Department of Surgery and Cancer
Imperial College London

Developing a Soft Inflatable Endorectal Actuator for Prostate Radiotherapy

Aryan Niknam Maleki

Supervised by:
Dr. George Mylonas
Dr. Julia Murray
Dr. Alexander Thompson
Prof. Julian Jones

Submitted in part fulfilment of the requirements for the degree of Master of Philosophy in Surgery and Cancer of Imperial College London and the Diploma of Imperial College London

Abstract

Prostate motion during radiotherapy—primarily caused by patient-specific variations in rectal filling—can compromise dose delivery accuracy, increasing the risk of biochemical recurrence and toxicity. Current rectal stabilisation devices suffer from poor tolerability or limited validation. This thesis aimed to design, fabricate, and validate a novel rectal stabilisation device—an endorectal actuator—addressing these limitations.

An initial trial comparing CT scans of patients who could and could not tolerate ProSpare™ found no significant anatomical differences (anorectal angle, rectal diameter, anal canal length), suggesting that reduced tolerability was caused by device geometry and rigidity rather than a mismatch to anorectal anatomy. These results helped establish the seven design criteria: deployability, radial stiffness, rectal retraction capability, self-insertion, image guidance, and low-cost manufacturing.

A hydraulically inflatable soft robotic actuator was developed through successive design iterations to improve device rigidity, control, and durability. Replacing conical pouch motors with elliptical pouch motor reduced internal membrane damage while increasing volume capacity and holding force. A dual-flexor configuration further improved resistance to opposing bending action. The final device achieved a baseline angle of 115.8°, rising to 122.8° under 0.72 N of opposing force.

Radiopaque markers for image guidance proved too thin to be visible on CT, but the water-inflated device itself was visible contrasting with air; a low-cost contrast-enhancing liquid may be viable.

Rectal phantom validation demonstrated the device’s ability to reduce diameter change (from 25 mm to <5 mm) and rectal wall displacement (from 15 mm to <5 mm) under dynamic compressions; and reduce rectal wall displacement (13 mm to 4 mm) and anorectal angle (+12° to +2°) after inducing anterior translation.

The final endorectal actuator met six of seven design criteria, suggesting it may reduce prostate displacement and improve radiotherapy outcomes. Future work should improve usability, soften device edges, and integrate sensing for treatment monitoring.

Declaration

This thesis contains the author's original work. Any work not completed by the author has been referenced as appropriate.

The copyright of this thesis rests with the author. Unless otherwise indicated, its contents are licensed under a Creative Commons Attribution-NonCommercial 4.0 International Licence (CC BY-NC).

Under this licence, you may copy and redistribute the material in any medium or format. You may also create and distribute modified versions of the work. This is on the condition that: you credit the author and do not use it, or any derivative works, for a commercial purpose.

When reusing or sharing this work, ensure you make the licence terms clear to others by naming the licence and linking to the licence text. Where a work has been adapted, you should indicate that the work has been changed and describe those changes.

Please seek permission from the copyright holder for uses of this work that are not included in this licence or permitted under UK Copyright Law.

Acknowledgements

I would like to express my gratitude to Garrick Wilson who gave me the opportunity to pursue this MPhil, my parents for financially supporting me and my decision to pursue this degree in between my BSc and completing my MBBS, and to Dr George Mylonas and Dr Julia Murray for their guidance, feedback, and expertise while I explored new ideas throughout these last four years. I would also like to thank Dr Alex Thompson and Prof Julian Jones for their guidance before the project underwent a change in direction.

I would like to thank the medical physicists at The Royal Marsden Hospital who helped me in furthering my understanding of radiotherapy. I would like to thank Rollo Moore and Angelos Vasilopoulos who helped me scan my device.

I would like the thank the research group in the office at South Kensington and the lab in the Paterson Building whose friendships kept me sane throughout these years. Special mentions go to Mark Runciman, Nilanjan, Amirhossein, Emilia, Jianlin, and Zhangxi for the office banter, political discussions, and who I was able to confide to when life was rough. Special thanks go to Dr Mark Runciman for his insights, helping me understand soft robotics, and maintaining the equipment I required for this project. His mentorship included teaching me how to create soft robots, improving my coding skills, and shaping me as an engineer.

Lastly I would like to thank my own friends, including the members of Post-Montrose Revival (PMR) and my high school friends (Portugal). These people have always been there for me and gave me a space to have fun outside of university. Most of all I would like to thank my fiancée, Molly Workman, who has been my light and rock during any times I struggled. She has continually supported my decisions during this project and helped me understand myself better.

Table of contents

Chapter 1 Introduction....22
1.1 Thesis overview....22
1.1.1 Thesis structure....22
1.1.2 Contributions....23
1.2 Clinical background....25
1.2.1 Overview of challenges in tracking rectal motion during pelvic radiotherapy....30
1.2.2 Adaptive radiation therapy and methods of tracking rectal motion 32
1.2.3 Interventions aimed at reducing rectal toxicity....36
1.2.4 Literature review on current rectal stabilisers for pelvic radiotherapy 38
1.2.5 Conclusions....41
1.2.6 Aims....41

Chapter 2 ProSpare™ tolerability is independent of rectal anatomy....52
2.1 Introduction....52
2.1.1 Existing rectal examination devices....52
2.1.2 Anorectal anatomy....53
2.1.3 Aims....55
2.2 Methods....55
2.3 Results....56
2.4 Discussion....57

Chapter 3 Background on soft robotics and fluid actuation....59
3.1 Actuation methods....59
3.2 Variable stiffness mechanisms....61
3.3 Literature review on pouch motors and pressure-driven actuators....63

3.3.1 Introduction....63
3.3.2 Pneumatic artificial muscles....64
3.3.3 Pleated PAMs....65
3.3.4 Embedded PAMs....66
3.3.5 Pouch motors/Peano Muscle....69
3.3.6 Electrohydraulic actuators....70
3.3.7 Gusseted pouch motors including Origami-inspired designs....75
3.3.8 Paired pouch motors....76
3.3.9 Kirigami inflatable actuators....77
3.3.10 Conical pouch motors....77
3.3.11 Other pouch motors....78
3.3.12 Applications of pouch motors in soft robots....81
3.3.13 Discussion....82
3.4 Revised aims....83

Chapter 4 Design and fabrication of a deployable endorectal actuator....85
4.1 Introduction....85
4.2 Laser welding methods....85
4.3 First design: a dual-truncated prism....87
4.3.1 Design and methods....87
4.3.2 Results....88
4.3.3 Discussion....89
4.4 Second design: perpendicular welds for a reinforced actuator....89
4.4.1 Radial welds to reinforce one side: Methods....89
4.4.2 Results....93
4.4.3 Discussion....95
4.5 Modifications that aimed to increase the angle....95
4.5.1 Increased width of device....96

4.5.2 Notching in the device 97
4.6 A working prototype: a notched wrist actuator with a flexor and extensor actuator 99
4.6.1 Introduction 99
4.6.2 Materials 103
4.6.3 Designs 103
4.6.4 Deployability of device 106
4.6.5 Extent of flexion and extension and angle control 107
4.6.6 Strength: radial stiffness and resistance to bending 108
4.6.7 Stress relaxation properties of device 111
4.6.8 Repeatability of inflation, flexion, and extension 113
4.7 Discussion 113
Chapter 5 Optimising the endorectal actuator for use in radiotherapy 117
5.1 Introduction 117
5.2 Optimising bending resistance 117
5.2.1 Design 118
5.2.2 Experimental methods 124
5.2.3 Results 128
5.2.4 Discussion 134
5.2.5 Conclusion 137
5.3 Additional modifications to device 138
5.3.1 Three-sided device 138
5.3.2 Making the device self-insertable 140
5.4 Adding fiducial markers 141
5.4.1 Methods 141
5.4.2 Results 143
5.4.3 Discussion 144

Chapter 6 Validating the endorectal actuator inside a rectal phantom 145
6.1 Introduction 145
6.2 Materials and methods 145
6.2.1 Fabrication of phantom 147
6.2.2 Validation of phantom 149
6.2.3 Validating the elastic ribbons 149
6.2.4 Validation of device 153
6.3 Results 156
6.3.1 Elastic ribbons 156
6.3.2 Barostat validations 157
6.3.3 Dynamic compressions 159
6.3.4 Reproducibility of volume and position 160
6.4 Discussion 162
6.5 Conclusion 166

Chapter 7 Discussion and Conclusion 167
Chapter 1 167
Chapter 2 167
Chapter 3 167
Chapter 4 168
Chapter 5 168
Chapter 6 169
General comments 170

Bibliography 172

Appendix 205
A.1 Copyright summary table for third party work 205
A.2 Copyright permission statement from IEEE 211

List of figures

Figure 1.1 Visualisation of different delineations and how motion can affect coverage. 26
Figure 2.1 Labelled schematic of the anorectum. 54
Figure 2.2 A patient's CT planning scan with annotations analysing the rectum shape and size....56
Figure 2.3 Distributions of measurements of patients' rectums....57
Figure 3.1 The main actuation methods discussed....61
Figure 4.1: Workflow visualization of the fabrication methods. 86
Figure 4.2 The design principle of two truncated prisms connected to each other to form a dual truncated prism. 87
Figure 4.3 Design and dimensions of a three-sided (Left) and four-sided (Right) dual-truncated prism. 88
Figure 4.4 Four-sided dual-truncated prism device. 89
Figure 4.5 Left: The initial design of a reinforced device with a channel for an inextensible tube and horizontal chambers. 90
Figure 4.6 Three-sided device with radial welds and with axial welds. 91
Figure 4.7 A 3-sided device containing axial or radial welds and its respective direction of contraction. 91
Figure 4.8 The sketch design of the reinforced actuator with axial welds on one side and radial welds on the other two sides. 92
Figure 4.9 Inflated 3D shape of the design with axial welds on one side to reinforce it. Left: lateral view of the device highlighting the angle. Right: Anterior side of the device showing the axial welds. 94
Figure 4.10 The reinforced actuator design superimposed on ProSpare™ on CBCT. 94
Figure 4.11 Radial stiffness of the reinforced actuator against gauge pressure. 95
Figure 4.12 Angle of the device at different widths. 96
Figure 4.13 The first notched device with a 16 mm cutout. 98
Figure 4.14 Design process of the angled inflatable endorectal actuator summarised as a flowchart. 99

Figure 4.15 The initial prototype with a flexor actuator. 101
Figure 4.16 Visualisation of a “disconnected” dual truncated prism 101
Figure 4.17 The flexor actuator is attached to the same side of the main actuator 103
Figure 4.18 Design and fabrication of the soft endorectal actuator showing weld patterns 104
Figure 4.19 Sagittal view of the device showing the mechanism of action of the internal flexor actuator 105
Figure 4.20 Dimensions of the device 106
Figure 4.21 The maximal angle of flexion and extension 108
Figure 4.22 Angle changes of the device while the flexor actuator is full and the extensor actuator is inflated from 0 ml to 4 ml. 108
Figure 4.23 Measuring force output from the main actuator of the device 109
Figure 4.24 Radial stiffness of the main actuator in relation to the volume it is inflated 110
Figure 4.25 Force measured vs displacement in compression of the main actuator 110
Figure 4.26 Relationship between the torque acting on the device and the increase in the angle of the device, opposing the bending action by the flexor actuator 111
Figure 4.27 The absolute pressure over time inside the actuators. 112
Figure 4.28 Compressive radial stiffness over time 113
Figure 5.1 The designs and dimensions of each pouch motor and their sub-actuator type. 119
Figure 5.2. Graphical visualisation of the elliptical end of the actuator. 121
Figure 5.3 Setup to determine contraction ratios and maximum volumes of the different flexor actuators. 125
Figure 5.4: Experimental setup assessing the actuators’ load bearing capacity 126
Figure 5.5 Experimental setup to determine the bending resistance of each prototype device with a differently-shaped flexor actuator and multiple flexor actuators. 127
Figure 5.6 The angle of the device was defined as the angle between the longitudinal axis of the device and the front wall of the device 128

Figure 5.7 Each pouch motor shape type visualized once fully inflated with water. 130
Figure 5.8 Maximum stroke ratio (stroke length as a proportion of uninflated length) vs load pulled. 130
Figure 5.9 Changes in pressure with stroke ratio for the different actuator iterations holding either no load, 150 grams, or 300 grams. 131
Figure 5.10 Internal pressure at maximum volume plateaus as the load increases on the actuators 132
Figure 5.11 The mean force measured on spring gauge in the bending resistance trials for a single or dual flexor actuator setup for each type of actuator. 134
Figure 5.12. Fabrication of the modified soft hydraulic endorectal actuator. ...139
Figure 5.13 Dimensions of the XXWE (Extra-extra wide elliptical) actuator 140
Figure 5.14 The main body of the endorectal actuator embedded with metallised thermoplastic.....142
Figure 5.15 Inflated endorectal actuator placed on CT bed prior to scan.....143
Figure 5.16 Three-dimensionally reconstructed CT view of the endorectal actuator in the sagittal plane (left) and transverse plane (right). 143
Figure 6.1. Rectal phantom used to validate the endorectal actuator 148
Figure 6.2: Expressing the dimensions of the rectal phantom to indirectly find the total length of the elastic ribbons.....152
Figure 6.3. Measuring anorectal angle (left) and position of the anterior rectal wall (right) in the rectal phantom. 156
Figure 6.4 The force-strain curves of the elastic ribbons used in the rectal phantom. 157
Figure 6.5 Diameters of the distal and proximal rectum with different motion protocols acting on the rectal phantom. 159
Figure 6.6 2-Dimensional displacements of the anterior rectal wall (ARW) and centre of rectum with different motion protocols acting on the rectal phantom.. 160
Figure 6.7 Anorectal angle positions with and without the device inside the rectal phantom when the proximal flange was moved to displace the rectal phantom. 161

List of tables

Table 1.1 Summary of studies exploring rectal stabilisers in radical prostate radiotherapy. 43
Table 1.2 Summary of studies exploring rectal stabilisers in post-prostatectomy radiotherapy. 49
Table 2.1 Mean (±SD) anorectal angle, anterior-posterior rectal diameter at the anorectal junction, and anal canal lengths in patients who could tolerate ProSpare™ (Group Y), patients who could not tolerate ProSpare™ (Group N), and patients who had ProSpare™ inside (Group PS), as seen on planning CT scan 57
Table 3.1 Summary of common pneumatic artificial muscle designs. 67
Table 3.2 Summary of design modifications made to pouch motors. 72
Table 4.1 Force by Newton meter and angle changes 111
Table 5.1. Equivalent volume ratios for inflatable pouch motors depending on the shape of the lateral ends 124
Table 5.2 Characteristics of the different shapes of actuators 129
Table 5.3 Measured angles of the device at maximum contraction of the flexor actuator, depending on the number of actuators and shape of the sub-actuator, and whether a force is applied to it with a spring gauge 133
Table 5.4 Dimensions and expansion ratio of the three-sided device across its different states of inflation. 139
Table 6.1: Desired ranges of anorectal properties to emulate in the rectal phantom 146
Table 6.2. Motion protocols simulated in the rectal phantom 153
Table 6.3 Elastic ribbon strains and corresponding forces associated with each induced level of tone in the rectal phantom. 158
Table 6.4. Rectal compliance of the rectal phantom at different levels of muscular tone. 158
Table 6.5. Outer diameter of the proximal rectum and calculated volume changes in the rectal phantom with and without the device. 161
Table 6.6. Anterior-posterior displacement of the anterior rectal wall (ARW) relative to control position in rectal phantom with and without the device. 162

List of acronyms

Acronym	Definition
2D	Two dimensional
3D	Three dimensional
3D-CRT	3-dimensional conformal radiation therapy
ANOVA	Analysis of variance
AP	Anterior-posterior
ARA	Anorectal angle
ART	Adaptive radiation therapy
BA	Bony alignment
BEV	Beam-eye-view
CAD	Computer-aided design
CBCT	Cone beam computed tomography
CI	Confidence interval
CT	Computed tomography
CTCAE	Common Terminology Criteria for Adverse Events
CTV	Clinical target volume
DRE	Digital rectal examination
EBRT	External beam radiation therapy
EM	Electromagnetic
ERB	Endorectal balloon
FM	Fiducial markers
GI	Gastrointestinal
GI	Gastrointestinal
GTV	Gross tumour volume
GU	Genitourinary
IGRT	Image-guided radiation therapy
IMRT	Intensity-modulated radiation therapy
KIM	Kilovoltage intra-fraction monitoring
LR	Left-right
MAUDE	Manufacturer and User Facility Device Experience
MOSFET	Metal-Oxide-Semiconductor Field-Effect Transistor

MRI	MRI (Magnetic Resonance Imaging
OAR	Organs at risk
PAM	Pneumatic artificial muscle
PTV	Planning target volume
RMC	Rectal motor complex
RT	Radiotherapy
SD	Standard deviation
SI	Superior-inferior
SMA	Shape memory alloy
US	Ultrasound
VMAT	Volumetric modulated arc therapy

Glossary

Term	Definition
3-dimensional conformal radiation therapy	Delivery of radiation shaped to the target's geometry using multiple fixed-angle beams
Actuator	A component in robotics or devices that converts energy (electric, pressure) into mechanical motion.
Adaptive radiation therapy	Strategy where plan is adjusted during treatment to compensate for anatomical changes
Anal canal	Terminal part of the large intestine, 2–4 cm long, ending at the anus
Analysis of variance	A statistical method used to compare the means of three or more groups to determine if at least one is significantly different from the others
Anorectal angle	Angle between rectum and anal canal maintained by puborectalis muscle, and is involved in maintaining continence
Anorectal manometry	Test measuring pressures in rectum and anus to assess function
Barostat balloon	A balloon in rectum used during manometry to test sensitivity, capacity, and compliance.
Beam-eye-view	A planning perspective showing target and organs from the beam's viewpoint
Bony alignment	Positioning based on skeletal structures seen via imaging
Brachytherapy	A type of internal radiation therapy where radioactive sources are placed directly inside or next to the treatment area, often used for prostate, cervical, or breast cancer
Chemotherapy	Use of cytotoxic drugs to treat cancer systemically

Clinical target volume	the tissue volume that contains the gross tumor and/or subclinical malignant disease that needs to be targeted to achieve therapeutic effects
Common Terminology Criteria for Adverse Events	Standardized system for grading side effects of cancer therapies.
Computed tomography	A diagnostic imaging procedure that uses X-rays to create detailed cross-sectional images of the body
Computer-aided design	The use of computer systems to assist in the creation, modification, analysis, or optimization of a design, often used in medical device development or treatment planning
Cone beam computed tomography	A type of CT imaging that uses a cone-shaped X-ray beam to create 3D images, frequently used in radiation therapy and dental imaging
Conventional fractionation	Standard radiation dose schedule—typically 1.8–2 Gy per fraction over ~6–7 weeks.
Defecography study	Imaging (often fluoroscopic or MRI) of rectal emptying and defecatory mechanics
Digital rectal examination	A physical exam where a healthcare provider inserts a gloved, lubricated finger into the rectum to check for abnormalities of the prostate or rectal wall.
Electromagnetic	Pertaining to the magnetic and electric fields produced by the movement of electrically charged particles; in medicine, it may relate to imaging techniques or therapeutic devices
Electromagnetic transponders	Implanted beacons that emit signals to track tumour position in real time
External beam radiotherapy	A type of radiation therapy where beams of high-energy rays are directed from outside the body toward the tumour.

Fiducial markers	Small radiopaque markers inserted in or near the tumour to enhance localization accuracy.
Gastrointestinal	Relating to the stomach and intestines, often referenced in the context of side effects or complications from therapy
Gaussian curvature (Theorema Egregium)	In differential geometry, states that intrinsic curvature is preserved under bending.
Genitourinary	Pertaining to the genital and urinary organs and systems, commonly involved in prostate and pelvic-related medical contexts
Geographical miss	Undercovering the target due to misalignment or anatomical changes
Gross tumour volume	The visible or palpable extent of malignant tissue as seen on imaging or during examination.
Hydrogel spacer (SpaceOAR)	A biodegradable gel injected between prostate and rectum to protect rectal tissue during prostate radiation
Hypofractionated radiotherapy	Larger dose per session over fewer visits (e.g., 2.5–7 Gy/fraction).
Image-guided radiation therapy	A type of radiation therapy that uses imaging during treatment to improve precision and accuracy of radiation delivery
Intensity-modulated radiation therapy	Advanced radiotherapy technique modulating beam intensity to deposit conformal dose around complex-shaped targets
Isodose	A line/surface in plans representing locations receiving equal radiation dose
Kilovoltage intra-fraction monitoring	Technique using kilovoltage X-rays during radiation delivery to track internal markers.
Kirigami	Extension of origami involving cuts as well as folds.
Laplace’s Law	Wall tension in a cylinder/sphere is directly proportional to the pressure inside and the radius

	of the vessel, and inversely proportional to the wall thickness. Used in vessel and organ wall stress analysis.
Magnetic Resonance Imaging	Medical imaging technique based on nuclear magnetic resonance to create images of the inside of the body
Manufacturer and User Facility Device Experience (MAUDE) Database	Public resourced maintained by the US Food and Drug Administration (FDA) that contains reports of adverse events associated with medical devices.
Metal-Oxide-Semiconductor Field-Effect Transistor (MOSFET)	A type of transistor used for switching and amplifying electronic signals in circuits
Organs at risk	Healthy tissues/organs near the target that are sensitive to radiation and must be spared.
Origami	Japanese art of folding paper into decorative shapes and figures.
Planning target volume	The CTV plus a margin for uncertainties in treatment delivery, such as patient movement or setup variations, used to ensure the entire target receives the prescribed dose.
Plastic scintillation detectors	Fiber-optic detectors emitting light proportional to radiation dose—used in quality assurance
Pneumatic artificial muscle	A soft actuator that expands or contracts in response to air pressure changes, mimicking natural muscle movement; used in robotics and assistive medical devices
Pouch motor	A type of soft actuator made of flexible materials that inflates like a pouch to produce motion, often used in wearable or robotic systems for rehabilitation or support
Prostatectomy	Surgical removal of the prostate gland.

Radiotherapy	Use of ionizing radiation (external or internal/brachytherapy) to control or eradicate cancer.
Radiotherapy fraction	One daily dose of radiation delivered in a treatment course
Rectal capacity	Maximum volume the rectum can hold before feeling urgent need to defecate
Rectal compliance	The rectum's ability to stretch in response to filling (Δvolume/Δpressure) (in ml/mmHg).
Rectal motor complex	Cyclic and coordinated neuromuscular activity in the rectum, facilitating stool propulsion
Rectum	Last 12–15 cm of the large intestine ending at anorectal junction
Shape memory alloy	Metals (e.g., Nitinol) that "remember" original shape and return to it when heated, used in actuators or stents.
Thermoplastic	polymers that can be softened through heating before being processed and then left to cool and harden
Ultrasound	medical imaging technique that uses high-frequency sound waves to create images of the inside of the body
Van Herk margins	Quantitative expansions applied to CTV to generate PTV, accounting for uncertainties and ensuring a minimum dose to the CTV of 95% for 90% of patients
Viscoelastic	Material exhibiting both viscous (time-dependent) and elastic (instantaneous recovery) behaviour—common in biological tissues and certain polymers
Volumetric modulated arc therapy	An advanced form of radiation therapy that delivers dose continuously as the treatment

	machine rotates around the patient, enabling precise and efficient treatment.
X-ray	Medical imaging technique using ionizing radiation to create images of inside of the body

List of publications

Niknam Maleki A, Runciman M, Murray J, Mylonas G. Hydraulic endorectal actuator for prostate radiotherapy reduces variations in motion in a silicone rectal phantom. *Frontiers in oncology*. 2026; 16 1686529. 10.3389/fonc.2026.1686529

Maleki AN, Runciman MS, Murray J, Mylonas GP. Elliptical-Shaped Pouch Motors Improve Bending Resistance of Endorectal Actuator for Prostate Radiotherapy. *IEEE International Conference on Robotics and Biomimetics (Online)*: IEEE; Dec 3, 2025. pp. 436–441. 10.1109/ROBIO66223.2025.11377826

Niknam Maleki A, Mylonas G, Murray J. ProSpare tolerability is independent of rectal anatomy. *Proceedings of the 10th World Congress on Electrical Engineering and Computer Systems and Sciences (EECSS'24),* : Avestia; 2024. pp. ICBES 145. 10.11159/icbes24.145.

Maleki AN, Thompson A, Runciman MS, Murray J, Mylonas GP. A soft hydraulic endorectal actuator for prostate radiotherapy. *2023 IEEE International Conference on Robotics and Biomimetics (ROBIO)* : IEEE; Dec 4, 2023. pp. 1–6.

Niknam Maleki A, Runciman M, Thompson A, Murray J, Mylonas G. Developing a customisable inflatable rectal obturator. *The 15th Hamlyn Symposium on Medical Robotics 2023* London; 2023. pp. 141–142.

Chapter 1 Introduction

1.1 Thesis overview

This thesis investigates the development of a soft endorectal actuator for prostate radiotherapy that can translate into the clinic. The initial prototypes of the endorectal actuator and how they inspired the working prototype are described. The motivations for this work were the high prevalence of prostate cancer, the high rate of patients suffering from cancer recurrence and gastrointestinal toxicity for those undergoing prostate radiotherapy, and the lack of uptake from current rectal stabilisers aiming to address this because of their inherent limitations. A soft endorectal actuator was hypothesized to address these limitations and improve outcomes in prostate radiotherapy.

A soft endorectal actuator was fabricated and validated with benchtop force measurements and a clinically simulated rectal phantom. The deployable endorectal actuator would be expected to be tolerated by most men inserting the device because of its inflatable nature and soft materials. It can inflate to a rigid, angled shape which provides rectal stabilisation which would improve outcomes in radiotherapy. Future work to verify this in human trials is needed.

1.1.1 Thesis structure

Firstly, the clinical background for the use of rectal devices in pelvic radiotherapy is outlined. This includes an overview of the challenges of rectal motion and existing rectal devices aiming to reduce rectal motion. This is followed by a preliminary trial ascertaining anatomical differences between patients who could tolerate one such device and patients who could not, based on (1). This directed the project into the design and fabrication of a soft endorectal actuator. A second overview is provided, which considers the structures of soft robotic actuators that can be incorporated into the device.

Chapter 4 expands on (2) and (3) and discusses initial prototypes that were tested but were ultimately unsuccessful in meeting the desired criteria of the device. The initial prototype that met 6 out 7 criteria is described and validated here.

Chapter 5 describes improvements made to the endorectal actuator including increasing the bending resistance, reducing shearing, and allowing self-insertion by the patient. This chapter also includes an attempt at making the device visible on CT and MRI scan.

Chapter 6 describes designing, manufacturing, and validating a motor-controlled rectal phantom for testing the endorectal actuator. The endorectal actuator's ability to stabilise the rectum is assessed with this phantom.

Finally, the discussion and conclusions of this thesis are presented in Chapter 7.

1.1.2 Contributions

The first overview in Chapter 1 is on the challenges of rectal motion in pelvic radiotherapy. It provides the clinical context behind the impact rectal motion has on pelvic radiotherapy outcomes and analyses existing methods for tracking or reducing rectal motion to improve outcomes. While the focus of this thesis is in prostate radiotherapy, the takeaways from radiotherapy in gynaecological and rectal cancers are used to guide this thesis. Specifically, a review of rectal stabilisation devices is presented in this chapter.

Chapter 2 presents the results from a preliminary trial ascertaining differences in the rectal anatomy between patients in the phase II Post-Operative use of ProSpare™ (POPS) trial (NCT02978014) is an extension of (1) and influenced the direction of this project to make a soft robotic device, instead of a personalised rigid device. The results from this preliminary trial were indicative that ProSpare's challenges on insertion may be because of difficulties bypassing the anal sphincter. This conclusion was not established prior, when ProSpare™ was undergoing design modifications before its current iteration. The images were collected from the POPS trial but results were analysed and interpreted by the author.

This is followed by an overview of soft robotic devices and their structure in Chapter 3. This overview discusses the benefits and limitations of different structures of existing soft robotic actuators, known as pouch motors. This chapter

analyses how the structure affects performance aspects such as contraction ratio and force output. These structures were considered when the author designed his device in Chapter 4.

Chapter 4 describes the initial prototypes designed that initially did not satisfy the device criteria but ultimately helped inspire the design and fabrication of the working endorectal actuator. This chapter also describes the design, manufacture, and testing of this endorectal actuator. The first half of the chapter (the initial prototypes) is based on (2) whereas the second half (the working endorectal actuator) is based on (3). The contribution of this chapter is to highlight the design of the endorectal actuator consisting of an inflatable external shell with an internal pouch motor that acts as a “flexor” actuator. The development of this novel rectal stabiliser device may enable improved outcomes in prostate radiotherapy.

Using the knowledge obtained from analysing structures of pouch motors, a novel pouch motor with elliptical ends is described in Chapter 5. This pouch motor with elliptical ends addresses the limitations seen in rectangular and conical pouch motors. This elliptical pouch motor reduced cutting risk of the internal membrane from the flexor actuator and improved the bending resistance of the endorectal actuator, by allowing for increased inflation volume within the same space. This design may be useful in wearable robotics, where sharp-edged inflatables would lead to discomfort. Additionally, the device was modified to a three-sided device instead of four to reduce shearing, and the tubing that inflates the device is inserted all the way to the tip of the device enabling self-insertion by pushing from the tube. The design of the actuators, design of experiments, testing and analysis of results were carried out by the author of this thesis.

The work in Chapter 6 included a validated rectal phantom with motor-controlled elastic ribbons that can induce dynamic changes in volume. A brief overview of rectal properties and analysis of other phantoms is included to justify the design and dimensions of this phantom. The author validated the phantom with a barostat balloon. The endorectal actuator was validated in this phantom by assessing its ability to resist dynamic changes in rectal volume and reproducibly

stabilise the rectal volume from different starting positions. These validations in the phantom show success in the development of the endorectal actuator and its ability to stabilise a rectum.

1.2 Clinical background

In the United Kingdom, prostate cancer is the most common cancer by diagnosis, and the 2nd most common cause of cancer death in males (4-6). In England, 45,000 – 50,000 men are diagnosed with prostate cancer each year (5,7,8). Only 13% of these diagnoses were in men under the age of 60, making age the single biggest non-modifiable risk factor for prostate cancer (8,9). Other non-modifiable risk factors include having a family history of prostate cancer (10) and being of Black, African, or Caribbean ethnicity (11). Modifiable risk factors include smoking and a high-fat diet (11,12).

Treatment options for prostate cancer include active surveillance, radical prostatectomy, chemotherapy, and radiotherapy. The majority of patients will first undergo active surveillance, where the patient is carefully observed with regular follow-ups. When the tumour shows signs of progression or there is an effect on the quality of life, interventional treatment takes place (13). Prostatectomy is surgical removal of the prostate. Chemotherapy is the administration of cytotoxic drugs which kill the cancer cells. Radiotherapy can be radical radiotherapy which is ionising energy targeted at the prostate to kill cancer cells or can be post-surgical radiotherapy where the prostate bed is targeted as the prostate has been removed. Between 2019 and 2021, in the United Kingdom, 33.1% of prostate cancer patients received radiotherapy (14).

Modern radiotherapy techniques use three-dimensional anatomical information and conformal treatment fields to deliver high doses to the target volume while sparing surrounding tissues (15). To create conformal treatment fields, the planning process of treatment includes image segmentation: delineation of regions of interest such as bony landmarks, the target volume, and healthy

structures which must be avoided (15,16). The target volumes consist of a clinical target volume (CTV)—the local spread of the disease and encompasses the gross tumour volume (GTV)—which is the primary target of the radiation beam and the planning target volume (PTV), which includes the CTV with a “safety margin” that accounts for setup errors and movement (17-19). Image segmentation is followed by selecting the beam’s directions and apertures, based on beam-eye view projections on the delineated structures, and volumetric dose calculations. Multiple treatment fields and multileaf collimators (MLCs) enable multiplicity low-energy beams, conforming high dose at the CTV/PTV and sparing surrounding tissues. MLCs have tungsten leaves, each of which can move independently of each other, allowing precise field boundaries and conformal shaping of the field (15).

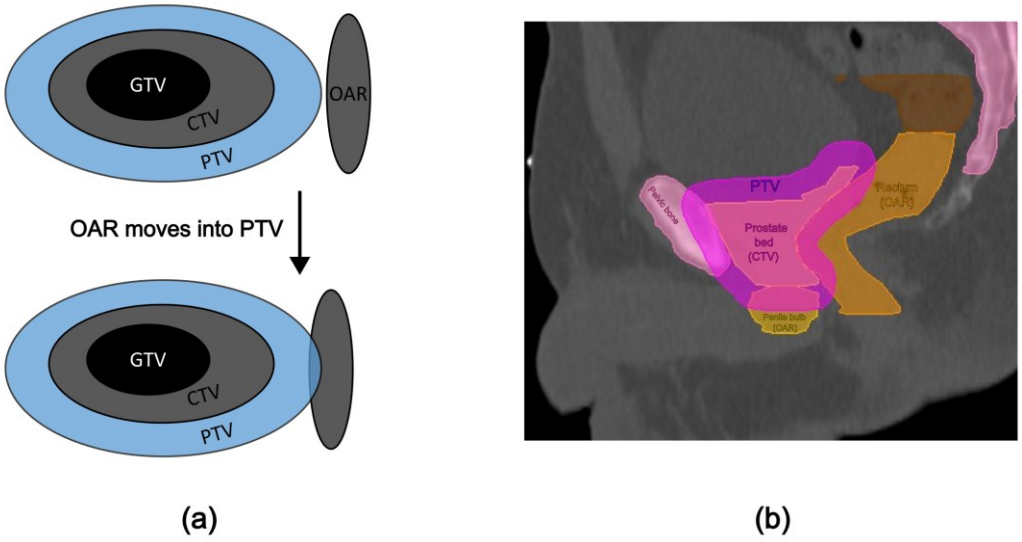

Figure 1.1 Visualisation of different delineations and how motion can affect coverage. (a) Example showing the OAR is not covered by the PTV but after the OAR moves into the PTV field it is covered by radiation; (b) How these delineations look like on a sagittal pelvic CT scan. GTV = gross tumour volume; CTV = clinical target volume; PTV = planning target volume; OAR = organ at risk.

These radiation techniques aim to deliver high doses to the target and spare surrounding organs at risk (OARs). However, a highly conformal and precise radiation beam is sensitive to motion of the target and OARs relative to the radiation beam. Figure 1.1 depicts how this can lead to geographical misses and inclusion of the OARs into high-dose regions. PTV can target OARs, including the rectum in the case of post-prostatectomy (Figure 1.1b). Inclusion of the OARs

in high-dose regions leads to increased exposure to radiation and consequent side effects. For prostate cancer and gynaecological radiotherapies, variations in rectal filling is the predominant cause of inter- and intra-fractional motion of the target and the rectum is the main OAR (20-25).

In both prostate and cervical cancer radiotherapy, there is a clear correlation between variations in rectal filling and shifts in the target (21,22,25-27). Eminowicz et al. found that in cervical cancer patients undergoing chemoradiation, each mm of rectum anterior-posterior diameter deviation from the planning scan would reduce the probability of the PTV covering the CTV by 5.6% (26). They recommended interventions in the form of laxatives and/or micro-enemas if needed to aim for a sub-4 cm rectal diameter (26). Jensen et al. found large rectal fillings on daily CBCT compared to pre-treatment scans were associated with a lack of target coverage during treatment (27). In prostate cancer radiotherapy, every cm^3 increase in rectal, on average, leads to a 0.05-0.06 mm anterior shift (28-30) and 0.085 degrees rotation in the prostate (29). It is not uncommon for the prostate to shift up to 5-10 mm in either direction (28-32). In the postsurgical setting, rectal filling is also predominant source of anterior-posterior prostate bed motion (33,34). This intra-fraction motion is larger in the upper half of the rectum than the lower half and leads to shifts in the CTV (34), which can contribute to marginal misses (35), as every 10 mm shift in the anterior rectal wall is also correlated with a 5 mm shift of the posterior border of the CTV (34).

Additional causes for variations in motion include prostate volume, and motion of surrounding organs, namely bowel movements and glute contractions. These lead to variations in radiotherapy delivery and toxicity risks. Firstly, radiotherapy to the prostate varies with prostate volume and prostate deformation. Larger prostate glands (higher volume) require larger PTVs. These larger PTVs lead to increased areas of healthy tissue exposed to radiation, which manifests as larger prostate glands being associated with a higher risk of acute and late GU toxicity (36,37). If required, a patient may need some neoadjuvant hormone therapy to shrink the gland before radiotherapy is feasible (38). This can help reduce toxicity as smaller glands require smaller margins which results in a lower risk of

associated toxicity. However, radiotherapy itself can affect gland size which in turn affects radiotherapy planning. The prostate volume changes over the course of radiotherapy fractions (39). Prostate volume increases by about 10-20% during the first week of radiotherapy, because of the radiation-induced oedema (40-42). As the patient progresses through the radiotherapy fractions, the cells die and the prostate shrinks towards the end of treatment (43). This shrinking can be more pronounced with hormonal treatment (44). As the prostate volume varies over the course of radiotherapy, re-planning is mandatory to reduce the risk of recurrence and increase sparing of healthy tissues. Additional factors that can affect prostate motion during prostate radiotherapy are factors that affect pelvic floor contractions and/or intrabdominal pressure. Increased intra-abdominal pressure can in turn lead to involuntary pelvic floor contractions. Such factors include digestive issues and irregular bowel movements, mental anxiety and irregular breathing, which can be prominent at the start of treatment due to the patient being nervous. All these factors can lead to involuntary pelvic floor and glute contractions, posteriorly tilting the pelvis and moving the prostate (45).

Because of these motion errors, it is important to accurately delineate the CTV and OARs and track target position between radiotherapy fractions (inter-fraction error) and within a fraction (intra-fraction error). This accurate delineation and position tracking is especially important in post-prostatectomy radiotherapy, where the anterior rectal wall forms the posterior border of the CTV (46-50). Virtually any anterior-posterior translation or any change in rectal diameter would mean the anterior rectal wall is either exposed to increased radiation doses (51,52), or part of the CTV is missed for that fraction. To reduce the likelihood of missing the CTV, large PTV margins of 10-15 mm are recommended in the post-prostatectomy setting (52-56), covering more of the OARs with radiation doses. Additionally, most sites of relapse in post-prostatectomy radiotherapy are nodal or metastatic sites (57), which are not targeted without additional pelvic radiotherapy. As a result, 30-40% of post-prostatectomy patients experience biochemical recurrence within 5-10 years after postprostatectomy salvage RT (58,59). In the UK, 1/3rd of men are expected to undergo salvage radiotherapy after radical prostatectomy (60). Of these, 1000 patients are estimated to require radiotherapy again to target the pelvic nodes to treat biochemical recurrence

(7,58). In radical prostate radiotherapy, the biochemical recurrence is around 5% within 5 years with modern hypofractionation techniques (61). The rate of acute and late grade ≥2 GI toxicity in prostate radiotherapy can range between 16-38% (62-64) and 1.5-3% (63,64), respectively. In the post-surgical setting, acute grade ≥2 GI toxicity can be as high as 30% (65) and late grade ≥2 GI toxicity between 3-4.5% (58,65). In cervical cancer patients, the rate of cancer recurrence within 5 years is around 30% (66,67). The rate of grade ≥2 rectal toxicity is between 12-23% in patients treated with external beam radiation therapy (EBRT) and brachytherapy (68-70).

In these pelvic cancer patients, emptying the bowels can reduce variations in rectal filling, thereby reducing target motion and this has formed part of the bowel prep of most centres. However, this is only feasible where the rectum is an organ at risk (OAR); this does not apply to patients who are treated for rectal cancer as they usually have severe bowel dysfunctions meaning they cannot empty their bowels for radiotherapy, reducing target motion (71). In these patients, it may be even more challenging to measure and address rectal motion as that is the target. In rectal cancer radiotherapy, delineating the tumour alone is not always possible. So, sometimes, the gross tumour volume (GTV) alone can already include the whole lumen at the tumour site (72). The CTV includes some of its surrounding structures. Depending on the stage of the tumour, the CTV will include at least the mesorectum, presacral nodes, and lateral lymph nodes, but may also include the other lymph nodes and ischiorectal fossa (73). The PTV margins will then add 5 or 10 mm, depending on the imaging protocol and centre, increasing the rectum’s exposure to radiation.

Possible solutions to address variations in rectal motion include tracking rectal or target motion or reducing rectal or target motion. Implementing these solutions have proven difficult, because of rectal anatomy, physiology, and the unpredictable nature of its motion. Because of this, image-based monitoring and image-guided radiotherapy techniques are necessary.

1.2.1 Overview of challenges in tracking rectal motion during pelvic radiotherapy

This overview:

- Discusses the challenges of rectal motion monitoring in pelvic radiotherapy,
- Explores methods to monitor and quantify rectal motion with various imaging and tracking technologies.
    - Including attempts at individualising PTV margins and a discussion on adaptive radiation therapy (ART).
- Explores interventions and devices that reduce rectal motion by stabilising the rectum or reduce rectal toxicity in another way.
- Aims to create the criteria that guide the development of the device.

While the focus of this thesis is in prostate and prostate bed radiotherapy, the impact of rectal motion on patient outcomes in gynaecological and rectal cancer radiotherapy, as well as methods employed to improve these outcomes, will also be reviewed. The methods used to improve outcomes in the management of these cancers may be translatable to the device in prostate radiotherapy.

While target motion is correlated with rectal motion, it cannot be systematically quantified. There may be correlations showing a set amount of target motion for every unit increase in rectal volume or increase in anterior-posterior diameter (28-30,32,74), but the range of target motion within a patient population is large. For prostate cancer patients, anterior-posterior prostate shifts can range anywhere from -10 to +10 mm when rectal volume changes anywhere between -50 or +50 cm^3, with no clear correlation. Some patients saw a shift of 5 mm with little to no change in rectal volume while other patients would see similar shifts with an increased rectal volume (30). Likewise, some patients with a 100 cm^3 decreased rectal volume would have a posterior prostate shift of 8 mm, while others would have a posterior shift of 4 mm (28). Jensen et al. (27) found that target coverage in cervical cancer patients was dependent on rectal/bowel fillings on daily cone beam computed tomography (CBCT) but found these to be patient-specific with no systematic pattern during treatment. The extent of target coverage was not predictable during pre-treatment scans, making CBCT-based monitoring of the

target and/or other image-guided radiation therapy (IGRT) methods necessary (27).

Rectal movement is unpredictable likely because of the complex variable nature of rectal motion. Firstly, the rectum is a hollow, viscoelastic organ that can move about in translation, expansion, and rotation about the anorectal angle. The rectum's contractions that bring about most of this motion, are cyclic and occur in waves, called rectal motor complexes (RMC) (75). These cyclic contractions occur during the day and the night and can be split into two types. First are clusters of fast contractions (last less than 15 seconds), where the rectum contracts 5-6 times per minute for 1-2 minutes. This type more often occurs after eating. Second are powerful contractions exhibiting a pressure of >50 mmHg, which occur 2-3 times per minute for 3-10 minutes. These powerful contractions recur, on average, every 92 minutes during the day and 56 minutes at night (76). There are also isolated, slower contractions that last 10-20 seconds at a time (76,77). The anal canal also exhibits isolated and bursts of contractions. However, these are unrelated to the rectum's contractions (76) and are not cyclic or periodic like the rectum's contractions (78). These frequent and seemingly random movements make rectal motion during each treatment session unpredictable. While larger rectal volumes on pre-treatment scans are correlated with worse outcomes, there are conflicting results on whether they predict target intra-fraction motion (79,80). In prostate bed radiotherapy, inter-fraction motion can be largely corrected with image guidance, but large PTV margins of up to 10mm are still recommended (52,56), especially if online correction is based on bony alignment only, where it can be up to 15mm (52-56). Bony alignment is standard procedure as there is no visible target in prostate bed radiotherapy unlike in prostate radiotherapy.

To summarise, there are unpredictable and patient-specific variations in rectal filling and anterior-posterior translation, which lead to unpredictable and patient-specific shifts in target position. The consequence of this is potentially erroneous PTV margins. Population-based PTV margins in cervical cancer radiotherapy can be large (up to 4 cm around the uterus) to make sure to cover everyone (25). However, organ motion patterns are patient-specific, leading to unnecessary

inclusion of the OAR in the target volume in some patients, or PTV margins that are too small in other patients (25).

This is a statistical problem with van Herk margins, which systematically add margins to the CTV by considering the population systematic set-up error, the random error in each individual patient, and the inter-patient variation in random errors (van Herk main paper). The patient's individual systematic set-up error is the deviation between the actual and expected position and is often the calculated shift in position between the current fraction and the reference scan. The patient's mean individual set-up error is then the arithmetic mean of these errors across fractions. The population set-up error is then given as the standard deviation of this mean individual set-up error in a population and is denoted by $\Sigma_{\text{set-up}}$. The individual's random error is the standard deviation of the individual's set-up errors across fractions. The population random error is then the arithmetic mean of these set-up errors across a population and is denoted by $\sigma_{\text{set-up}}$. The PTV margins are then calculated:

$$\text{PTV margins} = 2.5\,\Sigma_{set-up} + 0.7\,\sigma_{set-up}$$

Statistically, these margins would mean that the CTV of 90% of the population is covered with 95% of the prescribed isodose (21,81,82). However, in small patient populations, these can be erroneously large or small due to statistical variability in patient-specific motion errors that would not be well represented because of sampling bias. The main methods to address these pitfalls are by adopting anisotropic margins and adaptive radiation therapy, which considers patient-specific anatomy and motion (25,83).

1.2.2 Adaptive radiation therapy and methods of tracking rectal motion

PTV margins are based on systematic and random set-up errors from image-guided radiation therapy (IGRT). IGRT in its simplest form would include a daily image of the patient's internal anatomy to compare to the planning scan. Image

registration enables discrepancies in position—translational and rotational—to be corrected by moving the treatment couch and align the image of the day with the reference planning scan (84). Alignment can be carried out by using soft tissues, such as the prostate or anterior rectal wall (ARW), or bony alignment—standard procedure in postprostatectomy as there is no visible target (33)—or gold seed fiducial markers, which are discussed later (85-87). Anyhow, standard IGRT only considers the reference planning scan and does not correct for intra-fraction motion, or patient-specific variability.

Adaptive radiation therapy (ART) addresses these limitations. Each daily scan is re-planned regenerating margins based on the individual patient's set-up error (88-90) and includes deformable image registration, which considers complex shape changes and distortions when aligning images (91). Offline ART aims to create an adaptive plan based on patient-specific inter-fraction motion error, but does not measure intra-fraction motion. Intra-fraction motion scans can be taken before and after a fraction, enabling the clinician to assess the effect the patient-specific organ motion has on the CTV. This assessment can be done quickly with beam-eye-view (BEV) CT image comparisons of rectal shifts from CT scans. However, these scans may fail to capture the full extent of rectal motion that occurs during treatment, as they only measure positions before and after the fraction. This approach risks overlooking any larger shifts that happen mid-treatment but are not present at the end. This may happen because of the cyclic nature of rectal motion in RMCs discussed (75). On the other hand, online ART does measure real-time intra-fraction motion. The adaptive plan is created in real-time while the patient is on the treatment table. It has been shown to improve PTV coverage and better spare OARs due to reduced PTV margins, where this is appropriate to do so in prostate and cervical cancer patients (79,88,92-95). This means less OARs are exposed to unnecessary radiation doses. However, online ART's is time and resource intensive. The extra steps taken at each fraction may include clinician, radiographer or AI contouring, optimising the adaptive plan, final dose calculations of the adaptive plan, and review. This can take on average, an extra 15:58 to 19:11 minutes and costs an extra $103.58 **per fraction** (95,96). This is resource-intensive and longer treatment times lead to larger displacements of the target during the fraction (97).

Kilovoltage intra-fraction monitoring (KIM) provides real-time tracking of implanted markers by taking X-rays during the delivery of the beam (98-100). When the tumour displacement is greater than 3 mm during the fraction, the beam is paused, and the couch is moved to realign the tumour to the isocentre. This can be beneficial during hypofractionated treatment regimens, where treatment times are longer and more displacements >3 mm occur during a fraction (98). Keall et al. showed KIM-guided gating reduced the percentage of treatment time with a prostate displacement of >3 mm from 73% to 24% (99). However, a significant limitation of KIM is additional exposure to imaging radiation. CyberKnife works similarly by tracking tumour position with markers in real-time and adjusting the radiotherapy beam accordingly. This has been shown to reduce the dose delivered to the rectum, compared to VMAT and IMRT (101,102). However, their availability is limited (103) and it takes significantly longer to generate treatment plans and carry out the radiotherapy fraction. Planning can take 1.5 hours longer with CyberKnife compared to VMAT (102), while treatment times can take between 42 to 90 minutes per session compared to 4-6 minutes with VMAT (102,104).

Another method of tracking target motion by placing markers inside the tissue is also not feasible for tracking rectal motion. Fiducial markers or electromagnetic (EM) transponders (Calypso®) can track real-time displacements by using intra-fraction x-rays or EM waves, respectively, to align the radiation beam accurately. These fiducial markers such as gold seeds (85-87,98), surgical clips in the postsurgical setting (105-107), and EM transponders (105-107) have all been validated extensively in the treatment of prostate cancer (97,99,108-112). In prostate cancer, EM and fiducial marker insertion have their own associated co-morbidity, such as bleeding, inflammation, and infection, because it is a surgical procedure (112,113). Despite the invasive nature of the procedure, the rate of complications is similar to the rate of complications in prostate biopsy (114,115). Many authors report low complication rates and conclude that, on balance, fiducial markers are safe to use (116). A significant advantage of EM markers (Calypso®) is that they do not require exposure to imaging radiation.

However, they cannot be used in the post-surgical setting because there is no solid structure to insert the markers, only the space left behind in the prostate bed. Calypso transponders' use in gynaecological cancers has also been validated, albeit with limited studies (117,118). Gatcombe et al. were able to implant Calypso transponders inside an endocervical (Smit) sleeve which was sutured within the cervical os which demonstrated highlighted intra-fraction cervical motion during EBRT (118).

These markers are hard to use for rectal cancers. While rectal implantation of fiducial markers is generally successful (119,120), fiducial and EM markers are rarely used in tracking rectal motion in rectal cancer radiotherapy. This is because, unlike the prostate, the rectum is not a solid structure; it is hollow and viscoelastic with hyper-elastic properties (121-123). In a solid structure, like the prostate, the markers move together to accurately show the location of the fiducials about the tumour and/or the radiation beam. However, in an elastic structure like the rectum, the markers move in different directions and create too many differential movement points to accurately interpret positions. Additionally, retention rates for intratumoral fiducial markers in rectal cancer are inconsistent, going as low as 55% after 17 days in Rigter et al's study (120,124,125). While these markers may be used for target motion in prostate cancer, they are difficult to implant to track target motion in other pelvic cancers. They are limited in their ability to accurately track rectal motion, either as an OAR, or as the target in rectal radiotherapy.

Wagner et al. (126) validated computer-aided correction models that compensated for the rectum's deformation when tracking its motion with electromagnetic markers. They validated this method of real-time rectal motion monitoring in a phantom for laparoscopy so that intraoperative imaging would not be required. Their most complex model was feasible and had a mean target registration error of 2.9 mm. Kok et al. (127) showed the use of EM trackers to track rectal motion during laparoscopy in rectal cancer patients. They showed feasibility of the method, and their results were in accordance per Wagner et al.'s study with a median tumour registration accuracy of 3 mm. While this may show promise, the deformation model needs further research in humans. While this

level of accuracy may be appropriate for laparoscopic surgery, it is hard to justify the use of transponders in radiotherapy: Calypso has been shown to have submillimetre accuracy (128) but this accuracy goes down to 1.5 mm in prostate cancer (111).

Another attempt at real-time monitoring of rectal motion involved real-time rectal dose monitoring. Ultimately, the reason to monitor rectal motion is to ensure it does not receive unintended radiation doses as an OAR, and that it does receive coverage as the target. By monitoring the dose in real-time directly, measuring motion is redundant; you can adjust the beam when unintended doses target the OAR. Hardcastle et al. validated rectal balloons with MOSFET radiation detectors for real-time *in vivo* rectal wall dosimetry (129). In a phantom, they showed the MOSFET agreed within 2.5% of the ion chamber measurements and provided real-time dose measurements of the anterior rectal wall. The anterior rectal wall (ARW) dose measured was 2.6% and 3.2% lower than the expected dose on the treatment plan for 3DCRT and IMRT plans, respectively (129). Wootton et al. made plastic scintillation detectors (PSDs), which, when attached to an endorectal balloon, can be used to monitor the real-time dose delivered to the rectum during a fraction of EBRT (130). They validated it in 5 patients and found a mean difference of -0.4% between measured doses and calculated planned doses. These PSDs were previously validated in phantoms (131-133), which also showed a discrepancy between measured doses and expected doses of less than 1%. These PSDs can measure real-time doses to the rectum in a non-invasive, radiation-free method. As such, they have clinical potential as patient position can be adjusted in response to real-time measurements when these deviate from the expected dose, similarly to KIM and EM markers. However, they are in their early stage of development and more research on patients needs to be conducted.

1.2.3 Interventions aimed at reducing rectal toxicity

Since tracking rectal motion and then adjusting the radiotherapy beam from any motion measured is either impractical, inaccessible, or resource-intensive, alternative methods of reducing GI toxicity in pelvic radiotherapies must be

explored. Pharmaceutical and non-pharmaceutical interventions to mitigate gastrointestinal toxicity from pelvic radiotherapy have been reviewed previously (134-136).

Pharmaceutical interventions include aminosalicylates, mucosal protectives, anti-inflammatory agents, and other targeted therapies. Aminosalicylates including mesalazine and sulfasalazine, show varying effects, but generally increase acute GI toxicity and symptoms, such as diarrhoea and cramps (134). Sulfasalazine had conflicting results whether it reduced rectal toxicity (137,138). Corticosteroids are anti-inflammatory medications considered as the first-line therapy for radiation proctitis (139). There is limited data on corticosteroid enemas potentially being beneficial when this was compared with sucralfate enemas instead of placebo (140,141). Oral metronidazole, when combined with other therapies, has also been shown to be an effective treatment for chronic radiation proctitis, but these also had no control group (142,143). Rectal beclomethasone has been shown to reduce rectal bleeding (144). Sucralfate, a mucosal protectant, facilitates epithelial healing by forming a physical barrier over damaged tissue which should be effective in treating haemorrhagic radiation proctitis (145,146). Orally, it has little to no effect on rectal toxicity but may increase acute rectal bleeding (134). As an enema, it has little to no effect on rectal toxicity or rectal bleeding (134,136). The topical administration of sucralfate ointment has been shown to reduce acute radiation proctitis (147). Amifostine offers cytoprotection through free radical scavenging and DNA repair mechanisms (148). It has shown to be an effective prophylactic in reducing the incidence of acute rectal toxicity when administered intrarectally (149-151), intravenously (152,153), and subcutaneously (154,155). However, the data on chronic GI toxicity remains limited (134).Other interventions such as bile acid sequestrants, misoprostol suppositories, oral magnesium oxide, and octreotide injections all had limited evidence but have been shown to increase the incidence of acute GI toxicity (134). Orgotein (Superoxide dismutase) (156,157) and famotidine (158) been shown to reduce GI toxicity, but data is limited and its impact on chronic toxicity remains unclear. Antioxidants, including vitamins A, C, and E, have been shown to reduce oxidative stress and aid tissue recovery in chronic radiation proctitis

(159-162). Glutamine has limited and conflicting data on its efficacy in decreasing the severity of diarrhoea (163-165).

Non-pharmaceutical interventions include diet, protein supplementation, probiotics, and counselling. Five types of diets were included in Lawrie et al.'s meta-analysis (134): an elemental diet, a lactose-restricted diet, a high- and low-fibre diet, and a low-fat diet. An elemental diet may worsen GI toxicity but shows little effect on diarrhoea or quality of life (QoL) (166). A lactose-restricted diet appears to make little difference in acute or late GI toxicity or diarrhoea (167). A high-fibre diet may improve long-term GI toxicity and QoL, though its effect on diarrhoea is limited (168-170). Conversely, a low-fibre diet seems to offer little benefit in improving GI toxicity or diarrhoea (167,170,171). Lastly, a low-fat diet has minimal impact on GI toxicity, diarrhoea, or QoL during radiotherapy (168). Protein supplementation, probiotics, and counselling had limited data but may reduce diarrhoea (134).

1.2.4 Literature review on current rectal stabilisers for pelvic radiotherapy

Spacers, including biodegradable balloons, are biomaterial polymers (e.g., polyethylene glycol (PEG), hyaluronan) injected in between the target and anterior rectal wall. Spacers create a space between the target and rectum, moving the rectum away from the CTV and sparing the rectum from radiation doses. Spacers are effective at reducing rectal dosimetry in prostate EBRT (172-180) and cervical brachytherapy (181-185).

However, they become redundant in prostate bed radiotherapy, where they are simply placed inside the area targeted. For this reason, there is only one case report (186) and one retrospective study that has no control group. Both studies explored spacers in the post-prostatectomy setting (187), where they likely did not improve outcomes when compared to similar studies that used no spacer (58,59). The insertion of spacers is also an invasive surgical procedure. This procedure was thought to have similar rates of adverse events as gold marker

implantation (112). However, recent analysis from the MAUDE database identified worse potential side effects from spacers compared to FMs (188,189). The insertion of spacers is done by a trained member of staff who carries out the invasive procedure. The procedure is an obtained skill with its associated learning curve. It is hypothesised that because of this learning curve, SpaceOARs can lead to potential side effects worse than marker implantation (190).

A non-invasive alternative are endorectal balloons (ERBs). Endorectal balloons are inflatable devices that are inserted into the rectum and inflated with either water or air. They work by expanding and stabilising the rectum to reduce variations in rectal filling. Although they are well tolerated, there is no conclusive evidence on whether they reduce inter-fraction motion enough to reduce PTV margins during prostate radiotherapy (191-200). (192,198-200) One limitation of ERBs is a reduced efficacy in intra-fraction motion because of the build-up of gas proximal to the device (199,201). This gas build-up can be reduced by adding a gas-release conduit (202). Another limitation is that the device is inserted by a different therapist, meaning there is no positional feedback, which leads to errors in depth of insertion (203), worsening dosimetry (204). To reduce errors in depth of insertion, Jones et al. (204) and El-Bassiouni et al. (198) recommend additional localisation techniques such as gold seed markers or on-line CT to verify ERB positioning and reduce inter-fraction motion. The lack of agreement on ERB's efficacy persists in the post-surgical setting. While some studies point to favourable outcomes by reducing inter-fraction motion and anorectal dosimetry (205-207), some studies could not find a difference in anorectal dosimetry between patients using ERB and no ERB (208-210). Particularly, Ishiyama et al.'s retrospective study of 107 patients is one of the more promising, larger data sets. However, their study had no control group and should be compared to other studies which used no ERB. Comparing Ishiyama's results to Siepe et al.'s (58) and Tendulkar et al.'s (59) studies (cited earlier in subchapter 1.2) suggests that using ERB in Ishiyama's cohort did not improve late grade ≥2 GI toxicity and biochemical recurrence, respectively. The evidence in the post-surgical setting is limited which is another reason why ERBs have not been taken up in clinical practice. One subtype of ERB is an ERB with a NiTi SMA wire. The SMA actuates the ERB to retract the rectum, moving it away by 1 cm from the target volume to

improve rectal sparing. Parsai et al. validated this SMA ERB in a software simulation (211). The simulated DVH shows that this actuated ERB has reduced rectal dosimetry (211). This has potential but needs more validation in humans.

Rectal retractors aim to retract the rectum to pull the posterior rectal wall away from the CTV and thicken the anterior rectal wall to move the epithelial lining away from the CTV. This retraction decreases the likelihood of the OAR being targeted and reduces the rate of late GI toxicity in prostate cancer patients (212-217). A rectal retractor also acts as a stabiliser for the rectum, as it pushes the rectum down, reducing intrafraction motion during prostate radiotherapy (100,218,219). While promising in the radical prostate radiotherapy setting, there is limited evidence in the post-prostatectomy setting. In the post-prostatectomy setting, there is one case study of a single patient investigating the use of a rectal retractor. The use of a rectal retractor reduced rectal wall and anterior rectal wall volumes at high doses and rectal wall mean dose, but more research must be conducted to draw reliable conclusions on the rectal retractor's efficacy in the post-surgical setting (220). A financial burden of rectal retractors is that they are operated by another staff member, who requires training and remuneration. Another limitation is that rectal retractors are limited by pain as this determines the extent of extraction (100,216,221).

ProSpare™ is a novel rigid obturator that may be promising as it is self-insertable, meaning depth of insertion or hiring another staff member is not an issue, while maintaining favourable features of the other devices. ProSpare™ is shaped to retract the rectum away from the CTV, contains holes for gas passage, and steel ball bearings for localisation of the ARW with IGRT. These features have shown it to be effective in reducing intra-fraction motion, PTV margins, and improving anorectal dosimetry (222,223). However, there is inconclusive evidence on ProSpare's ability to reduce inter-fraction motion (222,224) and it has poorer tolerability compared to other rectal devices. ProSpare™ could not be inserted on the first attempt by 37% of men from initial data in the POPS trial. This would mean it needs to be inserted by a staff member anyway. On repeated attempts, ProSpare™ may still not be tolerated by the patient. This reduced tolerability is possibly because of its rigidity and angled nature, contributing to its bulkiness.

Despite being self-insertable, ProSpare™ also has poor reproducibility in the SI axis (225,226).

1.2.5 Conclusions

Variations in rectal filling cause shifts in target position during radiotherapy, leading to geographical misses that may lead to cancer recurrence. Variations in rectal filling may also lead to inclusions of the rectum into high dose regions. Rectal motor complexes make rectal motion unpredictable and patient specific. This further means that, where PTV margins are large to ensure target coverage, the OAR may be included in the high-dose regions.

Online ART aims to personalise PTV margins in real-time to improve coverage and spare OARs but is resource intensive. KIM tracks motion in real-time but exposes the patient to extra radiation. Electromagnetic markers do the same but cannot be used to accurately track rectal motion. Lastly, real-time rectal dose monitoring is in its infancy. Currently, a low-cost, accessible, and time-efficient method of real-time monitoring of the rectum does not currently exist because of the complexity of the physiology of the rectum.

Pharmaceutical interventions either show no effect or worsen GI toxicity or have limited evidence to support they do. Non-pharmaceutical interventions, in the form of a high-fibre diet may be beneficial, but rectal displacement devices or stabilisers, which aim to reduce rectal inter- and intra-fraction motion during pelvic radiotherapy, show promise. More research is required on these devices in post-prostatectomy and gynaecological patients.

1.2.6 Aims

With this review, the author created the criteria for the development of the device to be used in prostate radiotherapy, with justifications given below. The device should:

- Criterion 1: Be well tolerated (>80% of population)
- Criterion 2: Provide rigidity to resist compressive peristaltic forces

- Criterion 3: Retract the rectum away from target volume
- Criterion 4: Allow the passage of gas
- Criterion 5: Enable patient self-insertion
- Criterion 6: Have image-guidance capabilities.

Firstly, the device must be well tolerated (C1) as there is no justification for clinical translation of a device that is painful or difficult to use. To obtain a similar efficacy as ProSpare™, the rectal device should act as a rigid plug that accommodates and expands the rectum to reduce it moving (C2). Any rectal motor complexes that do occur would simply contract against a non-compliant device. By acting as a spacer and retracting the rectum, the device would reduce anterior translation of the rectum (C3), decreasing the likelihood of the rectum moving into the target volume **and** reducing variations in rectal filling. The latter would consequently reduce PTV margins, further reducing the chance the rectum moves into the target volume. The device should allow the passage of gas (C4) so this does not cause further intra-fraction variations from gas accumulation. The device needs to be self-insertable by the patient (C5) to provide positional feedback and reduce staff costs. Finally, if it can be used as an IGRT tool (C6), this would further enhance localisation abilities, especially in prostate bed radiotherapy. Should the device satisfy these criteria it may improve outcomes in prostate radiotherapy by reducing variations in rectal motion and reduce PTV margins.

Table 1.1 Summary of studies exploring rectal stabilisers in radical prostate radiotherapy.

Author year	Rectal device used	Description of study	Benefits	Limitations	Reference
Wilder et al., 2010	Spacer – Hyaluronan gel (Hylaform)	Phase I trial (n = 10) compared to historical controls.	Spacers are made of biodegradable polymers that are resorbed by the body making them safe. Spacers increase the distance between the prostate and rectum. This increased space leads to reduced mean rectal doses with reduced rectal toxicity rates. In the respective randomised controlled trials, this benefit was clearly demonstrated against a control group.	Insertion of spacers and biodegradable balloons is an invasive procedure with associated morbidity.	(172)
Wilder et al., 2011		Prospective phase I trial (n = 35 with hyaluronan gel; 5 controls no gel)			(173)
Yeh et al., 2016	Spacer – polyethylene glycol (PEG) hydrogel	Single arm retrospective study for patients receiving combined brachytherapy and IMRT (n = 326)			(174)
Strom et al., 2014		Retrospective cohort study of patients receiving combined brachytherapy and IMRT (n = 200; 100 used PEG hydrogel)			(175)
Uhl et al., 2014		Prospective single-arm phase II trial (n = 52) with PEG spacer undergoing IMRT			(176)
Mariados et al., 2015		Randomised controlled trial (n = 222) comparing spacer vs no spacer in patients undergoing IMRT.			(177)
Hamstra et al., 2017		Same study as Mariados et al., 2015 but reporting results at 3 year follow up.			(178)
Melchert et al., 2013	Inflatable biodegradable balloon spacer	Virtual dose planning in 26 patients undergoing 3D CRT or IMRT.			(179)
Pinkawa et al., 2013	Hydrogel spacer (SpaceOAR™)	Phase II trial (n = 15 with spacer; n = 30 no spacer) investigating inter-fractional			(227)

		prostate motion between start of treatment and end of treatment (10-12 weeks)		Opposing evidence on whether spacers reduce inter-fractional motion.	
Picardi et al., 2016		Phase II trial (n = 10 with spacer vs n = 10 no spacer) investigating inter-fractional prostate motion using fiducial markers and bony anatomy.			(228)
Juneja et al., 2015		Investigating spacers' effect on intra-fraction motion during each fraction using Calypso EM transponders. Spacers vs no spacer.			(109)
Hendrick et al., 2017	Spacer vs ERB	Comparing spacers and ERB's effect on intra-fraction motion using orthogonal x-rays before and after each fraction		Opposing evidence on whether spacers reduce intra-fractional motion	(229)
Su et al., 2021	Spacer vs ERB	Comparing spacers and ERB's effect on intra-fraction motion using orthogonal x-rays before and after each fraction			(230)
Ciernik et al., 2002	Endorectal balloon (ERB)	Study on nine patients and how ERB affects online corrections in EBRT.	Easy to operate and inflate with either water or air. Inflatable nature makes them well tolerated. Expands rectum and acts as a non-invasive rectal spacer and rectal stabiliser.	Limited evidence agreeing on their efficacy in reducing inter-fraction motion. Current evidence suggests reduced efficacy in reducing intra-fraction motion.	(191)
Smeenk et al., 2012		Controlled trial comparing real-time motion during each treatment fraction with daily air-filled ERB vs control (n = 15 with ERB; n = 15 no ERB)			(192)
Hille et al., 2005		Prospective study generating rectal dose-volume histograms in patients			(193)

		with no ERB and then with air-filled ERB or water-filled ERB.	By acting as a spacer, ERBs can reduce anal and rectal radiation exposure. ERBs may also reduce variations in rectal filling to reduce PTV margins and subsequently reduce radiation exposure to the rectum.	Inserted by staff member leading to errors in depth of insertion. Also a financial burden in hiring additional staff members. Additional localisation techniques required to confirm position and reduce inter-fraction motion.	
Wachter et al., 2002		Prospective study looking at prostate displacements and rectal DVHs in 10 patients			(194)
Smeenk et al., 2009		Prospective study (n = 24) investigating the effect of ERB on prostate PTV and anal wall dose volumes.			(196)
Hung et al., 2011		Comparative study (n = 29) comparing daily prostate motion using fiducial markers with ERB (n = 14) and without ERB (n = 15)			(200)
El-Bassiouni et al., 2006		Comparative study comparing the setup error with ERB vs no ERB.			(198)
Van Lin et al., 2005		A comparative study on how ERB affects off-line corrections in EBRT (n = 22 with ERB and n = 30 without ERB)			(199)
Wang et al., 2014		Exploratory study quantifying rectal stool and gas volumes and real-time prostate motion in 30 patients with daily ERB.			(201)
Wootton et al., 2012	ERB with a gas-release valve	Retrospective study comparing the amount of gas visible on lateral kilovoltage images in patients with a standard ERB (n = 15) to patients with an ERB with a gas-release valve (n = 15)	Gas-release ERB shows promise by reducing the build-up of gas proximal to the ERB	Further evidence is required to draw conclusions on whether this design improves outcomes	(202)

Parsai et al., 2019	SMA actuator	Software simulation study looking at DVHs in a NiTi SMA wire controlled ERB that actuates to retract the rectum	The SMA actuator retracts the rectum away from the target volume to improve rectal sparing. Simulated DVH showed reduced rectal exposure to radiation.	Has potential but requires further validation in patients	(211)
Arefpour et al., 2021	Rectal retractor	Randomised trial comparing anorectal dosimetry and late GI toxicity between patients with a rectal retractor (n = 18) and no rectal retractor (n = 18)	Across most studies, rectal retractor significantly reduced anorectal dosimetry in treatment plans or as measured. Rectal retractor subsequently reduced GI toxicity rates at 12 months.	Inserted and operated by staff member so is a financial burden. Insertion is not necessarily consistent as no positional feedback. Use of rectal retractor can lead to rectal discomfort and pain. Extent of retraction is determined by pain. Small sample sizes in existing studies making it difficult to draw definitive conclusions.	(213)
Mahdavi et al., 2019		Comparative study in 21 patients undergoing 3D CRT. Treatment plans with and without rectal retractor were generated and compared. For 6 patients, a dosimeter was inserted into the rectal retractor for in vivo dose verifications.	Reduce dose and toxicity rates		(214)
Nilsson et al., 2014		Comparative study (n = 10) creating treatment plans with and without rectal retractor in each patient using VMAT.	Reduced rectal dose exposure		(215)
Ghaffari et al., 2021		Comparative study (n = 12) undergoing IMRT and treatment plans generated with and without rectal retractor in each patient.	Reduce dose to rectal wall without compromising PTV.		(216)

De Leon et al., 2019		Investigated intrafraction motion using cine MRI and dosimetry in 10 patients with and without a rectal retractor	Reduced intrafraction motion, especially drift motion that accumulates over time. Also reduced rectal dose exposure.	Conflicting evidence on whether rectal retractors reduce intra-fraction motion. More evidence is required to draw reliable conclusions.	(218)
Nicolae et al., 2015		Comparative study (n = 20) investigating effect of rectal retractor on dosimetry and intrafraction motion during VMAT. Treatment plans generated for each patient with and without rectal retractor.	No statistical difference found in rectal dosimetry between the two groups in the treatment plans		(219)
Vanhanen et al., 2016		Investigated the impact of rectal retractor on intra-fractional motion using real-time EM trackers in 22 patients	Rectal retractor increased intra-fractional motion.		(221)
Murray et al., 2015	ProSpare	Randomised trial (n = 19) investigating the effect of ProSpare on interfraction and intrafraction motion errors by using Calypso transponders.	ProSpare reduced intrafraction prostate displacement, without changing interfraction errors.	Small sample sizes and only a few studies have been carried out on this novel device. ProSpare seems promising in prostate radiotherapy, but more research should be carried out before translation to the clinic.	(222)
Murray et al., 2014		Randomised trial (n = 21) with patients receiving prostate radiotherapy with ProSpare in the first half or second half of their treatment. Rectal dose-volume histograms created comparing ProSpare to no ProSpare.	ProSpare reduced the dose to the anal canal and rectum.		(223)
Murray et al., 2015		Randomised trial (n = 19) investigating the effect of ProSpare on interfraction prostate and seminal vesicle motion.	ProSpare reduced prostate and seminal vesicle interfraction motion. This		(224)

			would enable a reduction in PTV margins.		
Alexander et al., 2013		Re-assessment of ProSpare's superior-inferior reproducibility after design modifications were made. SI displacements were measured with fiducial markers in 11 men.	SI reproducibility was higher compared to the previous design and device was tolerable in 100% of patients.		(225)

Table 1.2 Summary of studies exploring rectal stabilisers in post-prostatectomy radiotherapy.

Author year	Name of rectal device	Description of study	Benefits	Limitations	Reference
Pinkawa et al., 2014	Hydrogel spacer (SpaceOAR™)	Case report (n = 1)	Spacers may be successfully applied in the post-surgical setting. Spacers have shown to reduce rectal doses in these studies.	The spacer would be inserted into the space that is targeted by radiotherapy, making it redundant. Limited studies with evidence in the post-surgical setting suggests a potential publication bias.	(186)
Lehrich et al., 2018	Polyethylene glycol (PEG) spacer	Five-year retrospective study with no control group (n = 21)			(187)
Joo et al., 2016	ERB	Prospective study analysing prostate bed motion using CT images in 46 patients with ERB	Interfraction motion reduced so PTV margins could be reduced to <5 mm to include 95% of interfraction variations with ERB	Studies with small sample sizes. Different studies show different evidence on whether ERBs reduce interfraction motion and thereby can reduce PTV margins. Also, conflicting evidence on whether ERBs reduce anorectal dosimetry. The lack of convincing consistent evidence has meant ERBs have not been	(205)
De Leon et al., 2015		Compared CTV and rectal stability using CBCT between patients with ERB (n = 7) and without ERB (n = 7)	ERBs increased CTV and rectal stability (i.e., reduced inter-fraction motion)		(206)
Smeenk et al., 2011		Compared anal wall and rectal wall doses in 20 patients, each of which underwent a scan with and without ERB.	ERB significantly reduced anal wall doses and rectal wall doses to a lesser extent.		(207)
Ishiyama et al., 2013		Retrospective study with no control group looking at outcomes after	Comparing to control studies there is no improvement in		(208)

		postprostatectomy radiotherapy with ERB (n = 107)	GI toxicity or biochemical recurrence, respectively.	taken up in clinical practice in the postsurgical setting.	
Streller et al., 2017		Evaluation of ERB on postprostatectomy VMAT in 10 patients	ERB did not lead to reduced anorectal dose during postsurgical VMAT		(209)
Jameson et al., 2013		Comparative study between ERB (n = 10, prospectively) and no ERB (n = 10, retrospectively) during IMRT and IGRT	ERB reduced inter-fractional motion but failed to show improvements in dosimetry		(210)
Ghaffari et al., 2019	Rectal retractor	Case report on a rectal retractor used during salvage prostate bed radiotherapy	Rectal retractor reduced rectal wall doses	More research must be conducted to draw reliable conclusions	(220)
Unpublished data (POPS trial)	ProSpare	Randomised controlled phase II trial	N/A	From initial 17 patients, 7 could not insert the device	N/A

Chapter 2 ProSpare™ tolerability is independent of rectal anatomy

2.1 Introduction

At the time of this preliminary study, ProSpare™ was undergoing a trial in post-prostatectomy radiotherapy (POPS trial NCT02978014) where initial data showed that 7/19 (37%) patients cannot tolerate the insertion of ProSpare™. This is despite multiple design modifications because of poor tolerance in prior populations (225). Patients who can tolerate the insertion of ProSpare™ can walk to the radiotherapy couch with the device inside and maintain it for the duration of the radiotherapy fraction, with no difficulty or discomfort. Before investigating why ProSpare may have such a high rate of patients unable to insert the device, an overview on rectal examination devices is provided. This is followed by a summary of anorectal anatomy to provide background information on the aims of this study.

2.1.1 Existing rectal examination devices

Firstly, a digital rectal examination (DRE)—the insertion of a lubricated gloved finger into the rectum to examine the prostate and rectum—is a simple, well-tolerated procedure. The average adult index finger size is approximately 20 mm (231). Romera et al. found that, while 61% of patients in their study (n = 100) complained of pain in a simple DRE, all of them were able to complete the procedure (232). A DRE, however, is a 5-10 second procedure, while a radiotherapy session lasts around 10 minutes.

Secondly, anorectal manometry is a procedure that measures pressures inside the anorectum with a probe in incontinence assessments. The probe measures a length of 6.4 cm and diameter of 10.75 mm (233). The patient information leaflet from the American Neurogastroenterology and Motility Society states the procedure “is unlikely to cause any pain” (234). Ho and Tan found all their patients (n = 18) were able to tolerate ambulatory anorectal manometry before and after their haemorrhoidectomies (235). In Gibbons and Read’s study of six patients with anorectal fissures, all patients tolerated the procedure well (236). The author

was unable to find any publications suggesting poor tolerance to anorectal manometry. Anorectal manometry takes approximately 30 minutes, so this may be more relevant to compare to a rectal device used in radiotherapy. However, the diameter of the probe is significantly smaller, at 10.75 mm, compared to ProSpare's 23 mm.

Lastly, the proctoscope or rigid sigmoidoscope is also well tolerated. While it has no absolute contraindications, severe pain and anal or rectal stenosis are considered relative contraindications (237,238). Pain is manageable with local anaesthesia or pain relief while stenosis may lead to failed insertion. In Makowiec et al.'s study on perianal abscesses in Crohn's disease, proctoscopy was still performed unless anal or rectal stenosis was present (239). That stands to reason, as these devices are made with toughened polystyrene, making it stiff, and have a diameter of 21-23 mm (240,241). Inserting such a device into a narrowed anal canal would prove difficult or impossible. Barring any presence of anal or rectal stenosis, no studies were found of patients unable to insert the device.

To the best of the author's knowledge, there is no existing evidence demonstrating a significant portion of people unable to tolerate other rectal examination devices.

2.1.2 Anorectal anatomy

The anorectum consists of the rectum and anal canal. The rectum is distal to the anorectal junction. The anorectal junction connects the rectum to the anal canal. The anorectal angle is the angle between the anal canal and the rectum. That is, the angle at the anorectal junction. Throughout this thesis, the terms "anorectal angle" and "anorectal junction" may be used interchangeably. The anal canal is defined as the space from the anorectal junction to the anal verge. The anal verge is the border between the internal anal canal and outer perianal skin. Together, the anal verge and perianal skin constitute the anus (242,243). The anorectal anatomy is visualised in Figure 2.1.

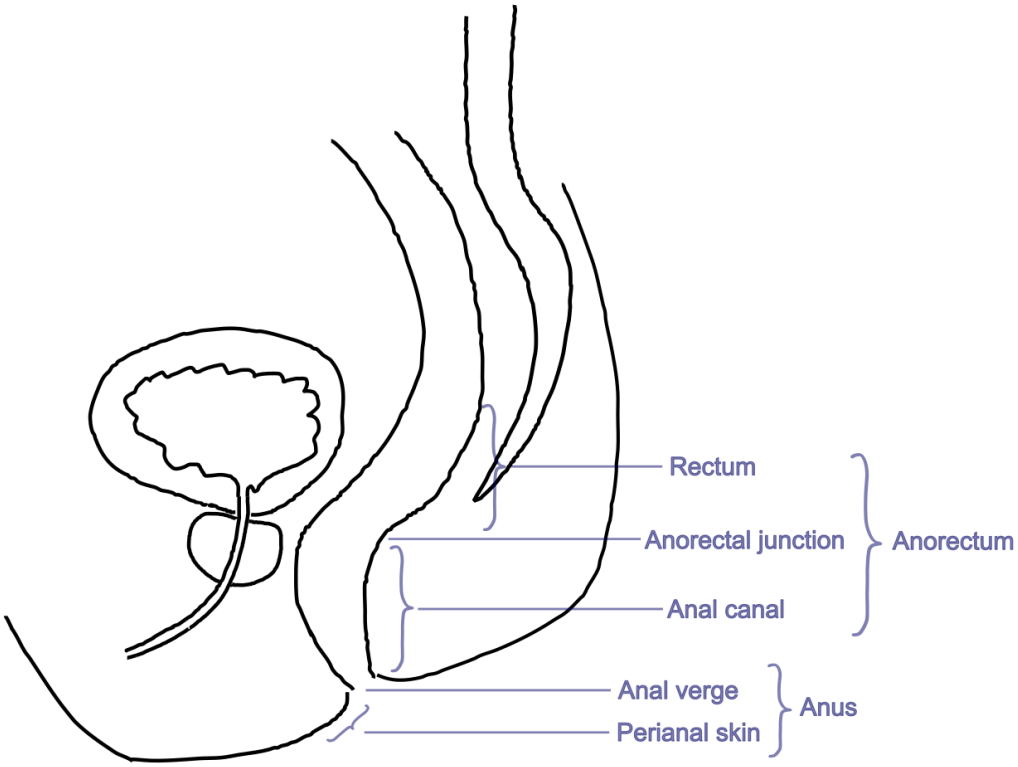

Figure 2.1 Labelled schematic of the anorectum. Drawing by Aryan Niknam Maleki.

Rectal retractors and proctoscopes have similar diameters to ProSpare™ at 20 mm (215), 21-23 mm (240), and 23 mm (244), respectively. Since other rectal devices for rectal examinations, such as the proctoscope, or for prostate radiotherapy, such as the rectal retractor, do not have as a high a rate of intolerance as ProSpare, it was hypothesised that ProSpare's tolerability is dependent on its shape matching the patient's rectal anatomy; ProSpare™ is a rigid device with a fixed shape, while rectal anatomy can vary significantly between patients.

Firstly, the angle at the anorectal junction, the anorectal angle, can vary significantly in healthy individuals. Piloni et al. (244) reported 95% of healthy volunteers (n=69) had an anorectal angle in the range of 84° to 125° and the American Society of Colon and Rectal Surgeons states the normal range is 90-110° (245). Secondly, the surgical anal canal—the length from the anorectal junction to the anal verge—can vary from 3-5 cm (246). Lastly, rectal diameter

can vary from 2.67 cm to 4.72 cm (247). Hence, it was hypothesised, some patients may not be able to insert ProSpare™ because either: the length of the anal canal does not allow sufficient insertion for ProSpare's to follow the anorectal angle; the angle of the rectum is not matched to ProSpare™, causing pain; or the rectum is too narrow, impacting insertion. While it is uncertain that anorectal angle is a significant problem in ProSpare, as the anorectal angle is a flexible structure held by the puborectalis muscle and the anorectal angle has such a large range, it is worth investigating for a rigid, angled device such as ProSpare.

2.1.3 Aims

The first aim was to ascertain differences in the rectal anatomy between patients who tolerated the insertion of ProSpare™ and those who could not tolerate the insertion. The second aim was to find a threshold for at least one of: anorectal angle, anal canal length, or rectum diameter, at which patients were able to insert ProSpare™. If the data support the hypotheses, this will form the case of this thesis that it is best to create personalised iterations of ProSpare™ based on rectal anatomy. This chapter is based on (1).

2.2 Methods

CT planning scans of patients in the POPS trial (NCT02978014) who could tolerate the insertion of ProSpare™ (Group Y), could not tolerate the insertion of ProSpare™ (Group N), and had ProSpare™ inside (Group PS) the rectum on planning scan were analysed using 3D Slicer. Group PS was also analysed to investigate how ProSpare™ affects the shape of the rectum. Measurements were taken in the sagittal plane at the level of the pubic symphysis. The anorectal angle, length of the surgical anal canal, and rectal diameter at the location of the anorectal angle were measured. Anal canal widths could not be measured because the anal sphincters could not be distinguished from the anal canals in the planning scans. Anorectal angle was defined as the angle between the longitudinal axis of the anal canal and a line parallel to the posterior rectal wall (Figure 2.2a). This is how anorectal angle is defined in defecography studies (248,249). Since the anorectal ring, the superior border of the surgical anal canal (246), could not be identified, a line was drawn from the most posterior point of

the pubic symphysis to the most posterior point on the anorectal junction to define the superior border of the anal canal on the CT planning scans (Figure 2.2b). The anal canal length was defined as the distance between this line and the anal verge along the longitudinal axis of the anal canal. Rectal diameter was measured in the anterior-posterior direction at the anorectal junction (Figure 2.2a). Length measurements were rounded to the nearest mm and angles to the nearest degree. One-way ANOVA tests determined if any means were significantly different between groups. If ANOVA tests yielded $p<0.05$, then unpaired t-tests were carried out between the groups.

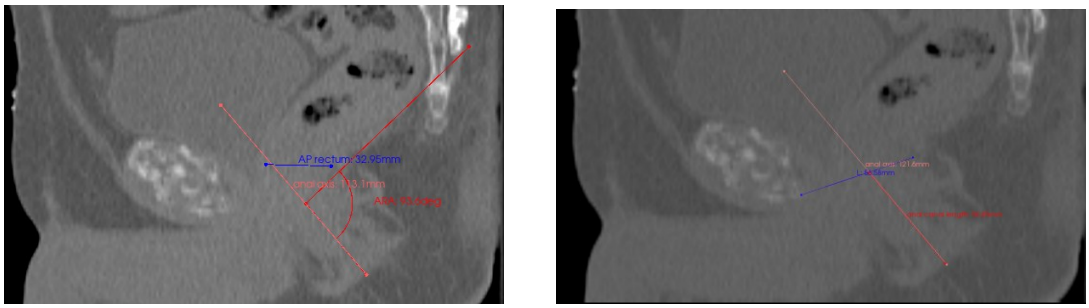

(a) (b)

Figure 2.2 A patient's CT planning scan with annotations analysing the rectum shape and size to assess features between patients who could insert ProSpare™ and those who could not. (a) The anorectal angle (red) and anterior-posterior rectal diameter (blue) at the anorectal angle are measured. (b) Anal canal length (red) is measured. Pink = longitudinal axis of the anal canal.; Purple = upper boundary of the anal canal. Copyright © 2024 Avestia

2.3 Results

Group Y consisted of five patients, Group N had seven patients, and Group PS had seven patients. Table 2.1 shows the means and standard deviations of anorectal angle, rectal diameter, and anal canal length for each group, as measured on CT planning scans. One-way ANOVA tests found that no means between Groups Y and N were significantly different ($p>0.05$). The anorectal angle and rectal diameter were significantly different between Group Y and Group PS ($p<0.01$, and $p<0.001$, respectively), and between Group N and Group PS ($p<0.05$ and $p<0.001$, respectively). Figure 2.3 shows the distributions of anorectal angle, rectal diameter, and anal canal length. No group had a clear cut-off threshold at which its distribution started uniquely to the other groups.

Table 2.1 Mean (±SD) anorectal angle, anterior-posterior rectal diameter at the anorectal junction, and anal canal lengths in patients who could tolerate ProSpare™ (Group Y), patients who could not tolerate ProSpare™ (Group N), and patients who had ProSpare™ inside (Group PS), as seen on planning CT scan; SD = standard deviation; [abc]Within the same row, values with a common superscript are statistically different ([a]p<0.05; [b]p<0.01; [cd]p<0.001). Copyright © 2024 Avestia

	Group Y	Group N	Group PS
Anorectal angle (°)	91.4 (±11.2)[b]	99.0 (±13.0)[a]	113.6 (±9.1)[a b]
AP rectal diameter at anorectal junction (mm)	27.8 (±4.9)[c]	26.1 (±5.7)[d]	39.3 (±3.1)[c d]
Anal canal length (mm)	43.0 (±13.9)	44.6 (±12.1)	45.4 (±12.6)

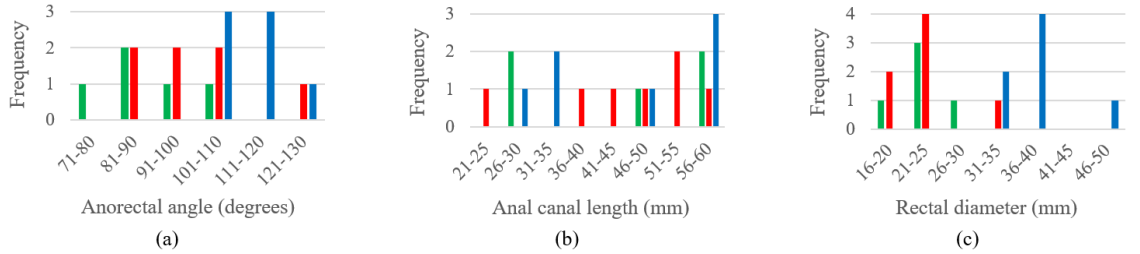

Figure 2.3 Distributions of measurements of patients' rectums who could insert ProSpare™ (Green), could not insert ProSpare™ (Red), and had ProSpare™ inside (Blue). (a) Distribution of anorectal angles (b) Distribution of anal canal lengths. (c) Distributions of rectal diameter in the anterior-posterior direction at the anorectal junction. Copyright © 2024 Avestia

2.4 Discussion

This preliminary study suggests macroscopic rectal anatomy is not the limiting factor in tolerating ProSpare™. The anorectal angle measurements of patients in this study were within the 85-125° range, despite differences in positioning compared to traditional defecography studies: patients were supine for CT imaging, but in the left lateral decubitus position in defecography studies (245,250). Anal canal lengths differ significantly because the anorectal ring could not be identified on CT scans. However, the systematic approach to approximating the upper boundary of the anal canal allowed for comparison between the groups. Lastly, the measured rectal diameters were below the normal range in Kuhlmann et al.'s study (247), because measurements were taken at the anorectal junction, whereas Kuhlmann et al. measured the widest part of the rectum. The anorectal junction is a narrower region transitioning to the anal canal and this was the region of interest. No macroscopic rectal anatomical features were identified that would impact the ability to insert ProSpare™. However, once inserted, ProSpare™ was observed to increase the anorectal

angle and rectal diameters, indicating its effectiveness as a spacer and rectal stabiliser in prostate radiotherapy, as the rectum conforms to ProSpare's shape and size.

Since the results were obtained using a small sample size in a modality that was readily available from an ongoing trial, a more comprehensive study investigating other parts of the anorectal anatomy—rectal wall thickness and stiffness, nociceptive sensitivity, and variations in shape, size, and stiffness, in surrounding tissue like the mesorectum and fascia—should be done to definitively exclude rectal anatomy as the limiting factor in ProSpare™ tolerance. However, this requires more time and imaging modalities. Nevertheless, it is reasonable to infer the problem is at the entry, since endorectal balloons are inflatable and have excellent tolerance, and linear devices like rectal retractors and proctoscopes have good tolerances; ProSpare's angle may make the device too bulky on insertion. The anal sphincter diameter or tone, or nociceptive sensitivity of the submucosa may be the limiting factor in tolerating ProSpare™. Anal sphincter tone decreases with age, as sphincter thickness increases (251). The age data of these patients were not available as all data were anonymised before image analysis. Burnett and Bartram (251) studied anal canal distension with an imaging probe and found that the anal canal maintains a diameter of approximately 5 mm with balloon inflation up to 40 mL of saline solution. Only at 50 mL did the anal canal distend to around 7 mm, demonstrating the anal canal's resistance to expansion. This resistance may explain why ERBs are easier to insert than ProSpare™.

The results of this study are the first to show that the ability to insert ProSpare™ is independent of rectal anatomy. This suggests that creating multiple device iterations or further modifying the device geometry to improve the rate of insertion is not the solution. Instead, the likely limiting factor is anal sphincter tone or size, and ProSpare's ability to bypass the anal sphincter. A deployable or inflatable device would improve tolerance while maintaining ProSpare's favourable features. This determined the direction of the thesis: by using soft robotics, the author was able to develop such a device.

Chapter 3 Background on soft robotics and fluid actuation

This chapter gives a brief overview on the main principles of soft robotics that would allow the device to be inflatable and therefore, easier to insert. The main working principles the development of the device should explore is fluid-driven actuation (for deployment and bending motion) and variable stiffness mechanisms. This review on soft robotic actuators enables the development of a device designed to meet Criteria 1,2,3, and 5. Criteria 1 will be met by nature of soft robotics. Variable stiffness methods must be employed for the device to meet Criterion 2. Appropriate actuation methods need to be chosen to satisfy Criterion 3. Lastly, attention must be paid to variable stiffness mechanisms or actuation methods that would preclude self-insertion of the device by the patient (Criterion 5).

3.1 Actuation methods

A brief description of different actuation methods is provided here. Different actuation methods provide different benefits and limitations that can be used to meet Criterion 3 of the device, retracting the rectum away from the target volume. The most common actuation methods include fluid actuation (pneumatic or hydraulic), cable or pulley driven actuation, shape memory actuators (SMAs), electroactive polymers (EAPs) or dielectric electro-activated polymers (DEAPs). These mechanisms are visualised in Figure 3.1. For a detailed review of these actuation methods, the reader is directed to Dr Runciman's review on soft robotics in minimally invasive surgery (252).

The main working principle behind pressure-driven actuation is that the work done by the pressurised fluid in an inextensible compartment is converted into a tension force and displacement (actuation) in the actuator:

$$-FdL = PdV$$

Pressure-driven actuation is described in more detail later, but the main benefits to using pressure-driven actuators is that they are lightweight, are easy to use

with fast response times, and can produce various types of motion including rotation, twisting, bending. The main limitations are that their response curves suggest these actuators are very sensitive to changes in the upper ends of the volume and pressure range, i.e., the relative change in contraction and change in force is increased exponentially per unit of pressure or unit volume. As Runciman et al. demonstrated, when their actuator was inflated to half its maximum volume, it contracted by approximately 10% of its maximum theoretical contraction ratio, but inflating it to 90% of its maximum volume contracts it to about 50% of its maximum contraction ratio (253). This makes precise control difficult, high pressures are required to exert large forces which may pose a problem when aiming to satisfy Criterion 3, and there is a risk of puncture that would render a device useless.

Cable or pulley driven actuators use flexible cables to transmit a tension force by changing the length of the cable. Their advantages include the ability to transmit large forces with fast response rates. However, they are often controlled by motors which may make it challenging to translate into to patient self-insertion as they would make any actuator increasingly bulky.

Shape memory alloys (SMAs) use temperature changes to change the shape of an alloy for actuation. These provide highly reproducible actuations and are inexpensive to make. However, there may be a safety risk to heat up a SMA for a device that is inserted into a mucosal membrane. Parsai et al. addressed this by incorporating a Nitinol core inside an endorectal balloon (211). In their computational simulation, they showed no temperature change in the rectum or balloon, despite the Nitinol core heating up to 100°C. They carried out a cadaver study showing the retraction of the rectum. Nevertheless, SMAs do not have precision control between their two phases. The SMA can only retract the device to its austenite shape but not in between.

Electroactive polymers (EAPs) or dielectric electro-activated polymers (DEAPs) work by applying a voltage to a dielectric elastomer film which provides actuation through electrostatic forces compressing and stretches the film (254). Again,

there is a safety concern and lack of patient self-insertion as these polymers require high voltages (> 1kV) to operate.

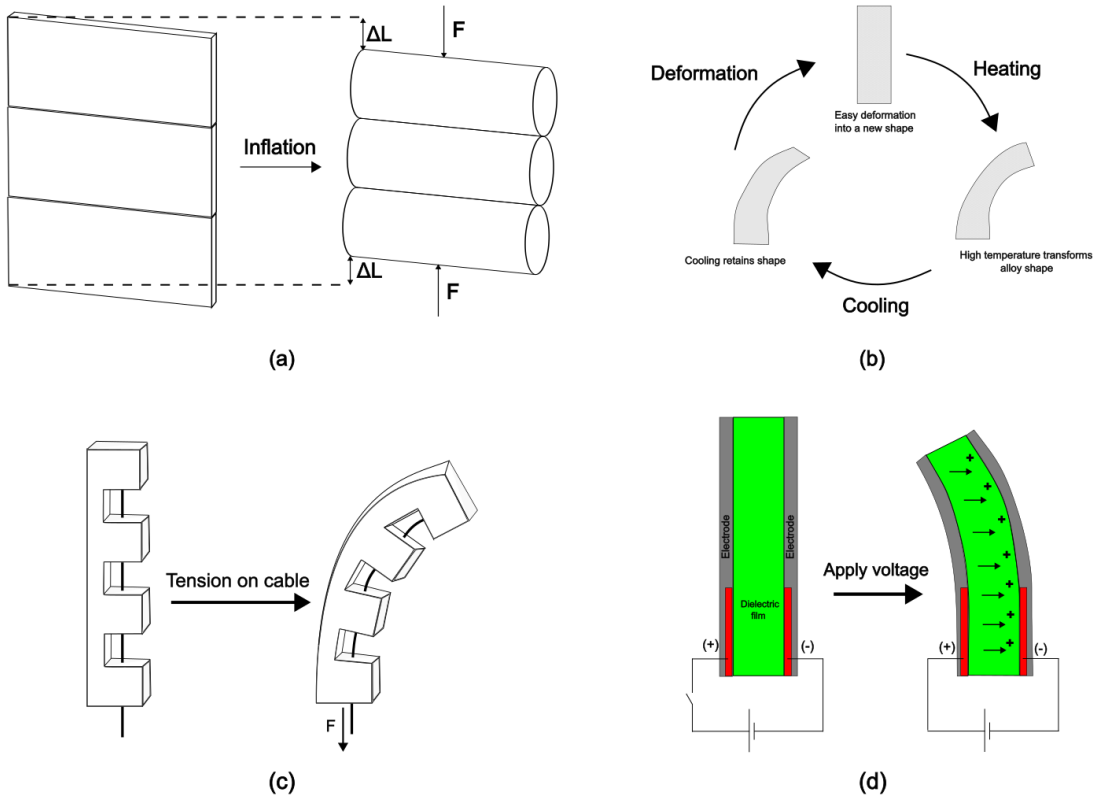

Figure 3.1 The main actuation methods discussed: (a) fluid actuation (b) shape memory alloys (c) cable-driven actuation (d) dielectric activated polymer

3.2 Variable stiffness mechanisms

Variable stiffness mechanisms allow the stiffness of the device to be reversibly changed (i.e., from soft to rigid). Evaluating different mechanisms will guide the development of the device to meet Criteria 1 and 2. Variable stiffness is an important requirement of the device so the device is soft on insertion for high tolerance and can become rigid enough to stabilise the rectum. A detailed review on variable stiffness in medical devices was done by Blanc et al. (255). This section reviews only fluid actuation and jamming, as both variable stiffness mechanisms are pressure-driven and so have potential to be used as a single mode of control which would help to meet Criterion 5 in the development of the device.

Fluid actuation alone can achieve variable stiffness. While fluid-driven actuators can work to move a soft robot, the internal pressure and structure of a membrane can influence the stiffness. Cross-sectional deformations of a beam cause stiffening because of the Poisson effect (256). The structure also affects stiffness. For instance, when multiple pouch motors close enough to each other are inflated, they create a corrugated surface with increased rigidity because of Gaussian curvature (Theorema Egregium) (257). Variable stiffness is impacted by the structure and material of the device being actuated by fluid. Another example is the inflatable CYCLOPS robot (258). The authors directly welded stiffening beams to the hexagonal prism to increase the stiffness by inflating this separate compartment simultaneously with the main hexagonal prism. The overview in 3.3 will go into more detail on how structure affects the performance of fluid-driven actuators.

Jamming provides variable stiffness but does not inherently produce motion, unlike fluid actuation. This means it can be used in conjunction with fluid actuation to bring about motion and variable stiffness. Types of jamming include granular or particle jamming, fibre jamming, and layer jamming (259). Fibre jamming involves a network of intertwined or bundled fibres. Layer jamming involves stacked flexible sheets or layers. Granular or particle jamming consist of small particles or grains. Their variable stiffness mechanisms all work similar in that the network or composition of particles, fibres, or layers, can freely move when unjammed. This makes the device soft. When either a positive or negative pressure is applied, these particles, fibres, or layers jam together, giving stiffness. The main disadvantage to this mechanism is that an extra layer or compartment is required that contains the items that are to be jammed. This increases the size of the device in the soft state which may make it harder to meet Criterion 1. This is especially pronounced with granular/particle jamming as these are bulky particles that take up more volume than layers or fibres. While fibre and layer jamming are lower profile, they cannot deform as much in the unjammed state as granular jamming can. In granular jamming systems, the particles are free to move and act as a fluid when unjammed. In fibre and layer jamming, the overall systems still retain some rigidity because of the inherent rigidity of the contents but also the friction between the fibres or layers.

Fluid-driven actuation methods are discussed in more detail, as they offer the greatest potential to meet Criteria 1 and 5. The use of multiple actuation methods, or those requiring the use of electronics (e.g. SMAs), reduces the feasibility of self-insertion by the patient. Additional actuation methods would necessitate additional methods of varying the stiffness. For instance, while cable-driven actuators could be used, fluid actuation would still be required to satisfy Criterion 2. Using fluid actuation as both the actuation and variable stiffness mechanism enables a single mode of control, increasing the potential for patient self-insertion.

3.3 Literature review on pouch motors and pressure-driven actuators

3.3.1 Introduction

This subchapter provides an overview of existing pressure-driven actuators which may be suitable to incorporate into the device. To better align with Criterion 5, the review primarily focussed on studies where the actuation mechanism was exclusively pressure-driven. In cases where a soft robotic system employed multiple actuation methods, studies were still reviewed if the pressure-driven mechanism could be separated from the other mechanisms.

Pressure-driven actuators can be subdivided into pneumatic (air) or hydraulic (liquid) actuators. Pneumatic actuation will not be appropriate to incorporate in the device design because it affects radiation dose due to scatter caused by the air. While pneumatic actuation does not qualify for the device, studies investigating this actuation method were still included in this overview. These studies are included because their design may still be incorporated into a device with hydraulic actuation. Additionally, some initial prototyping in this thesis involved pneumatic actuation as this was faster.

The aim of this overview is to review geometric design specifications of pressure-driven actuators that determine the shape, behaviour, and performance of these actuators. The primary performance metrics of these actuators that are of interest are contraction ratio and load-bearing capacity. These metrics are important for the device to hold the shape of the rectum and resist compressive stresses from

peristatic motion. Secondary performance metrics include speed of contraction, control or precision, and actuator durability. Speed of contraction is relevant to the practical applications of a device within a 10-minute radiotherapy fraction.

Control and precision are important for achieving a reproducible or adjustable shape if required. Durability is considered both to ensure performance during a single fraction and to assess feasibility of a reusable device over many fractions. Although these secondary metrics were important, they were not deprioritised in studies where an actuator exhibited poor primary performance metrics.

3.3.2 Pneumatic artificial muscles

Before examining structural designs for pouch motors and inflatable actuators, a review of pneumatic artificial muscles is provided (PAMs). Understanding the working mechanism and evolution of PAMs, particularly how their limitations have been addressed, is important to appreciate how pouch motors and their different structures address these limitations.

PAMs are soft mechanical actuators that can contract and produce force like an artificial muscle. The McKibben PAM consists of an elastomeric bladder within an inextensible braided mesh, which is attached to end-fittings on both ends of the muscle. As the bladder is pressurised, it increases in volume. Due to the inextensible braided mesh, as the bladder increases in volume, it must contract axially. This contraction shortens the PAM and produces a tension force. This tension force with the axial displacement of the PAM translates to the work done by the PAM. By the conservation of energy, the work done by the PAM must equal to the work put into the PAM by inflating it. This work done by inflating the PAM is the product of the pressure of the fluid and the change in volume (260-263). This gives the equation:

$$-FdL = PdV$$

This is one of the fundamental operating principles of soft actuators and will be referred to several times in this thesis. The inflation of the actuator brings about a tensile force output by the actuator that can be used in soft robotic applications

such as wearable robotics or minimally invasive surgery. PAMs are lightweight actuators which are simple and inexpensive to make, as they virtually only consist of a membrane and a mesh. However, the McKibben PAMs have limitations. The first limitation is the friction that arises between the braided mesh and the membrane. This friction causes substantial hysteresis, making it difficult to control and model the behaviour (axial contraction and force output) of these actuators. Secondly, there is a residual amount of volume in the PAMs when deflated, which leads to two consequences: the actuator takes up a large baseline amount of space despite uninflated; and the pressure in the actuator must exceed a threshold value before it can start inflating. Thirdly, rubber fatigue is a common cause of failure of the artificial muscle. Lastly, the contraction ratio is relatively low, between 20 and 30% (260-262,264). Other PAMs have been developed to address some of these limitations, namely embedded PAMs including the Baldwin type, the pleated PAMs, netted PAMs, and high contraction ratio PAMs (HCRPAMs). These PAMs are summarised in Table 1.1.

3.3.3 Pleated PAMs

Pleated PAMs aim to increase the contraction ratio of PAMs by incorporating folds, or pleats, along the central axis of the membrane. Pressurised air causes inflation by unfolding these pleats which leads to greater contraction ratios. In theory, a reasonably thin pleated PAM had a maximum contraction ratio of 45.5%. In experimental results, Daerden et al. achieved a maximum contraction ratio of 41.5% at pressures above 50 kPa (264). Verrelst et al. incorporated these pleated PAMs in a bipedal robot (265) before presenting their second-generation pleated PAM with greater longevity (266). They changed the stiffness of the fabric that made up the folded membrane structure. This meant the pleated membrane would unfold more evenly, reducing the extra parallel stresses on the fabric and its airtight coating (266). Villegas et al. published their third-generation pleated PAM (267) presenting a simpler manufacturing process and a 75% reduced production time. Terryn et al. developed a pleated PAM with a self-healing polymer to further improve the longevity of the actuator. Their pleated PAM achieved a contraction force of 20 N at only 10 kPa (268). While these more recent versions of pleated PAMs were improvements from the original pleated

PAM, the fundamental working principle remained the same. The main advantages of the pleated PAMs are that the unfolding of the pleats allow for a greater contraction ratio at a lower pressure, and that there is no external mesh like in the McKibben PAM which would cause friction. However, they still have a residual volume when deflated and their inflation causes significant lateral expansion. The large sizes would be impractical when multiple PAMs are used in parallel in applications such as wearable robotics.

3.3.4 Embedded PAMs

An embedded PAM is a rubber bladder which is reinforced with embedded fibres. The Baldwin type muscle consists of a rubber tube reinforced by straight inextensible fibres in the axial direction (269). This reinforcement has been made of Kevlar (270,271), glass (272), or carbon fibre (273). This fibre-reinforcement restrains the rubber tube significantly more in the axial direction than the McKibben PAM. This leads to increased contraction force and contraction ratio. The PAMs reinforced by glass fibres by Nakamura and Shinohara were able to contract approximately 28% with no load, 26% with a 20 N load, and 23% with a 40 N load (272). Since the reinforced fibres are embedded in the silicone, rather than on the outside of the membrane, this leads to less friction and greater longevity of the PAM (272). However, they still have a residual volume when deflated and a large cylindrical form when actuated, like the other types of PAMs. Wirekoh et al. try to address this by creating a flat PAM that is flat when deflated (274). The flat PAM is made by moulding a silicone layer on top of another mould with a water-soluble mask (e.g., mould release spray) in between. This mask prevents the top mould from adhering to the bottom mould, creating a “zero-volume air chamber” (ZAC) (274,275). This mould with the ZAC is then embedded with Kevlar fibres. The single-cell-unit PAMs achieved a contraction ratio of 20.5% and the multi-cell unit 22.5%. This is a lower contraction ratio but it solves the problem of a large empty PAM (274).

Table 3.1 Summary of common pneumatic artificial muscle designs.

Author year	Type of pouch motor	Description of design	Benefits	Limitations	Reference
Chou and Hannaford, 1996	McKibben PAM	Inextensible braided mesh constraining an elastomeric bladder or membrane.	Lightweight; high power:weight ratio; simple and inexpensive manufacturing.	Friction causes hysteresis; large initial volume when deflated; threshold pressure required to start inflating; relatively low contraction ratio (20-30%).	(260)
Tondu and Lopez, 2000					(261)
Daerden et al., 2001	Pleated PAM	Folds (pleats) along the central axis of the PAM. Pressurised air causes inflation by unfolding of these pleats.	No friction as there is no external layer or shell; higher contraction ratios (41.5%).	Requires large initial volume when deflated; Inflation causes significant lateral expansion for actuation, i.e., not compact enough.	(264)
Verrelst et al., 2006					(266)
Verrelst et al., 2005					(265)
Villegas et al., 2012					(267)
Terryn et al., 2018					(268)
Park and Wood, 2013	Embedded PAM	Rubber membrane embedded with inextensible but flexible fibre.	Less friction and greater longevity; slightly greater contraction ratios with load; relatively easy and inexpensive to fabricate.	Large initial volume when deflated; inflation causes significant lateral expansion on actuation.	(270)
Saga et al., 2003					(271)
Nakamura and Shinohara, 2007					(272)
Tomori and Nakamura, 2011					(273)
Wirekoh et al., 2017	Flat PAM with embedded fibres	Zero-volume layer silicone PAM with embedded Kevlar fibres.	Flat and compact when deflated.	Manufacturing consists of finicky/awkward and delicate manual work to achieve the zero-volume layer and to embed the fibres.	(274)

3.3.5 Pouch motors/Peano Muscle

The pouch motor is a flat fluidic muscle with a zero-volume chamber when deflated. Their working principle is like the conventional PAM: instead of an inextensible outer shell that turns radial expansion into axial contraction, the force transfer from a pressurised fluid is provided by the inextensible film or fabric they are made of. Because of their material properties and method of fabrication, the pouch motor addresses the limitations of conventional PAMs since they have no volume when deflated, are compact even when inflated, do not cause friction with an external shell as they are made of one material, have a much lower threshold pressure to start inflating, and are simple and inexpensive to manufacture through printable robotics (276,277). These pouch motors were first presented by Niiyama et al. (276,278) to enhance the speed of fabrication of printable robotics. These fluidic actuators have been referred to in other works as a Peano muscle (277,279,280) and a flat PAM (275,281). These all refer to the same type of actuator but in this thesis will from hereon be referred to as pouch motor or pouch. The pouch motors have been modelled, validated, and used to fabricate a soft gripper, robotic arm, quadruped robot, wearable robotics such as an orthosis or gait rehabilitation, and in sensing (275-280).

Niiyama et al.'s pouch motors were made of 0.102 mm thick PVC sheets, manually fabricated by a line heat sealer. The width, D, of the pouch motors was 85 and 75 mm with an initial length, L_0, of 25 mm. Both pneumatic pouch motors worked as intended, with the linear pouch motors achieving a maximum contraction ratio of 30% at 20 kPa and 28% at 40 kPa, respectively. The rotational pouch motors measured a maximum angle of between 90° at 10 kPa and 80° at 20 kPa, respectively (276,278). While force output was measured, load-bearing capacity was not. Force output in pouch motors is strongest at the beginning of inflation. This is not applicable to the device, which needs to stay inflated and resist compressive forces in the deployed state. This research group showed the flexibility in the design of the pouch motor by creating flat PAMs with different lengths, widths, and "pennate angle" of the PAM (282). The pennate angle of a biological muscle can be mimicked by printing pouches in series at an angle rather than parallel to the direction of force. In (282), the authors found that a

longer pouch (i.e., fewer pouches in series for a given length), did not significantly change the contraction ratio while a wider pouch did increase the contraction ratio significantly. A 50 mm wider pouch achieved a contraction ratio of 27% while a 20 mm pouch motor achieved a contraction ratio of 20% (282). Veale et al., using various materials and composites, consistently achieved a contraction ratio of 17% at a low pressure of 30 kPa and at higher pressures of 200 and 500 kPa (277,280). Kim et al.'s pouch motor (referred to as a flat PAM in their work) was made of 50 μm silicone and urethane impregnated nylon fabrics (281). These were bonded with silicone adhesive and achieved a contraction ratio of 24% at 172 kPa.

While the pouch motors have a flexible design and a flat deflated form with zero volume, they have a key limitation: a low theoretical contraction ratio of 36.3% which is not achievable experimentally because lateral expansion is restricted at the edges of the pouch motors (283). The edges of these rectangular-shaped pouch motors crinkle and buckle with inflation, preventing full contraction of an actuator (253), so the contraction ratio falls between a range of 17 and 28%. This is why a wider pouch motor exhibits greater contraction ratios, as there is less unintended deformation of the edges relative to the width of the pouch. The easiest method of improving contraction ratio and force output is therefore by increasing the width of the actuator or by placing multiple actuators in parallel. However, if there are constraints in width or thickness, this is not possible. Because of these constraints, variations of the pouch motor with a unique secondary or tertiary-ordered structure have been designed. The different changes seen in the literature are summarised in Table 3.2.

3.3.6 Electrohydraulic actuators

Electrohydraulic actuators or dielectric elastomer actuator (DEAs) use electrodes to apply an electric field to actuate a pouch (284,285). These are intended to self-sense their deformation with capacitance monitoring. These actuators have rapid response times and improved precision control because the fluid is already inside the pouch motor. The electric field is deployed instantly to displace a dielectric oil to cause contraction of the pouch. This is a significant advantage over hydraulic

or pneumatic actuation which are slower. However, their contraction ratio is lower because part of the pouch is covered by electrodes that apply the electric field to displace the liquid. Only the part not covered by electrodes is what ultimately contracts, reducing the total area of the pouch that can contract. However, there are biocompatibility and translatability issues with using a dielectric oil and high voltages in the kV range in a device that is inserted into the rectum and intended to be controlled by the patient.

Table 3.2 Summary of design modifications made to pouch motors.

Author year	Type of pouch motor	Description of design	Benefits	Limitations	Reference
Niiyama et al., 2014	Pouch motor/Peano muscle/flat PAM	Flat film, fabric, or silicone sealed to create an airtight chamber. Sealing may be done through heat sealing or adhesives.	Zero-volume when deflated; lower pressure threshold to start inflating; compact when inflated.	Low contraction ratio (<30%) due to buckling of the edges.	(276)
Niiyama et al., 2015					(278)
Sanan et al. 2014					(279)
Veale et al., 2015					(280)
Veale et al. 2016					(277)
Kim et al. 2021					(281)
Kellaris et al., 2018	Peano-HASEL muscle (dielectric actuator)	Dielectric diodes displace a dielectric oil on application of an electric field	Rapid response times; self-sensing through capacitive monitoring.	Biocompatibility issues; lower contraction ratio (less than a regular pouch).	(284)
Park et al., 2020	Electro hydraulic actuator				(285)
Jang et al., 2023	Gusset pouch motor	Gussets are side walls added between the seams of the pouch motor.	Gussets increase volume and reduce crinkling from the edges; increased force output; increased contraction ratio	Performs best when longer than wide.	(286)
Li et al., 2022	Origami gusset pouch motor				(283)
Oh et al., 2019	Paired pouch motor, regular pouch	Pair or multiple pairs of pouch motors connected in parallel.	Lateral expansion of pouch causes rotation that increased contraction ratio.	Paired actuators greatly increase the width of the system. Increased width would make a device too bulky.	(287)
Oh et al., 2019	Paired pouch motor, sPAM				(287)
Jang et al., 2023	Paired pouch motor, gusset pouch				(286)

Li et al., 2022	Paired pouch motor, origami gusset pouch				(283)
Chung et al., 2023	Kirigami actuators	Cutting around pouch motors to increase stretchability of pouch.	Highly extensible pouch motors leading to high contraction ratios.	Smaller volume for its stretched length => Reduced force output.	(288)
Runciman et al., 2021	Conical pouch motor	Triangular edges on pouch motor.	Reduced crinkling of edges; higher contraction ratio; constant curvature of inflated pouch.	Triangular edges have lower volume than rectangular edges of the same width => reduced force output.	(253)
Shen et al., 2021	Constrained pouch motor (flat PAM)	Orthogonal weaving of pouch motor with constrained PET layer and Kevlar wire.	Increases the maximum work pressure of the pouch allowing for greater force outputs.	Delicate manual work consisting of weaving the Kevlar wire and the flat PAM together; lower contraction ratios than a regular pouch motor.	(289)
Feng et al., 2023	X-crossing PAMs	Comb-like filaments of pouch motor form an “X” that provides the actuation.	Very high contraction ratio (87-93%). Constant force output throughout contraction.	Increased width with contraction, not compact enough.	(290)
Kwon et al, 2020	Pouch motor with constraints	Internal and external constraints added to pouch to increase contraction ratio.	Increased contraction ratio (46.3%).	Complex construction	(291)
Belforte et al., 2014	Bellows actuator	Corrugated actuator that contracts with negative	High contraction ratios (~90%)	Require negative pressure to actuate; no inherent rigidity.	(292)
Lee and Rodrigue., 2019	Bellows actuator				(293)

Paez et al., 2016	Yoshimura pattern bellows actuator	pressure and expands with positive pressure.	Origami patterns provide more rigidity; improve foldability to improve deploying ratio.	Folding adds another step in construction.	(294)
Wu et al., 2021	Kresling pattern bellows actuator				(295)
Yang et al., 2023	Miura-Ori pattern bellows actuator				(296)
Han et al., 2018	High contraction ratio PAMs (HCRPAMs)	Inner bellows-like actuator with external band that contracts perpendicularly to the expansion of the inner actuator.	High contraction ratios (60-65%); simple and inexpensive manufacturing;	Inflation causes significant lateral expansion for actuation. i.e., not compact enough.	(297)
Yang et al., 2019	High-displacement PAMs				(298)

3.3.7 Gusseted pouch motors including Origami-inspired designs

Gusseted pouch motors use additional side walls, called gussets, which are added to the “seams” between pouch motors in an actuator. These gussets increase the volume of and reduce the crinkling at the edges with inflation. This increased volume and reduced crinkling translates into an increased force output and improved contraction ratio. Jang et al. made a gusseted pouch motor with textiles containing nylon and a heat-sealable thermoplastic polyurethane (TPU) layer (286). The thickness of the material is not disclosed. The authors added an additional triangular corner seal to maximise volume. The gusseted pouches had a length of 7 cm and a width of 6 cm (i.e., it was longer than it was wide). With the triangular corner seal, the gusseted pouches reached a maximum contraction ratio of 42.6% while their pouch motors with no gussets only achieved a contraction ratio of around 16% at 80 kPa. At 40 kPa and at any payload from 1 kg to 13 kg, the gusseted pouch had significantly greater contraction ratio than the regular pouch. At 1 kg, the gusseted pouch had a contraction ratio of 36.3% compared to 16.3%, and at 13 kg it had a contraction ratio of 6.3% compared to 2% in the regular pouch. The blocked force for gusseted pouch was 331 N at a length of 110 mm and 40 kPa, while this was 176 N for the regular pouch. The maximum blocked force for the gusseted pouch was found to be 526.5 N at 210 kPa. The authors do admit that part of the reason the regular pouch motor performed so poorly against the gusseted pouch motor is because the regular pouch motors perform better when they are wider than they are long (286). The gusseted pouches perform well at a smaller aspect ratio (smaller width: length ratio) because there is more edge to add a gusset to, preventing crinkling of the edges.

The bio-inspired origami pouch motors by Li et al. integrate origami structures into the longitudinal edges of a pouch motor (283). These act like a gusset, adding an additional side wall to improve the contraction ratio of the inflatable actuator. These origami pouches were made by heat sealing 25 µm polyurethane films with a length of 70 mm and a width of 70 mm or 140 mm. The authors’ Type III pouches were made by additionally using hotmelt adhesive to seal the lateral edges within the origami structure. These Type III pouches performed best. The

maximum theoretical contraction ratio for these pouches was 42.5%. For a single pouch, at 15 kPa and with a 30g weight, the contraction ratio was around 40%, which is a significant improvement from the original pouch motors. Force output was measured but no pulling load-bearing capacity. Using a pair of gripper actuators, each made of two pouches attached to a rigid scaffold to allow for rotation, they were able to hold up to 466 g with an input pressure of 25 kPa. A circular gripper design attached to a rigid scaffold could hold up to 3000 g with an input pressure of 10 kPa (283).

3.3.8 Paired pouch motors

Pairing pouch motors uses the lateral expansion from each pouch to induce a rotation. This rotation increases the contraction ratio. Oh et al. showed this working in pouch motors and serial pneumatic artificial muscles (sPAMs) (287). Their pouch motors made from heat sealing thermoplastic polyurethane (TPU) were inflated to 90 kPa and achieved a contraction ratio of 41.9% with no load, 26.67% with a 5 kg load, and 19.22% with a 10 kg load. The pouch motors had a width of 7.5 cm and a length of 2.5 cm. By increasing the number of pairs (higher-order pairs) the authors were able to keep increasing the contraction ratio. A second-order pair of pouch motors, which is two pairs of first-order pouch motors joined together at the top and bottom, achieved a contraction ratio of 45.97% at 20 kPa. Oh et al. achieved similar results with their sPAMs. They created an sPAM with PE film with a 3.18 mm diameter and 50 um thickness. A zero-order sPAM consisted of a single actuator of four sPAMs. This zero-order configuration had maximum contraction ratio of 42.09%. A paired sPAM (first-order) had a contraction ratio of 47.3%. A second-order paired sPAM had a contraction ratio of 50.35% and a third-order paired configuration 51.78% (287).

The two studies discussed above by Jang et al. and Li et al. also investigated their pouch motors in a pair (283,286). The paired gusseted pouch motors by Jang et al. reached a contraction ratio of 50.3%, which is higher than the 42.6% contraction ratio of a single pouch. Li et al.'s Type III origami pouch motor was

directly compared to a regular pouch motor of the same materials and dimensions. The regular pouch motor reached a contraction ratio of 39.4% in a pair, which agrees with Oh et al.'s results, while pairing their origami pouch motor reached a contraction ratio of 55.9%. Both methods of adding a gusset to the pouch motor generated more lateral expansion which meant more rotation occurred when the pouches were paired. This increased rotation led to a higher contraction ratio. Naturally, having a pair of pouch motors would also double the load-bearing capacity. This may not be feasible in the rectal device if it makes the device too bulky.

3.3.9 Kirigami inflatable actuators

Kirigami is a variation of Origami where paper is cut as well as folded. Pneumatic Kirigami actuator were presented by Chung et al. (288). These actuators consisted of pouch motors connected in series but with laser cut patterns around the sealed edges. These cuts created highly compliant regions surrounding the pouch motors. This meant the deflated actuators were highly extensible. Their parallel Kirigami actuator could be stretched to a strain of 2.37 under a 100 g payload. At 200 kPa, this actuator then reached a contraction ratio of 78.5% from this stretched length. These are significantly higher contraction ratios than discussed previously. However, this high contraction ratio only exists because the contracted actuator is being compared to the stretched deflated actuator. While this is promising for creating high displacements, it comes at the expense of losing volume. The actuator occupies a small surface area in this stretched length. This smaller surface area, as a result of the cuts, means the actuator is inflated with a lower volume than an actuator that is not cut and takes up a larger surface area. While the contraction ratio may be high, the force output and load-bearing capacity are lower.

3.3.10 Conical pouch motors

The conical pouch motors are a hydraulic pouch motor inspired by Niiyama et al.'s work (276,278) and were developed by Runciman et al. to work with the

inflatable CYCLOPS robot (253,258). The conical pouch motors were designed because the edges of the original rectangular pouch motors would crinkle and buckle the membrane when filled with water. Since this caused an irregular shape in the pouch motors, it prevented contraction of the actuator. The rectangular ends were replaced with a triangular pattern, making the curvature of the pouch more constant along the actuator's width (253). The conical pouch motors were made by laser welding two thermoplastic triple laminate sheets (PE/PET/PE, 30/60/30 μm). These conical pouch motors would have the same theoretical contraction ratio as the rectangular pouch motors (36.3%). When filled hydraulically up to a pressure of 75 kPa, the conical actuators reached a contraction ratio of approximately 25%. Similarly to other studies, load-bearing capacity was not measured but force output was. While these conical pouch motors solve the issue of crinkling seen in rectangular pouch motors, the removal of material means that, for a given width, there is less volume inside the actuator working to displace the actuator. Less volume in the actuator should mean a lower load-bearing capacity. This may be a worthwhile trade-off but was not explored by the authors. Another limitation with thin film conical pouch motors may be that the edges of the triangular ends are sharp which may prevent their uptake in other fields of soft robotics. Consideration must be given to these sharp edges if these pouch motors are to be used in a rectal device.

3.3.11 Other pouch motors

Other modifications to the pouch motors, which cannot be easily grouped into one distinct category, are reviewed in this subsection. A pouch motor that is constrained with PET and Kevlar wire was presented by Shen et al. (289) . The authors aimed to increase the maximum work pressure of the pouch motor while maintaining its light weight and low profile. Their "flat PAM" (FPAM) consisted of an inextensible balloon made of a 0.09 (90 μm) mm thick aluminium plastic film welded and cut into a specified pattern to create pouch motors connected to one inlet in parallel. The constrained layer was a 0.15 mm (150 μm) thick PET cut in such a way that the pouch motors, Kevlar wire, and PET layer can be orthogonally woven together. The maximum contraction ratio of this FPAM was 22.4% at 200 kPa, but this went down to 17% with a load of 65.9 N. These are lower contraction

ratios than the original pouch motor can achieve. While these FPAMs can withstand significantly greater pressures than previous pouch motors reviewed, part of the reason may well be that the films used were thicker. Nevertheless, orthogonally weaving the inextensible balloon, constrained layer, and Kevlar wire would involve delicate manual work that may be difficult to translate.

X-crossing PAMs consist of two pouch motors with comb-like filaments which connect in an X-crossing mechanism when folded. These comb-like filaments in the X-crossing mechanism provide linear contraction along the actuation axis (290). These X-crossing PAMs achieved a very high contraction ratio of 87.6-92.9% depending on the dimensions of the PAMs. While other pouch motors and PAMs have the greatest force output at the start of inflation and reduce this force output sharply with inflation, the X-crossing PAMs maintain their high force output throughout contraction. For their type 2 X-PAM, force was consistently similar at 70% as it was at 0% contraction, regardless of the pressure. While the actuator's performance is excellent, they act similarly to paired pouch motors and rotate and increase in width as they actuate. This increase in width may be a limitation where compactness is favoured.

The pneumatic pouch motor by Kwon et al. contains extra internal and external constraints to increase the theoretical contraction ratio from 36.3% to 55.3% (291). The authors achieved a contraction ratio of 46.3% at 10 kPa, which did not change when increased to 30 kPa because it was a geometric constraint leading to this contraction ratio, not the pressure being the limiting factor. Material on the inner layer was a triple laminate of linear low-density polyethylene (LLDPE), nylon, LLDPE, 32.5 μm/15 μm/32.5 μm. For the outer layer it was a double laminate of nylon 15 μm/LLDPE 125 μm. While the contraction ratio was clearly improved, the construction of these pouch motors was complex and may not be translated into the clinic.

Bellows actuators' working principle is similar to the pouch motor. They are made of round discs of fabric which are connected along their centres. A comparison would be if pouch motors were connected parallel to each other, where the lateral expansion of the motor is greatest, rather than in series, where the edges are

connected. Because they are connected in this fashion, they contract to extremely flat shapes, achieving contraction ratios of 90% with high load bearing capacity (292,293,299). Lee and Rodrigue showed their bellows-like actuator was able to lift a 40 kg payload with an 87% contraction ratio (293). However, these actuators contract with negative pressure (i.e., they are vacuum-powered) and do not provide any inherent rigidity.

Origami-inspired fluid-driven actuators are another form of bellows actuator. While bellows actuators have their limitations, Origami principles improve these actuators for three reasons. Origami principles can be used to fold a device into a compact form prior deployment, induce rigidity in the device, and induce motion such as translation, rotation, and twisting. This section briefly reviews the use of the Yoshimura pattern, the Kresling pattern, and the Miura-Ori pattern. Paez et al.'s Origami shell reinforced the exterior of their bellows actuator using a Yoshimura pattern (294). The shell allowed for bending on inflation like a bellows actuator while the folds in the shell provided a restoring force limiting this bending to a desired value. Wu et al. used Kresling patterns to achieve omnidirectional bending in their magnetically controlled Origami robotic arms (295). The Kresling pattern has two stable states: the folded state and the deployed state. The bistable Kresling pattern allows for omnidirectional motion between states but will "lock" and provide rigidity when it reaches either stable state. The Miura-Ori tessellation is capable of being folded into a compact size and its ridges and valleys provide rigidity in its own plane (300). It has only one degree of freedom, but the tessellation can be used as a tendon-induced bellows actuator with axial rigidity (296). These patterns may be useful to consider in the design of the device to induce bending while maintaining rigidity, compactness, and deployability of any actuators used in the device.

Other methods of improving the bellows-actuator include the "high-contraction ratio pneumatic artificial muscle" (HCRPAM) and "high-displacement pneumatic artificial muscle" by Han et al. (297) and Yang et al. (298), respectively. These "PAMs" consist of an inner bellows-like actuator, that expands with positive pressure, with an external diamond-shaped band wrapped around the bellows actuator that contracts in the perpendicular direction of the expansion of the

bellow. The HCRPAM's inner bellows actuator was made of TPU, was 53 mm in length when deflated and was split into 6 chambers. This was made by 3D printing which allowed for rapid and inexpensive prototyping. The diamond-shaped band was a bow string with a high Young's modulus to adequately convert the force output from the bellows actuator to the band. This diamond-shaped band was 170 mm in height at its longest. The whole actuator weighed in at 27.00 g. In contrast to the HCRPAM, the components of the high-displacement PAM by Yang et al. were made of the same material. This material was a heat sealable Oxford fabric and thermal adhesive film. Han et al.'s HCRPAM achieved a contraction ratio of 64.7% at 300 kPa and Yang et al.'s high-displacement PAM a contraction ratio of 60% at 34.5 kPa. However, like the other PAMs, the main drawback of these PAMs is that they become significantly wider as they actuate.

3.3.12 Applications of pouch motors in soft robots

Having reviewed the different structures and modifications used to improve conventional PAM and pouch motors, this section summarises how these designs integrate into applications within soft robotics and how they may inform the design of the device. Relevant applications include wearable robotics for rehabilitation, endoscopy, and minimally invasive surgery.

While there are examples of the application of pouch motors in wearable soft robotics, such as Niiyama et al.'s pouch motors in gait rehabilitation of paralysed rats, or Yilmaz et al.'s capacitive sensing pouch motor to aide with foot drop syndrome, most wearable robotics consist of a simple bellows actuator that is strapped around a joint (301,302) or a rotational pouch motor that rotates about a joint (303). There is usually no need for an elaborate quaternary ordered structure in rehabilitative exoskeletons.

The soft pneumatic inchworm double balloon (SPID) by Manfredi et al. consists of two balloons connected to a 3 DOF soft pneumatic actuator (304). The soft pneumatic actuator acts as the inchworm and provides the locomotion around the tortuous colon, while the balloons provide anchorage. A similar design could be employed, featuring a central soft pneumatic actuator that is capable of bending

to the anorectal angle, but with an alternative external structure that provides rigidity to resist compressive forces. The challenge here is that the structure that replaces the balloons would need to be deployable while providing radial rigidity when deployed.

A deployable soft robotic arm was presented by Fathi et al. (305). The quaternary ordered structure could be described as a soft robotic arm consisting of three honeycomb backbones, each with a Yoshimura Origami pattern. Each backbone acts as a bellows-actuator and the whole arm is tendon actuated to induce bending. While a tendon-actuated arm may not be suitable for a patient-operated rectal device, modifications to the deployable arm may make it appropriate. For instance, through separate pressure modulation of each backbone. If one backbone is pressurised while the other two sides are not, bending would be expected. This may be useful to lock in the anorectal angle and resist rotational forces about the anorectal angle. The honeycomb structure, when inflated, provided axial stiffness, but it is unclear whether it would provide radial stiffness to resist compressive peristaltic forces. Also, a hollow arm could be designed by creating a centre space between the three backbone when binding these together to meet Criterion 4 of the device, allowing the passage of gas.

The inflatable CYCLOPS robot by Runciman et al. is a proposed soft robot intended to deploy inside the lumen as a platform for endoscopic mucosal dissection (258). The quaternary structure of the inflatable CYCLOPS robot can be described as 6 actuators, each made of rectangular pouch motors, connected in parallel and then bound together to form a (hexagonal) cylinder. This inflatable robot could be folded down to a diameter of 25 mm around the endoscope but deployed such that each side of the hexagonal cylinder was 28.5 mm, meaning the width of the robot was 57 mm.

3.3.13 Discussion

The CYCLOPS robot which is to be used in minimally invasive surgery is a good foundation to base the device off. This inflatable robot and pouch motors have an inherent variable stiffness mechanism enabling the fabrication of a deployable

device while providing radial rigidity to expand and hold open the lumen. Additional criteria it needs to meet are being hollow for gas passage and angled to lock into the anorectal angle. Making a similar robot such that it is angled may be promising to lock the device into the anorectal angle. Using conical pouch motors in the design may be appropriate to achieve this since it has good performance criteria (contraction ratio, load-bearing capacity, and rigidity) while keeping the device low-profile, low-cost, and with a single mode of control for translatability. This thesis explains how the author initially tried to meet the device criteria with a truncated prism design before using an antagonistic pair of conical pouch motors to achieve and control the desired angle. This is followed by presenting a new design of elliptical pouch motors which improve the device's ability to resist changes to its angle.

3.4 Revised aims

The primary aim of this thesis is to develop a soft deployable endorectal actuator that meets the criteria hypothesised to improve outcomes in prostate radiotherapy. These criteria are repeated below with modifications that have arisen because of the preliminary trial in 1.3. and the pouch motor overview in 1.5. The modifications made from 1.2.5 are underlined. The device should:

- Criterion 1: Be well tolerated (>80% of population) <u>through a deployable mechanism which enables the device to be linear and as large as an index finger when folded</u>
- Criterion 2: Provide <u>radial</u> rigidity to resist compressive peristaltic forces <u>once deployed</u>
- Criterion 3: Retract the rectum away from target volume <u>by angling the rectum to 110°</u>
- Criterion 4: Allow the passage of gas
- Criterion 5: Enable patient self-insertion <u>with a single mode of control</u>
- Criterion 6: Have image-guidance capabilities <u>with the integration of radiopaque markers</u>
- <u>Criterion 7: Have simple and inexpensive manufacturing methods to translate to the clinic</u>

Criterion 7 was added here as part of clinical translatability includes the ease and cost of manufacturing.

Once an initial prototype was developed, additional aims were formed to meet these criteria. The aims of this thesis are to:

1. Characterise and optimise the mechanical properties of the soft endorectal actuator.
2. Enable the endorectal actuator to be self-insertable, self-inflatable, and act as an IGRT tool
3. Develop and validate a silicone rectal phantom to validate the endorectal actuator in vivo simulated.
4. Validate the endorectal actuator inside the rectal phantom.

Chapter 4 Design and fabrication of a deployable endorectal actuator

4.1 Introduction

This chapter describes the fabrication methods and design of the initial working prototype that met the criteria required of the device. The criteria that the device must meet are laid out in the aims. Criteria 1,2, and 4 were achieved by basing the device on the same design principles of the inflatable CYCLOPS robot (258). That is, it consists of a shell made of a 3D folded sheet of pouch motors that inflates (C1) to provide radial rigidity (C2) but must be angled to and maintain this angle through deployment at 110° (C3). By nature of being a hollow shell, it satisfied Criterion 4. This section outlines the initial design choices that aimed to satisfy Criterion 3. Although these early designs did not fully satisfy this criterion, they informed the development of the working prototype that ultimate met the desired requirements. The working prototype design consisted of an external shell that deploys to provide radial stiffness, with an internal pouch motor that acts as a “flexor” actuator. This novel design enabled the development of a deployable device that may be suitable to stabilise the rectum, while bypassing the anal sphincter on insertion. The chapter then describes the methods of validating the working prototype. In the fabrication of this device, thermoplastic sheets are used because they are highly flexible, meaning chambers that inflate with pressure are created to allow deformation of the sheets and a soft robot made of pouch motors could be made. Laser welding was used as it allows for rapid prototyping with CAD software editing designs. The manufacturing methods are easy to replicate and inexpensive, satisfying Criterion 7. This chapter is an extension of (2) and (3), both of which are written by the author of this thesis. Devices were fabricated by the author of this thesis. Designs of the device were created by the author with Dr Mark Runciman’s help and feedback. All experimental work, data collection, and analysis was carried out by the author.

4.2 Laser welding methods

The devices were fabricated using an established laser welding system developed at The Hamlyn Centre, St. Mary’s Hospital (258). Designs were

created in SolidWorks (Dassault Systèmes) and then converted to DXF files. DXF files were converted into G-code of the laser welding system using a DXF-to-G-code converter. These G-codes were input into the laser welding software. Triple-laminate (30/60/30 µm PE/PET/PE) thermoplastic sheets were used, which were cleaned with isopropyl alcohol (IPA) before being placed on a vacuum top. A marker pen with infrared absorptive dye (Clearweld LD940B, Crysta-Lyn Chemical Company, USA) was used to draw the design (as G-code) onto the first sheet. After removal of the pen, another thermoplastic sheet was placed on top of the first sheet. A larger transparent acetate sheet was used to hold down the two thermoplastic sheets on the vacuum top. The thermoplastic sheets were laser welded together in the prescribed design. The laser was set to 5.1 A, which corresponds to 11.97 Watts with a 0.8 mm spot diameter weld speed of 1500 mm/min. The resulting welds were then cut with a 1.5 mm cutting margin using a Beamo (FLUX Europe) laser cutter. Edges were manually soldered at 160°C. The workflow of the fabrication of the device is shown in Figure 4.1. These were the fabrication methods used throughout this chapter.

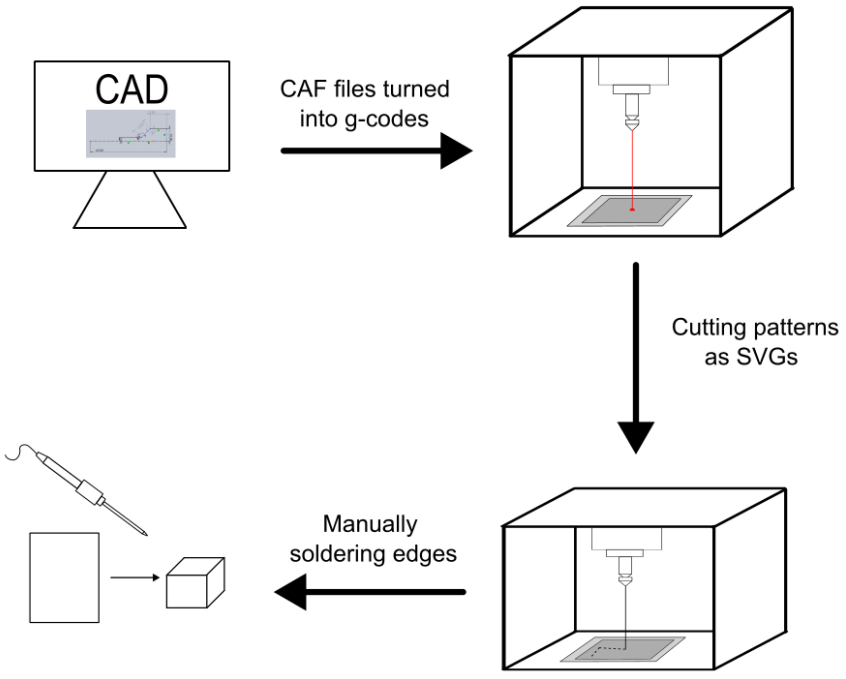

Figure 4.1: Workflow visualization of the fabrication methods to create the endorectal actuator.

4.3 First design: a dual-truncated prism

4.3.1 Design and methods

The first prototype design that was explored was a dual-truncated prism. The dual-truncated prism contains two truncated prisms connected to each other, visualised in Figure 4.2. This can be laser welded as one continuous design which is then manually welded together. The angle can be determined from the design, so to satisfy Criterion 3 (110° angle). This lets the device lock in the anorectal angle and prevent anterior translation of the rectum. Figure 4.3 shows the design and dimensions of a 3-sided and 4-sided dual-truncated prism. The angle of the design was 70°, which pinched in at 70 mm along the axial length of the device. The 2D design was 115 mm in length. Horizontal welds for the inflatable chambers were 10 mm apart in the vertical direction and 7mm apart in the horizontal direction; vertical welds in the middle between horizontal welds were 5 mm in length; the inlet for inflation was 22 mm in length and 5.5mm in width. For the 3-sided device, each side of the device was 28 mm in width, totalling a 2D width of 84 mm and the horizontal welds for the inflatable chambers were 22 mm in length. For the 4-sided device, each side had a width of 17.7 mm, totalling a 2D width of 70.8 mm, and the horizontal welds were 10.7 mm in length. The device's deployability, rigidity, and bursting pressure was tested by inflating them with a pneumatic compressor with an integrated pressure gauge. Devices were inflated in increments of 50 kPa until failure.

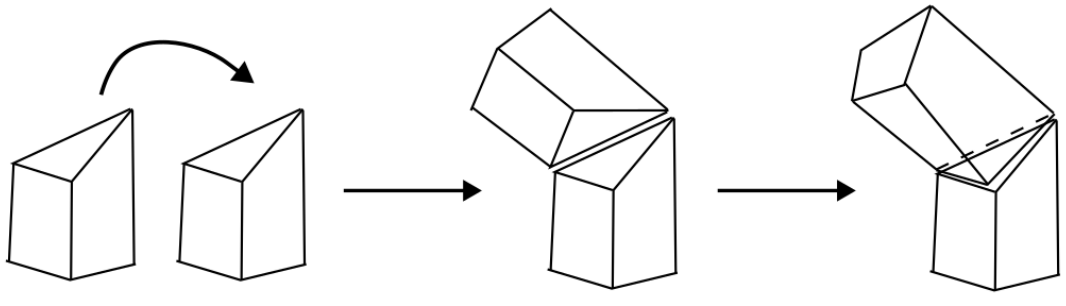

Figure 4.2 The design principle of two truncated prisms connected to each other to form a dual truncated prism.

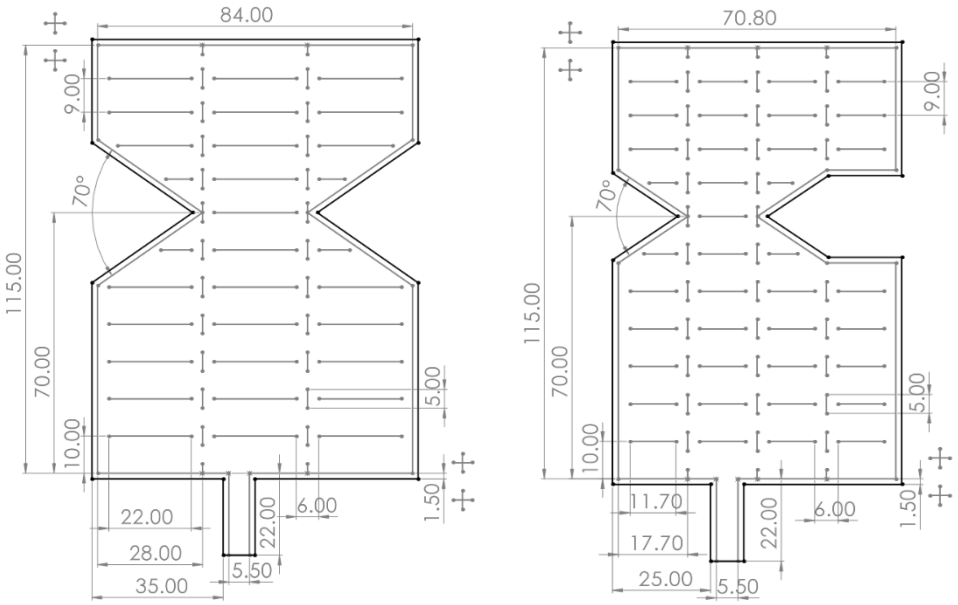

Figure 4.3 Design and dimensions of a three-sided (Left) and four-sided (Right) dual-truncated prism.

4.3.2 Results

The 3-sided device could not be folded into a linear device because the 3-sided device had increased rigidity along its longitudinal axis. This increased rigidity meant the device could not be folded along the longitudinal axis without breakage because of Gaussian curvature law (Theorema Egregium) (257) and would not be feasible for a deployable rectal actuator. The 4-sided device was made to address this, and it allowed folding. However, the nature of expansion was deemed impractical and uncomfortable; the device would significantly push and stretch against the posterior anal wall as it expanded to its final form (Figure 4.4). Because of this inappropriate expansion, no other testing was carried out.

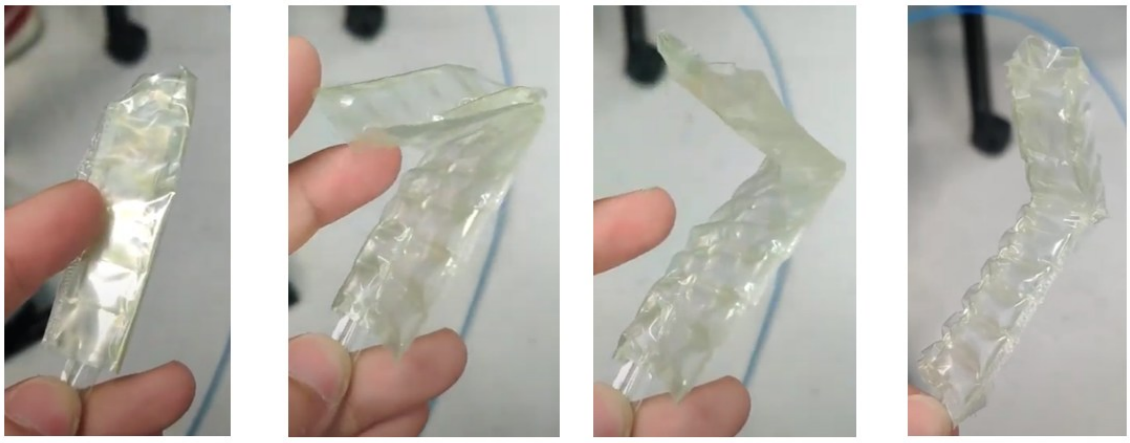

Figure 4.4 Four-sided dual-truncated prism device. (a) when deflated and folded, (b-c) when expanding and deploying, (d) In its final deployed shape.

4.3.3 Discussion

The dual-truncated prism design was unable to fully satisfy device Criterion 1 despite a successful angle (C3) and deployable mechanism. The inflation of the device was impractical for the rectum. An alternative method to satisfy the device criteria was pursued by fabricating a reinforced actuator.

4.4 Second design: perpendicular welds for a reinforced actuator

4.4.1 Radial welds to reinforce one side: Methods

The next design was based on a reinforced actuator that attempted to meet the angle criterion. In its simplest form, a reinforced actuator is an inflatable balloon that is constrained from expanding radially. When constrained radially, it can only expand axially. A sheet of inextensible material is added to one side of the balloon, restricting axial expansion on that side. One side is axially restricted; the rest of the balloon is not. On inflation, the rest of the balloon expands axially, causing the balloon to bend.

The initial attempt to replicate this behaviour consisted of a 3-sided device with a channel in which a Tygon tube was inserted to reinforce that side to cause bending (Figure 4.5, left). This tube did not bend the device as intended (Figure

4.5, right). Instead, creating a reinforced actuator by changing the orientation of the welds was explored. The orientation of the welds was first confirmed to determine the device's actuation behaviour. A three-sided device was fabricated with welds oriented either radially or axially along its length. Depending on their orientation, the welds effectively create rows or columns of pouch motors, that actuate on inflation (Figure 4.6). Radially oriented welds are expected to contract the device axially; axially oriented welds should contract the device radially. This was quickly confirmed and shown in Figure 4.7.

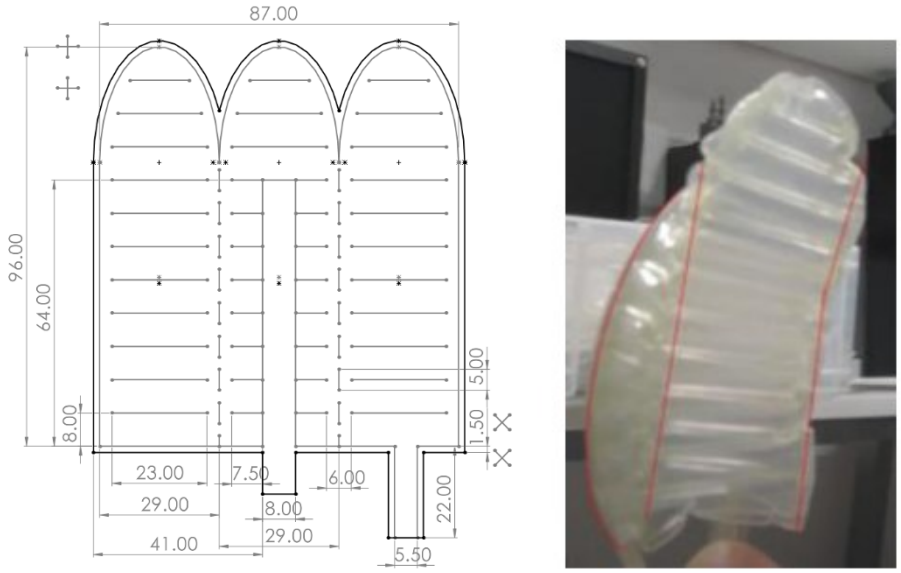

Figure 4.5 Left: The initial design of a reinforced device with a channel for an inextensible tube and horizontal chambers. Right: Inflated shape of this first design containing an embedded inextensible tube.

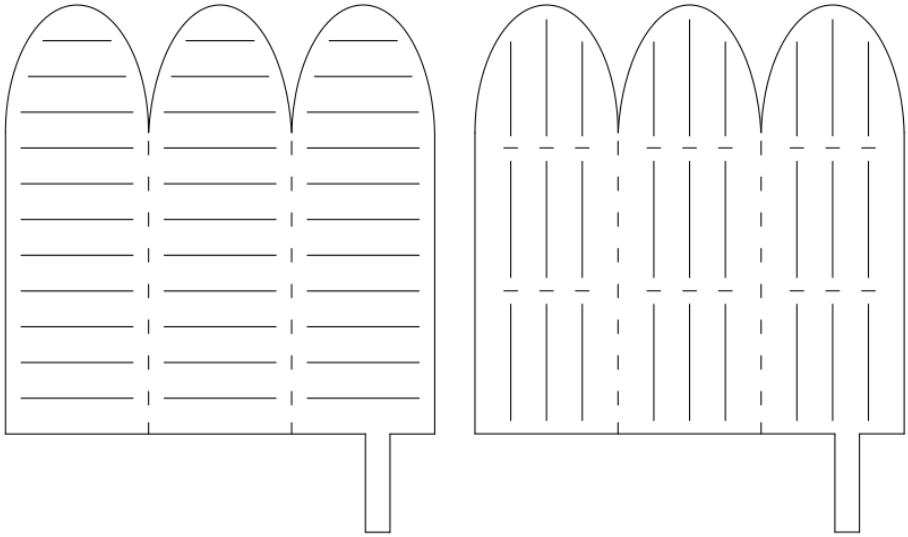

Figure 4.6 Three-sided device with radial welds expecting to actuate the device axially (left), and with axial welds expecting to actuate the device radially (right). Device dimensions and weld separations were constant.

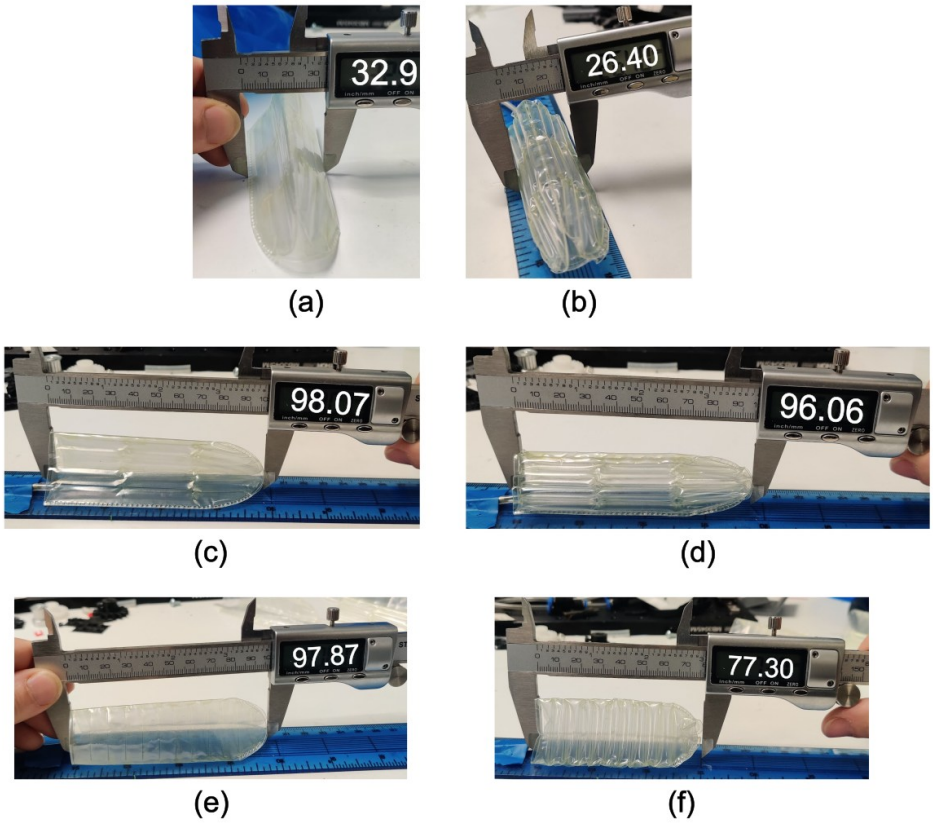

Figure 4.7 A 3-sided device containing axial or radial welds and its respective direction of contraction. Top: Axial welds showing radial contraction from (a) uninflated to (b) inflated device. Middle: Axial welds showing no radial contraction from (c) uninflated to (d) inflated device. Bottom: Radial welds showing axial contraction from (e) uninflated to (f) inflated device. Measurements (in mm) are added in white for better contrast and visibility.

Based on these findings, the design was implemented as a three-sided device with one side reinforced by axially oriented welds (Figure 4.8). This side's axial actuation will be restricted, while radial welds on the other two sides enable axial actuation. On inflation, the device is expected to bend. The tip of the device was also rounded to future-proof increased comfort on insertion. The device's deployability, angle on inflation, and radial stiffness were assessed. The device was inflated in increments of 50 kPa using a pneumatic compressor with integrated pressure gauge. To assess deployability, the device's dimensions were measured with digital calliper and rounded to the nearest millimetre when the device was folded and uninflated, and when fully inflated. The expansion ratio was calculated by taking the ratio of the inflated volume of the device to the folded volume. The angle on inflation was measured with a protractor.

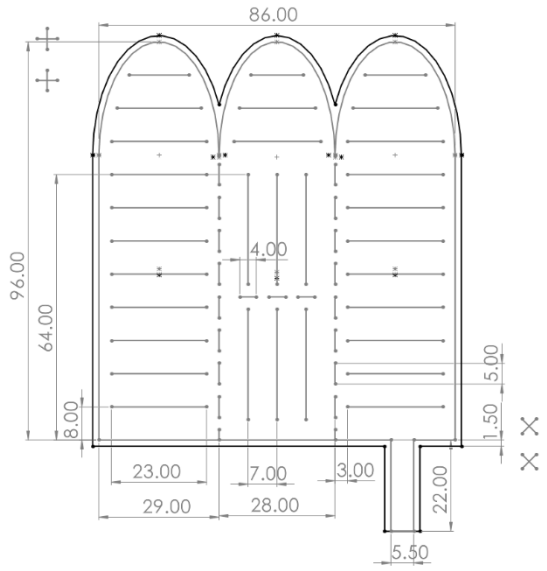

Figure 4.8 The sketch design of the reinforced actuator with axial welds on one side and radial welds on the other two sides.

Radial stiffness (force/displacement) was obtained by compressing the devices between two flat surfaces that were 3D-printed from PLA and measuring the force applied with a force sensor (Nano 17, ATI Automation, USA) and displacement with a digital calliper. At low displacements and forces, the device's bend caused force measurements to fluctuate in the same measurement. Instead of gradually increasing compression, devices were compressed as much as possible and then moved back 1 mm at a time. Leakage under pressure was tested by inflating

the device with water with a 50 ml syringe, on top of a dry paper towel, and examining the paper towel for leakage.

4.4.2 Results

While deflated, the device was folded axially three times to reduce the dimensions down to 3 mm by 17 mm with a length of 96 mm. Once inflated, the device reached a width by depth of 25 mm by 30 mm, with the length remaining at 96 mm, which resulted in an expansion ratio of 14.7 by volume ($V_{inflated}$:V_{folded}). The inflated device is shown in Figure 4.9.

The angle of the device was measured to be 160°. Figure 4.10 compares this to ProSpare™, which has an angle of 110°, on a cone-beam CT scan of the pelvis. While deflated, the device was folded axially in three to reduce the dimensions down to 3 mm by 17 mm with a length of 96 mm, which was not reduced. Once inflated and deployed, the device reached a width by depth of 25 mm by 30 mm, with the length remaining at 96 mm. This equated to an expansion ratio of 14.7 by volume ($V_{inflated}$:V_{folded}). Figure 4.11 shows the radial stiffness increased as the pressure of the pneumatic compressor increased. Internal welds burst at 150 kPa, but the soldered edges did not fail. Water did not leak from the main body but did leak from the inlet and the tubing connected to the syringe.

Figure 4.11 shows the radial stiffness increased as the pressure of the pneumatic compressor increased. Internal welds burst at 150 kPa, but the soldered edges did not fail. Water did not leak from the main body but did leak from the inlet and the tubing connected to the syringe.

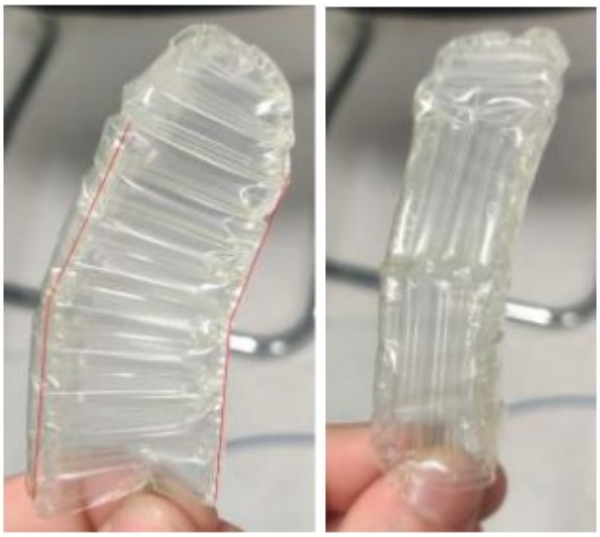

Figure 4.9 Inflated 3D shape of the design with axial welds on one side to reinforce it. Left: lateral view of the device highlighting the angle. Right: Anterior side of the device showing the axial welds.

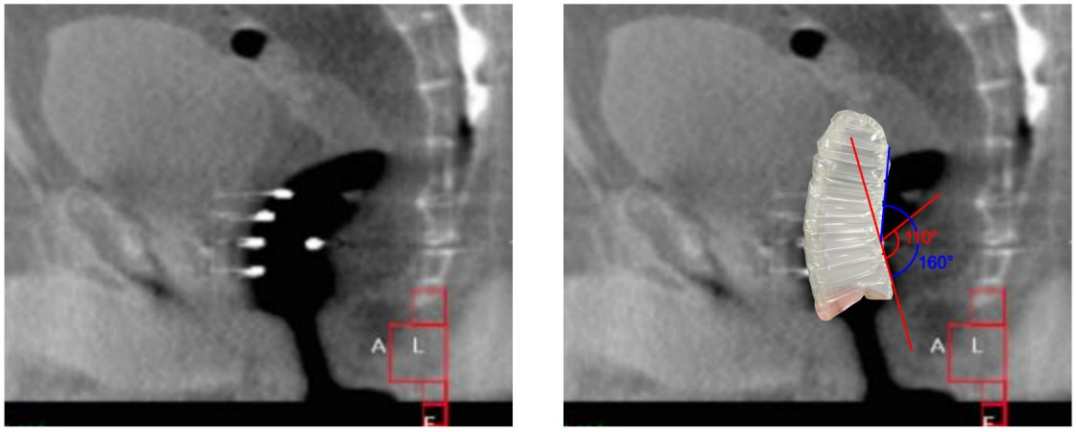

Figure 4.10 Left: Sagittal view of ProSpare™ on cone-beam CT scan. Right: The reinforced actuator design superimposed on ProSpare™ on CBCT comparing the angle of the bend in each device and its relation to the anorectum.

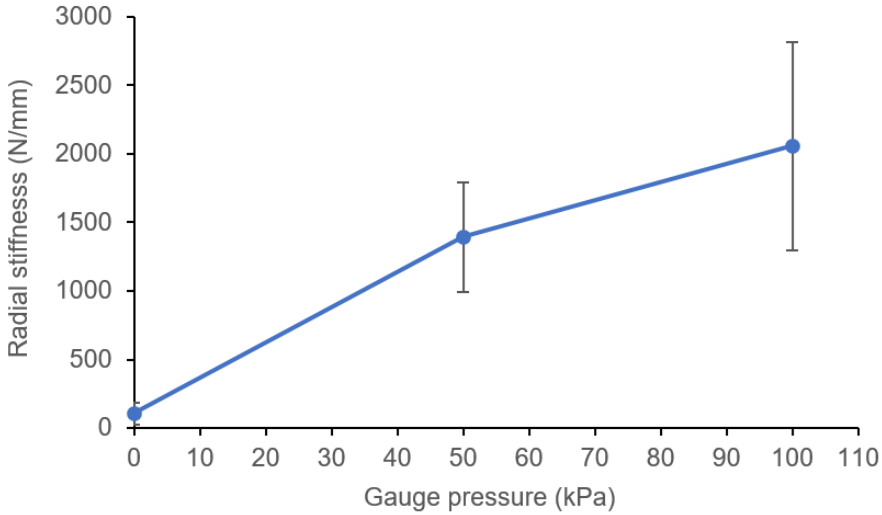

Figure 4.11 Radial stiffness of the reinforced actuator against gauge pressure. Values are means ± standard deviations from 8 measurements. Internal welds failed at 150 kPa.

4.4.3 Discussion

An inflatable device that inflates to a rigid, angled shape while being compact and linear when uninflated was successfully fabricated. This iteration of a reinforced actuator has met some of the desired criteria. It is fully compressible so it is linear when folded and uninflated which should enable easy insertion past the anal sphincter (C1). Its radial stiffness increased as it was inflated (C2) and the shape of the device should allow the passage of gas (C4). A single mode of control was maintained through pneumatic inflation (C5). Although this iteration achieved an angle (C3), the angle was insufficient to retract the rectum, as highlighted in Figure 4.10. The desired angle is 110°, as this would enable adequate retraction of the rectum.

Since the other criteria were met, the fundamental design of this reinforced actuator was maintained. The next subchapter describes modifications made to this design to increase the angle.

4.5 Modifications that aimed to increase the angle

Both initial modifications made to the device attempted to increase the angle of the device by increasing the contraction ratio of the sides with the radial welds.

An increased contraction of the sides with the radial welds, while the side with the axial weld is still reinforced, would mean the device bends more. The two modifications described here are increasing the width of the device, and adding notches to the device.

Lateral view images were taken of these modified devices, and angles on the “posterior” side of the device were measured with an onscreen protractor (306).

4.5.1 Increased width of device

First, the device’s width was increased. As discussed in 0, the edges of the rectangular pouch motors crinkle and buckle with inflation, preventing the pouch to achieve its maximum practical contraction ratio. Because of the edges crinkling, the contraction ratio of these rectangular pouch motors is between 17 and 28%, despite a theoretical maximum ratio of 36.3%. The edges of these pouches are what impede the contraction. To refresh the reader’s mind, Niiyama et al. found a wider (50 mm) pouch motor had a greater contraction ratio (27%) compared to a narrower (20 mm) pouch motor (20%). A wider pouch motor exhibits a greater contraction ratio because the edges make up less of the pouch relative to the width (282). Increasing the width of the device would therefore be expected to increase the contraction ratio which would in turn improve the angle of the device. The original device was 32 mm in width. The width was changed in increments of 8 mm down to 16 mm and up to 40 mm to assess how this affects the angle.

From 16 mm width to 32 mm width, the increase in width made a minimal difference (<5 degrees), as shown in Figure 4.12. The widest device at 40 mm had the worst angle at 151°.

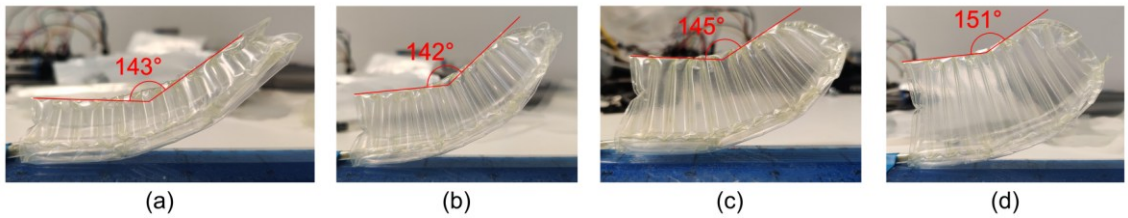

Figure 4.12 Angle of the device at different widths. (a) 16 mm width, (b) 24 mm width, (c) 32 mm width, (d) 40 mm width.

Because the crinkling of the edges continues to affect the contraction ratio of the radial sides, adding notches to the device was explored to increase the angle.

4.5.2 Notching in the device

A notched actuator, inspired from notched-wrist robots, is investigated here. Notched-wrist robots consist of blocks of Nickel-Titanium (Nitinol) with notches removed from it with a tendon actuator attached to the top of the robot. The tendon actuator pulls on the robot to bend it and the notches remove material that would otherwise obstruct this bending and create compliant regions that enable more bending (28). For the device, it was hypothesized that if the edges had gaps between them, there would be no material to impede the bending. Notches would prevent crinkling of the edges and increase the contraction ratio, increasing the angle. This increased contraction ratio was seen with Dr Mark Runciman's conical pouch motors (253), which worked with a similar principle. The rectangular sub-actuators (with the radial welds only) were turned into conical sub-actuators by using triangular cutouts. The drawback is that part of the actuator is removed, reducing the volume that it is inflated by. This reduction in volume reduces the force output and extent of contraction. While more notching is expected to lead to less buckling and a higher angle, it will simultaneously reduce the volume of the actuator, and in turn reduce bending. It was expected that a certain degree of notching would sufficiently reduce the effect of buckling, resulting in increased bending despite the associated reduction in volume.

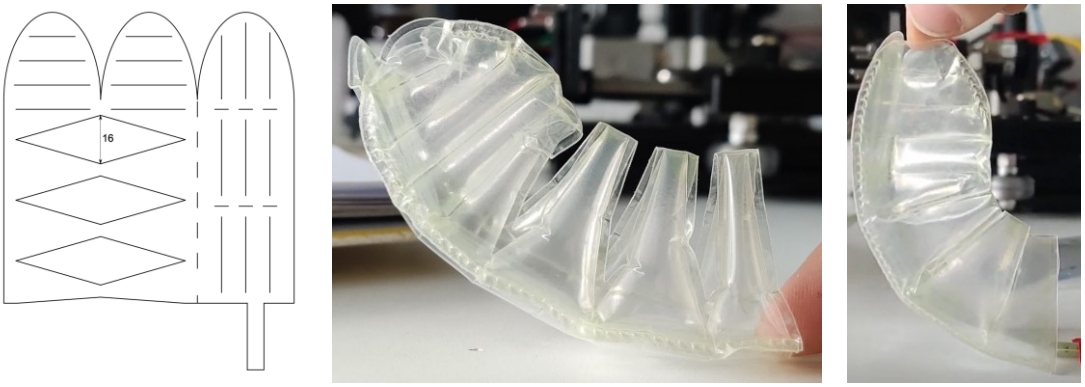

Figure 4.13 The first notched device with a 16 mm cutout. Left: 2D sketch of the design. Middle, inflated device leaving space which leaves potential for more bending. Right: Uninflated device manually pulling the device further in to highlight the potential for more bending.

However, after one trail, it was observed that while notching does help in reducing buckling, it also leaves spaces that could enable further bending. These spaces that are left by the notching are highlighted in Figure 4.13. The middle and right image in Figure 4.13 clearly illustrating the extent of the gaps created by the notches. This available space represents potential for increased bending, suggesting that a higher bending angle could be achieved compared to the current method. Like the notched-wrist robotic actuator, a mechanism to pull the notches closer together was required. The next subchapter describes the working prototype that employed this feature to satisfy Criterion 3. The entire design process has been summarised as a flowchart in Figure 4.14.

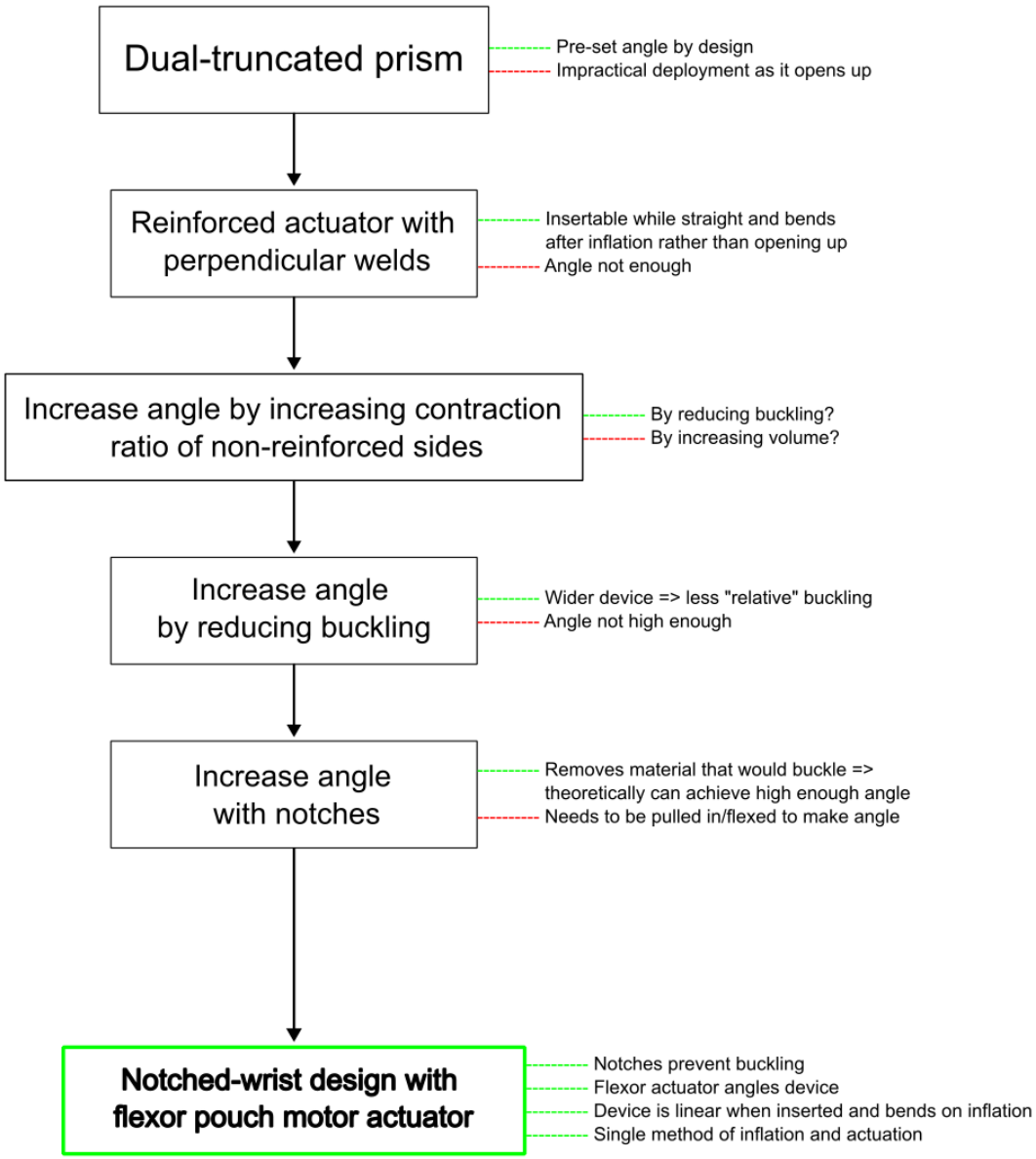

Figure 4.14 Design process of the angled inflatable endorectal actuator summarised as a flowchart. Each step represents an intermediate prototype with green lines highlighting justifications and advantages of that prototype, and red lines its limitations.

4.6 A working prototype: a notched wrist actuator with a flexor and extensor actuator

4.6.1 Introduction

For the initial design, an inflatable actuator—a “flexor” actuator—was attached directly to the main actuator and welded as one inflatable system (Figure 4.15a).

As it is all one closed system, it would inflate in order—first the main actuator and then the “flexor” actuator. This also maintains a single mode of control in the device as it is inflatable with a single syringe (C5). Since the flexor actuator pulls the device to bend it, more notches are not required to prevent buckling of the edges. Therefore, a single large notch will suffice. An efficient way to achieve this single notch is by designing a dual-truncated prism again as in subchapter 4.3 but not welding the inner edges together. This is visualised in Figure 4.16. The flexor actuator just needs to have a sufficient pulling force to bend the device. Initially, the flexor actuator was connected to the opposite side of the dual truncated prism (Figure 4.15). For this type of connection, the device had to become a 4-sided device again. This connection was suboptimal and did not bend the device sufficiently. This insufficient bending is because the connection is further away from the “joint”. This larger distance led to a larger moment arm the flexor actuator had to have a greater contraction ratio for the same degree of bending.

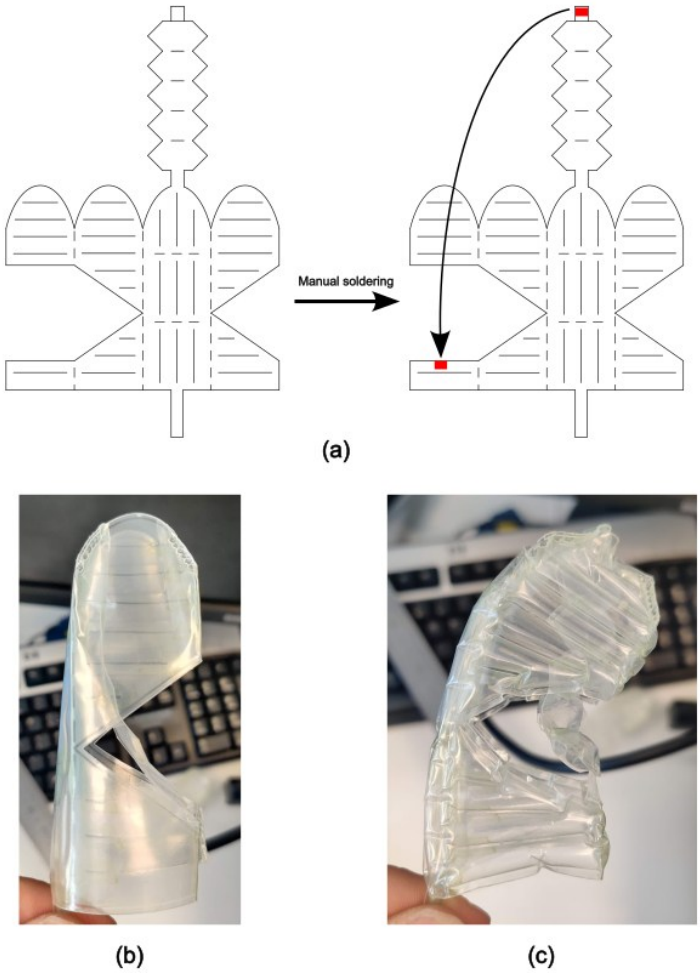

Figure 4.15 The initial prototype with a flexor actuator (a) Design and fabrication (b) Uninflated shape (c) Inflated shape.

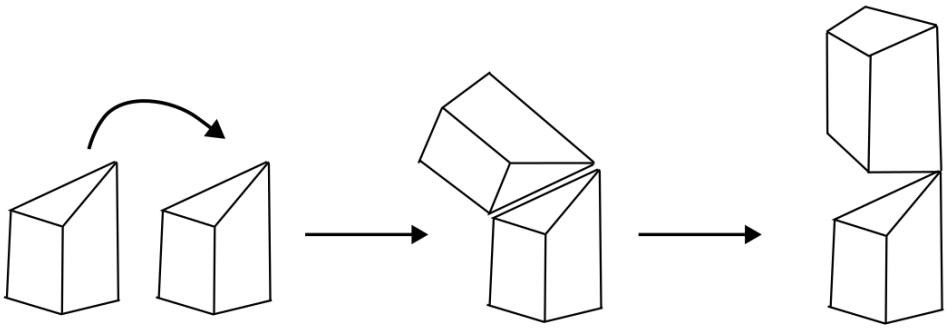

Figure 4.16 Visualisation of a "disconnected" dual truncated prism

To solve this, the flexor actuator was attached to the same side of the main actuator. By attaching the flexor actuator to the same side of the main actuator,

the force output is closer to the joint so a lower contraction ratio is required to achieve the desired angle. While increased the angle to 130°, it was still insufficient (Figure 4.17). Hydraulic inflation was then chose over pneumatic inflation because the incompressibility of water was expected to improve the contraction length. However, the inlet into the flexor actuator kinked at the top of the device, preventing the flow of water into the flexor actuator. The flexor actuator was made as a separate component and manually soldered to the main actuator. This method was successful in creating the desired angle. An additional “extensor” actuator was subsequently explored on the exterior of the device. This extensor actuator can be inflated simultaneously to control the angle more precisely. The rest of this chapter describes the fabrication, validations, and limitations of the working endorectal actuator and is based on (3).

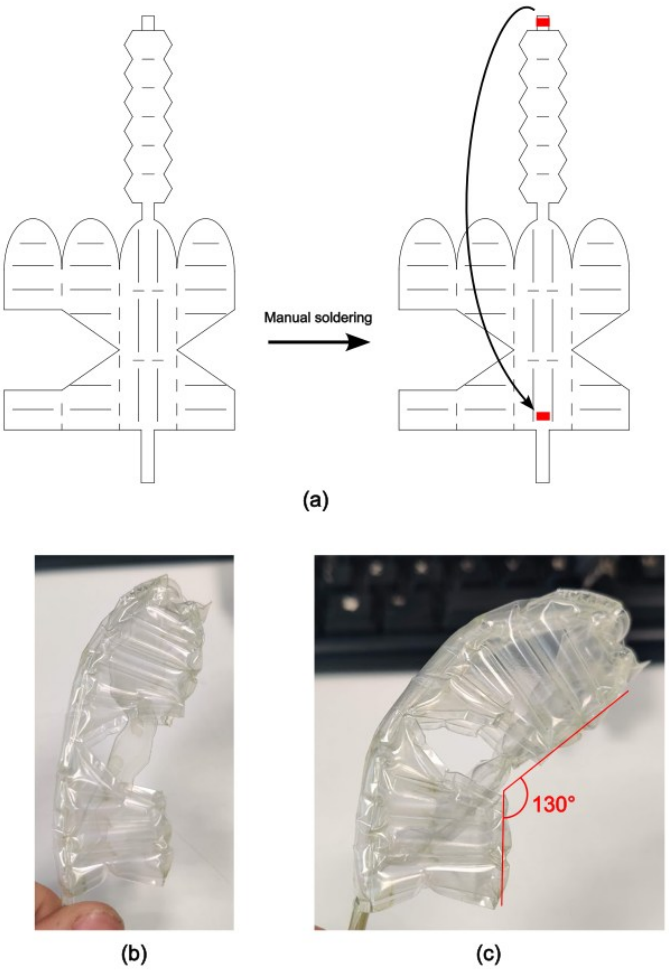

Figure 4.17 The flexor actuator is attached to the same side of the main actuator. (a) Design and fabrication (b) Uninflated flexor actuator (c) Inflated flexor brings the device to an angle of 130°

4.6.2 Materials

The device was fabricated with the same method as described in Chapter 4.2. Thermoplastic sheets used were a tiple laminate, 30/60/30 μm PE/PET/PE. Cutting margins were 1.5 mm and edges were manually soldered at 160°C.

4.6.3 Designs

Since the device is now a 4-sided device, each side was made smaller in width so the device would not be too big for insertion into the rectum. The widths were changed from 32 mm sides to 24 mm sides (Figure 4.18a). This way the deployed device will be of approximately the same volume. Upon confirming the open dual-truncated prism with a “flexor” actuator works, an “extensor” actuator was added

externally to enable more precise control of the angle (Figure 4.18b-c). The “flexor” actuator and an “extensor” actuator are manually soldered on the inside and outside of the main backbone, respectively, creating an antagonistic muscle pair (Figure 4.18d-e).

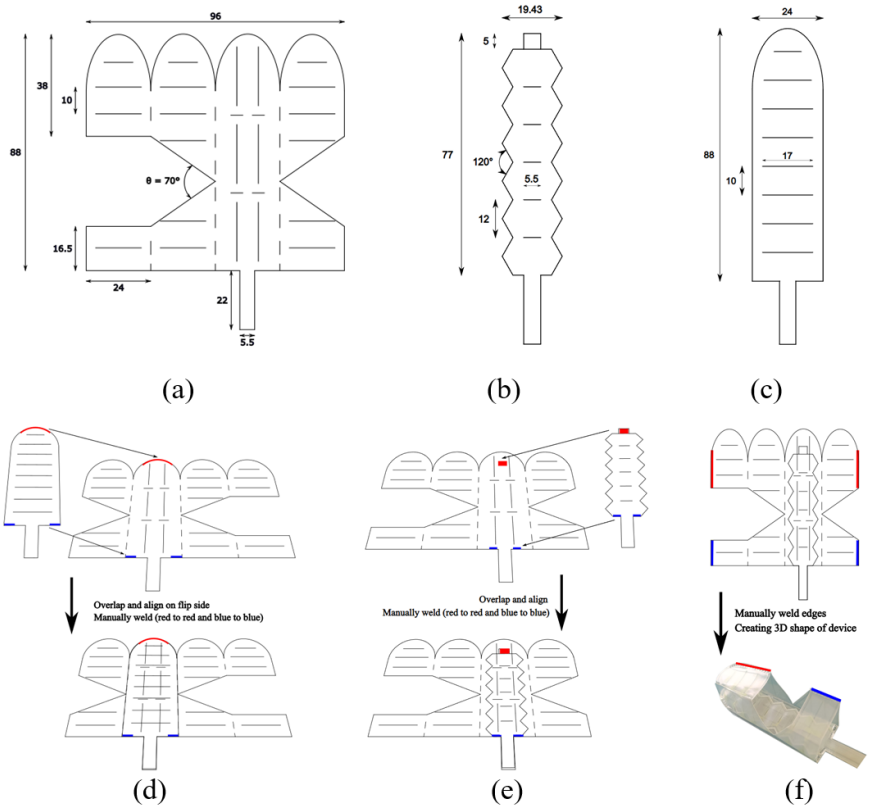

Figure 4.18 Design and fabrication of the soft endorectal actuator showing weld patterns of the (a) main body actuator, (b) flexor actuator, and (c) extensor actuator; the process of manually welding the (d) flexor actuator onto the main actuator, (e) extensor actuator onto the main actuator (on the back), and (f) edges of the device to create a cuboid structure. Dimensions are in mm. Copyright © 2023 IEEE

These muscle actuators act like biceps and triceps on an elbow joint. This creates a hydraulic soft robot capable of unidirectional movement. The starting length of the empty actuator muscle (L_0) is defined as

$$L_0 = y + \frac{d}{2} + u \quad (1)$$

where y is the length from the bottom cut edge to the bottom of the actuator, d is the distance between the cut edges, and u is the distance by which L_0 extends

past the joint (Figure 4.19). Using the cosine rule, the final length of the actuator when fully inflated, L_i, can be defined as

$$L_i^2 = u^2 + \left(y + \frac{d}{2}\right)^2 + 2u\left(y + \frac{d}{2}\right)\cos(\pi - \theta) \tag{2}$$

where d and u are defined as

$$d = 2x \tan\left(\frac{\theta}{2}\right) \tag{3}$$

$$0 < u < h + \frac{d}{2} \tag{4}$$

and x is the horizontal length of one of the sides for a four-sided device where all sides are equal in length.

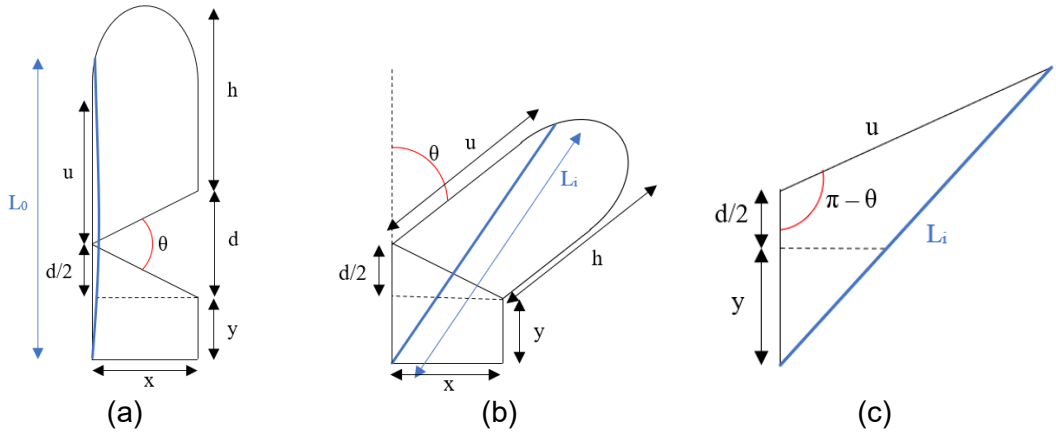

Figure 4.19 Sagittal view of the device showing the mechanism of action of the internal flexor actuator (in blue). (a) Initial position with an empty actuator with initial length L0. (b) The device is angled because of inflation and shortening of the flexor actuator. (c) Triangle showing how the inflated actuator relates to the dimensions of the device. L0 is the initial length of the empty actuator, Li is the length of the actuator when inflated, Li < L0. θ is the angle of rotation in radians.
Copyright © 2023 IEEE

The muscle actuators could not be laser-welded to the main body as they required cutting before attachment. Consequently, each muscle forms a separate chamber, necessitating a distinct inlet for each. The device consists of three chambers: one for the external extensor muscle, one for the central main body,

and one for the internal flexor muscle. Each actuator was inflated hydraulically with a syringe.

4.6.4 Deployability of device

The deployability of the device is shown in Figure 4.20. When folded down, the device had a volume of 4368 mm^3. When deployed and inflated, the volume was 47124 mm^3. This constitutes an expansion ratio of 10:8. It is important to note that 47124 mm^3 is the volume of space the device displaces as it expands in the rectum, while unflexed. This is not the actual volume of the device, as the device is ultimately hollow to accommodate the muscle actuators and allow the passage of intestinal gas. This is therefore the maximum volume the device will take up and can be used to predict whether the patient may feel discomfort during inflation. The volume of water with which the actuator could maximally be filled was 12 ml. However, some trials burst at 12 ml, so the main actuator was filled to 11 ml in all subsequent trials.

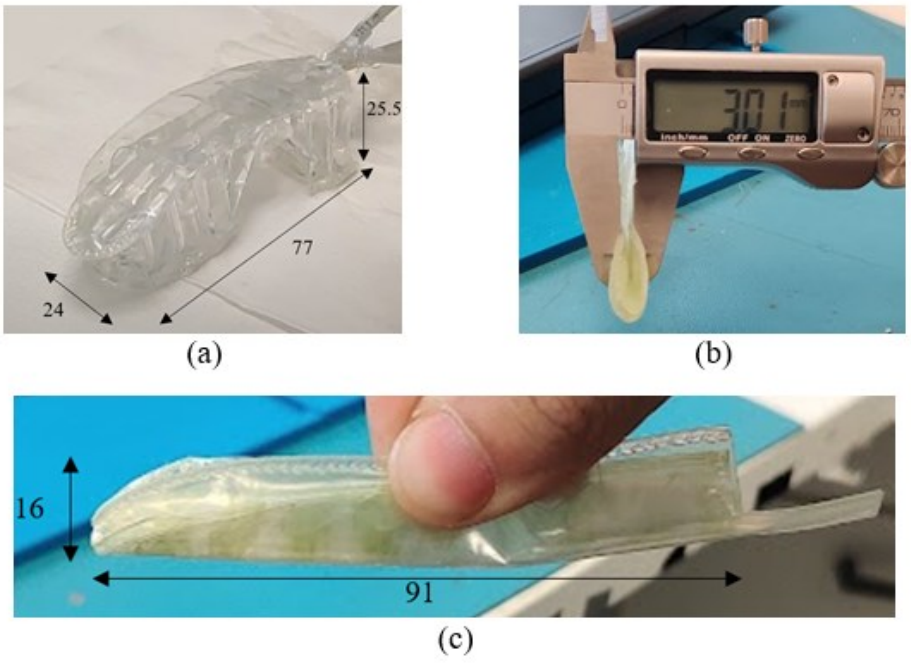

Figure 4.20 Dimensions of the device when (a) deployed and inflated and (b and c) undeployed and folded. Dimensions are in mm. Copyright © 2023 IEEE

4.6.5 Extent of flexion and extension and angle control

The maximal angle of flexion and extension were measured when the flexor actuator (Figure 4.21a) and extensor actuator (Figure 4.21b), respectively, were fully inflated with water. Food dye was used to visualize the muscle actuators. Measurements were taken when the main actuator body was deflated and when inflated. Angles were measured by taking a birds-eye view photograph, using an on-screen protractor to determine mean angles on the anterior and posterior sides of the device. Angle control was investigated by varying the inflation volumes of the flexor and extensor muscle actuators. Measurements were taken while inflating the flexor muscle in 1 ml increments with an empty extensor actuator, and vice versa. Mean maximal angles of flexion and extension were 116° (range 111-121°) and 241° (235-250°), respectively, while the main actuator was inflated (Figure 4.21), and 116° (range 110-120°) and 255° (250-262°), while the main actuator was uninflated. Figure 4.21b demonstrates the extensor actuator's function; the device would never assume this position in practice as this does not follow the anorectal angle. There was limited angle precision (i.e., high angle variation per ml of inflation) with isolated flexor (50° over 3 ml) or extensor (80.5° over 5 ml) inflation. With isolated flexor inflation, this included a large 35.5° increase from 161.0° to 125.5° from 1 ml to 2 ml. With isolated extensor inflation, this included a significant jump of 44° from 173.5° to 217.5° from 3 ml to 4 ml inflation. When inflating the extensor actuator in conjunction with a filled flexor actuator, more precise control over the angle was achieved: 30.0° over 4 ml inflation (Figure 4.22). Each ml increase in extensor volume consistently caused between a 5-11° (average 7.5°) increase in angle.



Figure 4.21 (a) The maximal angle of flexion with the flexor actuator fully inflated with red-dyed water, and (b) maximal angle of extension with the extensor actuator filled with black-dyed water. © 2023 IEEE

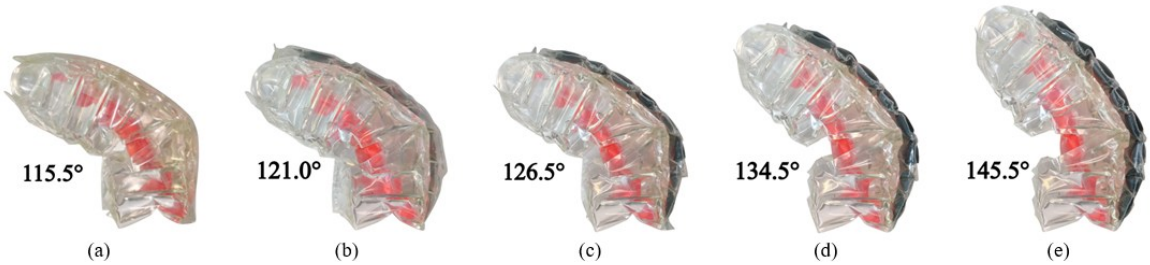

Figure 4.22 Angle changes of the device while the flexor actuator is full and the extensor actuator is inflated from 0 ml to 4 ml. (a) Extensor muscle at 0 ml, device at 115.5° (b) Extensor muscle at 1 ml, device at 121.0° (c) Extensor muscle at 2 ml, device at 126.5° (d) Extensor muscle at 3 ml, device at 134.5° (e) Extensor muscle at 4 ml, device at 145.5°. Flexor actuator contains red-dyed water; extensor actuator contains black-dyed water; main actuator contains clear water. © 2023 IEEE

4.6.6 Strength: radial stiffness and resistance to bending

Radial stiffness of the main actuator was assessed in the left-right (L-R) and anterior-posterior (A-P) directions using PLA surfaces and a linear stage to compress the device (Figure 4.23a and b, respectively). Force was measured with a force/torque sensor (Nano 17, ATI Automation, USA), while displacement was measured with a digital calliper, obtaining radial stiffness (force/displacement). The effect of volume on radial stiffness was investigated by increasing the device's volume by 2 ml increments at a 3 mm displacement, measuring force output over 5 minutes. Bending resistance was measured with a 5N Newton Meter by attaching a condom to bend the inflated device while its base was held in place (Figure 4.23c). This applied a distributed force on the device to mimic the application in the rectum. Attaching a cable onto a single point of the device (e.g., at the tip) had caused local deformation and tearing, so

this was avoided. The radial stiffness in both L-R and A-P directions increased with increased inflation volume until the device bursts at 12 ml (Figure 4.24a and b). The force-displacement curves in the A-P direction (Figure 4.25b) and L-R direction (Figure 4.25c) had gradients of 2.022 N/mm and 1.395 N/mm, respectively. These closely matched the results from Figure 4.24b and c, respectively. Error bars in Figure 4.25a-c are small showing the device's reproducible radial stiffness.

Challenges with obtaining a repeatable force output at a 1 mm A-P displacement, due to the device's slight bending, led to its exclusion from data analysis. Shearing of the device was observed at all displacements when compressed in the LR (unflexed) direction, which can also be seen in Figure 4.23a. It noticeably increased at 5 mm displacement, causing a dip in radial stiffness (Figure 4.25a). At 6 mm, significant shearing occurred, resulting in the device's failure. This shearing did not happen in the A-P or L-R direction when flexed, indicating the device's greater stability in those orientations. Therefore, shearing is of little concern since the intended use of the device is in the flexed position. The inability to measure A-P compression in the flexed position led to the assessment of the bending resistance. Table 4.1 contains the angle increase from forces applied at 53 mm from the hinge of the device. Torque calculations and their impact on angle are visualized in Figure 4.26. Error bars are relatively small here confirming the flexor actuator's reproducible, albeit insufficient, ability to resist bending.

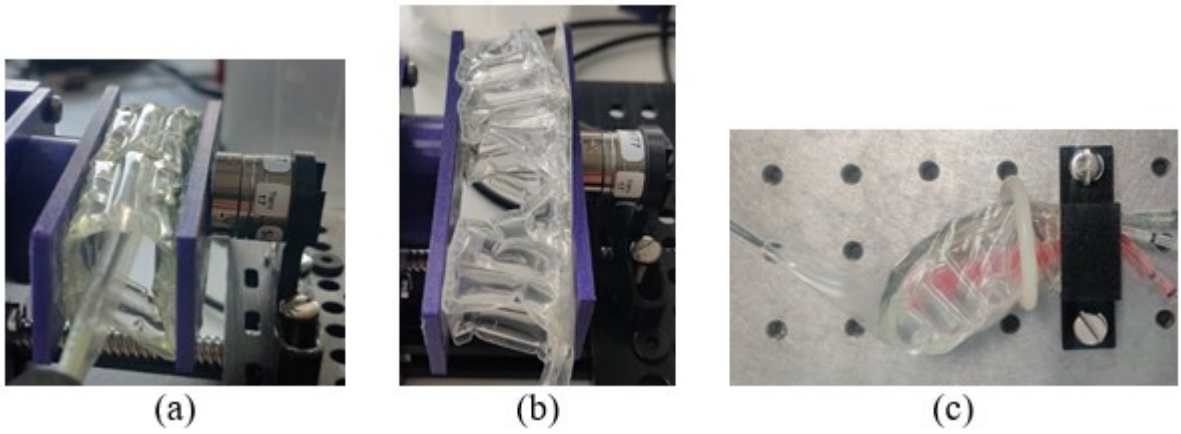

Figure 4.23 Measuring force output from the main actuator of the device in the (a) left-right direction and (b) anterior-posterior direction of the device. (c) A Newton Meter is attached to the device via a condom to pull on the upper part of the device and measure its resistance to opposite bending. © 2023 IEEE

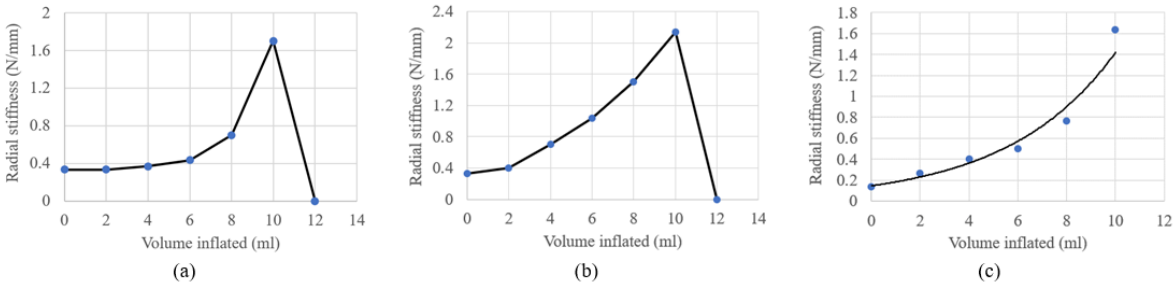

Figure 4.24 Radial stiffness of the main actuator in relation to the volume it is inflated by. (a) Compression in the left-right direction while unflexed. (b) Compression in the anterior-posterior direction while unflexed. The main actuator bursts and starts leaking at 12 ml in the unflexed positions. (c) Compression in the left-right direction while flexed. © 2023 IEEE

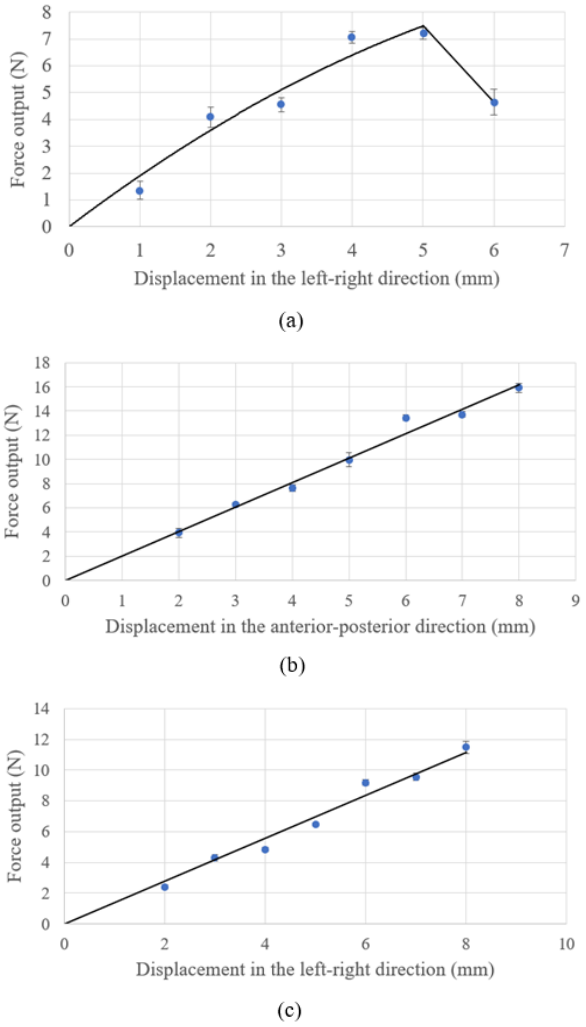

Figure 4.25 Force measured vs displacement in compression of the main actuator in the (a) left-right direction while unflexed (b) anterior-posterior direction while unflexed (c) left-right position while flexed. Error bars are standard error of mean from 4 trials. Some bars are too small to be visible. © 2023 IEEE

Table 4.1 Force by Newton meter and angle changes. Copyright © 2023 IEEE

Force (N)	Angle (°)	Angle change (°)
0	120.5	-
0.5	128.3	+7.8
1.0	144.8	+24.3
1.5	161.8	+41.3

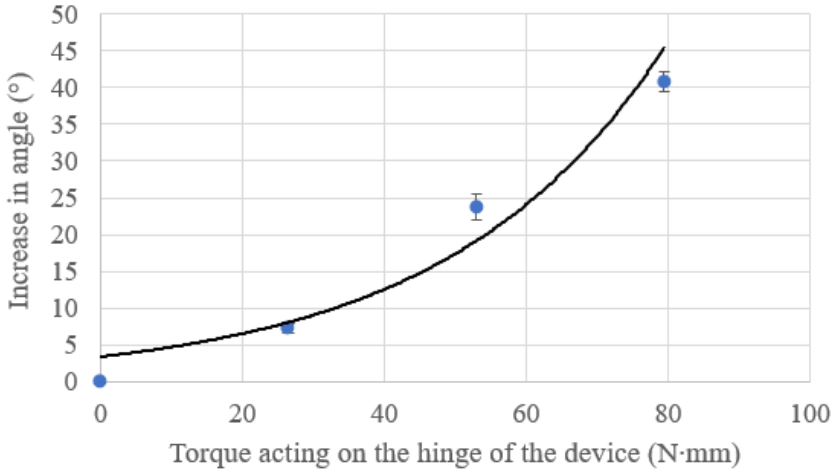

Figure 4.26 Relationship between the torque acting on the device and the increase in the angle of the device, opposing the bending action by the flexor actuator. Error bars are standard error of mean from 4 trials. © 2023 IEEE

4.6.7 Stress relaxation properties of device

The device's suitability for radiotherapy fractions, which can extend up to 10 minutes, was evaluated. The tubing was clamped with a pinch clamp upon full inflation of the main actuator and flexor actuator, and force measurements were taken every 30 seconds over 5 minutes. Using a tee connecter, a pressure sensor (MS5803-14BA Breakout SEN12909) was connected to the main actuator, measuring its pressure at the same time as the force output every 30 seconds. These steps were repeated for the flexor muscle, with pressure measured every second for 10 minutes and the device's angle tracked every minute to evaluate angle stability over time. Figure 4.28 shows the time-dependent exponential

decay in the force output of the device in all three directions (L-R unflexed, A-P unflexed, and L-R flexed). Error bars after 60 seconds are minute, showing the device's radial stiffness over time is reproducible for multiple copies of the device. The main body of the device exhibits stress relaxation properties that were confirmed via pressure readings, results shown in Figure 4.27a. The device's angle remained constant, implying no change in the length of the flexor actuator. This was confirmed by isolated measurements of the flexor actuator outside the device, showing no length change over 5 minutes. The pressure inside the flexor actuator during device flexion and in isolation over time is depicted in Figure 4.27b and c, respectively. The slight increase in pressure around 270s (Figure 4.27c) corresponds to device handling for length measurement after 5 minutes; pressure then returned to the trendline after handling ceased.

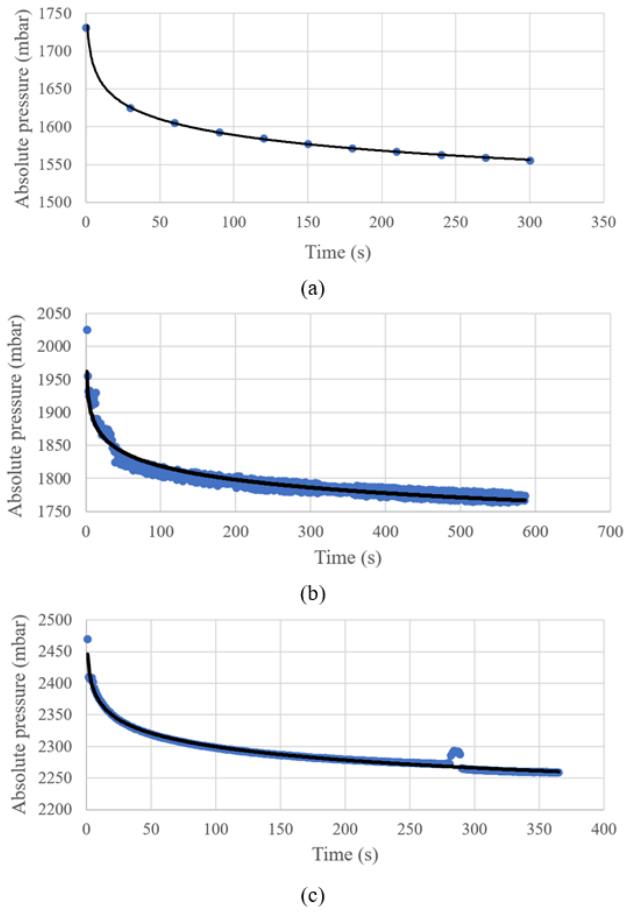

Figure 4.27 The absolute pressure over time inside (a) the main body of the device while undergoing anterior-posterior compression. (b) the flexor actuator while flexing the device (c) the flexor actuator in isolation, outside the device. © 2023 IEEE

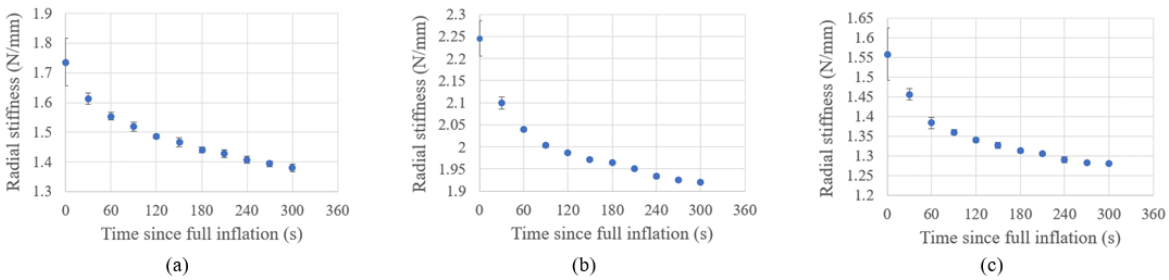

Figure 4.28 Compressive radial stiffness over time in the (a) left-right direction while unflexed (b) anterior-posterior direction while unflexed (c) left-right direction while flexed. Error bars are standard deviation of mean from four trials. Some bars are too small to be visible. © 2023 IEEE

4.6.8 Repeatability of inflation, flexion, and extension

The repeatability of the use of the device was investigated to explore the possibility of making the device reusable for a single patient over the course of their radiotherapy. This may be more environmentally friendly and cost-effective. Repeatability of the device was explored by fully inflating and deflating the flexor and extensor actuators 100 times while the main actuator was deflated, and while the main actuator was inflated. The main actuator was also separately fully inflated and deflated up to 100 times. The main actuator, flexor, and extensor actuators, separately, could handle repeated inflation and deflation well over 100 times. However, flexion and extension of the device while the main actuator was inflated were not repeatable after 5-6 cycles because of leaks caused by the sharp edges of the flexor muscle cutting through the membrane of the main actuator. Rounding the edges of the flexor actuator design or making the main actuator bigger so there is no contact between the edges of the flexor and the main actuator membrane may prevent this.

4.7 Discussion

By incorporating design aspects from soft robotics—using a pouch motor as a flexor actuator inside a notched-wrist inflatable prism—a working prototype has successfully been made. This working prototype meets Criteria 1-5: a deployable mechanism enables a linear deflated device that is as compact as the index finger; the weld pattern on the prism provides radial rigidity; the flexor actuator angles the device to potentially retract the rectum away from the target volume;

the prism allows the passage of gas; a single mode of control is possible as all parts are hydraulically inflated.

This working prototype is from here on referred to as a soft hydraulic endorectal actuator. The endorectal actuator for prostate radiotherapy can be compressed down to bypass the anal sphincter, occupying a volume of 47125 mm^3 on deployment, comparable to the average threshold volume for first sensation, as seen on anorectal barometry (44-53 cm^3) (307,308). This makes it likely that the device's deployment will be well tolerated. Its controllable angle, to suit a patient's anatomy, may improve superior-inferior displacements and comfort on insertion. The device underwent stress relaxation (Figure 4.28), as confirmed by pressure readings (Law of Laplace) (Figure 4.27), which may be monitored and corrected. Figure 4.28 and Figure 4.27 show the force and pressure, respectively, reach close to their plateau within 100 seconds.

Figure 4.25b and c show the endorectal actuator can withstand at least up to 16 N in the anterior-posterior direction, and 12 N in the left-right direction. A displacement of 8 mm was recorded with these high forces in their respective directions. These are very high forces that would not typically be produced by a rectum at rest. Therefore, the endorectal actuator will likely be capable of resisting compressive forces from the rectum and stabilise rectal volume.

The main limitation of the device is that the sharp edges of the conical flexor actuator cut the inner membrane of the main actuator. If this were to happen in a patient, it renders the device useless. Additionally, the device lacks resistance to opposing bending forces.

The next chapters show efforts to mitigate the sharp edges of the flexor actuator and strengthen the device's resistance to bending forces. Additionally, the inflation tubing was modified to enable self-insertion and the device's stabilisation properties were validated in a biomechanically representative phantom.

The soft hydraulic endorectal actuator will fundamentally remain the same over the course of this thesis. It consists of a dual-truncated prism, welded from plastic

film, with a “flexor” actuator of the same material attached to the inside which bends the device. The “extensor” actuator was excluded to reduce device complexity. Efforts were made to simplify the operation of the device, by avoiding the combination of multiple actuation methods, thereby reducing the operational burden on the patient user. Inflating three separate actuators through distinct supply tubes in a specific sequence would have introduced complexity contrary to this goal. A single mode of control means the whole endorectal actuator can potentially be inflated with one syringe and supply tube. An easier inflation method means the patient is more likely to be able to follow instructions for self-insertion and feel confident in their ability to make the device work.

Chapter 5 Optimising the endorectal actuator for use in radiotherapy

5.1 Introduction

The previous chapter presented the working prototype that meets criteria 1-4 and partially fulfilled the first aim of characterising the mechanical properties of the device. The device's properties pertaining to its performance as a rectal actuator need to be improved. These properties are the longevity and bending resistance of the device. Improving the longevity will consist of reducing the cutting risk from the flexor actuator's edges sliding along the inner membrane of the main actuator. Improving the bending resistance means the device will be able to hold its angle better, locking in the rectum better and resisting anterior rotation about the anorectal angle. This chapter describes the modifications to the design of the flexor actuator to 1. reduce the cutting risk of the inner membrane of the main actuator, and 2. improve the force output from the flexor actuator to improve the bending resistance of the device. After optimising the device, methods to explore improve the self-operability of the device are outlined. The self-operability of the device consists of making the device self-insertable—the patient can insert the device themselves with no third-party help—and inflatable with a single syringe that the patient can use. Lastly, a method of embedding fiducial markers into the device is presented so the endorectal actuator can be used as an IGRT tool. Devices were fabricated by the author of this thesis. All experimental work was carried out by the author. Designs of the device were created by the author unless otherwise indicated.

5.2 Optimising bending resistance

From Chapter 4 it was found that the bending resistance was poor and that the flexor actuators would cut the inner membrane of the main body. Modifications were made to the flexor actuator aiming to address these limitations. The edges of the flexor actuators were made less sharp by modifying the conical pouch motor structure to an elliptical shape. It was hypothesised that the elliptical

actuator would perform comparably to the conical actuator for a given volume. Therefore, if performance remained equivalent while reducing the risk of membrane damage, this would constitute an improvement. To improve the device's bending resistance, an additional actuator was incorporated, and a longer "tendon" length in the flexor actuator was employed to increase the moment arm. It was further hypothesised that the combination of a second actuator and a longer tendon would increase the holding force of the flexor actuators and thereby improve the bending resistance. This subchapter is based on (308).

5.2.1 Design

The laser welding methods used were the same as the previous fabrication methods. Here, the author used a thinner triple laminate thermoplastic sheet (30/12/35 um PE/PET/PE) as the previous ones had finished stock.

The design of the main actuator remained unchanged. The flexor actuator positioned on the inside of the device is changed to investigate the effect of shape. The leftmost actuator shown in Figure 5.1 was the flexor actuator in the original prototype. It features a "tendon" of 5 mm that is manually soldered to the interior of the main actuator. The second actuator from the left in Figure 5.1 has a longer "tendon" of 10 mm. This was used to investigate whether a longer tendon, and consequently a longer moment arm, would enhance the bending resistance of the device. These actuators are derived from conically shaped pouch motors, which offer higher contraction ratios than traditional rectangular pouch motors. This is due to the tendency of rectangular pouch motor ends to crinkle and buckle as they inflate. The material at the end bends perpendicular to the major axis of the cylindrical central segment, which inhibits the contraction of the actuator (54,55). In contrast, conically shaped pouch motors have triangular ends, making the pouch motor conical when inflated. A modified version of this conical pouch motor was employed in the endorectal actuator, as the width of the flexor actuator is constrained by the internal width of the main actuator when inflated. To mitigate the cutting risk of the device, a pouch motor with elliptically shaped sub-actuators was trialled. This is the middle actuator in Figure 5.1.

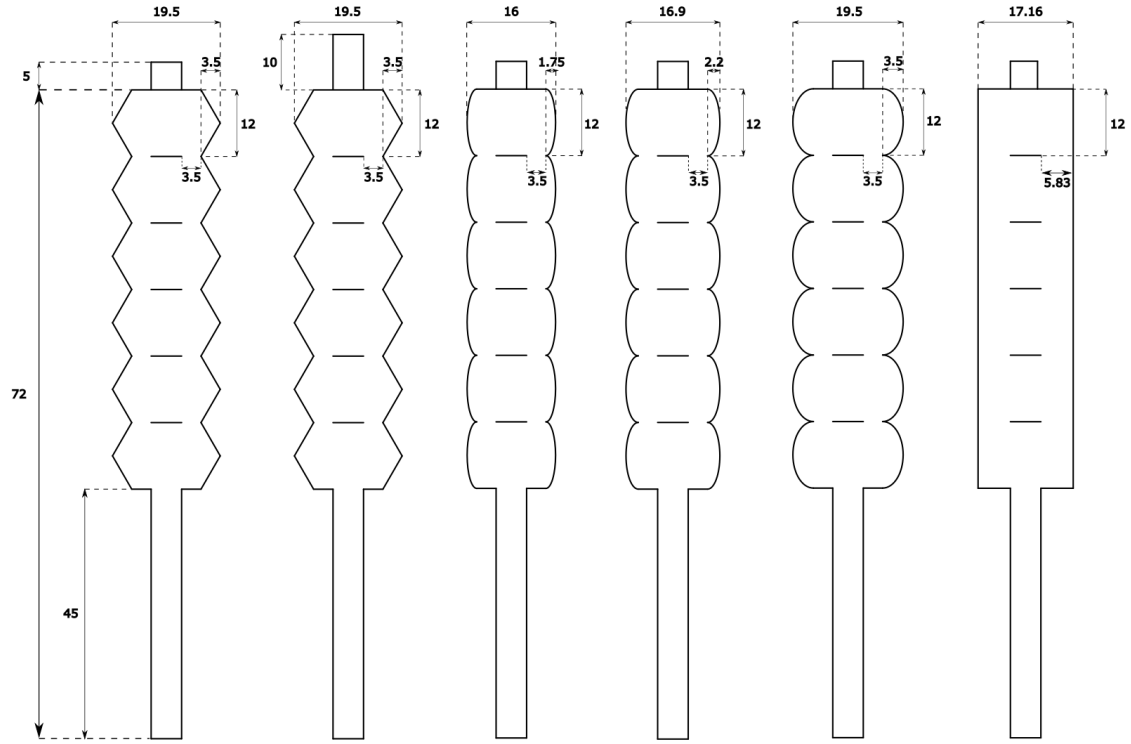

Figure 5.1 The designs and dimensions of each pouch motor and their sub-actuator type. From left to right: conical with a short tendon, conical with a long tendon, narrow-width elliptical, medium-width elliptical, extra-wide elliptical, rectangular. All aim to have the same volume except for the wide elliptical one.

As the shape of the sub-actuators is different, it was expected that the maximal inflated volume would change if dimensions remained the same. Keeping the volume constant is important because the work done by the fluid is its volume times the pressure of the fluid. The work done by the fluid is transformed into the displacement of the actuator and its restoring force.

$$-F\Delta L = P\Delta V \tag{1}$$

Where *F* is the restoring force, *P* is the internal pressure of the actuator, and *ΔL* and *ΔV* are the changes in length and volume, respectively (278). The volume of an actuator for a given extent of contraction is determined by the equation:

$$V(\theta) = \frac{{L_0}^2 D}{2}\left(\frac{\theta - \cos\theta \sin\theta}{\theta^2}\right) \tag{2}$$

Where L_0 is the length of the flat, uninflated actuator, D is the width of the actuator, and θ is the half the central angle made when the actuator is contracted. The angle, θ, is related to the arc length of the circular segment (278). Effectively, the term in brackets describes the extent of contraction. The restoring force of an actuator is expressed in terms of its angle as:

$$F_r(\theta) = L_0 DP \frac{\cos\theta}{\theta} \tag{3}$$

Where F_r is the restoring force that brings the inflated actuator to an equilibrium position, when a tension force is applied to it. Note, these equations apply to a rectangular pouch motor, where L_0 is the same along the length of D. For a conical actuator, resulting volume, V_c, of an actuator with two triangular ends, each of width d_c, and a centre section of width D_s, is given in the following equation, derived by Dr Mark Runciman:

$$V_c(\theta) = \frac{{L_0}^2}{2}\left(\frac{d_c}{3} + \frac{D_s}{2}\right)\left(\frac{\theta - \cos\theta \sin\theta}{\theta^2}\right) \tag{4}$$

This makes sense when compared to the volume of a cone with respect to a cylinder having the same base: for the volume of a cone to be the same as that of a cylinder, the cone's height must be three times as large (253).

The volume of the elliptical actuators was derived by integrating the cross-sectional area along the width of the elliptical ends, like how Dr Runciman did for the triangular ends of a conical actuator. The elliptical end can be visualised as shown in Figure 5.2. The top half of this shape was then derived as a function of L_0 by using the equation of an ellipse centred at point a on the x-axis.

$$y = b\sqrt{1 - \frac{(x-a)^2}{a^2}} \tag{5}$$

Point a in this case is d as this is the width of the elliptical end, and the x-axis is D so it can be expressed as a function of D.

$$\frac{L_0}{2} = b\sqrt{1 - \frac{(D-d)^2}{d^2}} \tag{6}$$

This is visualised Figure 5.2.

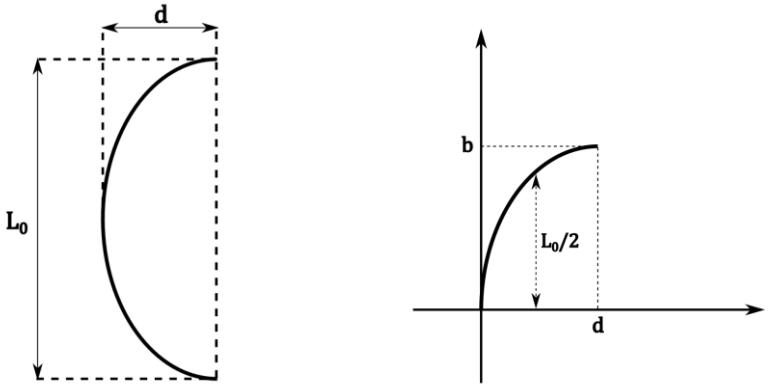

Figure 5.2. Graphical visualisation of the elliptical end of the actuator. Left shows the dimensions of an elliptical end of the actuator. Right shows how the top half would show on an x-y axis.

The equation for the cross-sectional area of a segment is:

$$A = \frac{L_0^2}{2}\left(\frac{\theta - \sin\theta\cos\theta}{\theta^2}\right) \tag{7}$$

Re-arranging (6) so it is in terms of L_0, and then replacing the term L_0 in (7), gives the equation for the area in terms of D:

$$A = 2b^2 \cdot \frac{2dD - D^2}{d^2} \cdot \left(\frac{\theta - \sin\theta\cos\theta}{\theta^2}\right) \tag{8}$$

Now that the area is expressed in terms of D, the author integrated the area with respect to D to obtain the volume:

$$V = \int_0^d 2b^2 \cdot \frac{2dD - D^2}{d^2} \cdot \left(\frac{\theta - \sin\theta\cos\theta}{\theta^2}\right) \delta D \quad (9)$$

$$V = \frac{4b^2 d}{3} \cdot \left(\frac{\theta - \sin\theta\cos\theta}{\theta^2}\right) \quad (10)$$

At $D = d$, $b = \frac{L_0^2}{2}$, the volume becomes expressed as:

$$V = L_0^2 \frac{d}{3} \left(\frac{\theta - \sin\theta\cos\theta}{\theta^2}\right) \quad (11)$$

Since this is the equation for one elliptical end. The total theoretical volume for the whole elliptical sub-actuator is therefore:

$$V(\theta) = L_0^2 \left(\frac{2d_e}{3} + \frac{D_s}{2}\right) \left(\frac{\theta - \sin\theta\cos\theta}{\theta^2}\right) \quad (12)$$

Which again makes intuitive sense since the volume of an ellipsoid or sphere has 4 times the volume of a cone with the same base length. The two elliptical ends add up to one ellipsoid. Since there are two cones in the conical actuator, the ratio becomes 2:1.

From equation (1) it is understood that for a given pressure and extent of contraction, the volume determines the actuator's force output (278). In this study, the pressure is not controlled but is measured to account for any force differences that volume control alone would not explain. Controlling the volume, without controlling the pressure, is also part of the translatability of the device.

Operating the device by administering a single controlled volume of water with a single syringe is simple and this further reinforces why hydraulic actuation is more favourable than pneumatic actuation for the device's purpose. Pneumatic actuation would require a separate input to regulate pressure, while this is uncommon for hydraulics. This volume-based control increases the likelihood that the device can be self-inserted and inflated by the patient.

The equations for volume for each of the rectangular, conical, and elliptical actuators enable the ends to be designed with dimensions for a constant volume. To ensure a constant volume across the actuator designs, each actuator was modelled as a rectangle of 12 x 12.5 mm, with shape-dependent additions on either side. The ratios in the width of the shape-dependent ends of the actuators are 1:1.5:2 for the shape-dependent additions (Table 5.1) for the conical:rectangular:elliptical actuators. For the original conical actuator, these additions were triangles with a width of 3.5 mm, (height of 12 mm) on either side. For the rectangular actuators, 2.33 mm was added on both sides, creating a 12 x 17.16 mm rectangle. The elliptical pouch motor included semi-ellipses with a minor axis of 1.75 mm (major axis: 12 mm), totalling 16 mm in width. It was found these first-iteration elliptical pouch motors crinkled a little, like how Mark Runciman found the rectangular pouch motors did. Since these first-iteration elliptical pouch motors crinkled, it was hypothesised that a slightly wider elliptic end would solve this issue. The first-iteration elliptical actuator is more "rectangular" than "elliptical", so it crinkles at the edges. Making it wider would leave more space for the material to actuate unimpeded. Additionally, this elliptical actuator had slightly less volume than the conical actuator, likely because of the crinkling, but this would make it underperform significantly because volume is directly correlated to force output.

It was hypothesised that, because of these practical limitations, using surface area as a surrogate for controlling volume would be more appropriate. Additionally, the restoring force of a pouch motor is also given by:

$$F_r(\theta) = L_0 D P \frac{\cos\theta}{\theta} \tag{13}$$

Where the cosine term describes the angle related to the arc length of the circular segment when the pouch contracts. This term describes the extent of contraction. Therefore, for a given extent of contraction and constant pressure, barring any additional practical limitations, the force output can be controlled with the surface area of the pouch motor. This is another way of describing equation (1)—the actuator's force output is determined by its volume for a given pressure and change in length—as surface area is used as a surrogate to control volume.

The first iteration of elliptical pouch motor will from hereon be referred to as the narrow-width elliptical (NWE) pouch motor, and the pouch motor which used surface area as a control for volume be referred to as the medium-width elliptical (MWE) pouch motor. To ensure the same surface area for the MWE as the conical pouch motor, the MWE pouch had semi-ellipses with a minor axis of 2.2 mm (major axis 12 mm). This slightly wider minor axis meant the MWE pouch had a total width of 16.9 mm and a surface area of 191.47 mm^2, which is approximately the same as the 192 mm^2 surface area of the conical pouch. The NWE and MWE pouch motors were smaller in width than the original conical flexor actuators. This smaller width meant the elliptical actuator did not contact the inner membrane of the main actuator of the device. To address this width discrepancy, one more extra-wide elliptical (EWE) actuator, with a minor axis of 3.5 mm, and the same width as the original conical actuator, was made. This wider design allows greater inflation volume for a given contraction and pressure, potentially improving bending while retaining the rounded edges.

Table 5.1. Equivalent volume ratios for inflatable pouch motors depending on the shape of the lateral ends

Actuator type	**Conical**	**Rectangular**	**Elliptical**
3D shape when inflated	Cone	Cylinder	Ellipsoid/sphere
Shape-dependent addition length for same volume.	$\frac{d_c}{3}$	d_r	$\frac{2d_e}{3}$
Ratio $V:V_{conical}$ for same width	1	3	2
Width (mm)	3.5	1.17	1.75

5.2.2 Experimental methods

To ensure the same inflation volume and stroke ratio between actuators, actuator stroke length was measured at maximum inflation using a spring gauge. A 175 mm plastic loop was manually welded to the actuator base for anchoring, and a

slit in the tendon enabled the spring gauge to be hooked onto the actuator (Figure 5.3). Actuators were placed horizontally, pulled taut by the spring gauge, and inflated in 0.2 ml increments using a 5 ml syringe until failure or until no more fluid could be injected by physical strength. The latter relates to how the device would be expected to use by a patient. Each device was filled from empty five times and the volume change measured from the graduated syringe. The standard deviation could then be calculated for each. Initial and contracted lengths were measured with a digital calliper, and force readings on the spring gauge at maximum inflation were recorded. While the calliper can record measurements to 1/100th of a mm, readings were rounded to the nearest 0.1 mm because pouch motor lengths were manually measured using the ends of the calliper.

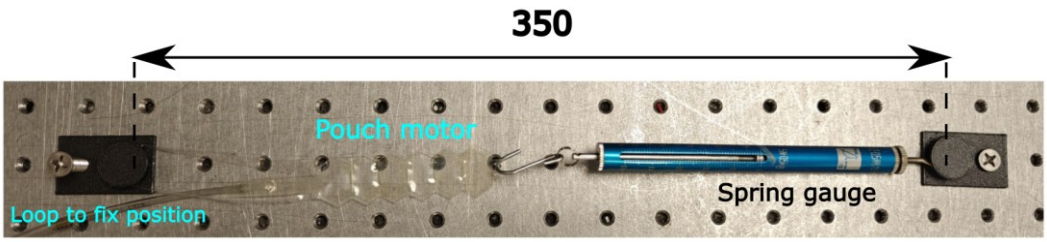

Figure 5.3 Setup to determine contraction ratios and maximum volumes of the different flexor actuators. Dimensions are in mm.

To measure the restoring force of each actuator at maximum inflation, actuators were hung vertically from a table. The syringe that inflates each actuator was fixed in position on the table, and calibrated weights were added in 50 g increments after inflating to the maximum volume. A tee connector connected the actuator and syringe to a pressure sensor (MS5803-14BA Breakout SEN 12909), which measured the pressure to ensure this was similar between actuators. Each trial was repeated four times for each shape actuator and as a single- and dual-actuator setup. Single-actuator setups were inflated in 0.2 ml increments with a 5 ml syringe and dual-actuator setups were inflated in 1 ml increments with a 20 ml syringe connected with a tee connector. A camera, which was placed directly in front of the hanging actuator, recorded each trial and actuator lengths were measured post-recording using the screen ruler available in Microsoft PowerToys. The experimental set-up is shown in Figure 5.4. To mitigate the effect of parallax errors in recording actuator lengths, the camera and tripod were set

to the same height from the floor at each trial, and the same length tubing was used when hanging the actuator off the table. This ensured any parallax error would be consistent across trials and comparisons would remain reliable. The stroke length (L_{stroke}), and stroke ratio (L_{sr}) were calculated as follows:

$$L_{stroke} = L_0 - L(\theta) \tag{14}$$

$$L_{sr} = \frac{L_0 - L(\theta)}{L_0} \times 100\% \tag{15}$$

where $L(\theta) = L_0 \frac{\sin\theta}{\theta}$. This means the theoretical maximum contraction occurs at $\theta = \frac{\pi}{2}$, giving a stroke ratio of 36.3% (278).

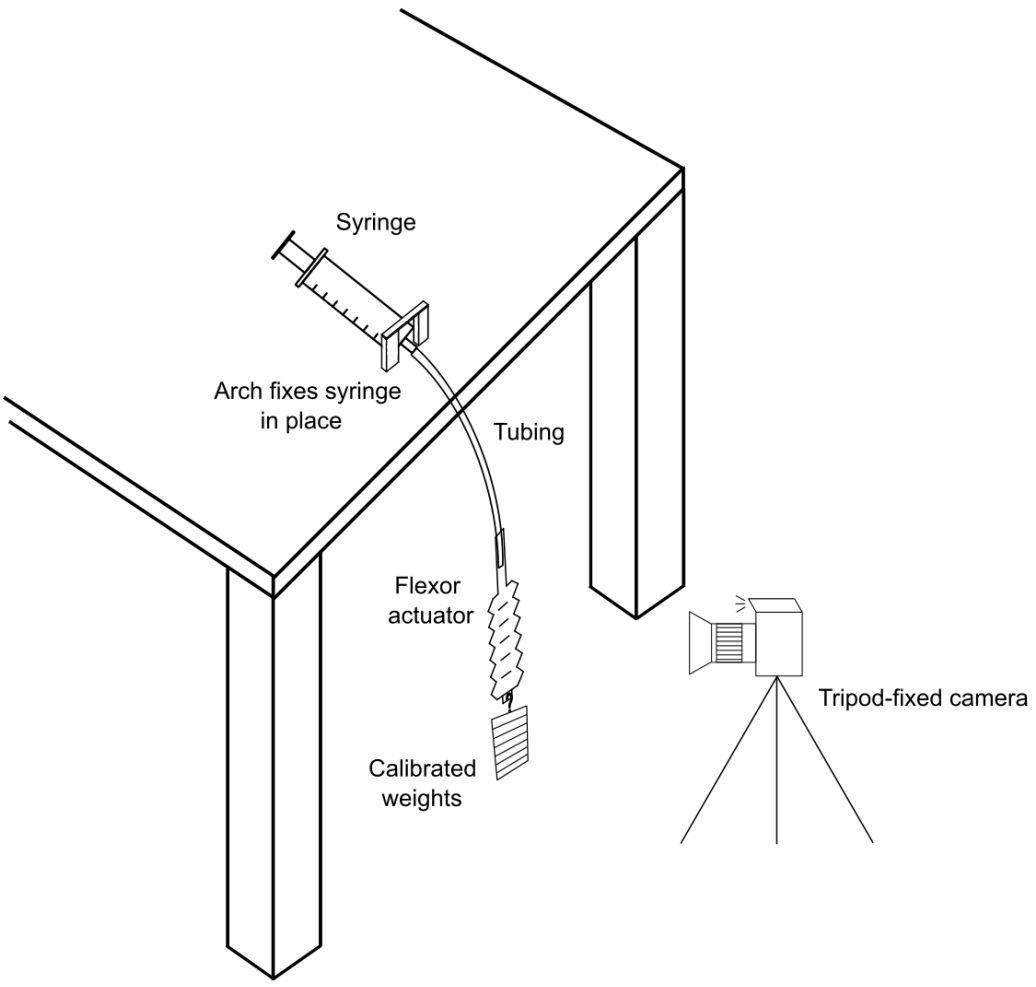

Figure 5.4: Experimental setup assessing the actuators' load bearing capacity

Bending resistance was tested by fixing prototypes to an optical table and attaching a spring gauge at 215 mm and 55° to the longitudinal axis (Figure 3). The main actuator was inflated to 11 ml, as previously this was found to burst at 12 ml. The flexor actuators were rounded down to the nearest 0.2 ml of the average maximum volumes. Actuators were fully inflated and clipped closed before attaching the spring gauge to the device. Force readings from the spring gauge were recorded for each shape actuator, and single- and dual-actuator setups. Angles were measured using an on-screen protractor from recorded videos. The angles were defined as the angle between the longitudinal axis of the base of the device, and the front wall of the device (Figure 4).

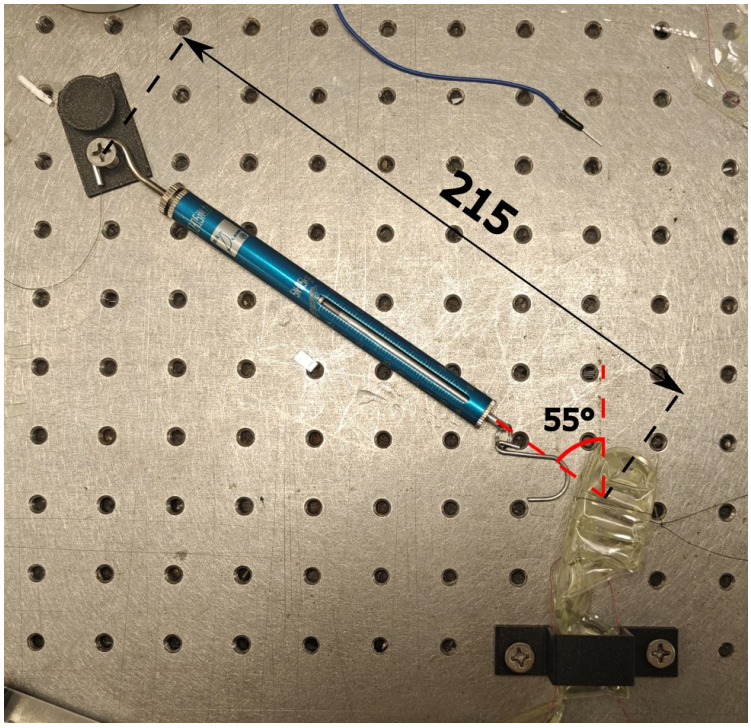

Figure 5.5 Experimental setup to determine the bending resistance of each prototype device with a differently-shaped flexor actuator and multiple flexor actuators. Dimensions are in mm and degrees.

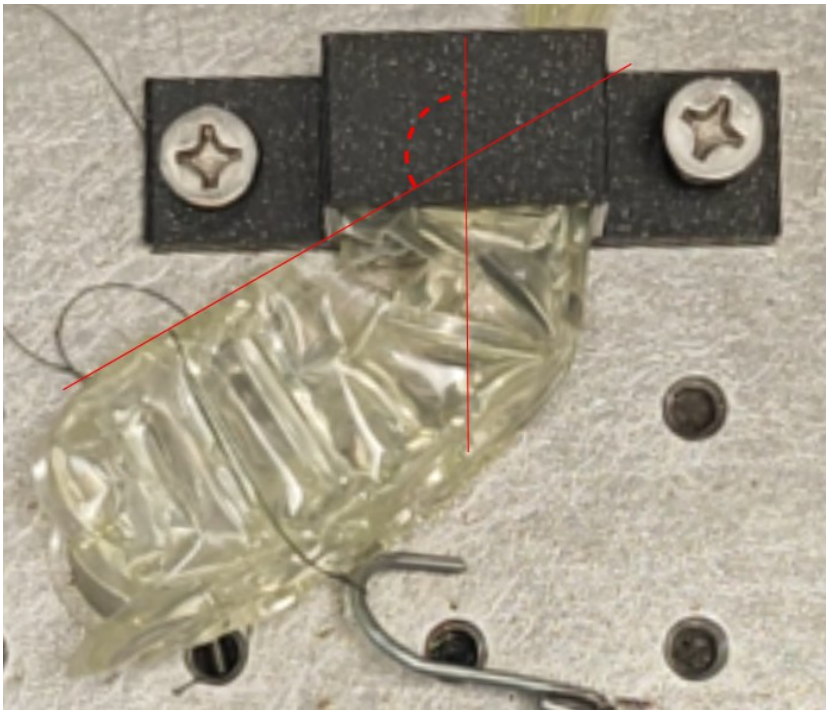

Figure 5.6 The angle of the device was defined as the angle between the longitudinal axis of the device and the front wall of the device

5.2.3 Results

As mentioned in the methods, the NWE pouch maximal inflation volume was lower than the conical pouch. Because of its crinkling it had a slightly lower contraction ratio than the conical and MWE pouch. The rectangular actuator exhibited the same behaviour but worse, with consequent lower volume and contraction ratio. The visual behaviour of each actuator is shown in Figure 5.7 and each actuator's characteristics, such as average maximum volume and stroke length, are summarised in Table 5.2. Because the NWE and rectangular pouch exhibited crinkling and buckling on the edges, with a lower inflated volume, these pouch motors were not investigated further. This thesis does not model the mechanical behaviour of these actuators but rather focuses on identifying improved designs to optimise and enhance the bending resistance of the existing device. The MWE and conical actuator had similar volume per actuator, allowing for appropriate comparison of their shapes and how the shape difference impacts performance. The load pulling capacity and contraction efficiency was also similar. The performance of the dual conical actuator is also shown to confirm the dual actuator configuration does not affect individual actuator performance. The

volume per actuator and contraction ratios were similar. The dual conical and single EWE actuators could hold a load of over 550 grams before the tubing failed where the actuator would detach from the tubing. No internal or external welds failed; the actuator could comfortably hold 550 grams, but the tubing was the limiting factor. The EWE actuator had significantly more volume and slightly more contraction at maximum inflation.

Table 5.2 Characteristics of the different shapes of actuators

	Volume per actuator (±SD) (ml)	Average failure load (±SD) (grams)	Average maximum contraction length (±SD) (mm)	Average maximum contraction ratio (±SD) (%)
Single conic	3.02 ± 0.12	212.5 ± 62.5	14.1 ± 1.1	19.2 ± 1.2
NWE	2.64 ± 0.17	212.5 ± 62.5	13.6 ± 0.4	18.8 ± 0.6
MWE	3.08 ± 0.18	225.0 ± 28.9	14.2 ± 0.9	19.4 ± 1.2
EWE	3.28 ± 0.23	>550	15.4 ± 0.3	21.2 ± 0.5
Single rectangular	2.76 ± 0.09	N/A	10.1 ± 1.0	13.9 ± 1.4
Dual conic	3.02 ± 0.12	>550	14.1 ± 1.1	19.2 ± 1.2

The stroke ratios for each actuator change with increasing load, shown in Figure 5.8. The conic and elliptical actuators had a similar drop-off in stroke ratio as the load increased to 150 g, beyond which the actuators failed. A dual conic actuator setup holds close to its original stroke ratio for much longer. At a load of 300 g, the average stroke ratio was 15.8%. The EWE actuator had a similar slope to the dual conic actuator. At 300 g, the average stroke ratio for the EWE actuator was 17.1%.

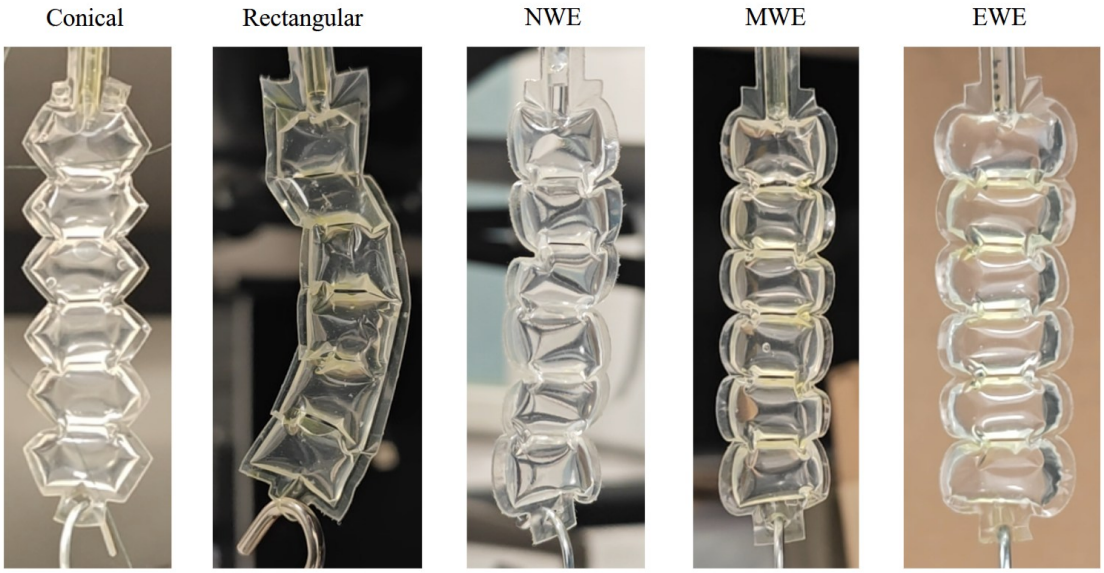

Figure 5.7 Each pouch motor shape type visualized once fully inflated with water. Buckling and crinkling is visible on the NWE and rectangular pouch motors. NWE = narrow-width elliptical; MWE = medium-width elliptical; EWE = extra-wide elliptical.

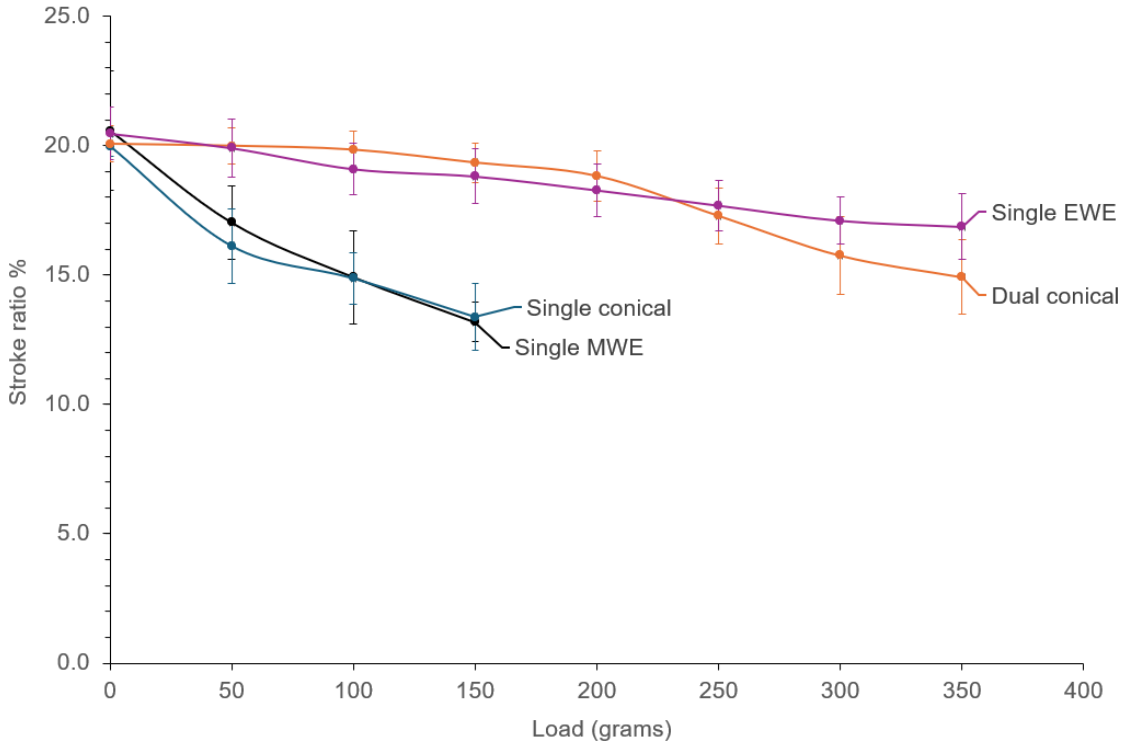

Figure 5.8 Maximum stroke ratio (stroke length as a proportion of uninflated length) vs load pulled.

The actuators underwent pressure changes as they held different loads, with the same inflation of volume. As shown in Figure 5.9, all three configurations (single conical, dual conical, and single EWE) had similar pressure-stroke gradients at no load. At 150 g, the single conical actuator had significantly higher pressures at similar stroke ratios to when it had no load. This pressure-stroke gradient is comparable with the dual conical configuration pulling 300 g. The single EWE actuator had a similar pressure-stroke gradient at 300 g, offset by about 10 kPa.

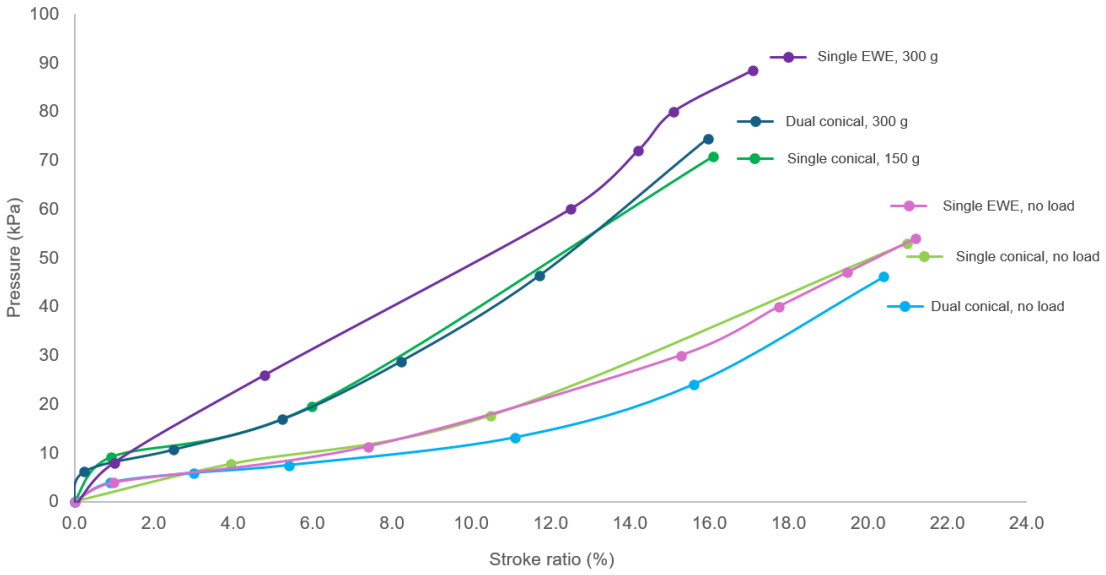

Figure 5.9 Changes in pressure with stroke ratio for the different actuator iterations holding either no load, 150 grams, or 300 grams. EWE = Extra wide elliptical.

To explain why the single EWE actuator had a similar pressure-stroke gradient at 300 g as that of a dual conical setup, despite only a ~15% increase in volume, a comparison of pressures at maximum volume under increasing load was conducted. Both actuators were set up as described in section 5.2.2, hanging vertically with the syringe fixed. Actuators were inflated to maximum volume, after which the supply tube was clipped to maintain a fixed volume. Increasing loads from 0 to 500 g were then applied and corresponding pressures measured.

The pressures, at maximum volume, when pulling a load of 0-500 grams in a dual conical setup and a single EWE actuator are compared in Figure 5.10. Both setups rapidly rise in pressure with a load of 150 g and then plateau in pressure

at 300 g and beyond. The single EWE actuator plateaued at around 10-13 kPa higher than its dual conical counterpart.

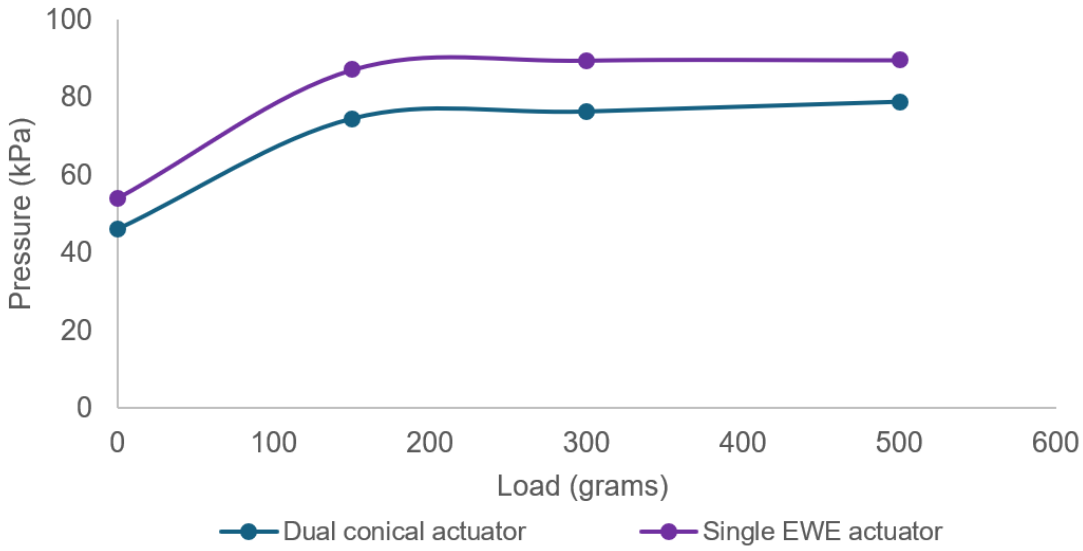

Figure 5.10 Internal pressure at maximum volume plateaus as the load increases on the actuators. EWE = Extra wide elliptical

Table 5.3 and Figure 5.11 compare the bending resistance of the EWE actuator to the conical elliptical actuator. Table 5.3 shows the angle of the device with and without a spring gauge pulling on it as in Figure 5.5, depending on what flexor actuator setup was inside the device. Figure 5.11 shows the force expressed by the spring gauge in these cases.

The conical and normal-width elliptical actuator have the same force expressed on the spring gauge as it resists opposing bending action (Figure 5.11), regardless of tendon length. The dual actuator setup had an increased force expressed on the spring gauge in response to opposing bending action. Here again there was no difference between the conical and normal-width elliptical setups, regardless of tendon length. This translated into the device's angle at baseline and with spring gauge as well. The normal-width elliptical actuator had angles within 1.0° of the conical actuator, with a single and dual-actuator setup. For this reason, the normal-width elliptical actuator is not included in the

visualisation in Table 5.3. Instead, the conical actuator is directly compared to the EWE actuator. This is also more relevant because the elliptical actuator does not touch the inner edges of the device's main actuator and so there is no cutting risk. The conical and EWE actuators do touch the inner edges of the device, so this comparison is more useful. The single EWE setup performs similarly to the single conical setup, at baseline and with a spring gauge pulling. Figure 5.11 also shows the force is the same for a single elliptical as that of a dual conical flexor setup. This is where a dual EWE setup outperformed every other setup. The dual EWE setup had an angle of 122.8° and a force of 0.72 N pulling on the spring gauge. This is a 36% increase in the holding force of the dual conical actuator while maintaining a 3° reduced angle.

Table 5.3 Measured angles of the device at maximum contraction of the flexor actuator, depending on the number of actuators and shape of the sub-actuator, and whether a force is applied to it with a spring gauge

	Single conical	Dual conical	Single EWE	Dual EWE
Angle at baseline				
Angle with a spring gauge				

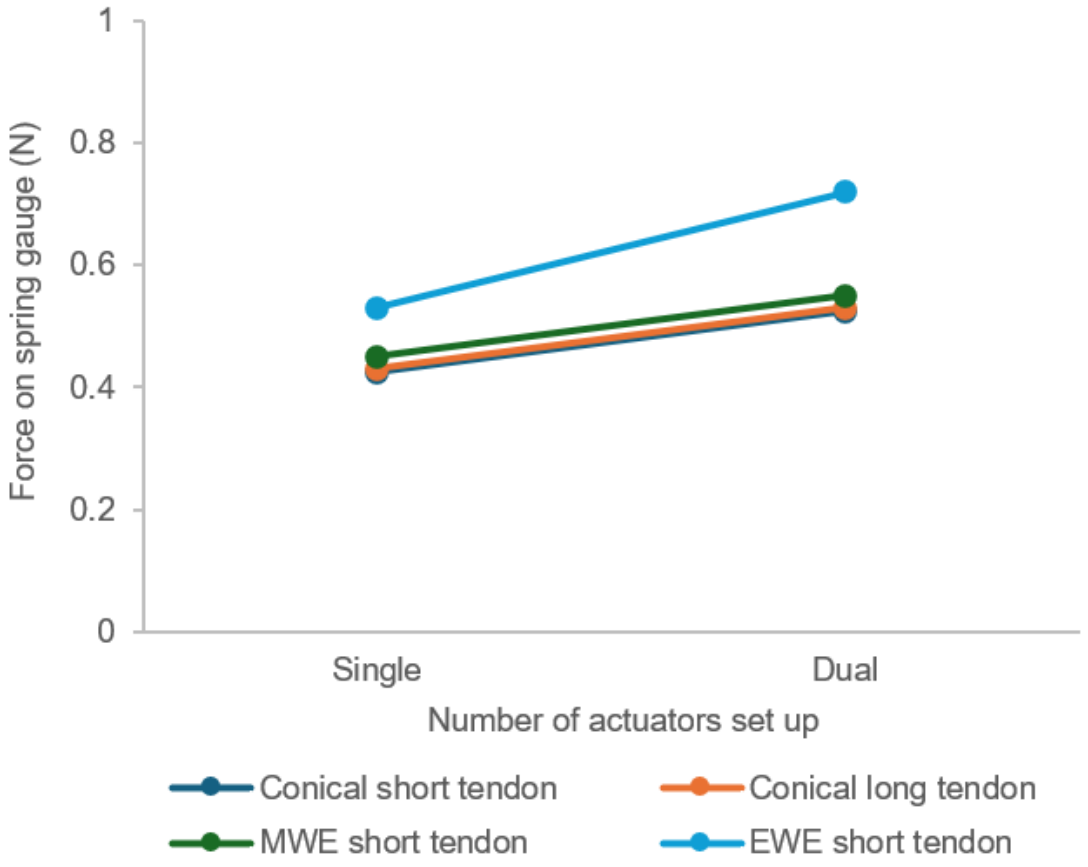

Figure 5.11 The mean force measured on spring gauge in the bending resistance trials for a single or dual flexor actuator setup for each type of actuator.

5.2.4 Discussion

The dual EWE flexor actuator had the highest bending resistance among the tested designs. While the NWE actuator performed comparably to the conical actuator, for a given volume and pressure, the EWE actuator outperformed the conical design because of its greater volume and pressure capacity. This meant the EWE actuator matched the performance of two conical actuators, despite only a ~15% increased volume. This is partially in agreement Niiyama et al.'s work (282) with but a more detailed discussion on why follows below.

The rectangular actuator's poor contraction ratio was expected, as its edges crinkled during inflation, limiting full contraction (Figure 5.7). In contrast, the conical actuator's shape prevented this issue. The better performance in the dual conic setup in Figure 5.8Figure 5.9Figure 5.11 was expected as two actuators

holding the same load means the load per actuator is halved. The EWE actuator's performance, similar to a dual conical setup despite only a 10-20% volume increase, was unexpected. This can be attributed to pressure differences and the material's viscoelastic properties, as explained by Laplace's Law, where wall tension increases with pressure, *P*, and radius, *R* (309).

$$T = PR$$

The rectangular actuator's poor contraction ratio was expected because of its shape: the edges of the rectangular actuator would crinkle and buckle with inflation, preventing full contraction of the actuator (Figure 5.7). This is why the conical actuator is more effective; the conical edges do not bend this way. The EWE elliptical actuator had a similar slope to the dual conic actuator which was unexpected since the additional volume is only 0.28 ml, on average, or an extra 9.3%, and it is only one actuator holding the weight versus two conical actuators.

The results from 3.7 and 3.8 are unexpected, as they suggest the restoring force of a single EWE elliptical actuator is roughly the same as that of two conical actuators, despite only a ~15% increase in volume per actuator. The similar pulling capacity and contraction ratio between these two setups is partially explained by the pressure difference (Figure 5.9) and Equation 3. According to Equation 3, increasing the load on the actuator increases the pressure for a given volume and contraction ratio. As shown in Figure 5.9, pressure rises rapidly when a 300 g load is attached, while the stroke ratio is slightly reduced (Figure 5.8). Since water is incompressible, it was assumed the cross-sectional area remains constant when the actuator is at its maximum contraction ratio. If the cross-sectional area remains constant, then to maintain the stroke ratio with increasing load, a constant cross-sectional radius is required. According to Laplace's Law (309), as the load is increased and increases the tension in the pouch membrane, the pressure inside the membrane must increase. However, this does not occur: Figure 5.10 shows the pressure plateaus with increased load. Since the pressure plateaus with increased load, and therefore increased wall tension, the cross-sectional radius must increase, which explains the reduced contraction ratios. Since water is incompressible, the initial assumption that the cross-sectional area

remains constant may be wrong. The cross-sectional area likely increased as the pressure plateaued. This may happen with some degree of stretch. While the material was thought to be inextensible, Chapter 4.6.7 showed that these thermoplastic sheets exhibit viscoelastic behaviour. The lowered stroke ratio and stretch over time with increasing load may be accommodated by the material's viscoelastic properties. The EWE actuator's larger stroke ratio at baseline (Table 5.2) and smaller cross-sectional radius allow higher pressures for the same maximum tension (Figure 5.10), and greater stretch under load for the same stroke ratio. Future work to characterise the tensile strength of the film material would help to confirm this. Additionally, the wall tension in the EWE actuator may be better distributed along its weld pattern. The triangular pattern may have a high concentration of tension at the edge where the weld pattern converges. This could be investigated by changing the "slope" or aspect ratio of the triangular ends of the conical actuators, while maintaining constant volume. A more acute triangle would be hypothesised to be more likely to fail whereas a more obtuse edge would be more likely to allow some degree of stretch. Regardless, the current data do not fully explain why the EWE elliptical pouch had such a disproportionately better performance than the conical pouch. Nevertheless, this subchapter aimed to, and successfully did, improve the bending resistance and longevity of the device

Table 3.3 shows that, in some trials, the main actuator had some motion within the placeholder as the spring gauge pulled on it. In these cases, the longitudinal axis of the device did not align with the longitudinal axis of the placeholder in the single EWE image. However, the longitudinal axis of the device was still clearly visible and measuring the angle of the tip relative to the base was still possible. For force measurements, the device had to be manually reset into place and held by the base to ensure correct readings of the holding force by the flexor actuator.

Stroke ratios in this study are lower than other film-based actuators described in the literature. This may be because of the use of thin (0.065 mm) material and limited hydraulic pressurisation of 70-90 kPa, whereas others inflated to high pressures, enabling more compression. Niiyama et al. (310) used thicker (0.102 mm) polyethylene sheets, achieving a 28% contraction ratio and 100 N force

output at 40 kPa and larger pouches (75 mm x 25 mm). Li et al. (283) used thinner polyurethane films, which has higher tensile strength than polyethylene, in Origami pouches, reducing edge crinkling. They also used larger pouch sizes (70 mm x 70 mm or 70 mm x 140 mm). Lee et al. (293) achieved contraction ratios up to 90% with bellowed actuators, which are often fabric-based in wearable soft robotics, but comfort for skin contact remains underexplored. One study found that rounded fabric bellowed actuators were more comfortable for infants, while maintaining performance (301). Rounded edges distribute pressure more evenly reducing tissue damage. The elliptical actuator, a novel design, offers potential for wearable robotics by improving comfort and safety (311,312). This design could inspire further advancements in film-based pouch motors for soft robotics application.

Future work involves validating the device in a rectal phantom. This includes integrating the dual elliptical flexor actuators and testing the device's ability to stabilise the rectum and lock its angle. The elliptical shape of the flexor actuator reduces leakage risks compared to the conical design, while maintaining potential for single-syringe control for self-insertability. Next, elongated tubing with a rigid tip will be developed to prevent folding during insertion, ensuring the device remains self-insertable for pelvic radiotherapy applications.

5.2.5 Conclusion

The elliptical pouch motor design succesfully improves the bending resistance and performance of the existing endorectal actuator. This elliptical design reduces the sharpness of the edges that pose cutting risks and discomfort. It improves the longevity and performance of devices like this soft inflatable endorectal actuator but also may allow improved comfort and safety of film-based actuators in wearable soft robotics. The additional volume in the EWE actuator contributes to greater force exertion to angle device. The addition of an extra actuator further emphasises a stronger force holding the device's angle. Together, this endorectal actuator is more likely to adequately meet Criterion 3 (retracting the rectum) as not only does it reach the desired angle, but it can resist more force that would pull the device away from this angle.

5.3 Additional modifications to device

At this point, some modifications were made to improve the device that cannot be directly quantified. These modifications are that the main body of the endorectal actuator consists of three sides instead of four sides, and the tubing was pushed all the way into the device to reach the tip, rather than just the inlet. This assists with insertion where the endorectal actuator can be pushed in from the tubing as it pushes on the top of the device. This also prevents the device from folding on itself axially as it is inserted in the rectal phantom in the next chapter.

5.3.1 Three-sided device

The main body of the endorectal actuator consists of a three-sided dual truncated prism instead of four sides. This is because of the shearing found earlier in 4.6.6. A three-sided device does not undergo this shearing on inflation. The design specifications of the main actuator are outlined in Figure 5.12. The fabrication method is also outlined. Because the device is three sided, each side was made wider than before to ensure the volume it occupies on expansion remains roughly the same. The device is made of two sides at 32 mm each, and the anterior side is 40 mm. The anterior side is slightly wider to allow for space for a central channel which the tubing is inserted and slid into, which is explained further in the next subchapter.

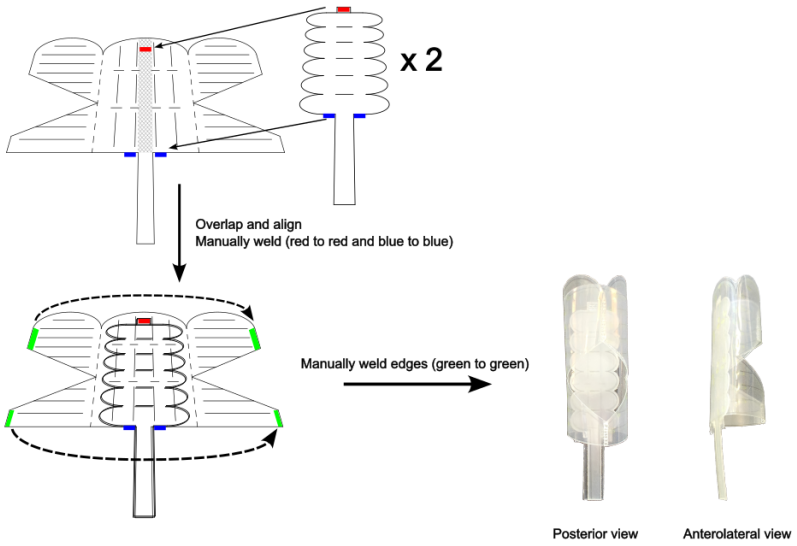

Figure 5.12. Fabrication of the modified soft hydraulic endorectal actuator.

The volume was calculated by taking the cross-sectional area of the triangular shape and multiplying it by length. The cross-sectional area was calculated by measuring the anterior side of the device and take this as the “base” of the triangle, and the anterior-posterior width of the device as the “height” of the triangle accordingly. This area was multiplied by the length of the device to obtain the volume.

Table 5.4 Dimensions and expansion ratio of the three-sided device across its different states of inflation.

	Undeployed, folded	Deployed uninflated	Deployed and inflated
Shape	Flat sheet	Triangular prism	Triangular prism
Dimensions (ant side, AP width, length)	6 x 15 x 91 mm	36 x 30 x 91 mm	23.5 x 40.5 x 88.5 mm
Volume, V	8.2 cm^3	49.1 cm^3	42.1 cm^3
Ratio $V:V_{deployed}$	1:5.13	1:0.86	1:1
Volume change, %	80.5%	-16.7%	-

Consequently, a wider elliptical flexor actuator could be employed as there was more space available within the device. Given the greater restoring force of the elliptical actuators compared to conical ones, elliptical actuators were employed. Because the three-sided main actuator was wider, it provided additional space for the flexor actuators, prompting the design of an elliptical pouch motor wider

than those described in 5.2.1. These are extra-extra wide elliptical (XXWE) actuators and their dimensions are outlined in Figure 5.13. Two of these actuators were employed in the endorectal actuator.

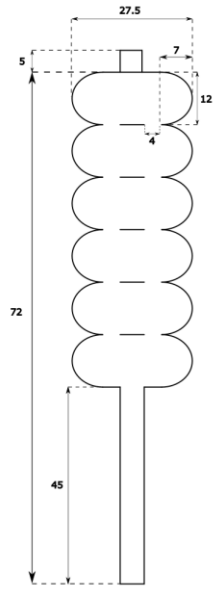

Figure 5.13 Dimensions of the XXWE (Extra-extra wide elliptical) actuator

5.3.2 Making the device self-insertable

The device needs to have a method of being insertable into the rectum by the patient. Self-insertion by the patient allows for positional feedback and would not make the device a burden on staff resources. On initial trials in a rectal phantom, the endorectal actuator will just dig into the inner side of the rectum as it is inserted. Since the actuator is of a soft material and flimsy when uninflated, it just folds and does not hold shape when pushing it from the bottom of the device. It collapses axially before it can be fully inserted into the rectum and inflated.

The tubing used to inflate the main actuator is now inserted and routed fully to the tip of the device. This design enables the device to be advanced from the top of the device rather than the bottom, enabling one-handed insertion by holding the tubing at the inlet, like a catheter.

5.4 Adding fiducial markers

Criterion 6 of the thesis is for the endorectal actuator to be used as an IGRT tool. ProSpare™ does this with steel ball bearings inside the device and improves outcomes in pelvic radiotherapy this way. To incorporate radiopaque markers into this device, steel discs were initially explored. Discs were punched from a 0.05 mm feeler gauge using a 5-mm leather hole puncher. The intent was to incorporate these 5-mm discs into the laser welding fabrication process of the device. After the dye had been applied these discs could be placed on top of the first layer of plastic before placing the second layer on top. A small circular weld would enclose each steel disc. The hypothesis was that these feeler gauges are thin, and good contact could be achieved despite placing something in between the plastic layers to be welded. However, because they were so thin it meant it was too delicate to work with. It was cumbersome to precisely place the thin discs in the right place to align with the prescribed pattern and no devices were produced with this method. Instead, metallised thermoplastic films were obtained which could be cut into discs and incorporated easily into the device via manual welding. No precision is required here to align with the g-code of the laser welder.

5.4.1 Methods

A triple laminate thermoplastic sheet (Camplex® Thermal by Camvac International) of 30-micron PE, 12-micron metallised PE, and 35-micron PE was cut into 5 mm diameter discs using Beamo laser cutter. These discs were manually soldered to the inside of the main body as highlighted in Figure 5.14 below. The main body was then folded into its truncated prism shape as usual. The discs were placed here as this is the anterior side of the device when inflated. It was hypothesised the discs would show the anterior side of the device on CT scan to localise the anterior rectal wall, like ProSpare's steel ball bearings (224).

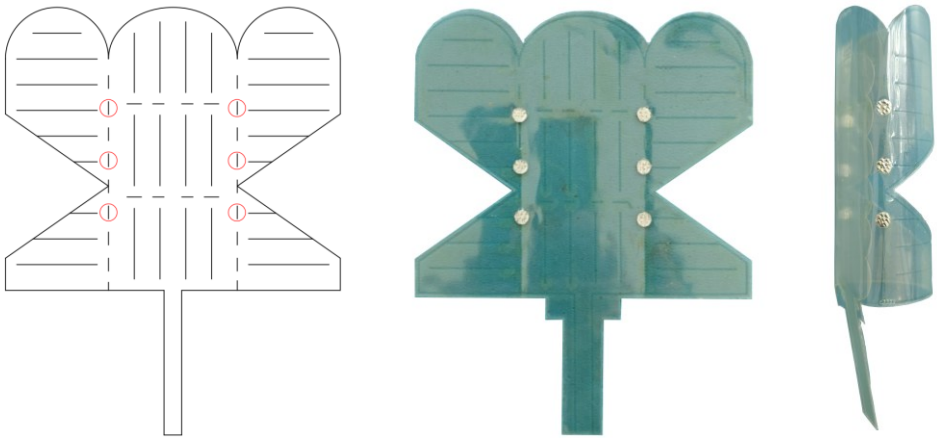

Figure 5.14 The main body of the endorectal actuator embedded with metallised thermoplastic. Left: Red circles denote where the metallised plastic was manually welded before 3D folding of the device. Middle: Metallised plastic manually welded on the main body before assembly. Right: The assembled device with aluminium markers clearly visible.

The endorectal actuator was assembled and inflated with water as per the author's previous methods. The device was inflated and placed on the CT bed (Figure 5.15) before and scanned using a brain scan protocol for the highest possible resolution. The CT scanner used was a SOMATOM Confidence® RT Pro by Siemens Healthineers and was set to 120 kV with a 0.6 mm slice thickness. Angelos Vasilopoulos ran the scan and exported the images as DICOM files for the author to process on 3D-Slicer software.



Figure 5.15 Inflated endorectal actuator placed on CT bed prior to scan.

5.4.2 Results

The CT scanner obtained 70 images at 0.6 mm slice thickness. Figure 5.16 shows the sagittal and transverse views of the device. The corrugations of the inflated sides and the contracted pouch motor inside the device are visible. The aluminium markers could not be seen on any images.

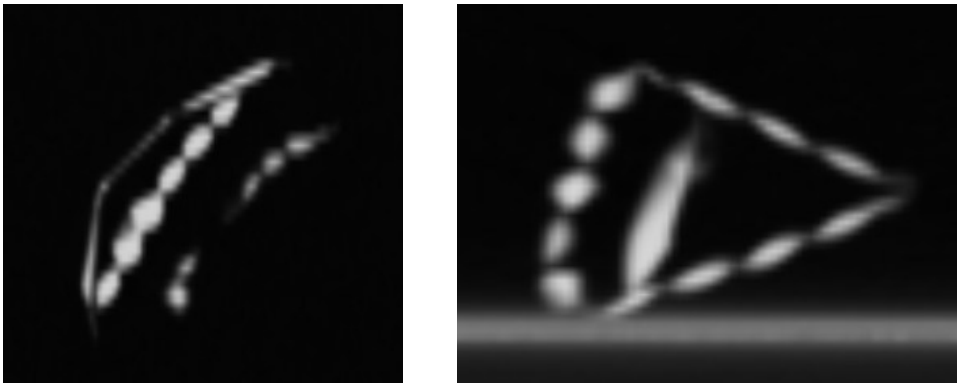

Figure 5.16 Three-dimensionally reconstructed CT view of the endorectal actuator in the sagittal plane (left) and transverse plane (right).

5.4.3 Discussion

The device itself was visible but the aluminium markers were not. The device was visible because it was filled with water and placed in air. The markers were not visible, likely because the markers were too thin and not of a dense enough metal to show on imaging. The metallised plastic was a triple laminate with a total thickness of 77 micrometres. This is less than 0.1 mm and would not show on imaging when the material is not a dense metal. The medical physicists Rollo Moore and Angelos Vasilopoulos suggested this is too thin to show on imaging due to the slice thickness of the images. The metallised plastic was used because it was easy to incorporate into the device. Gold pellets would show up imaging, but they would have the same limitations as the steel feeler gauges discussed earlier. Gold pellets can be placed between the thermoplastic sheets during laser welding but need to be of a small enough size to maintain sufficient contact between the sheets. It is suspected that the size required to maintain adequate contact would render the fabrication of the device too delicate and difficult to reproduce. If thermoplastic can be metallised with copper or gold instead, these can be manually welded following laser welding. These metals are presumed to be sufficiently dense to show on imaging owing to their higher atomic number. However, a dense metal would pose additional challenges such as artifacts on planning scans, affecting dose calculations. The corrugations on the device are visible which is promising. Since the device is in air, the water is visible as it is contrasted to the air surrounding the device. In a rectum, the device would likely not be visible as it is surrounded by organs that are primarily water. The water that normally inflates the device could be replaced with a radiopaque liquid such as barium sulphate or iodine. These are contrast agents used in gastrointestinal and arterial imaging, respectively. These are safe to ingest and therefore would be safe to use in the device. Future work should confirm the visibility of the device inflated with a contrast agent in a water phantom under CT imaging. Due to time constraints during this project, the author was unable to explore this himself.

Chapter 6 Validating the endorectal actuator inside a rectal phantom

6.1 Introduction

This chapter presents the fabrication of a rectal phantom that exhibits mechanically accurate tonal properties, followed by its validation and the validation of the endorectal actuator inside the phantom. Chapter 4 presented initial validations of the endorectal actuator with benchtop force/torque sensors but lacked a clinically applicable simulation. This work presents the fabrication and validation of a rectal phantom with biomechanical properties—compliance and capacity—representative of a healthy human rectum. The phantom uses motor-controlled elastic ribbons that simulate peristaltic variations in rectal motion and rectal tone, enabling an assessment of the device's ability to resist the dynamic compression and reduce variations in rectal volume. This study also aimed to assess the device's ability to reproduce rectal volume and anorectal angle on insertion. Reproducing the anorectal angle would allow the device to "lock in" the rectum and act as a spacer by pulling the ARW away from the target volume. These assessments gauge whether the device would improve radiotherapy outcomes. This chapter is based on (313).

The author of this thesis designed the rectal phantom with input from Dr Reza Haghighi Osgouei and Dr Emma Carrington. The author then fabricated the phantom and borrowed Dr Emma Carrington's equipment to validate the phantom. The author of this thesis carried out all experimental work, data collection, and data analysis of validating the device inside the phantom.

6.2 Materials and methods

The properties the phantom must emulate for mechanical representation are rectal anatomy, accurate fracture and tone properties, and the ability to translate and rotate about the anorectal angle. The anatomical properties of the rectum to emulate are rectal diameter and wall thickness, anal canal length, rectum length,

and anorectal angle. Table 6.1 summarises the quantitative ranges to emulate these properties with references.

Table 6.1: Desired ranges of anorectal properties to emulate in the rectal phantom

Property	Range	References
Rectal diameter	30-40 mm	(123,314)
Wall thickness	1.6 – 4.5 mm (median 2.6 mm)	(315)
Anal canal length	25 – 53 mm	(246,316)
Rectum length	80 mm	(314)
Anorectal angle	85° – 125°	(244)
Tensile strength	0.84 MPa	(317)
Rectal compliance	Low	(122,318,319)

Dal Lago et al. reported the radius of the rectum at first sensation or sensation of gas at low pressured distension using a barostat balloon and MRI. They reported a rectal radius of 19.9 mm using MRI and 18.7 mm using an electronic barostat at a pressure of 7 mmHg. The lowest rectal cross-sectional area reported by Dall et al. (123) was approximately 800 mm^2 at a distension pressure of less than 2 mmHg. This corresponds to a radius of approximately 16 mm. To reflect this range, the rectal phantom was designed as a silicone cylinder capable of contracting to a 30-40 mm diameter, which represents the rectum at rest.

Rectal wall thickness, ranging from 1.6 to 4.5 mm (315), affects fracture properties and is important for safety assessment of the device. Initial attempts to cast a phantom with a 1.5 mm wall failed because of wall tearing during silicone demoulding. A 2.5 mm rectal wall was adopted instead.

The anal canal ranges from 25-53 mm in length. Following Dal Lago et al. (314) who assumed an 8-cm long cylinder in their volume and radius calculations, a straight 80 mm cylinder was chosen for the phantom. This excludes the sacral flexure (320) which is not a region of interest to the clinical assessment of the endorectal actuator. As discussed in Chapter 2, the anorectal angle can range from 85° to 125°. Here, a thick elastic band that wraps around the phantom is incorporated, inspired by Stokes et al.'s defecatory model (317).

Emulating mechanical properties was emphasised to directly assess the endorectal actuator's radial stiffness in a more clinical context. Cadaveric studies show the ultimate tensile strength of passive rectal tissue is 0.84 MPa with failure at 62% strain (321). Ecoflex™ 00-10 silicone, with a tensile strength of 0.827 MPa (322), was chosen to match this. Matching the tensile strength ensures the phantom exhibits realistic fracture properties. However, this silicone has a low elastic modulus (0.05 MPa) (323) which does not adequately represent rectal tone. In vivo, the rectum is an active organ that resists expansion (122,123,319), maintaining itself within a physiological expansion range of 0-35% (317). Rectal compliance values vary widely within the literature: Papaconstantinou shared a normal range of 3-15 ml/mmHg (318); Van den Berg et al. found a mean rectal compliance of 16 ml/mm with a 5th-95th percentile range of 12-20 ml/mmHg in their study of healthy adolescents (122); And Fox et al. reported a mean rectal compliance of 11.9 ml/mmHg (range 13-38 ml/mmHg) (319). Additionally, it is unclear what volume ranges these compliance ranges correspond to. Because of these large, reported variations in rectal compliance, a phantom with deliberately low compliance was designed. This approach enabled a harsher assessment of the endorectal actuator: if the endorectal actuator can reproducibly expand the phantom to a stable volume despite the phantom's high resistance to distension, the actuator is likely to perform reliably in patients and improve radiotherapy outcomes.

6.2.1 Fabrication of phantom

The rectal phantom was fabricated by casting silicone (Ecoflex™ 00-10) in a 3D-printed cylindrical mould. The cure formed a 120 mm long tapered cylinder, with an inner diameter of 50 mm at the proximal (rectal) end and 23 mm at the distal (anal) end. The "anal canal" is 25 mm in length and conically tapers to the 50-mm rectal diameter. A tapered design was made because the rectum narrows as it transitions to the anal canal. The phantom had a 2.5 mm wall thickness.

A silicone flange was attached to the distal end and bolted to a 3D printed flange to suspend the phantom in the air. Additional flanges were placed at 30mm, 70 mm, and 120 mm along the length, allowing elastic bands to connect the phantom

to a proximal flange. This proximal flange suspended the phantom in the air while permitting anterior-posterior motion. Tone was induced using four NEMA17 stepper motors and elastic ribbons (Trimming Shop, Hamburg, Germany). To reduce friction between the ribbons and the silicone material, a fabric mesh was wrapped around the silicone rectum before wrapping the ribbons around it. Two elastic ribbons (5 mm wide, 1 mm thick) were wrapped around the motor shafts before being looped twice around the phantom. The proximal ribbon was 60 mm in length and the distal ribbon 50 mm. A thick elastic band (50 mm wide, 5 mm thick) was placed 25 mm from the distal end and looped around a 3D printed hook that was bolted in place. This band simulated the puborectalis muscle and creates the angle of the rectum. Figure 6.1 shows a beam-eye view of the phantom with directional references and motors labelled. A 30 cm ruler is placed on the optical platform for image and video calibration.

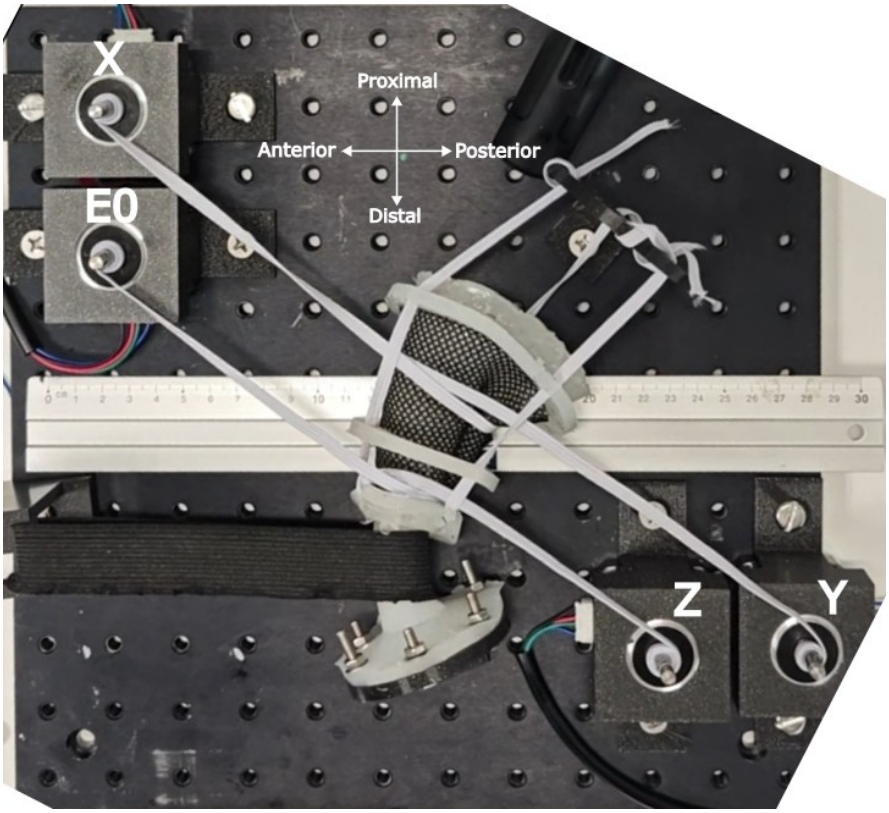

Figure 6.1. Rectal phantom used to validate the endorectal actuator. Stepper motors are labelled. Orientation cross shows the anatomical directions of the phantom.

6.2.2 Validation of phantom

A barostat balloon was used to assess whether the rectal phantom is mechanically representative of a healthy rectum. The phantom was validated with a barostat balloon connected to a rapid barostat bag pump (Mui Scientific, model #P1-RBB-1). The barostat balloon was inserted into the rectal phantom with a water-based lubricant until the 5 cm mark aligned with the phantom's "anal canal". This is in line with manufacturer's instructions (324). On the pump, the maximum bag pressure was set to 40 mmHg, maximum bag volume to 700 ml, inflation rate to 120 ml/min, and deflation rate to 180 ml/min. A rapid barostat bag (RBB) test was performed by following instructions displayed on the pump screen: the balloon was emptied and then automatically inflated while recording pressure and volume. The balloon was inflated to the maximum bag pressure. No sensation test was conducted. Raw data from each RBB test were exported via USB and analysed in MS Excel. Rectal capacity tests were performed across four levels of simulated "muscular tone", determined by the number of revolutions each elastic ribbon made around the motor shafts. The first level of tone was defined as barely taut elastic ribbons around the phantom. The number of revolutions the elastic ribbons made around each motor shaft was noted for this level of tone. Tone was increased with one additional revolution around each motor shaft, up to three additional revolutions. Rectal compliance was taken as the slope of the pressure-volume curves over three volume ranges: 40-60 ml, 60-100 ml, and 100 ml to rectal capacity. These ranges were chosen because a steep inflation curve below 40 ml was observed, where the balloon fills an empty rectum with no external resistance. The rectal compliance should decrease with increasing volume (123), this property was also validated in the phantom. The 40-60 ml range is most relevant because this is the endorectal actuator's operating range; the deployed volume of the inflated actuator.

6.2.3 Validating the elastic ribbons

The elastic ribbons used to contract the rectum were validated to ensure consistent stress-strain behaviour. Consistent contraction of the elastic ribbons ensures the motor-controlled elastic ribbons provide reproducible volume

changes in the rectal phantom. Reproducible volume changes are essential to draw reliable conclusions about the clinical efficacy of the endorectal actuator. The elastic ribbons were laid flat on a desk with one end fixed with duct tape. The other end had a small slit to hook a spring gauge onto. A 5 m tape ruler was placed next to the ribbon to measure the changing length of the ribbon throughout the experiment. The spring gauge was used to extend the elastic ribbon and the new lengths of the ribbon were measured with every 0.2 N increase on the spring gauge until either the ribbon was pulled loose from the duct tape, or the spring gauge reached a force of 3 N. The strains were calculated by dividing the displacements of the elastic ribbon by its starting length. Starting lengths of 20 cm, 40 cm, 60 cm, 70 cm, and 80 cm were used. Each starting length underwent 3 trials of the same ribbon and 2 additional trials with a “new” ribbon of the same length which had not been stretched yet. Comparing a “new” ribbon to a “used” ribbon was done to test whether the elastic ribbons undergo plastic deformation.

At each level of tone in the rectal phantom, outer diameters at the distal and proximal ribbon sites were measured using a digital calliper. Using these measurements, the strain experienced by the elastic ribbons at each level of tone was calculated. Since direct measurements of the ribbon length during contraction of the rectal phantom was not possible, the ribbon length was estimated indirectly based on the phantom’s dimensions. Figure 6.2a is a transverse view of how the elastic ribbons relate to the dimensions of the rectal phantom. This is related back to the phantom set up from Figure 1, but is shown again in Figure 6.2b. The total length of the elastic ribbons is the sum of the distance between the motor shafts, the circumference around the rectum multiplied by the number of loops the ribbon makes around the rectum, and length around each motor shaft. The last term, the length around each motor shaft, is challenging to find as it relates to the number of revolutions the ribbon makes around the shaft. Because the thickness of the ribbon is small relative to the radius of the shaft, each additional revolution significantly adds to the radius that the next revolution covers. The distance the ribbon covers around the first revolution around the motor shaft is of course given by the circumference of the motor shaft. As the elastic ribbon stacks on itself with each revolution, the radius of the circle it covers is increased by the thickness of the ribbon for each additional

revolution. This increases the circumference it covers. Indeed, the circumference covered by the ribbon on the *n*th revolution is given by:

$$C(n) = 2\pi\big(r_s + t_e(n-1)\big) \tag{16}$$

Where r_s is the radius of the motor shafts, and t_e is the thickness of the elastic ribbon. The length of the ribbon around one motor shaft after *n* revolutions is therefore the sum of the series

$$\sum_{i=1}^{n} 2\pi\big(r_s + t_e(n-1)\big) = t_e n^2\pi + n\pi(2r_s - t_e) \tag{17}$$

Therefore, the total length of the elastic ribbon, L_e, around the rectal phantom is expressed as:

$$L_e = x + 2l\pi r_r + 2\big(t_e n^2\pi + n\pi(2r_s - t_e)\big) \tag{18}$$

As some of these terms are constants specific to the phantom, the equation can be simplified. To the nearest cm, the distance between the proximal motor shafts, X and Y, was measured to be 33 cm and the distance between the distal shafts, Z and E0, to be 25 cm. The elastic ribbon only loops around the phantom once, and the thickness of the elastic ribbon was 1 mm. The radius of the shafts was 2.5 mm. Therefore, the simplified equations expressing the length of the proximal and distal elastic ribbons are, in mm:

$$L_{e,proximal} = 330 + 5\pi + 2(n^2\pi + 4n\pi) \tag{19}$$

$$L_{e,distal} = 250 + 5\pi + 2(n^2\pi + 4n\pi) \tag{20}$$

Using Equations 4 and 5, the length of the elastic ribbons was calculated at each level of tone, which increased with each additional revolution. The length of the ribbon at each level of tone was subtracted to the original length of the ribbon to obtain a strain, δ_e, in percent:

$$\varepsilon_e = \frac{L_e - L_{\text{initial}}}{L_e} \times 100\% \quad (21)$$

Where L_{initial} was the original length of the elastic ribbon. The strain was calculated for both the proximal and distal elastic ribbon. This is expected to differ between the proximal and distal ribbon as the rectal radii and the distance between the motor shafts at these positions are different.

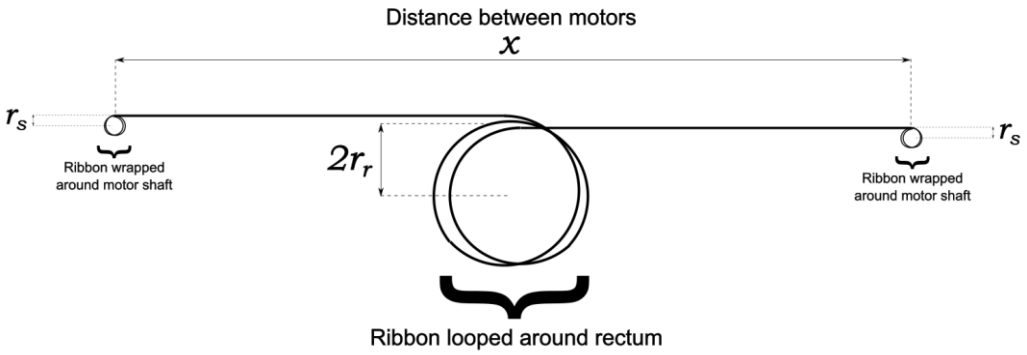

(a)

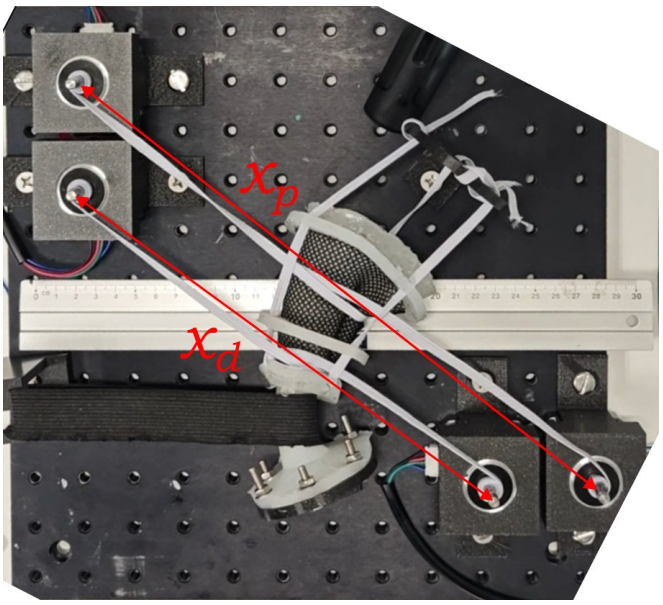

(b)

Figure 6.2: Expressing the dimensions of the rectal phantom to indirectly find the total length of the elastic ribbons.

6.2.4 Validation of device

Following fabrication of the endorectal actuator, using the same methods as described in Chapter 4.2 and modifications added as described in Chapter 5.3, it was validated in the rectal phantom. The endorectal actuator folded and inserted into the phantom by pushing the tubing into the rectum. The main body of the endorectal actuator burst between 15 and 16 ml of inflation. Therefore, once the endorectal actuator was inside the phantom, the main body was inflated to 14 ml to leave a safety buffer. Once inflated to this volume, the tubing was clipped shut to the main body to maintain a constant volume. The flexor actuators were then inflated to 4.4 ml, and their respective tubing were clipped shut. Once the endorectal actuator was inflated, its ability to reduce rectal motion in the phantom was evaluated.

Dynamic compressions:

The endorectal actuator was validated by simulating dynamic variations in rectal volume and assessing the actuator's ability to resist these rectal volume variations. Since rectal motion and prostate motion are closely correlated, the rectal phantom was subject to contractions by motor-controlled elastic ribbons that mimicked prostate intra-fraction motion (53,98). The motors were programmed to induce rectal volume changes through compression as summarised in Table 6.2:

Table 6.2. Motion protocols simulated in the rectal phantom

Motion type	Description	Contraction profile and timings
Continuous drift	Slow, gradual change in rectal motion	Elastic ribbons contract slowly and continuously over 40 s
Transient excursion	Large motions, which rapidly resolve	Elastic ribbons rapidly contract down to 50% of the original diameter over 5 s, followed by 5 s

		relaxation back to baseline. Repeated once after 15 s
Persistent excursion	Constant, large displacement which does not resolve	Elastic ribbons rapidly contract down to 75% of original diameter over 5 s, maintaining this diameter for at least 30 s
High-frequency excursions	Repeated rapid motions over short intervals	Elastic ribbons rapidly contract down to 67% of original diameter, followed by immediate relaxation back to baseline. Repeated 3 times, 3 s apart.

During each motion protocol, the rectal phantom was filmed from above using a smartphone camera placed 50 cm above the phantom's platform, fixed with a tripod. This generated a beam-eye view of the AP plane. Videos were analysed using Tracker software (325), with rectal diameter, anterior rectal wall (ARW) position, and centre of proximal rectum tracked every 5th frame.

Reproducibility of rectal volume

The actuator's ability to reproduce rectal volume and anorectal angle on insertion and inflation was assessed. The actuator was inserted and inflated inside the phantom across the four levels of tone used prior: baseline to +3 revolutions around each motor shaft. The control was defined as baseline tone + 3 revolutions. This assessed the device's ability to reproducibly expand the rectum. At each level of tone, rectal diameters were measured, and rectal volumes were calculated by assuming a perfect cylinder 80 mm in length. The difference in rectal volume from the control was used to estimate expected prostate displacements associated with these volume changes. The extent of anterior prostate displacement expected is 0.06 mm per cm^3 volume increase in rectal volume (28-30). Hence, the rectal volume difference was multiplied by 0.06 mm

to calculate expected prostate displacements at each level of tone. Displacements were compared with and without the actuator inflated inside the phantom to assess the actuator's ability to stabilise the phantom.

Reproducibility of anorectal angle and ARW position.

The proximal flange was moved on the optical platform to simulate changes in anorectal angle and ARW position. Using the holes on the platform as a coordinate system, the flange was bolted at the following defined coordinates: The control position, as in Figure 1, was defined as (9,9); Posterior rotation was at (10,9); and Anterior rotation was at (9,10) and (8,10).

Images were taken from above with a tripod-fixed smartphone camera at 50 cm above the platform. A black pen was used to mark the top of the centre of the rectum. Using Inkscape software, a straight line, denoting the rectal axis, was drawn on the image from this black mark to the centre hole on the distal flange around the rectum (Figure 6.3). The anorectal angle was defined as angle between this rectal axis and another line that follows the longitudinal axis of the anal canal. The device's ability to reproduce this angle on insertion was assessed by comparing these angles with and without the device inside. ARW position reproducibility was also assessed. The position of the ARW was defined as the point where the ARW of the phantom coincided with the top edge of the ruler in the image. Using the ruler as a reference, the position of the ARW in each case was compared to the control to assess the actuator's ability to "lock" in the rectum and consistently retract the ARW away from the target volume.

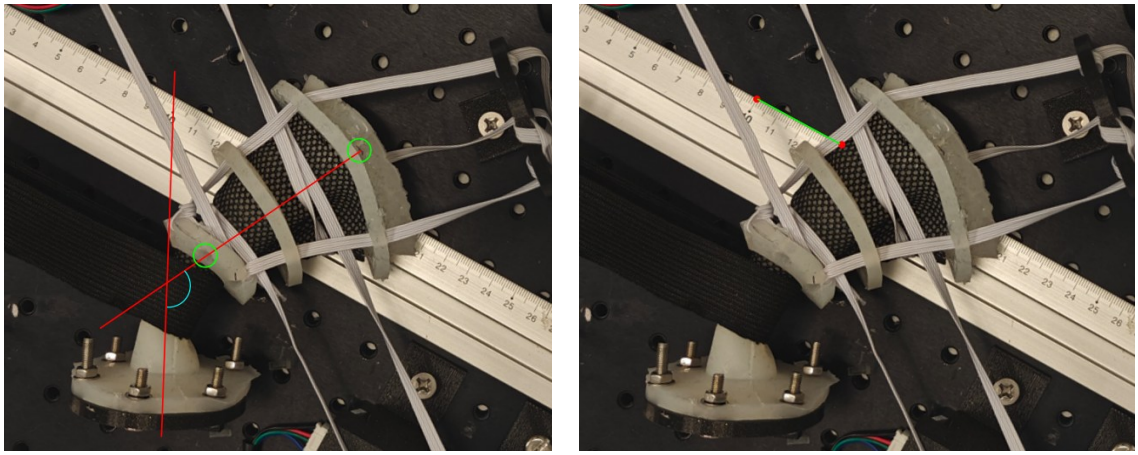

Figure 6.3. Measuring anorectal angle (left) and position of the anterior rectal wall (right) in the rectal phantom.

6.3 Results

6.3.1 Elastic ribbons

The elastic ribbons consistently had similar strains for a given force on the spring gauge. The averages for 20 trials are shown in Figure 6.4, including standard deviations denoted as error bars. Figure 6.4 on the left shows the elastic ribbons exhibiting hyperelastic behaviour. The stress-strain curve is steep at lower strains but then exhibits linearly elastic behaviour between 10-80% strain. Beyond 80% strain, the stress-strain curve has a higher gradient again. The linear region is highlighted on the right of Figure 6.4 and has an equation of $F = 0.0224\varepsilon + 0.5031$, where F is the force measured on the spring gauge required to stretch the ribbon to a strain, ε, expressed as a percentage. The strain was consistent, as denoted by the small standard deviation in the error bars. Used ribbons had slightly more strain (around 3% more in the linear region of the graph) than a “new” ribbon. This increase in strain did not stack if the ribbon was strained no more than 70%. Beyond 70% strain, the elastic ribbons underwent some plastic deformation causing the initial length of the elastic ribbon to be longer.

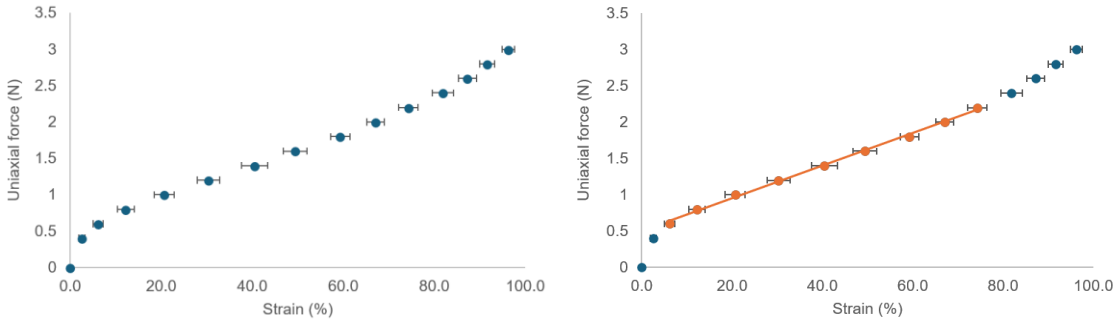

Figure 6.4 The force-strain curves of the elastic ribbons used in the rectal phantom. Left: Hyperelastic behaviour is clear. Right: Linear part is highlighted in orange. Error bars are standard deviation from 20 trials.

6.3.2 Barostat validations

The superior rectal diameter decreased with increased tone but the inferior rectal diameter was mostly unchanged as it was the minimum diameter of the barostat balloon. As mentioned, the first level of tone established was when the elastic ribbons were just taut around the phantom. This was found to be when the elastic ribbons had 2.5, 2.5, 3.5, and 3.5 revolutions around the motor shafts labelled X, Y, Z, and E0, respectively, in Figure 6.1. Table 6.3 shows the proximal and distal rectum's radius, elastic ribbon strains and corresponding force associated each level of tone induced. Ribbon lengths and strain in Table 6.3 were calculated using the methods described in 6.2.3. Both ribbons were within the linear strain region under 70% strain, allowing the force exerted by the ribbons to be determined using the gradient in Figure 6.4. Throughout the rest of this chapter, each level of tone is referred to by its level of strain. The rectal capacity and compliance at each volume range and level of contraction of each elastic ribbon is shown in Table 6.4.

Table 6.3 Elastic ribbon strains and corresponding forces associated with each induced level of tone in the rectal phantom.

Revolutions around motor shafts.	Proximal rectum				Distal rectum			
	Radius (mm)	Ribbon length (mm)	Ribbon strain (%)	Ribbon force (N)	Radius (mm)	Ribbon length (mm)	Ribbon strain (%)	Ribbon force (N)
Just taut	**26.25**	**597**	**-0.5**	**0.5**	**13.5**	**500**	**0**	**0.5**
Taut + 1 revolution	**24**	**646**	**7.6**	**0.7**	**13.25**	**574**	**15**	**0.8**
Taut + 2 revolutions	**18.5**	**687**	**14.4**	**0.8**	**12.75**	**658**	**32**	**1.2**
Taut + 3 revolutions.	**13**	**740**	**23.3**	**1.0**	**11.5**	**751**	**51**	**1.6**

Rectal capacity was between 130-140 ml at all levels of tone. At a baseline tone, the rectal compliance was 4.19 ml/mmHg between 40-60 ml. The rectal compliance decreased after one additional revolution around each motor shaft, but further additional revolutions did not have a significant effect on the rectal compliance. Likewise, the rectal compliance decreased as the volume of the rectum expanded. This was true at all levels of tone. Over 100 ml, the rectal compliance did not significantly differ between the different levels of tone, as the volume of the balloon reached closer to capacity. With no elastic around the rectal phantom, the rectal compliance was high at 24.82 and decreased sharply with increased volume.

Table 6.4. Rectal compliance of the rectal phantom at different levels of muscular tone.

Elastic ribbon strain	Rectal diameter (mm)		Rectal capacity (ml)	Rectal compliance within volume range (ml/mmHg)		
	Superior	Inferior		40-60 ml	60-100 ml	100+ ml
No elastic	55	26	166	24.82	10.26	4.09
Baseline tone	52.5	27	140	4.19	3.11	1.92
Baseline + 1 rev	48	26.5	134	3.30	2.22	2.00
Baseline + 2 rev	37	25.5	136	2.92	2.47	2.17
Baseline + 3 rev	26	23	139	2.98	2.32	2.19

6.3.3 Dynamic compressions

Figure 6.5 shows how the anterior-posterior diameter changes over time in the proximal and distal rectum with and without the device for each motion protocol. Figure 6.6 shows the same but for 2-dimensional displacements in the anterior-posterior direction for the anterior rectal wall and centre of rectum instead. In both graphs, divergence between tracked positions can be seen between rectums with and without the device inside. In Figure 6.5, the upper rectum's diameter consistently changed less than 5 mm with the device, while without the device the diameter changed up to 25 mm as seen in Figure 6.5b. Likewise, the ARW and centre of rectum did not move more than 3 mm with the device inflated inside (Figure 6.6). Without the device, both the ARW and centre of the rectum consistently moved more than 5 mm, with the ARW at times displacing more than 15 mm (Figure 6.6b and d).

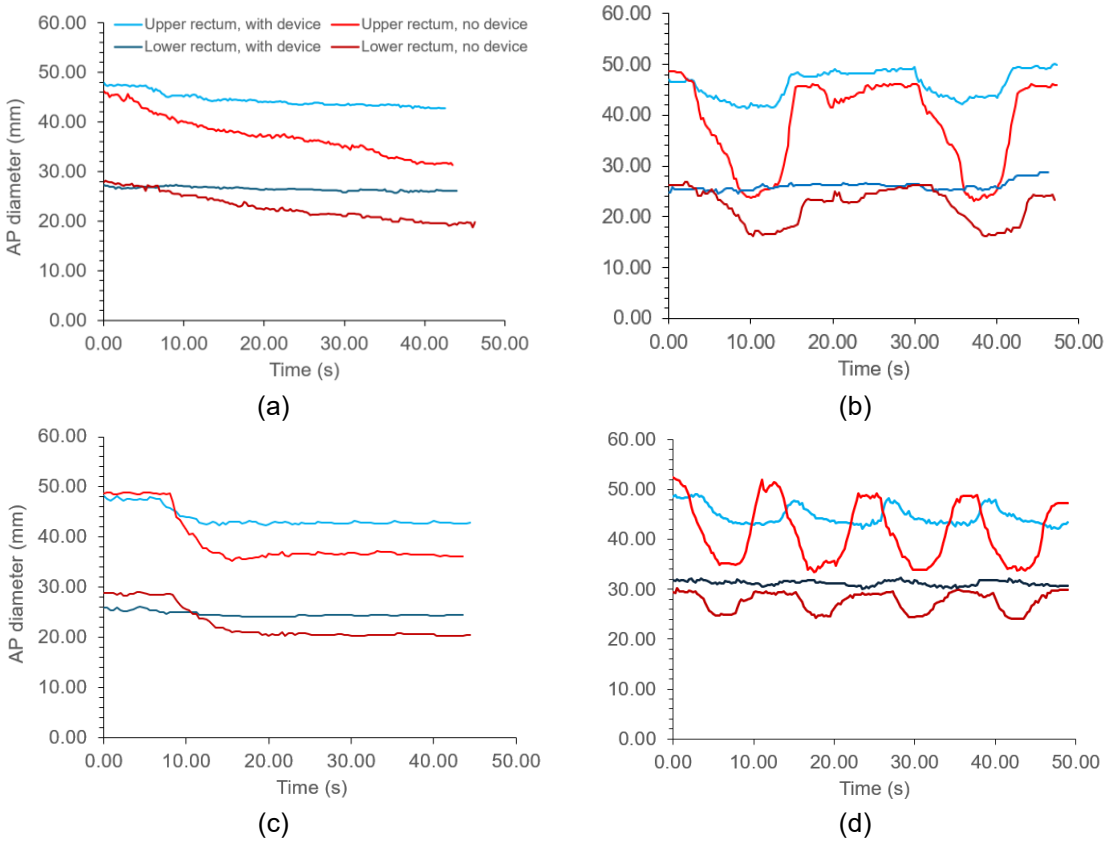

Figure 6.5 Diameters of the distal and proximal rectum with different motion protocols acting on the rectal phantom. (a) Continuous drift; (b) Transient excursion; (c) Persistent excursion; (d) High frequency excursion. Light blue: Proximal rectum, with device. Dark blue: Distal rectum, with device. Light red: Proximal rectum, no device. Dark red: Distal rectum, no device.

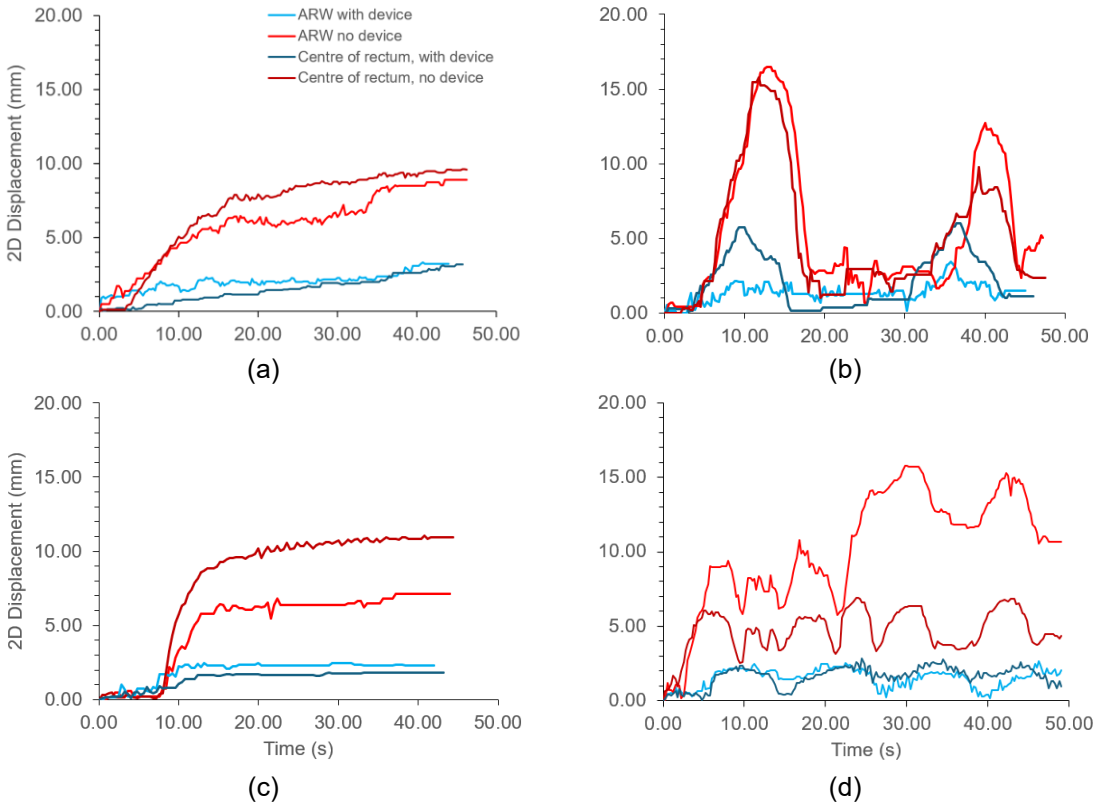

Figure 6.6 2-Dimensional displacements of the anterior rectal wall (ARW) and centre of rectum with different motion protocols acting on the rectal phantom. (a) Continuous drift; (b) Transient excursion; (c) Persistent excursion; (d) High frequency excursion. Light blue: ARW with device. Dark blue: Centre of rectum, with device. Light red: ARW, no device. Dark red: Centre of rectum, no device.

6.3.4 Reproducibility of volume and position

Table 6.5 shows the diameters with and without the device at different extents of contraction by the elastic ribbons. Without the device, the rectum underwent a 132.3 cm^3 change in volume from 40.9 cm^3 to 173.2 cm^3. For this change in rectal volume the prostate is expected to undergo an anterior translation of 7.94 mm. With the device, the volume change between the control and the lowest tone was 59.7 cm^3. This change in volume would be expected to anteriorly translate the prostate by 3.58 mm. This is less than half the translation expected without the device, for this extent of change in rectal volume.

Table 6.5. Outer diameter of the proximal rectum and calculated volume changes in the rectal phantom with and without the device at different extents of contraction. Expected estimated prostate displacements as a result of volume changes from the control are included.

Proximal rectum ribbon strain (%)	Measurement	**Without device**	**With device**
Control = 23.3%	Rectal diameter (mm)	25.5	42.5
	Volume (cm^3)	40.9	113.5
	Est. prostate displacement relative to control (mm)	Control	Control
14.4%	Rectal diameter (mm)	37.0	43.0
	Volume (cm^3)	86.0	116.2
	Est. prostate displacement relative to control (mm)	2.70	0.16
7.6%	Rectal diameter (mm)	48.0	48.0
	Volume (cm^3)	144.8	144.8
	Est. prostate displacement relative to control (mm)	6.23	1.88
-0.5%	Rectal diameter (mm)	52.5	52.5
	Volume (cm^3)	173.2	173.2
	Est. prostate displacement relative to control (mm)	7.94	3.58

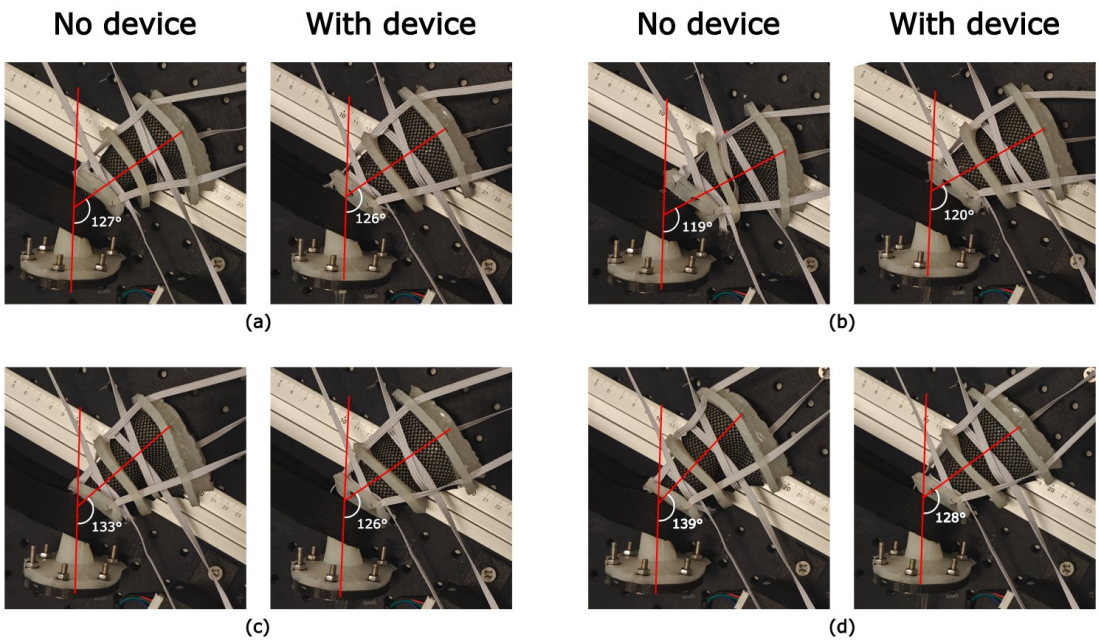

Figure 6.7 Anorectal angle positions with and without the device inside the rectal phantom when the proximal flange was moved to displace the rectal phantom. Device not visible as it is inside phantom. (a) Control position; (b) Posteriorly rotated phantom; (c) Anteriorly rotated phantom; (d) Further anterior rotation.

Table 6.6. Anterior-posterior displacement of the anterior rectal wall (ARW) relative to control position in rectal phantom with and without the device. Positive displacements are in the anterior direction.

Position of superior flange on platform (x, y)	ARW displacement (mm)	
	Without device	With device
Control (9, 9)	Control	Control
Posterior rotation (10, 9)	-8	-6
Anterior rotation (9, 10)	7	3
Further anterior rotation (8, 10)	13	4

The device's ability to reproduce the anorectal angle is shown in Figure 6.7. Figure 6.7a and b show the anorectal angle of the phantom was similar with the device inside and no device inside. Figure 6.7c and d show the device reduced the angle of the phantom with significant anterior rotation. The anterior rotations increased the anorectal angle from 127° to 133° and 139°, respectively. In contrast, with the device the angle did not change significantly from the control position. There was only 2° increase in anorectal angle between Figure 6.7a and d.

Table 6.6 shows the anterior-posterior displacement in the ARW position, as defined in the methods, at the different rectal positions. With anterior rotations the ARW was displaced anteriorly by 7 and 13 mm compared to the control position. Compared to the control when the device was inserted, the rectal phantom translated by 3 and 4 mm respectively.

6.4 Discussion

Our results demonstrate that the endorectal actuator effectively reduced motion in the validated rectal phantom, particularly motion from simulated peristaltic forces. By minimising variations in rectal diameter (Figure 6.5), the device is expected to reduce prostate motion errors during radiotherapy fractions. Additionally, it limited anterior displacement of the ARW during each simulation (Figure 6.6), reducing the likelihood of the ARW entering the target volume. This is especially significant in the post-surgical setting, where the ARW delineates the target volume.

The phantom was validated using a barostat balloon, exhibiting a lower compliance of 4 ml/mmHg. Although this suggests the phantom exhibits a higher resistance to distension that what might be expected in an average patient (122,318,319), this enabled the endorectal actuator to undergo a harsher assessment. Despite the phantom's higher resistance to distension, the actuator successfully expanded the rectum across varying levels of tone, as shown in Table 6.5. If an *in situ* rectum is more compliant, the device should perform at least as well in vivo. By reproducibly expanding the rectum, the device reduces variations in rectal volume between fractions that would have been caused by gas or peristaltic relaxations. Figure 6.7 and Table 6.6 also show the device reproduce the anorectal angle and ARW position on insertion. When the phantom was anteriorly rotated compared to the control position, the actuator "locked in" the anorectal angle at a consistent angle. This consistency could reduce motion within a patient but also provide consistent position across patients with differing anatomies. This reproducible positioning, particularly the reduction in anterior displacement of the ARW, will likely prevent the rectum from moving into the target volume, potentially improving outcomes by reducing rectal toxicity.

Indeed, the phantom exhibited additional features of human rectums: representative anatomical features such as an anorectal angle in the upper bound of the range (85° to 125°), a reducing compliance with increasing cross-sectional area or volume (123), and a rectal capacity of 134-140 ml at 40 mmHg—within the normal range of 100-250 ml (318). The anorectal angle of the phantom was slightly higher than that seen in the literature because measurements were taken using slightly different methods: in defecography studies the anorectal angle is usually measured using the posterior wall of the rectum on imaging (245), whereas this study measured it using the central longitudinal rectal axis. This axis was chosen because of the challenges in identifying the whole axis of the posterior rectal wall. As the phantom's diameter is tapered along its length, the angle is expected be slightly higher along the centre than the posterior wall.

Stokes et al. made a defecatory model including an anal sphincter complex and a puborectalis "muscle" attached to a load cell that can change the anorectal angle (317). The paper describes the modelling and results of their simulated

defecations in this model. The authors of this study were studying the rectal dynamics behind incontinence with their model. As the authors were investigating rectal incontinence, they did not employ dynamic volume changes or compressive forces. Instead, they used a stiffer silicone with hardness 10A to 30A, but they do not provide data or validations to match rectal compliance. Bohoudi et al. validated an anthropomorphic deformable pelvis phantom to validate dosimetry in MRI-guided ART (326). Their phantom contained the bladder and prostate in addition to a rectum. The authors of this study validated dosimetry on varying organ volumes and inter-fraction changes seen based on patient scans. This created more realistic and patient-specific changes in volume seen in the phantom. However, they also did not employ dynamic compression.

While the primary goal of this chapter was to demonstrate the device's potential to reduce variations in motion in a physical simulated environment, the design and fabrication of the rectal phantom itself may of interest to the wider scientific community. Investigating how different variables of the phantom, such as the number of elastic bands, the distance between the bands, and the extent of friction between the bands and the silicone, may make the phantom more representative of a realistic human rectum. A realistic rectal phantom could be translated into a validation tool for other rectal devices or a training tool for clinicians (327).

Despite efforts to develop and validate a biomechanically accurate rectal phantom, several limitations remain. Firstly, the phantom does not reproduce physiological temperatures (37°C), resulting in an approximate 15°C increase from room temperature. Under constrained-volume conditions—our endorectal actuator when it is clamped shut after inflation—such a temperature rise would theoretically induce a pressure rise of 7-8 MPa. This thermal expansion is estimated using the linear thermoelastic relation. This pressure increase is more than an order of magnitude higher than the endorectal actuator's typical operating pressure (0.155-0.175 MPa (3). Such a pressure increase would lead to device failure. Clinically, this necessitates adjustments to the inflation protocol: the actuator should be inflated very gradually to allow thermal equilibrium in vivo, or the water with which the device is inflated should be kept at 37°C. Since inflation

of the endorectal actuator is pressure-limited, to reduce the risk of bursting, there is a temperature-dependent change in achievable inflation volume. The bulk modulus of water is about 3% higher at 37°C than at 22°C (328), corresponding to a small change in the achievable inflation volume (< 0.5 ml for a 14 ml inflation). While this change is unlikely to impact rectal stabilisation, inflation protocols will require adjustments for human trials. Future burst-pressure and burst-volume investigations with water at 37°C are warranted to further validate device safety.

A second limitation is that the phantom does not simulate anorectal humidity, which may affect the endorectal actuator's ease of insertion compared with in vivo conditions. Although the actuator will require a soft silicone sleeve or external shell to cover the sharp plastic edges, the insertion methods used in this study are representative of the intended clinical process.

Finally, we used a simple water-based lubricant to simulate the rectal mucosa. This is consistent with prior colorectal phantom studies (329-332). While this approach does not replicate the complex rheological and adhesion properties of rectal mucous—important properties when studying microscopic behaviour such as particle transport and particle penetration (333)—the primary objective of our study was to assess the endorectal actuator's ability to stabilise the rectum following device insertion and inflation. Variations in rectal motion are primarily driven by peristalsis and gas. For this mechanically focused goal, using a simple water-based lubricant was sufficient and does considerably affect our conclusions.

To the author's knowledge, this is the first published validation of a rectal device in a mechanically representative phantom. The findings support the device's potential to reduce variations in rectal volume and therefore reduce target motion error during prostate radiotherapy. This study only looked at motion in the anterior-posterior plane. However, motion error is three-dimensional and displacements in left-right and superior-inferior direction can also impact radiotherapy outcomes. The experimental methods could be repeated with 3D positional trackers. This would assess the device's ability to reduce displacements in the other two planes and may enable the assessment of rectal

deformations. Future work will focus on improving device usability. A soft silicone sleeve or external shell will cover the plastic edges for improved safety and easier insertion. This will enable the assessment of the device's safety and tolerability in a phase I trial. A subsequent phase II trial should compare this actuator to a control group and other devices like ProSpare™ or ERBs. A current limitation is the need for multiple syringes to operate the device, preventing seamless patient self-insertion. To address this, future versions should inflate the device with a single syringe, possibly through embedding automatic valves that control the direction of flow.

6.5 Conclusion

The endorectal actuator demonstrated its ability to reduce variations in rectal motion in this phantom by stabilising rectal volume and position. These findings support the device's potential to improve target accuracy and reduce ARW exposure in prostate radiotherapy. The device is translatable with improved usability for patient self-insertion. Future clinical trials will further validate these findings.

Chapter 7 Discussion and Conclusion

Chapter 1

The challenges posed by rectal motion in pelvic radiotherapy were discussed. The review on these challenges concluded that there was a lack of low-cost and accessible methods of tracking real-time rectal motion, and that existing rectal stabilisation devices have limitations or lack sufficient evidence at this time to justify clinical adoption.

Chapter 2

The preliminary study determined that there were no differences in gross rectal anatomy in patients who could insert ProSpare™ and those who could not. From these results it was inferred that ProSpare™ has limited ability to bypass the anal sphincter. These results showed that the device's geometry is not the limiting factor in enabling patient insertion and that further modifications to the device geometry would likely not increase tolerance rates. ProSpare™ has excellent features with promising data supporting its ability to improve outcomes in prostate radiotherapy. The preliminary trial determined the direction of this thesis: to implement these beneficial elements of ProSpare™ —a hollow, rigid, and angled device with radiopaque markers—into a soft endorectal actuator to improve tolerance.

Chapter 3

To understand how these features may be implemented, an overview of soft robotic actuators, with an in-depth analysis of pouch motors and how their structure affects their performance is provided. The review in Chapter 1 and the review on pouch motors influenced the criteria for the endorectal actuator. This review on pouch motors enabled the author to incorporate a flexor pouch motor inside of an external inflatable shell, providing radial stiffness and an angled shape to stabilise the rectum. This review also identified limitations with current designs which enabled the author to design a novel elliptical pouch motor in Chapter 5.

Chapter 4

This chapter presented the successful fabrication of an endorectal actuator that partially satisfies six out of the seven predefined criteria. The initial prototypes were developed based on design principles from the soft robotic review in 0. First, a dual-truncated prism was shown to deploy in a manner that would likely be uncomfortable inside the patient. This dual-truncated prism was turned into a regular triangular prism with one side reinforced by axially oriented welds, perpendicular to the radial welds on the other two sides. This allowed for bending to occur similarly to a reinforced actuator. As the resulting angle was insufficient, the use of notches was explored to mitigate the distortions seen at the edges of rectangular pouch motors. Several features from the initial prototypes were integrated into the working prototype. This working prototype comprised of a shell formed from a disconnected dual-truncated prism and incorporated an internal flexor actuator that enabled the device to reach the desired angle. Variable stiffness was achieved with corrugations that appear on inflation, which are an inherent part of inflatable pouch motors. Initial validations quantified the radial stiffness and bending resistance of the device. Limitations in this working prototype were a low bending resistance and a risk of damage to the internal membrane of the main actuator. This damage was due to the sharp edges of the triangular ends of the conical pouch motor that made up the flexor actuator. These limitations were addressed with design modifications in the next chapter.

Chapter 5

The device's bending resistance was optimised here to fulfil the 2nd and 3rd aims of the project. The fundamental structure of the endorectal actuator remained the same: a flexor actuator inside a disconnected dual-truncated prism. The aim was to retain the existing pouch motors as flexor actuators rather than use another mechanism. The pouch motors are low profile, easy and inexpensive to fabricate, integrate easily within the inner membrane of the main actuator, and preserve a single mode of control for patient self-insertion. To mitigate the risk of membrane damage caused by the sharp edges of the conical actuators, a new pouch motor with elliptical ends was developed. Rounding the edges reduced the risk of

membrane damage while also increasing the maximum inflatable volume of the pouch motor for a given deflated width. Contraction ratios remained unchanged, ensuring the device's angle was unaffected. The extra volume increased the restoring force which improved the resistance to opposing bending action. Other design strategies, such as increasing the moment arm by increasing the "tendon length" were ineffective. A second flexor actuator was added to double the restoring force.

Further modifications to the device were implemented to improve it meeting the defined criteria. The inflation tubing was routed fully to the top of the endorectal actuator, enabling the actuator to be advanced from the tip like a catheter, despite being held at the inlet. This design was important to fulfilling Criterion 5, to enable patient self-insertion. To satisfy Criterion 6, capability for image-guidance, metallised thermoplastic sheets were embedded into the device during fabrication. Unfortunately, these were not visible on CT scan because they were too thin. Other methods of enabling the device to be used as an IGRT tool could be explored, such as inflating the device with a radiopaque fluid, although this may be too costly.

Chapter 6

The motivation for this chapter stem from the initial validations presented in Chapter 4, which characterised the device's radial stiffness and angle. This chapter aimed to further validate the endorectal actuator within the context of its intended clinical application. A rectal phantom was successfully fabricated using motor controlled elastic ribbons. These ribbons induced tone into the phantom, which other similar phantoms had not included. The phantom was validated with a barostat balloon, showing it was appropriate to assess the endorectal actuator in this phantom. The actuator's ability to resist dynamic compressive forces and to reproducibly stabilise rectal volume, the anterior position of the anterior rectal wall, and the anorectal angle was assessed. The endorectal actuator successfully reduced variations in rectal motion under these test conditions. Based on the correlations between prostate motion and rectal motion, the prostate displacements from the variations in rectal volume would be less with this

endorectal actuator compared to a control (no device). These results suggest that the endorectal actuator may improve outcomes in prostate radiotherapy.

General comments

The work presented has shown that a soft endorectal actuator that meets most of the predefined criteria, as outlined in Chapter 1 and 0, can be developed for the use in prostate radiotherapy. The deployability, radial stiffness, ability to hold the anorectal angle, and hydraulic inflation methods demonstrate the potential translatability of the device in patients.

This thesis focussed on prostate radiotherapy and the device's ability to reduce prostate motion. However, since rectal motion impacts other pelvic radiotherapies, such as gynaecological cancers, the endorectal actuator has potential applications in these radiotherapies too. Future work should assess the device in human trials to assess safety and feasibility (phase I) and efficacy (phase II).

The current endorectal actuator has partially met the first and fifth criteria—improved tolerance and self-insertion through a deployable mechanism—due to the device's soft materials, inflatable nature, and modified tubing that enables the device to be pushed in by holding the tubing alone. It has only partially met these criteria as the device is not yet feasible for self-insertion, because its inflation requires multiple syringes, and plastic edges of the external shell will likely lead to discomfort. It is necessary to improve the device's feasibility for self-insertion before human trials can take place. The endorectal actuator should be covered with a thin silicone sleeve to increase its softness and reduce the risk of the plastic edges causing discomfort. Although, this may increase the device's dimension in the uninflated state. Additionally, the endorectal actuator should be inflated with a single syringe. This may be achieved through embedding automatic valves that control the direction of flow. Having a single syringe to inflate the device and including clear instructions on how the device is inserted, using markers on the tubing to aid with insertion depth, will make it easier to use for the patient. Indeed, involving patients through Patient and Public Involvement and Engagement

(PPIE) in the design of improving its user friendliness will be crucial in increasing acceptance by patients to use this device. The device enters an intimate space so patient-centred co-design will help in ensuring comfort and ease of use. Further practical considerations include finding a reproducible burst volume assessing different pressures to determine when the device is expected to fail in a patient. Multiple iterations of the device could be fabricated, for instance to address differences in anorectal angle. Although less common, patients whose anorectal angle is 90° do exist. These patients may not benefit from the current iteration like a patient whose anorectal is at 120° might benefit.

Future work can also include integrating sensing in the endorectal actuator. Sensing modalities to integrate could include diffuse reflectance spectroscopy (DRS) and dynamic instrumented palpation (DIP). DRS involves emitting a light and measuring the intensity of the reflected light at a specific wavelength to assess the oxygenation of cells. The oxygenation of cells can indicate cancer cells becoming resistant to radiotherapy (334). DIP repeatedly palpates a tissue at a high frequency, measuring the dynamic stiffness of the tissue. The dynamic stiffness differs between cancer cells and healthy cells, enabling DIP to track response to radiotherapy; cancer cells are more elastic and softer (335). These sensing techniques would enable clinicians to track treatment progress during radiotherapy and aid their decision making. This informed decision making in adaptive radiotherapy may further reduce biochemical recurrence (336,337).

Bibliography

(1) Niknam Maleki A, Mylonas G, Murray J. ProSpare tolerability is independent of rectal anatomy. *Proceedings of the 10th World Congress on Electrical Engineering and Computer Systems and Sciences (EECSS'24),* : Avestia; 2024. pp. ICBES 145. 10.11159/icbes24.145.

(2) Niknam Maleki A, Runciman M, Thompson A, Murray J, Mylonas G. Developing a customisable inflatable rectal obturator. *The 15th Hamlyn Symposium on Medical Robotics 2023* London; 2023. pp. 141–142.

(3) Maleki AN, Thompson A, Runciman MS, Murray J, Mylonas GP. A soft hydraulic endorectal actuator for prostate radiotherapy. *2023 IEEE International Conference on Robotics and Biomimetics (ROBIO)* : IEEE; Dec 4, 2023. pp. 1–6.

(4) Sung H, Ferlay J, Siegel RL, Laversanne M, Soerjomataram I, Jemal A, et al. Global Cancer Statistics 2020: GLOBOCAN Estimates of Incidence and Mortality Worldwide for 36 Cancers in 185 Countries. *CA: a cancer journal for clinicians.* 2021; 71 (3): 209–249. 10.3322/caac.21660.

(5) Cancer Research UK. *Prostate cancer statistics.* https://www.cancerresearchuk.org/health-professional/cancer-statistics/statistics-by-cancer-type/prostate-cancer [Accessed 18 May 2022].

(6) Cancer Research UK. *Cancer mortality for common cancers.* https://www.cancerresearchuk.org/health-professional/cancer-statistics/mortality/common-cancers-compared [Accessed 18 May 2022].

(7) The Royal College of Surgeons of England. *Results of the NPCA Prospective Audit in England and Wales for men diagnosed from 1 April 2019 to 31 March 2020 and the Impact of COVID-19 in England during 2020 (published January 2022).* London: 2022.

(8) The Royal College of Surgeons of England. *Results of the NPCA Prospective Audit in England and Wales for men diagnosed from 1 April 2018 to 31 March 2019 (published January 2021).* London: 2021.

(9) Cuzick J, Prof, Thorat MA, MBBS, Andriole G, Prof, Brawley OW, Prof, Brown PH, Prof, Culig Z, MD, et al. Prevention and early detection of prostate cancer. *The lancet oncology.* 2014; 15 (11): e484–e492. 10.1016/S1470-2045(14)70211-6.

(10) Kiciński M, Vangronsveld J, Nawrot TS. An epidemiological reappraisal of the familial aggregation of prostate cancer: a meta-analysis. *PloS one.* 2011; 6 (10): e27130. 10.1371/journal.pone.0027130.

(11) Wallace TJ, Anscher MS. *Prostate Cancer.* https://bestpractice.bmj.com/topics/en-gb/254 [Accessed 10 December 2021].

(12) Kumar V, Abbas AK, Aster JC, Perkins JA. *Robbins basic pathology.* Robbins PathologyTenth edition ed. Philadelphia, Pennsylvania: Elsevier; 2018.

(13) National Institute for Health and Care Excellence. *Prostate cancer: diagnosis and management.* 2019.

(14) Cancer Research UK. *Cancer Research UK Treatment Hub.* https://crukcancerintelligence.shinyapps.io/Treatment/ .

(15) Khan FM, Gibbons JP. 19 Three-Dimensional Conformal Radiation Therapy. In: Khan FM, Gibbons JP. (eds.) *Khan's the Physics of Radiation Therapy - Fifth ed.* Philadelphia: Wolters Kluwer; 2014. pp. 413–429.

(16) Ezzell GA, Galvin JM, Low D, Palta JR, Rosen I, Sharpe MB, et al. Guidance document on delivery, treatment planning, and clinical implementation of IMRT: Report of the IMRT subcommittee of the AAPM radiation therapy committee. *Medical physics (Lancaster).* 2003; 30 (8): 2089–2115. 10.1118/1.1591194.

(17) Keall PJ, Balter JM. Patient and Organ Movement. In: Khan FM, Gibbons JP, Sperduto PW. (eds.) *Khan's Treatment Planning in Radiation Oncology.* Philadelphia: Wolters Kluwer; 2016. pp. 298–313.

(18) No authors listed. 4. Definition of volumes. *Journal of the ICRU.* 2010; 10 (1): 41–53. 10.1093/jicru_ndq009.

(19) Landberg T, Chavaudra J, Dobbs J, Gerard J-, Hanks G, Horiot J-, et al. 2. Volumes. *Reports of the International Commission on Radiation Units and Measurements.* 1999; os-32 (1): 3–20. 10.1093/jicru_os32.1.3.

(20) Langen KM, Jones DTL. *Organ motion and its management.* Elsevier BV; 2001.

(21) van Herk M. Errors and margins in radiotherapy. *Seminars in radiation oncology.* 2004; 14 (1): 52–64. 10.1053/j.semradonc.2003.10.003.

(22) Padhani AR, Khoo VS, Suckling J, Husband JE, Leach MO, Dearnaley DP. Evaluating the effect of rectal distension and rectal movement on prostate gland position using cine MRI. *International journal of radiation oncology, biology, physics.* 1999; 44 (3): 525–533. 10.1016/S0360-3016(99)00040-1.

(23) Ghilezan MJ, Jaffray DA, Siewerdsen JH, Van Herk M, Shetty A, Sharpe MB, et al. Prostate gland motion assessed with cine-magnetic resonance imaging (cine-MRI). *International journal of radiation oncology, biology, physics.* 2005; 62 (2): 406–417. 10.1016/j.ijrobp.2003.10.017.

(24) Bell LJ, Cox J, Eade T, Rinks M, Kneebone A. The impact of rectal and bladder variability on target coverage during post-prostatectomy intensity

modulated radiotherapy. *Radiotherapy and oncology.* 2014; 110 (2): 245–250. 10.1016/j.radonc.2013.10.042.

(25) Jadon R, Pembroke CA, Hanna CL, Palaniappan N, Evans M, Cleves AE, et al. A Systematic Review of Organ Motion and Image-guided Strategies in External Beam Radiotherapy for Cervical Cancer. *Clinical Oncology.* 2014; 26 (4): 185–196. 10.1016/j.clon.2013.11.031.

(26) Eminowicz G, Motlib J, Khan S, Perna C, McCormack M. Pelvic Organ Motion during Radiotherapy for Cervical Cancer: Understanding Patterns and Recommended Patient Preparation. *Clinical oncology (Royal College of Radiologists (Great Britain)).* 2016; 28 (9): e85–e91. 10.1016/j.clon.2016.04.044.

(27) Jensen NBK, Assenholt MS, Fokdal LU, Vestergaard A, Schouboe A, Kjaersgaard EB, et al. Cone beam computed tomography-based monitoring and management of target and organ motion during external beam radiotherapy in cervical cancer. *Physics and imaging in radiation oncology.* 2019; 9 14–20. 10.1016/j.phro.2018.12.002.

(28) Melian E, Mageras GS, Fuks Z, Leibel SA, Niehaus A, Helen L, et al. Variation in prostate position quantitation and implications for three-dimensional conformal treatment planning. *International Journal of Radiation OncologyBiologyPhysics.* 1997; 38 (1): 73–81. 10.1016/S0360-3016(97)00221-6.

(29) van Herk M, Bruce A, Guus Kroes AP, Shouman T, Touw A, Lebesque JV. Quantification of organ motion during conformal radiotherapy of the prostate by three dimensional image registration. *International Journal of Radiation OncologyBiologyPhysics.* 1995; 33 (5): 1311–1320. 10.1016/0360-3016(95)00116-6.

(30) Beard CJ, Kijewski P, Bussière M, Gelman R, Gladstone D, Shaffer K, et al. Analysis of prostate and seminal vesicle motion: Implications for treatment planning. *International Journal of Radiation OncologyBiologyPhysics.* 1996; 34 (2): 451–458. 10.1016/0360-3016(95)02081-0.

(31) Roeske JC, Forman JD, Mesina CF, He T, Pelizzari CA, Fontenla E, et al. Evaluation of changes in the size and location of the prostate, seminal vesicles, bladder, and rectum during a course of external beam radiation therapy. *International Journal of Radiation OncologyBiologyPhysics.* 1995; 33 (5): 1321–1329. 10.1016/0360-3016(95)00225-1.

(32) Tinger A, Michalski JM, Cheng A, Low DA, Zhu R, Bosch WR, et al. A critical evaluation of the planning target volume for 3-D conformal radiotherapy of prostate cancer. *International journal of radiation oncology, biology, physics.* 1998; 42 (1): 213–221. 10.1016/S0360-3016(98)00189-8.

(33) Klayton T, M.D, Price R, Ph.D, Buyyounouski, Mark K., M.D., M.S, Sobczak M, M.D, Greenberg R, M.D, Li J, Ph.D, et al. Prostate Bed Motion During

Intensity-Modulated Radiotherapy Treatment. *International journal of radiation oncology, biology, physics.* 2012; 84 (1): 130–136. 10.1016/j.ijrobp.2011.11.041.

(34) Fiorino C, Foppiano F, Franzone P, Broggi S, Castellone P, Marcenaro M, et al. Rectal and bladder motion during conformal radiotherapy after radical prostatectomy. *Radiotherapy and oncology.* 2005; 74 (2): 187–195. 10.1016/j.radonc.2004.10.002.

(35) Bell LJ, Eade T, Hruby G, Bromley R, Kneebone A. Intra-fraction displacement of the prostate bed during post-prostatectomy radiotherapy. *Radiation oncology (London, England).* 2021; 16 (1): 20. 10.1186/s13014-020-01743-9.

(36) Natesan D, Carpenter DJ, Floyd W, Oyekunle T, Niedzwiecki D, Waters L, et al. Effect of Large Prostate Volume on Efficacy and Toxicity of Moderately Hypofractionated Radiation Therapy in Patients With Prostate Cancer. *Advances in radiation oncology.* 2021; 7 (2): 100805. 10.1016/j.adro.2021.100805.

(37) Pinkawa M, Fischedick K, Asadpour B, Gagel B, Piroth MD, Nussen S, et al. Toxicity Profile With a Large Prostate Volume After External Beam Radiotherapy for Localized Prostate Cancer. *International journal of radiation oncology, biology, physics.* 2008; 70 (1): 83–89. 10.1016/j.ijrobp.2007.05.051.

(38) Tomida M, Okudaira K, Kamomae T, Oguchi H, Miyake Y, Yoneda K, et al. Relationship between prostate volume changes and treatment duration of neoadjuvant androgen deprivation during intensity-modulated radiation therapy for Japanese patients with prostate cancer. *Nagoya journal of medical science.* 2016; 78 (3): 313–321. https://www.ncbi.nlm.nih.gov/pubmed/27578915. .

(39) Roeske JC, Forman JD, Mesina CF, He T, Pelizzari CA, Fontenla E, et al. Evaluation of changes in the size and location of the prostate, seminal vesicles, bladder, and rectum during a course of external beam radiation therapy. *International Journal of Radiation OncologyBiologyPhysics.* 1995; 33 (5): 1321–1329. 10.1016/0360-3016(95)00225-1.

(40) Alexander SE, McNair HA, Oelfke U, Huddart R, Murray J, Pathmanathan A, et al. Prostate Volume Changes during Extreme and Moderately Hypofractionated Magnetic Resonance Image-guided Radiotherapy. *Clinical oncology (Royal College of Radiologists (Great Britain)).* 2022; 34 (9): e383–e391. 10.1016/j.clon.2022.03.022.

(41) Gurewitz J, Woo S, Oh C, Bruzzese A, Chen T, Wang H, et al. Changes in Prostate Volume during Prostate SBRT Delivered on an MR-Linac and Correlation with Acute Toxicity. *International journal of radiation oncology, biology, physics.* 2025; 123 (1): e559. 10.1016/j.ijrobp.2025.06.2776.

(42) Vanhanen A, Reinikainen P, Kapanen M. Radiation-induced prostate swelling during SBRT of the prostate. *Acta oncologica.* 2022; 61 (6): 698–704. 10.1080/0284186X.2022.2062682.

(43) Park J, Butler WM, Merrick GS, Kurko BS, Reed JL, Murray BC. Prostate Volume Changes Monitored during a Course of External Beam Radiation Therapy and for the Next Six Months using Electromagnetic Transponders. *International journal of radiation oncology, biology, physics.* 2010; 78 (3): S699. 10.1016/j.ijrobp.2010.07.1623.

(44) Zechmann CM, Aftab K, Didinger B, Giesel FL, Zamecnik P, Thieke C, et al. Changes of prostate gland volume with and without androgen deprivation after intensity modulated radiotherapy – A follow-up study. *Radiotherapy and oncology.* 2009; 90 (3): 408–412. 10.1016/j.radonc.2008.09.006.

(45) Chai H, Miyasaka Y, Hagiwara Y, Souda H, Ishizawa M, Sato H, et al. Investigation of pelvic floor influence on prostate displacement in image-guided radiotherapy. *The Prostate.* 2025; 85 (2): 123–129. 10.1002/pros.24808.

(46) Sidhom MA, Kneebone AB, Lehman M, Wiltshire KL, Millar JL, Mukherjee RK, et al. Post-prostatectomy radiation therapy: Consensus guidelines of the Australian and New Zealand Radiation Oncology Genito-Urinary Group. *Radiotherapy and oncology.* 2008; 88 (1): 10–19. 10.1016/j.radonc.2008.05.006.

(47) Michalski JM, M.D, Lawton C, M.D, El Naqa I, Ph.D, Ritter M, M.D, O'Meara E, C.M.D, Seider MJ, M.D, et al. Development of RTOG Consensus Guidelines for the Definition of the Clinical Target Volume for Postoperative Conformal Radiation Therapy for Prostate Cancer. *International journal of radiation oncology, biology, physics.* 2010; 76 (2): 361–368. 10.1016/j.ijrobp.2009.02.006.

(48) Wiltshire KL, M.D, Brock KK, Ph.D, Haider MA, M.D, Zwahlen D, M.D, Kong V, B.Sc, Chan E, M.D, et al. Anatomic Boundaries of the Clinical Target Volume (Prostate Bed) After Radical Prostatectomy. *International journal of radiation oncology, biology, physics.* 2007; 69 (4): 1090–1099. 10.1016/j.ijrobp.2007.04.068.

(49) Poortmans P, Bossi A, Vandeputte K, Bosset M, Miralbell R, Maingon P, et al. Guidelines for target volume definition in post-operative radiotherapy for prostate cancer, on behalf of the EORTC Radiation Oncology Group. *Radiotherapy and oncology.* 2007; 84 (2): 121–127. 10.1016/j.radonc.2007.07.017.

(50) Robin S, Jolicoeur M, Palumbo S, Zilli T, Crehange G, De Hertogh O, et al. Prostate Bed Delineation Guidelines for Postoperative Radiation Therapy: On Behalf Of The Francophone Group of Urological Radiation Therapy. *International journal of radiation oncology, biology, physics.* 2021; 109 (5): 1243–1253. 10.1016/j.ijrobp.2020.11.010.

(51) Latorzeff I, Sargos P, Loos G, Supiot S, Guerif S, Carrie C. Delineation of the Prostate Bed: The "Invisible Target" Is Still an Issue? *Frontiers in oncology.* 2017; 7 108. 10.3389/fonc.2017.00108.

(52) Vilotte F, Antoine M, Bobin M, Latorzeff I, Supiot S, Richaud P, et al. Post-Prostatectomy Image-Guided Radiotherapy: The Invisible Target Concept. *Frontiers in oncology.* 2017; 7 34. 10.3389/fonc.2017.00034.

(53) Kupelian PA, Langen KM, Willoughby TR, Wagner TH, Zeidan OA, Meeks SL. Daily variations in the position of the prostate bed in patients with prostate cancer receiving postoperative external beam radiation therapy. *International journal of radiation oncology, biology, physics.* 2006; 66 (2): 593–596. 10.1016/j.ijrobp.2006.05.071.

(54) Ost P, M.D, De Meerleer, Gert, M.D., Ph.D, De Gersem W, Ir. Ph.D, Impens A, R.N, De Neve, Wilfried, M.D., Ph.D. Analysis of Prostate Bed Motion Using Daily Cone-Beam Computed Tomography During Postprostatectomy Radiotherapy. *International journal of radiation oncology, biology, physics.* 2011; 79 (1): 188–194. 10.1016/j.ijrobp.2009.10.029.

(55) Huang, Kitty, M.D.C.M., M.Sc, Palma, David A., M.D., M.Sc., F.R.C.P.C., Ph.D, Scott, Danielle, M.R.T.T., B.Sc, McGregor, Danielle, B.Sc. (Hons.), M.R.T.T, Gaede S, Ph.D, Yartsev S, Ph.D, et al. Inter- and Intrafraction Uncertainty in Prostate Bed Image-Guided Radiotherapy. *International journal of radiation oncology, biology, physics.* 2012; 84 (2): 402–407. 10.1016/j.ijrobp.2011.12.035.

(56) Ramiandrisoa F, Duverge L, Castelli J, Nguyen TD, Servagi-Vernat S, De Crevoisier R. Clinical to planning target volume margins in prostate cancer radiotherapy. *Cancer radiothérapie.* 2016; 20 (6-7): 629. 10.1016/j.canrad.2016.07.095.

(57) Gonzalez-Moya A, Supiot S, Seegers V, Lizée T, Legouté F, Perennec T, et al. Mapping of Recurrence Sites Following Adjuvant or Salvage Radiotherapy for Prostate Cancer Patients. *Frontiers in oncology.* 2021; 11 787347. 10.3389/fonc.2021.787347.

(58) Siepe G, Buwenge M, Nguyen NP, Macchia G, Deodato F, Cilla S, et al. Postoperative Hypofractionated Radiation Therapy in Prostate Carcinoma: A Systematic Review. *Anticancer research.* 2018; 38 (3): 1221–1230. 10.21873/anticanres.12343.

(59) Tendulkar RD, Agrawal S, Gao T, Efstathiou JA, Pisansky TM, Michalski JM, et al. Contemporary update of a multi-institutional predictive nomogram for salvage radiotherapy after radical prostatectomy. *Journal of clinical oncology.* 2016; 34 (30): 3648–3654. 10.1200/JCO.2016.67.9647.

(60) Parker CC, Clarke NW, Cook AD, Kynaston HG, Petersen PM, Catton C, et al. Timing of radiotherapy after radical prostatectomy (RADICALS-RT): a randomised, controlled phase 3 trial. *The Lancet (British edition).* 2020; 396 (10260): 1413–1421. 10.1016/S0140-6736(20)31553-1.

(61) van As N, Griffin C, Tree A, Patel J, Ostler P, van der Voet H, et al. Phase 3 Trial of Stereotactic Body Radiotherapy in Localized Prostate Cancer. *The New*

England journal of medicine. 2024; 391 (15): 1413–1425. 10.1056/NEJMoa2403365.

(62) Aluwini S, Dr, Pos F, MD, Schimmel E, MD, van Lin E, MD, Krol S, MD, van der Toorn PP, MD, et al. Hypofractionated versus conventionally fractionated radiotherapy for patients with prostate cancer (HYPRO): acute toxicity results from a randomised non-inferiority phase 3 trial. *The lancet oncology.* 2015; 16 (3): 274–283. 10.1016/S1470-2045(14)70482-6.

(63) Catton CN, Lukka H, Gu C, Martin JM, Supiot S, Chung PWM, et al. Randomized Trial of a Hypofractionated Radiation Regimen for the Treatment of Localized Prostate Cancer. *Journal of Clinical Oncology.* 2017; 35 (17): 1884–1890. 10.1200/jco.2016.71.7397.

(64) Dearnaley D, Prof, Syndikus I, MD, Mossop H, MMathStat, Khoo V, MD, Birtle A, FRCR, Bloomfield D, FRCR, et al. Conventional versus hypofractionated high-dose intensity-modulated radiotherapy for prostate cancer: 5-year outcomes of the randomised, non-inferiority, phase 3 CHHiP trial. *The Lancet Oncology.* 2016; 17 (8): 1047–1060. 10.1016/S1470-2045(16)30102-4.

(65) Picardi C, Perret I, Miralbell R, Zilli T. Hypofractionated radiotherapy for prostate cancer in the postoperative setting: What is the evidence so far? *Cancer treatment reviews.* 2018; 62 91–96. 10.1016/j.ctrv.2017.11.004.

(66) Reiko Kobayashi, Hideomi Yamashita, Kae Okuma, Kuni Ohtomo, Keiichi Nakagawa. Details of recurrence sites after definitive radiation therapy for cervical cancer. *Journal of gynecologic oncology.* 2016; 27 (2): 28. https://kiss.kstudy.com/ExternalLink/Ar?key=3400881. .

(67) Li J, Liu G, Luo J, Yan S, Ye P, Wang J, et al. Cervical cancer prognosis and related risk factors for patients with cervical cancer: a long-term retrospective cohort study. *Scientific reports.* 2022; 12 (1): 13994. 10.1038/s41598-022-17733-8.

(68) Lee SJ, Kim M, Kwak Y, Kang HJ. The Clinical Course of the Late Toxicity of Definitive Radiotherapy in Cervical Cancer. *Medicina (Kaunas, Lithuania).* 2024; 60 (8): 1364. 10.3390/medicina60081364.

(69) Georg P, M.D, Lang S, Ph.D, Dimopoulos JCA, M.D, Dörr, Wolfgang, D.V.M., Ph.D, Sturdza AE, M.D, Berger D, Ph.D, et al. Dose–Volume Histogram Parameters and Late Side Effects in Magnetic Resonance Image–Guided Adaptive Cervical Cancer Brachytherapy. *International Journal of Radiation OncologyBiologyPhysics.* 2011; 79 (2): 356–362. 10.1016/j.ijrobp.2009.11.002.

(70) Chen SW, Liang JA, Hung YC, Yeh LS, Chang WC, Lin WC, et al. Late toxicities in concurrent chemoradiotherapy using high-dose-rate intracavitary brachytherapy plus weekly cisplatin for locally advanced cervical cancer: a historical cohort comparison against two previous different treatment schemes. *European journal of gynaecological oncology.* 2010; 31 (5): 504–509. https://www.ncbi.nlm.nih.gov/pubmed/21061789. .

(71) Ippolito E, Mertens I, Haustermans K, Gambacorta MA, Pasini D, Valentini V. IGRT in rectal cancer. *Acta oncologica.* 2008; 47 (7): 1317–1324. 10.1080/02841860802256459.

(72) The Royal College of Radiologists. *National rectal cancer intensity-modulated radiotherapy (IMRT) guidance.* 2021.

(73) Valentini V, Gambacorta MA, Barbaro B, Chiloiro G, Coco C, Das P, et al. International consensus guidelines on Clinical Target Volume delineation in rectal cancer. *Radiotherapy and oncology.* 2016; 120 (2): 195–201. 10.1016/j.radonc.2016.07.017.

(74) Roeske JC, Forman JD, Mesina CF, He T, Pelizzari CA, Fontenla E, et al. Evaluation of changes in the size and location of the prostate, seminal vesicles, bladder, and rectum during a course of external beam radiation therapy. *International Journal of Radiation OncologyBiologyPhysics.* 1995; 33 (5): 1321–1329. 10.1016/0360-3016(95)00225-1.

(75) Orkin BA, Hanson RB, Kelly KA. The Rectal Motor Complex. *Neurogastroenterology and motility.* 1989; 1 (1): 5–8. 10.1111/j.1365-2982.1989.tb00138.x.

(76) Kumar D, Williams NS, Waldron D, Wingate DL. Prolonged manometric recording of anorectal motor activity in ambulant human subjects: evidence of periodic activity. *Gut.* 1989; 30 (7): 1007–1011. 10.1136/gut.30.7.1007.

(77) Whitehead WE, Engel BT, Schuster MM. Irritable bowel syndrome: physiological and psychological differences between diarrhea-predominant and constipation-predominant patients. *Digestive diseases and sciences.* 1980; 25 (6): 404–413. 10.1007/BF01395503.

(78) Orkin BA, Hanson RB, Kelly KA, Phillips SF, John D. Human anal motility while fasting, after feeding, and during sleep. *Gastroenterology.* 1991; 100 (4): 1016–1023. 10.1016/0016-5085(91)90277-R.

(79) Oates R, Brown A, Tan A, Foroudi F, Lim Joon M, Schneider M, et al. Real-time Image-guided Adaptive-predictive Prostate Radiotherapy using Rectal Diameter as a Predictor of Motion. *Clinical oncology (Royal College of Radiologists (Great Britain)).* 2017; 29 (3): 180–187. 10.1016/j.clon.2016.09.019.

(80) Alexander SE, Oelfke U, Westley R, McNair HA, Tree AC. Prostate cancer image guided radiotherapy: Why the commotion over rectal volume and motion? *Clinical and translational radiation oncology.* 2023; 43 100685. 10.1016/j.ctro.2023.100685.

(81) van Herk M, Remeijer P, Rasch C, Lebesque JV. The probability of correct target dosage: dose-population histograms for deriving treatment margins in radiotherapy. *International Journal of Radiation OncologyBiologyPhysics.* 2000; 47 (4): 1121–1135. 10.1016/S0360-3016(00)00518-6.

(82) The Royal College of Radiologists, Institute of Physics and Engineering in Medicine, Society and College of Radiographers. *On target: ensuring geometric accuracy in radiotherapy.* 2008. .

(83) Di Yan, Frank Vicini, John Wong, Alvaro Martinez. Adaptive radiation therapy. *Physics in Medicine & Biology.* 1997; 42 (123): 1230132. 10.1088/0031-9155/42/1/008.

(84) Burmeister JW, Joiner MC. Physics of radiation therapy for the radiobiologist. In: Joiner MC, van der Kogel AJ. (eds.) *Basic Clinical Radiobiology.* CRC Press/Taylor & Francis Group; 2018. pp. 61–80.

(85) Ålander E, Visapää H, Kouri M, Keyriläinen J, Saarilahti K, Tenhunen M. Gold seed fiducials in analysis of linear and rotational displacement of the prostate bed. *Radiotherapy and oncology.* 2013; 110 (2): 256–260. 10.1016/j.radonc.2013.10.037.

(86) Schiffner DC, M.D, Gottschalk, Alexander R., M.D., Ph.D, Lometti M, M.S, Aubin M, M.Sc.E.E, Pouliot J, Ph.D, Speight, Joycelyn, M.D., Ph.D, et al. Daily electronic portal imaging of implanted gold seed fiducials in patients undergoing radiotherapy after radical prostatectomy. *International journal of radiation oncology, biology, physics.* 2007; 67 (2): 610–619. 10.1016/j.ijrobp.2006.09.042.

(87) Fortin I, Carrier J-, Beauchemin M-, Béliveau-Nadeau D, Delouya G, Taussky D. Using fiducial markers in the prostate bed in postprostatectomy external beam radiation therapy improves accuracy over surgical clips. *Strahlentherapie und Onkologie.* 2014; 190 (5): 467–471. 10.1007/s00066-014-0631-3.

(88) Yen A, Shen C, Albuquerque K. The New Kid on the Block: Online Adaptive Radiotherapy in the Treatment of Gynecologic Cancers. *Current oncology.* 2023; 30 (1): 865–874. 10.3390/curroncol30010066.

(89) Lim-Reinders S, BSc, Keller BM, PhD, Al-Ward S, MSc, Sahgal, Arjun, MD, FRCPC, Kim A, PhD. Online Adaptive Radiation Therapy. *International journal of radiation oncology, biology, physics.* 2017; 99 (4): 994–1003. 10.1016/j.ijrobp.2017.04.023.

(90) Ghilezan, Michel, MD, PhD, Yan D, DSc, Martinez A, MD. Adaptive Radiation Therapy for Prostate Cancer. *Seminars in Radiation Oncology.* 2010; 20 (2): 130–137. 10.1016/j.semradonc.2009.11.007.

(91) Chetty IJ, Rosu-Bubulac M. Deformable Registration for Dose Accumulation. *Seminars in radiation oncology.* 2019; 29 (3): 198–208. 10.1016/j.semradonc.2019.02.002.

(92) Yen A, Zhong X, Lin M, Nwachukwu C, Albuquerque K, Hrycushko B. Optimizing Online Adaptation Timing in the Treatment of Locally Advanced Cervical Cancer. *Practical Radiation Oncology.* 2024; 14 (2): e159–e164. 10.1016/j.prro.2023.10.004.

(93) Waters M, Price A, Laugeman E, Henke L, Hugo G, Stowe H, et al. CT-based online adaptive radiotherapy improves target coverage and organ at risk (OAR) avoidance in stereotactic body radiation therapy (SBRT) for prostate cancer. *Clinical and translational radiation oncology.* 2024; 44 100693. 10.1016/j.ctro.2023.100693.

(94) Christiansen RL, Dysager L, Hansen CR, Jensen HR, Schytte T, Nyborg CJ, et al. Online adaptive radiotherapy potentially reduces toxicity for high-risk prostate cancer treatment. *Radiotherapy and oncology.* 2022; 167 165–171. 10.1016/j.radonc.2021.12.013.

(95) Byrne M, Archibald-Heeren B, Hu Y, Teh A, Beserminji R, Cai E, et al. Varian ethos online adaptive radiotherapy for prostate cancer: Early results of contouring accuracy, treatment plan quality, and treatment time. *Journal of Applied Clinical Medical Physics.* 2022; 23 (1): e13479–n/a. 10.1002/acm2.13479.

(96) McComas KN, Yock A, Darrow K, Shinohara ET. Online Adaptive Radiation Therapy and Opportunity Cost. *Advances in radiation oncology.* 2023; 8 (3): 101034. 10.1016/j.adro.2022.101034.

(97) Langen KM, Ph.D, Willoughby TR, M.S, Meeks SL, Ph.D, Santhanam A, Ph.D, Cunningham A, B.A, Levine L, Ph.D, et al. Observations on Real-Time Prostate Gland Motion Using Electromagnetic Tracking. *International journal of radiation oncology, biology, physics.* 2008; 71 (4): 1084–1090. 10.1016/j.ijrobp.2007.11.054.

(98) Ng JA, Booth JT, PhD, Poulsen PR, PhD, Fledelius W, PhD, Worm ES, MS, Eade T, MD, et al. Kilovoltage Intrafraction Monitoring for Prostate Intensity Modulated Arc Therapy: First Clinical Results. *International journal of radiation oncology, biology, physics.* 2012; 84 (5): e655–e661. 10.1016/j.ijrobp.2012.07.2367.

(99) Keall PJ, PhD, Ng JA, PhD, Juneja P, PhD, O'Brien RT, PhD, Huang C, PhD, Colvill E, MSc, et al. Real-Time 3D Image Guidance Using a Standard LINAC: Measured Motion, Accuracy, and Precision of the First Prospective Clinical Trial of Kilovoltage Intrafraction Monitoring–Guided Gating for Prostate Cancer Radiation Therapy. *International journal of radiation oncology, biology, physics.* 2016; 94 (5): 1015–1021. 10.1016/j.ijrobp.2015.10.009.

(100) Legge K, Nguyen D, Ng JA, Wilton L, Richardson M, Booth J, et al. Real-time intrafraction prostate motion during linac based stereotactic radiotherapy with rectal displacement. *Journal of applied clinical medical physics.* 2017; 18 (6): 130–136. 10.1002/acm2.12195.

(101) Borowicz DM, Skrobała A, Kruszyna-Mochalska M, Malicki J. Does CyberKnife improve dose distribution versus IMRT and VMAT on a linear accelerator in low-risk prostate cancer? *Radiology and oncology.* 2022; 56 (2): 259–266. 10.2478/raon-2022-0010.

(102) Scobioala S, Kittel C, Elsayad K, Kroeger K, Oertel M, Samhouri L, et al. A treatment planning study comparing IMRT techniques and cyber knife for stereotactic body radiotherapy of low-risk prostate carcinoma. *Radiation Oncology.* 2019; 14 (1): 143–10. 10.1186/s13014-019-1353-6.

(103) Tawfik ZA, Farid ME, El Shahat KM, Hussein AA, Eldib AA, Al Etreby M. A dosimetric study comparing Cyberknife and LINAC-based stereotactic radiotherapy or radiosurgery treatments. *Journal of Radiation Research and Applied Sciences.* 2024; 17 (1): 100781. 10.1016/j.jrras.2023.100781.

(104) Koh D, Kim J, Kim H, Chang Y, Kim HJ. Clinical Outcomes of CyberKnife Radiotherapy in Prostate Cancer Patients: Short-term, Single-Center Experience. *Korean journal of urology.* 2014; 55 (3): 172–177. 10.4111/kju.2014.55.3.172.

(105) Song S, Yenice KM, Kopec M, Liauw SL. Image-guided radiotherapy using surgical clips as fiducial markers after prostatectomy: A report of total setup error, required PTV expansion, and dosimetric implications. *Radiotherapy and oncology.* 2012; 103 (2): 270–274. 10.1016/j.radonc.2011.07.024.

(106) Bell LJ, Cox J, Eade T, Rinks M, Kneebone A. Prostate bed motion may cause geographic miss in post-prostatectomy image-guided intensity-modulated radiotherapy. *Journal of medical imaging and radiation oncology.* 2013; 57 (6): 725–732. 10.1111/1754-9485.12089.

(107) Sandhu A, Sethi R, Rice R, Wang J, Marcus L, Salem C, et al. Prostate bed localization with image-guided approach using on-board imaging: Reporting acute toxicity and implications for radiation therapy planning following prostatectomy. *Radiotherapy and oncology.* 2008; 88 (1): 20–25. 10.1016/j.radonc.2008.05.009.

(108) Keall PJ, Colvill E, O'Brien R, Ng JA, Poulsen PR, Eade T, et al. The first clinical implementation of electromagnetic transponder-guided MLC tracking. *Medical Physics.* 2014; 41 (2): 020702–n/a. 10.1118/1.4862509.

(109) Juneja P, Kneebone A, Booth JT, Thwaites DI, Kaur R, Colvill E, et al. Prostate motion during radiotherapy of prostate cancer patients with and without application of a hydrogel spacer: a comparative study. *Radiation oncology (London, England).* 2015; 10 (1): 215. 10.1186/s13014-015-0526-1.

(110) Shah AP, Kupelian PA, Willoughby TR, Langen KM, Meeks SL. An evaluation of intrafraction motion of the prostate in the prone and supine positions using electromagnetic tracking. *Radiotherapy and oncology.* 2011; 99 (1): 37–43. 10.1016/j.radonc.2011.02.012.

(111) Willoughby TR, Kupelian PA, Pouliot J, Shinohara K, Aubin M, Roach M, et al. Target localization and real-time tracking using the Calypso 4D localization system in patients with localized prostate cancer. *International journal of radiation oncology, biology, physics.* 2006; 65 (2): 528–534. 10.1016/j.ijrobp.2006.01.050.

(112) Kupelian P, M.D, Willoughby T, M.Sc, Mahadevan A, M.D, Djemil T, Ph.D, Weinstein G, M.D, Jani S, Ph.D, et al. Multi-institutional clinical experience with the Calypso System in localization and continuous, real-time monitoring of the prostate gland during external radiotherapy. *International journal of radiation oncology, biology, physics.* 2007; 67 (4): 1088–1098. 10.1016/j.ijrobp.2006.10.026.

(113) Langenhuijsen JF, Donker R, McColl GM, Kiemeney LALM, Witjes JA, Lin ENJTv. Postprostatectomy ultrasound-guided transrectal implantation of gold markers for external beam radiotherapy : Technique and complications rate. *Strahlentherapie und Onkologie.* 2013; 189 (6): 476–481. 10.1007/s00066-013-0323-4.

(114) Wagenlehner FME, van Oostrum E, Tenke P, Tandogdu Z, Çek M, Grabe M, et al. Infective Complications After Prostate Biopsy: Outcome of the Global Prevalence Study of Infections in Urology (GPIU) 2010 and 2011, A Prospective Multinational Multicentre Prostate Biopsy Study. *European Urology.* 2013; 63 (3): 521–527. 10.1016/j.eururo.2012.06.003.

(115) Loh J, Baker K, Sridharan S, Greer P, Wratten C, Capp A, et al. Infections after fiducial marker implantation for prostate radiotherapy: are we underestimating the risks? *Radiation Oncology.* 2015; 10 (1): 38. 10.1186/s13014-015-0347-2.

(116) O'Neill AGM, Jain S, Hounsell AR, O'Sullivan JM. Fiducial marker guided prostate radiotherapy: a review. *British journal of radiology.* 2016; 89 (1068): 20–20160296. 10.1259/bjr.20160296.

(117) Fehniger J, Schiff PB, Pothuri B. Successful treatment of platinum refractory ovarian clear cell carcinoma with secondary cytoreductive surgery and implantable transponder placement to facilitate targeted volumetric arc radiation therapy. *Gynecologic oncology reports.* 2019; 27 11–14. 10.1016/j.gore.2018.11.004.

(118) Gatcombe HG, Liu T, Chen H, Godette KD, Diaz R, Rossi P. Calypso 4D Localization and Cone-beam CT Evaluation of Cervical Motion during External Beam Radiotherapy for Intact Cervix Cancer. *International journal of radiation oncology, biology, physics.* 2010; 78 (3): S41–S42. 10.1016/j.ijrobp.2010.07.133.

(119) Camus M, Karsenti D, Levy J, Moreno M, Coron E, Esch A, et al. Success rate of fiducial marker placement for treatment of esophageal or rectal cancers: a prospective multicenter study (FIDECHO study) (with video). *Gastrointestinal endoscopy.* 2024; 10.1016/j.gie.2024.08.014.

(120) Rigter LS, Rijkmans EC, Inderson A, van den Ende RPJ, Kerkhof EM, Ketelaars M, et al. EUS-guided fiducial marker placement for radiotherapy in rectal cancer: feasibility of two placement strategies and four fiducial types. *Endoscopy International Open.* 2019; 7 (11): E1357–E1364. 10.1055/a-0958-2148.

(121) Rubod C, Brieu M, Cosson M, Rivaux G, Clay J, de Landsheere L, et al. Biomechanical Properties of Human Pelvic Organs. *Urology.* 2012; 79 (4): 968.e17–968.e22. 10.1016/j.urology.2011.11.010.

(122) van den Berg MM, Voskuijl WP, Boeckxstaens GE, Benninga MA. Rectal compliance and rectal sensation in constipated adolescents, recovered adolescents and healthy volunteers. *Gut.* 2008; 57 (5): 599–603. 10.1136/gut.2007.125690.

(123) Dall FH, Jørgensen CS, Houe D, Gregersen H, Djurhuus JC. Biomechanical wall properties of the human rectum. A study with impedance planimetry. *Gut.* 1993; 34 (11): 1581–1586. 10.1136/gut.34.11.1581.

(124) Vorwerk H, Liersch T, Rothe H, Ghadimi M, Christiansen H, Hess CF, et al. Gold markers for tumor localization and target volume delineation in radiotherapy for rectal cancer. *Strahlentherapie und Onkologie.* 2009; 185 (2): 127–133. 10.1007/s00066-009-1928-5.

(125) Moningi S, BA, Walker AJ, MD, Malayeri AA, MD, Rosati LM, BS, Gearhart SL, MD, Efron JE, MD, et al. Analysis of fiducials implanted during EUS for patients with localized rectal cancer receiving high-dose rate endorectal brachytherapy. *Gastrointestinal endoscopy.* 2015; 81 (3): 765–769.e1. 10.1016/j.gie.2014.11.004.

(126) Wagner M, Gondan M, Zöllner C, Wünscher JJ, Nickel F, Albala L, et al. Electromagnetic organ tracking allows for real-time compensation of tissue shift in image-guided laparoscopic rectal surgery: results of a phantom study. *Surgical Endoscopy.* 2016; 30 (2): 495–503. 10.1007/s00464-015-4231-9.

(127) Kok END, Eppenga R, Kuhlmann KFD, Groen HC, van Veen R, van Dieren JM, et al. Accurate surgical navigation with real-time tumor tracking in cancer surgery. *NPJ precision oncology.* 2020; 4 (1): 8. 10.1038/s41698-020-0115-0.

(128) Balter JM, Wright JN, Newell LJ, Friemel B, Dimmer S, Cheng Y, et al. Accuracy of a wireless localization system for radiotherapy. *International Journal of Radiation OncologyBiologyPhysics.* 2005; 61 (3): 933–937. 10.1016/j.ijrobp.2004.11.009.

(129) Hardcastle N, Cutajar DL, Metcalfe PE, Lerch MLF, Perevertaylo VL, Tomé WA, et al. In vivo real-time rectal wall dosimetry for prostate radiotherapy. *Physics in medicine & biology.* 2010; 55 (13): 3859–3871. 10.1088/0031-9155/55/13/019.

(130) Wootton L, Kudchadker R, Lee A, Beddar S. Real-time in vivo rectal wall dosimetry using plastic scintillation detectors for patients with prostate cancer. *Physics in medicine & biology.* 2014; 59 (3): 647–660. 10.1088/0031-9155/59/3/647.

(131) Cartwright LE, Suchowerska N, Yin Y, Lambert J, Haque M, McKenzie DR. Dose mapping of the rectal wall during brachytherapy with an array of scintillation

dosimeters. *Medical physics (Lancaster).* 2010; 37 (5): 2247–2255. 10.1118/1.3397446.

(132) Archambault L, Ph.D, Briere TM, Ph.D, Pönisch F, Ph.D, Beaulieu L, Ph.D, Kuban DA, M.D, Lee A, M.D, et al. Toward a Real-Time In Vivo Dosimetry System Using Plastic Scintillation Detectors. *International Journal of Radiation OncologyBiologyPhysics.* 2010; 78 (1): 280–287. 10.1016/j.ijrobp.2009.11.025.

(133) Klein D, Briere TM, Kudchadker R, Archambault L, Beaulieu L, Lee A, et al. In-phantom dose verification of prostate IMRT and VMAT deliveries using plastic scintillation detectors. *Radiation Measurements.* 2012; 47 (10): 921–929. 10.1016/j.radmeas.2012.08.005.

(134) Lawrie TA, Green JT, Beresford M, Wedlake L, Burden S, Davidson SE, et al. Interventions to reduce acute and late adverse gastrointestinal effects of pelvic radiotherapy for primary pelvic cancers. *Cochrane database of systematic reviews.* 2018; 2020 (11): CD012529. 10.1002/14651858.CD012529.pub2.

(135) Fuccio L, Frazzoni L, Guido A. Prevention of pelvic radiation disease. *World journal of gastrointestinal pharmacology and therapeutics.* 2015; 6 (1): 1–9. 10.4292/wjgpt.v6.i1.1.

(136) van de Wetering FT, Verleye L, Andreyev HJN, Maher J, Vlayen J, Pieters BR, et al. Non-surgical interventions for late rectal problems (proctopathy) of radiotherapy in people who have received radiotherapy to the pelvis. *Cochrane database of systematic reviews.* 2016; 2016 (4): CD003455. 10.1002/14651858.CD003455.pub2.

(137) Kilic D, Ozenirler S, Egehan I, Dursun A. Sulfasalazine decreases acute gastrointestinal complications due to pelvic radiotherapy. *The Annals of pharmacotherapy.* 2001; 35 (7): 806–810. 10.1345/aph.10055.

(138) Miller RC, Petereit DG, Sloan JA, Liu H, Martenson JA, Bearden JD, et al. N08C9 (Alliance): A Phase 3 Randomized Study of Sulfasalazine vs Placebo in the Prevention of Acute Diarrhea in Patients Receiving Pelvic Radiation Therapy. *International journal of radiation oncology, biology, physics.* 2016; 95 (4): 1168–1174. 10.1016/j.ijrobp.2016.01.063.

(139) Dalsania RM, Shah KP, Stotsky-Himelfarb E, Hoffe S, Willingham FF. Management of Long-Term Toxicity From Pelvic Radiation Therapy. *American Society of Clinical Oncology educational book.* 2021; 41 (41): 1–157. 10.1200/EDBK_323525.

(140) Kochhar R, Patel F, Dhar A, Sharma SC, Ayyagari S, Aggarwal R, et al. Radiation-induced proctosigmoiditis. Prospective, randomized, double-blind controlled trial of oral sulfasalazine plus rectal steroids versus rectal sucralfate. *Digestive diseases and sciences.* 1991; 36 (1): 103–107. 10.1007/BF01300096.

(141) SANGUINETI G, FRANZONE P, MARCENARO M, FOPPIANO F, VITALE V. Sucralfate versus mesalazine versus hydrocortisone in the prevention of acute

radiation proctitis during conformal radiotherapy for prostate carcinoma: A randomized study. *Strahlentherapie und Onkologie.* 2003; 179 (7): 464–470. 10.1007/s00066-003-1082-4.

(142) Sahakitrungruang C, Patiwongpaisarn A, Kanjanasilp P, Malakorn S, Atittharnsakul P. A Randomized Controlled Trial Comparing Colonic Irrigation and Oral Antibiotics Administration Versus 4% Formalin Application for Treatment of Hemorrhagic Radiation Proctitis. *Diseases of the colon & rectum.* 2012; 55 (10): 1053–1058. 10.1097/DCR.0b013e318265720a.

(143) Cavcić J, Turcić J, Martinac P, Jelincić Z, Zupancić B, Panijan-Pezerović R, et al. Metronidazole in the treatment of chronic radiation proctitis: clinical trial. *Croatian medical journal.* 2000; 41 (3): 314–318. https://www.ncbi.nlm.nih.gov/pubmed/10962052. .

(144) Fuccio L, Guido A, Laterza L, Eusebi LH, Busutti L, Bunkheila F, et al. Randomised clinical trial: preventive treatment with topical rectal beclomethasone dipropionate reduces post-radiation risk of bleeding in patients irradiated for prostate cancer. *Alimentary pharmacology & therapeutics.* 2011; 34 (6): 628–637. 10.1111/j.1365-2036.2011.04780.x.

(145) Chruscielewska-Kiliszek MR, Regula J, Polkowski M, Rupinski M, Kraszewska E, Pachlewski J, et al. Sucralfate or placebo following argon plasma coagulation for chronic radiation proctitis: a randomized double blind trial. *Colorectal disease.* 2013; 15 (1): e48–e55. 10.1111/codi.12035.

(146) McElvanna K, Wilson A, Irwin T. Sucralfate paste enema: a new method of topical treatment for haemorrhagic radiation proctitis. *Colorectal disease.* 2014; 16 (4): 281–284. 10.1111/codi.12507.

(147) Saei S, Sahebnasagh A, Ghasemi A, Akbari J, Alipour A, Lashkardoost H, et al. Efficacy of sucralfate ointment in the prevention of acute proctitis in cancer patients: A randomized controlled clinical trial. *Caspian journal of internal medicine.* 2020; 11 (4): 410–418. 10.22088/cjim.11.4.410.

(148) Kouvaris JR, Kouloulias VE, Vlahos LJ. Amifostine: The First Selective-Target and Broad-Spectrum Radioprotector. *The Oncologist.* 2007; 12 (6): 738–747. 10.1634/theoncologist.12-6-738.

(149) Singh AK, Ménard C, Guion P, Simone NL, Smith S, Crouse NS, et al. Intrarectal amifostine suspension may protect against acute proctitis during radiation therapy for prostate cancer: A pilot study. *International journal of radiation oncology, biology, physics.* 2006; 65 (4): 1008–1013. 10.1016/j.ijrobp.2006.02.030.

(150) Kouloulias VE, Kouvaris JR, Pissakas G, Kokakis JD, Antypas C, Mallas E, et al. A Phase II Randomized Study of Topical Intrarectal Administration of Amifostine for the Prevention of Acute Radiation-Induced Rectal Toxicity. *Strahlentherapie und Onkologie.* 2004; 180 (9): 557–562. 10.1007/s00066-004-1226-1.

(151) Kouloulias VE, Kouvaris JR, Pissakas G, Mallas E, Antypas C, Kokakis JD, et al. Phase II multicenter randomized study of amifostine for prevention of acute radiation rectal toxicity: Topical intrarectal versus subcutaneous application. *International journal of radiation oncology, biology, physics.* 2005; 62 (2): 486–493. 10.1016/j.ijrobp.2004.10.043.

(152) KOUVARIS J, KOULOULIAS V, MALAS E, ANTYPAS C, KOKAKIS J, MICHOPOULOS S, et al. Amifostine as radioprotective agent for the rectal mucosa during irradiation of pelvic tumors: A phase II randomized study using various toxicity scales and rectosigmoidoscopy. *Strahlentherapie und Onkologie.* 2003; 179 (3): 167–174. 10.1007/s00066-003-0970-y.

(153) Athanassiou H, Antonadou D, Coliarakis N, Kouveli A, Synodinou M, Paraskevaidis M, et al. Protective effect of amifostine during fractionated radiotherapy in patients with pelvic carcinomas: Results of a randomized trial. *International journal of radiation oncology, biology, physics.* 2003; 56 (4): 1154–1160. 10.1016/S0360-3016(03)00187-1.

(154) Koukourakis MI, Kyrias G, Kakolyris S, Kouroussis C, Frangiadaki C, Giatromanolaki A, et al. Subcutaneous Administration of Amifostine During Fractionated Radiotherapy: A Randomized Phase II Study. *Journal of Clinical Oncology.* 2000; 18 (11): 2226–2233. 10.1200/jco.2000.18.11.2226.

(155) Katsanos KH, Briasoulis E, Tsekeris P, Batistatou A, Bai M, Tolis C, et al. Randomized phase II exploratory study of prophylactic amifostine in cancer patients who receive radical radiotherapy to the pelvis. *Journal of experimental & clinical cancer research.* 2010; 29 (1): 68. 10.1186/1756-9966-29-68.

(156) Esco R, Valencia J, Coronel P, Carceller JA, Gimeno M, Bascón N. Efficacy of orgotein in prevention of late side effects of pelvic irradiation: A randomized study. *International journal of radiation oncology, biology, physics.* 2004; 60 (4): 1211–1219. 10.1016/j.ijrobp.2004.04.038.

(157) Menander-Huber KB, Edsmyr F, Huber W. Orgotein (superoxide dismutase): a drug for the amelioration of radiation-induced side effects. A double-blind, placebo-controlled study in patients with bladder tumours. *Urological research.* 1978; 6 (4): 255–257. 10.1007/BF00262630.

(158) Razzaghdoust A, Mozdarani H, Mofid B. Famotidine as a radioprotector for rectal mucosa in prostate cancer patients treated with radiotherapy. *Strahlentherapie und Onkologie.* 2014; 190 (8): 739–744. 10.1007/s00066-014-0602-8.

(159) Hall S, Rudrawar S, Zunk M, Bernaitis N, Arora D, McDermott CM, et al. Protection against Radiotherapy-Induced Toxicity. *Antioxidants.* 2016; 5 (3): 22. 10.3390/antiox5030022.

(160) Patel P, Subhas G, Gupta A, Chang Y, Mittal VK, McKendrick A. Oral Vitamin A Enhances the Effectiveness of Formalin 8% in Treating Chronic

Hemorrhagic Radiation Proctopathy. *Diseases of the colon & rectum.* 2009; 52 (9): 1605–1609. 10.1007/DCR.0b013e3181afbe3a.

(161) Kennedy M, Bruninga K, Mutlu EA, Losurdo J, Choudhary S, Keshavarzian A. Successful and sustained treatment of chronic radiation proctitis with antioxidant vitamins E and C. *The American journal of gastroenterology.* 2001; 96 (4): 1080–1084. 10.1016/S0002-9270(01)02305-X.

(162) EHRENPREIS ED, JANI A, LEVITSKY J, AHN J, HONG J. A Prospective, Randomized, Double-Blind, Placebo-Controlled Trial of Retinol Palmitate (Vitamin A) for Symptomatic Chronic Radiation Proctopathy. *Diseases of the colon & rectum.* 2005; 48 (1): 1–8. 10.1007/s10350-004-0821-7.

(163) KOZELSKY TF, MEYERS GE, PILEPICH MV, NOVOTNY PJ, MARTENSON JA, SLOAN JA, et al. Phase III Double-Blind Study of Glutamine Versus Placebo for the Prevention of Acute Diarrhea in Patients Receiving Pelvic Radiation Therapy. *Journal of clinical oncology.* 2003; 21 (9): 1669–1674. 10.1200/JCO.2003.05.060.

(164) Kucuktulu E, Guner A, Kahraman I, Topbas M, Kucuktulu U. The protective effects of glutamine on radiation-induced diarrhea. *Supportive Care in Cancer.* 2013; 21 (4): 1071–1075. 10.1007/s00520-012-1627-0.

(165) Vidal-Casariego, Alfonso, M.D., Ph.D, Calleja-Fernández, Alicia, R.D., Ph.D, Cano-Rodríguez, Isidoro, M.D., Ph.D, Cordido, Fernando, M.D., Ph.D, Ballesteros-Pomar, María D., M.D., Ph.D. Effects of oral glutamine during abdominal radiotherapy on chronic radiation enteritis: A randomized controlled trial. *Nutrition (Burbank, Los Angeles County, Calif.).* 2015; 31 (1): 200–204. 10.1016/j.nut.2014.08.003.

(166) MCGOUGH C, WEDLAKE L, BALDWIN C, HACKETT C, NORMAN AR, BLAKE P, et al. Clinical trial: normal diet vs. partial replacement with oral E028 formula for the prevention of gastrointestinal toxicity in cancer patients undergoing pelvic radiotherapy. *Alimentary pharmacology & therapeutics.* 2008; 27 (11): 1132–1139. 10.1111/j.1365-2036.2008.03665.x.

(167) Pettersson A, Johansson B, Persson C, Berglund A, Turesson I. Effects of a dietary intervention on acute gastrointestinal side effects and other aspects of health-related quality of life: A randomized controlled trial in prostate cancer patients undergoing radiotherapy. *Radiotherapy and oncology.* 2012; 103 (3): 333–340. 10.1016/j.radonc.2012.04.006.

(168) Wedlake LJ, McGough C, Shaw C, Klopper T, Thomas K, Lalji A, et al. Clinical trial: efficacy of a low or modified fat diet for the prevention of gastrointestinal toxicity in patients receiving radiotherapy treatment for pelvic malignancies. *Journal of human nutrition and dietetics.* 2012; 25 (3): 247–259. 10.1111/j.1365-277X.2012.01248.x.

(169) Itoh Y, Mizuno M, Ikeda M, Nakahara R, Kubota S, Ito J, et al. A Randomized, Double-Blind Pilot Trial of Hydrolyzed Rice Bran versus Placebo

for Radioprotective Effect on Acute Gastroenteritis Secondary to Chemoradiotherapy in Patients with Cervical Cancer. *Evidence-based complementary and alternative medicine.* 2015; 2015 (2015): 1–6. 10.1155/2015/974390.

(170) Wedlake L, Shaw C, McNair H, Lalji A, Mohammed K, Klopper T, et al. Randomized controlled trial of dietary fiber for the prevention of radiation-induced gastrointestinal toxicity during pelvic radiotherapy. *The American journal of clinical nutrition.* 2017; 106 (3): 849–857. 10.3945/ajcn.116.150565.

(171) Pettersson A, Nygren P, Persson C, Berglund A, Turesson I, Johansson B. Effects of a dietary intervention on gastrointestinal symptoms after prostate cancer radiotherapy: Long-term results from a randomized controlled trial. *Radiotherapy and oncology.* 2014; 113 (2): 240–247. 10.1016/j.radonc.2014.11.025.

(172) Wilder RB, M.D, Barme GA, M.D, Gilbert RF, M.D, Holevas RE, M.D, Kobashi LI, M.D, Reed RR, M.D, et al. Cross-Linked Hyaluronan Gel Reduces the Acute Rectal Toxicity of Radiotherapy for Prostate Cancer. *International journal of radiation oncology, biology, physics.* 2010; 77 (3): 824–830. 10.1016/j.ijrobp.2009.05.069.

(173) Wilder RB, Barme GA, Gilbert RF, Holevas RE, Kobashi LI, Reed RR, et al. Cross-linked hyaluronan gel improves the quality of life of prostate cancer patients undergoing radiotherapy. *Brachytherapy.* 2011; 10 (1): 44–50. 10.1016/j.brachy.2009.12.005.

(174) Yeh J, Lehrich B, Tran C, Mesa A, Baghdassarian R, Yoshida J, et al. Polyethylene glycol hydrogel rectal spacer implantation in patients with prostate cancer undergoing combination high-dose-rate brachytherapy and external beam radiotherapy. *Brachytherapy.* 2016; 15 (3): 283–287. 10.1016/j.brachy.2015.12.007.

(175) Strom TJ, Wilder RB, Fernandez DC, Mellon EA, Saini AS, Hunt DC, et al. A dosimetric study of polyethylene glycol hydrogel in 200 prostate cancer patients treated with high-dose rate brachytherapy ± intensity modulated radiation therapy. *Radiotherapy and oncology.* 2014; 111 (1): 126–131. 10.1016/j.radonc.2014.02.011.

(176) Uhl M, Herfarth K, Eble MJ, Pinkawa M, van Triest B, Kalisvaart R, et al. Absorbable hydrogel spacer use in men undergoing prostate cancer radiotherapy: 12 month toxicity and proctoscopy results of a prospective multicenter phase II trial. *Radiation oncology (London, England).* 2014; 9 (1): 96. 10.1186/1748-717X-9-96.

(177) Mariados N, MD, Sylvester J, MD, Shah D, MD, Karsh L, MD, Hudes R, MD, Beyer D, MD, et al. Hydrogel Spacer Prospective Multicenter Randomized Controlled Pivotal Trial: Dosimetric and Clinical Effects of Perirectal Spacer Application in Men Undergoing Prostate Image Guided Intensity Modulated

Radiation Therapy. *International journal of radiation oncology, biology, physics.* 2015; 92 (5): 971–977. 10.1016/j.ijrobp.2015.04.030.

(178) Hamstra, Daniel A., MD, PhD, Mariados N, MD, Sylvester J, MD, Shah D, MD, Karsh L, MD, Hudes R, MD, et al. Continued Benefit to Rectal Separation for Prostate Radiation Therapy: Final Results of a Phase III Trial. *International journal of radiation oncology, biology, physics.* 2017; 97 (5): 976–985. 10.1016/j.ijrobp.2016.12.024.

(179) Melchert C, Gez E, Bohlen G, Scarzello G, Koziol I, Anscher M, et al. Interstitial biodegradable balloon for reduced rectal dose during prostate radiotherapy: Results of a virtual planning investigation based on the pre- and post-implant imaging data of an international multicenter study. *Radiotherapy and oncology.* 2013; 106 (2): 210–214. 10.1016/j.radonc.2013.01.007.

(180) Levy Y, Paz A, Yosef RB, Corn BW, Vaisman B, Shuhat S, et al. Biodegradable inflatable balloon for reducing radiation adverse effects in prostate cancer. *Journal of Biomedical Materials Research Part B: Applied Biomaterials.* 2009; 91B (2): 855–867. 10.1002/jbm.b.31467.

(181) Kobayashi R, Murakami N, Chiba T, Okuma K, Inaba K, Takahashi K, et al. Effect of Hyaluronate Acid Injection on Dose-Volume Parameters in Brachytherapy for Cervical Cancer. *Advances in radiation oncology.* 2022; 7 (3): 100918. 10.1016/j.adro.2022.100918.

(182) Murakami N, Nakamura S, Kashihara T, Kato T, Shibata Y, Takahashi K, et al. Hyaluronic acid gel injection in rectovaginal septum reduced incidence of rectal bleeding in brachytherapy for gynecological malignancies. *Brachytherapy.* 2020; 19 (2): 154–161. 10.1016/j.brachy.2019.11.004.

(183) Kashihara T, Murakami N, Tselis N, Kobayashi K, Tsuchida K, Shima S, et al. Hyaluronate gel injection for rectum dose reduction in gynecologic high-dose-rate brachytherapy: initial Japanese experience. *Journal of Radiation Research.* 2019; 60 (4): 501–508. 10.1093/jrr/rrz016.

(184) Viswanathan AN, Damato AL, Nguyen PL. Novel Use of a Hydrogel Spacer Permits Reirradiation in Otherwise Incurable Recurrent Gynecologic Cancers. *Journal of clinical oncology.* 2013; 31 (34): e446–e447. 10.1200/JCO.2012.47.9931.

(185) Marnitz S, Budach V, Weisser F, Burova E, Gebauer B, Vercellino FG, et al. Rectum separation in patients with cervical cancer for treatment planning in primary chemo-radiation. *Radiation oncology.* 2012; 7 (1): 109. 10.1186/1748-717X-7-109.

(186) Pinkawa M, Schubert C, Escobar-Corral N, Holy R, Eble MJ. Application of a hydrogel spacer for postoperative salvage radiotherapy of prostate cancer. *Strahlentherapie und Onkologie.* 2014; 191 (4): 375–379. 10.1007/s00066-014-0769-z.

(187) Lehrich BM, Moyses HM, Ravera J, Yoshida J, Torrey R, Baghdassarian R, et al. Five-year results of post-prostatectomy patients administered a hydrogel rectal spacer implant in conjunction with dose escalated external beam radiation therapy. *Journal of radiation oncology.* 2018; 8 (1): 31–38. 10.1007/s13566-018-0369-0.

(188) Millot JC, Arenas-Gallo C, Silver E, Goldman M, Picciotto S, Jia AY, et al. Major Complications and Adverse Events Related to Use of SpaceOAR Hydrogel for Prostate Cancer Radiotherapy. *Urology (Ridgewood, N.J.).* 2024; 188 94–100. 10.1016/j.urology.2023.12.034.

(189) Aminsharifi A, Kotamarti S, Silver D, Schulman A. Major Complications and Adverse Events Related to the Injection of the SpaceOAR Hydrogel System Before Radiotherapy for Prostate Cancer: Review of the Manufacturer and User Facility Device Experience Database. *Journal of Endourology.* 2019; 33 (10): 868–871. 10.1089/end.2019.0431.

(190) Pinkawa M, Klotz J, Djukic V, Schubert C, Escobar-Corral N, Caffaro M, et al. Learning Curve in the Application of a Hydrogel Spacer to Protect the Rectal Wall During Radiotherapy of Localized Prostate Cancer. *Urology.* 2013; 82 (4): 963–968. 10.1016/j.urology.2013.07.014.

(191) Ciernik IF, Baumert BG, Egli P, Glanzmann C, Lütolf UM. On-line correction of beam portals in the treatment of prostate cancer using an endorectal balloon device. *Radiotherapy and oncology.* 2002; 65 (1): 39–45. 10.1016/S0167-8140(02)00187-1.

(192) Smeenk RJ, M.D, Louwe RJW, Ph.D, Langen KM, Ph.D, Shah AP, Ph.D, Kupelian PA, M.D, van Lin, Emile N.J.Th., M.D., Ph.D, et al. An Endorectal Balloon Reduces Intrafraction Prostate Motion During Radiotherapy. *International journal of radiation oncology, biology, physics.* 2012; 83 (2): 661–669. 10.1016/j.ijrobp.2011.07.028.

(193) Hille A, Schmidberger H, Töws N, Weiss E, Vorwerk H, Hess C. The Impact of Varying Volumes in Rectal Balloons on Rectal Dose Sparing in Conformal Radiation Therapy of Prostate Cancer. *Strahlentherapie und Onkologie.* 2005; 181 (11): 709–716. 10.1007/s00066-005-1443-2.

(194) Wachter S, Gerstner N, Dorner D, Goldner G, Colotto A, Wambersie A, et al. The influence of a rectal balloon tube as internal immobilization device on variations of volumes and dose-volume histograms during treatment course of conformal radiotherapy for prostate cancer. *International journal of radiation oncology, biology, physics.* 2002; 52 (1): 91–100. 10.1016/S0360-3016(01)01821-1.

(195) Smeenk RJ, Teh BS, Butler EB, van Lin ENJT, Kaanders JHAM. Is there a role for endorectal balloons in prostate radiotherapy? A systematic review. *Radiotherapy and oncology.* 2010; 95 (3): 277–282. 10.1016/j.radonc.2010.04.016.

(196) Smeenk RJ, van Lin ENJT, van Kollenburg P, Kunze-Busch M, Kaanders JHAM. Anal wall sparing effect of an endorectal balloon in 3D conformal and intensity-modulated prostate radiotherapy. *Radiotherapy and oncology.* 2009; 93 (1): 131–136. 10.1016/j.radonc.2009.05.014.

(197) Ronson BB, Yonemoto LT, Rossi CJ, Slater JM, Slater JD. Patient tolerance of rectal balloons in conformal radiation treatment of prostate cancer. *International journal of radiation oncology, biology, physics.* 2006; 64 (5): 1367–1370. 10.1016/j.ijrobp.2005.11.001.

(198) El-Bassiouni M, Davis J, El-Attar I, Studer G, Lütolf U, Ciernik I. Target Motion Variability and On-Line Positioning Accuracy during External-Beam Radiation Therapy of Prostate Cancer with an Endorectal Balloon Device. *Strahlentherapie und Onkologie.* 2006; 182 (9): 531–536. 10.1007/s00066-006-1581-1.

(199) van Lin ENJT, van der Vight LP, Witjes JA, Huisman HJ, Leer JW, Visser AG. The effect of an endorectal balloon and off-line correction on the interfraction systematic and random prostate position variations: A comparative study. *International journal of radiation oncology, biology, physics.* 2005; 61 (1): 278–288. 10.1016/j.ijrobp.2004.09.042.

(200) Hung AY, M.D, Garzotto M, M.D, Kaurin D, Ph.D. Minimal Benefit of an Endorectal Balloon for Prostate Immobilization as Verified by Daily Localization. *Medical dosimetry : official journal of the American Association of Medical Dosimetrists.* 2011; 36 (2): 195–199. 10.1016/j.meddos.2010.03.003.

(201) Wang KK, Vapiwala N, Bui V, Deville C, Plastaras JP, Bar-Ad V, et al. The impact of stool and gas volume on intrafraction prostate motion in patients undergoing radiotherapy with daily endorectal balloon. *Radiotherapy and oncology.* 2014; 112 (1): 89–94. 10.1016/j.radonc.2014.05.008.

(202) Wootton LS, Kudchadker RJ, Beddar AS, Lee AK. Effectiveness of a novel gas-release endorectal balloon in the removal of rectal gas for prostate proton radiation therapy. *Journal of applied clinical medical physics.* 2012; 13 (5): 190–197. 10.1120/jacmp.v13i5.3945.

(203) Steiner E, MSc, Georg D, PhD, Goldner G, MD, Stock M, PhD. Prostate and Patient Intrafraction Motion: Impact on Treatment Time-Dependent Planning Margins for Patients With Endorectal Balloon. *INTERNATIONAL JOURNAL OF RADIATION ONCOLOGY BIOLOGY PHYSICS.* 2013; 86 (4): 755–761. 10.1016/j.ijrobp.2013.02.035.

(204) Jones BL, Gan G, Kavanagh B, Miften M. Effect of endorectal balloon positioning errors on target deformation and dosimetric quality during prostate SBRT. *Physics in medicine & biology.* 2013; 58 (22): 7995–8006. 10.1088/0031-9155/58/22/7995.

(205) Joo JH, Kim YJ, Kim YS, Cho YP, Lee HY, Jeong CY, et al. Analysis of prostate bed motion using an endorectal balloon and cone beam computed

tomography during postprostatectomy radiotherapy. *OncoTargets and Therapy.* 2016; 9 3095–3100. 10.2147/OTT.S98112.

(206) de Leon JF, Jameson MG, Windsor A, Cloak K, Keats S, Vial P, et al. Superior target volume and organ stability with the use of endorectal balloons in post-prostatectomy radiotherapy. *Journal of medical imaging and radiation oncology.* 2015; 59 (4): 507–513. 10.1111/1754-9485.12300.

(207) Smeenk RJ, van Lin ENJT, van Kollenburg P, McColl GM, Kunze-Busch M, Kaanders JHAM. Endorectal balloon reduces anorectal doses in post-prostatectomy intensity-modulated radiotherapy. *Radiotherapy and oncology.* 2011; 101 (3): 465–470. 10.1016/j.radonc.2011.07.019.

(208) Ishiyama H, Teh BS, Blanco AI, Paulino AC, Mai W, Caillouet J, et al. Salvage intensity modulated radiotherapy using endorectal balloon after radical prostatectomy: Clinical outcomes. *International journal of urology.* 2013; 20 (12): 1178–1183. 10.1111/iju.12145.

(209) Streller T, Rusch U, Herraiz Lablanca MD, Minneken I, Najafi Y, Shrestha B, et al. The effect of endorectal balloon on anorectal dose during postoperative volumetric arc radiotherapy of prostate cancer. *Radiotherapy and oncology.* 2017; 123 (3): 454–458. 10.1016/j.radonc.2017.04.014.

(210) Jameson MG, De Leon J, Windsor AA, Cloak K, Keats S, Dowling JA, et al. Endorectal balloons in the post prostatectomy setting: Do gains in stability lead to more predictable dosimetry? *Radiotherapy and oncology.* 2013; 109 (3): 493–497. 10.1016/j.radonc.2013.08.024.

(211) Parsai EI, Jahadakbar A, Lavvafi H, Elahinia M. A novel and innovative device to retract rectum during radiation therapy of pelvic tumors. *Journal of applied clinical medical physics.* 2019; 20 (1): 194–199. 10.1002/acm2.12517.

(212) Arefpour AM, Abbasi M, Mahdavi SR, Shafieesabet M, Fadavi P. Clinical effects of rectal retractor application in prostate cancer radiotherapy. *Medical journal of the Islamic Republic of Iran.* 2021; 35 69. 10.47176/mjiri.35.69.

(213) Mahdavi SR, Ghaffari H, Mofid B, Rostami A, Reiazi R, Janani L. Rectal retractor application during image-guided dose-escalated prostate radiotherapy. *Strahlentherapie und Onkologie.* 2019; 195 (10): 923–933. 10.1007/s00066-019-01445-6.

(214) Nilsson K, Johansson AK, Montelius A, Turesson I, Heikkinen RO, Ljung G, et al. Decreasing the Dose to the Rectal Wall by Using a Rectal Retractor during Radiotherapy of Prostate Cancer: A Comparative Treatment Planning Study. *Journal of Radiotherapy.* 2014; 2014 1–7. 10.1155/2014/680205.

(215) Ghaffari H, Rostami A, Ardekani M, Mofid B, Mahdavi S. Rectal wall sparing effect of a rectal retractor in prostate intensity-modulated radiotherapy. *Journal of cancer research and therapeutics.* 2021; 17 (2): 383–388. 10.4103/jcrt.JCRT_701_19.

(216) Ghaffari H, Mahdavi SR, Mofid B, Reiazi R. Rectal Sparing Using a Rectal Retractor During Dose Escalated Prostate Radiotherapy. *Medical Physics.* 2018; 45 (6): E254. https://aapm.onlinelibrary.wiley.com/doi/epdf/10.1002/mp.12938?saml_referrer. .

(217) de Leon J, Jameson MG, Rivest-Henault D, Keats S, Rai R, Arumugam S, et al. Reduced motion and improved rectal dosimetry through endorectal immobilization for prostate stereotactic body radiotherapy. *British journal of radiology.* 2019; 92 (1098): 20190056. 10.1259/bjr.20190056.

(218) Nicolae A, Davidson M, Easton H, Helou J, Musunuru H, Loblaw A, et al. Clinical evaluation of an endorectal immobilization system for use in prostate hypofractionated Stereotactic Ablative Body Radiotherapy (SABR). *Radiation oncology (London, England).* 2015; 10 (1): 122. 10.1186/s13014-015-0426-4.

(219) Ghaffari H, Afkhami Ardekani M, Molana SH, Haghparast M, Sanei M, Mahdavi SR, et al. Application of rectal retractor for postprostatectomy salvage radiotherapy of prostate cancer: A case report and literature review. *Clinical case reports.* 2019; 7 (11): 2102–2107. 10.1002/ccr3.2430.

(220) Vanhanen A, Kapanen M. The effect of rectal retractor on intrafraction motion of the prostate. *Biomedical physics & engineering express.* 2016; 2 (3): 35021. 10.1088/2057-1976/2/3/035021.

(221) Murray JR, Gulliford S, Alexander EJ, Mcnair H, Dearnaley DP. P028 The effect of ProSpare, a rectal obturator on anorectal doses in prostate radiotherapy. *European urology supplements : official journal of the European Association of Urology.* 2014; 13 (5): 119. 10.1016/S1569-9056(14)61253-7.

(222) Murray J, McNair H, Alexander E, Thomas K, Dearnaley D. ProSpare, a Rectal Obturator and its Effect on Prostate and Seminal Vesicle Interfraction Motion. *Clinical oncology (Royal College of Radiologists (Great Britain)).* 2015; 28 (5): e13–e14. 10.1016/j.clon.2015.12.015.

(223) Murray J, McNair H, Alexander E, O'Shea T, Thomas K, Nill S, et al. B90: ProSpare, a rectal obturator reduces intrafraction target motion in prostate cancer radiotherapy. *Abstracts from the NCRI Cancer Conference, 2015.*

(224) Alexander E, McNair H, Landeg S, Hansen V, Dearnaley D. Initial Results of a Prospective Clinical Trial Examining a Novel Rectal Obturator to Localise the Prostate and Spare the Rectum during Radical Prostate Radiotherapy. *Clinical oncology (Royal College of Radiologists (Great Britain)).* 2013; 26 (2): e3. 10.1016/j.clon.2013.11.006.

(225) Maleki AN, Thompson A, Runciman MS, Murray J, Mylonas GP. A soft hydraulic endorectal actuator for prostate radiotherapy. *2023 IEEE International Conference on Robotics and Biomimetics (ROBIO)* Piscataway: IEEE; Dec 4, 2023. pp. 1–6.

(226) Pinkawa M, Piroth MD, Holy R, Escobar-Corral N, Caffaro M, Djukic V, et al. Spacer stability and prostate position variability during radiotherapy for prostate cancer applying a hydrogel to protect the rectal wall. *Radiotherapy and oncology.* 2013; 106 (2): 220–224. 10.1016/j.radonc.2012.11.010.

(227) Picardi C, Rouzaud M, Kountouri M, Lestrade L, Vallée JP, Caparrotti F, et al. Impact of hydrogel spacer injections on interfraction prostate motion during prostate cancer radiotherapy. *Acta oncologica.* 2016; 55 (7): 834–838. 10.3109/0284186X.2015.1128118.

(228) Hedrick SG, Fagundes M, Robison B, Blakey M, Renegar J, Artz M, et al. A comparison between hydrogel spacer and endorectal balloon: An analysis of intrafraction prostate motion during proton therapy. *Journal of applied clinical medical physics.* 2017; 18 (2): 106–112. 10.1002/acm2.12051.

(229) Su Z, Henderson R, Nichols R, Bryant C, Hoppe B, Mendenhall W, et al. A comparative study of prostate PTV margins for patients using hydrogel spacer or rectal balloon in proton therapy. *Physica medica.* 2021; 81 47–51. 10.1016/j.ejmp.2020.11.033.

(230) Johnson PW, Blackstone JM. Children and gender-differences in exposure and how anthropometric differences can be incorporated into the design of computer input devices. *Scandinavian journal of work, environment & health.* 2007; 26. https://www.proquest.com/docview/201491746. .

(231) Romero FR, Romero AW, Brenny Filho T, Bark NM, Yamazaki DS, de Oliveira FCJ. Patients' perceptions of pain and discomfort during digital rectal exam for prostate cancer screening. *Archivos españoles de urología.* 2008; 61 (7): 850–854. 10.4321/S0004-06142008000700018.

(232) Lee TH, Bharucha AE. How to Perform and Interpret a High-resolution Anorectal Manometry Test. *Journal of Neurogastroenterology and Motility.* 2016; 22 (1): 46–59. 10.5056/jnm15168.

(233) American Neurogastroenterology and Motility Society. *Patient Information on Anorectal Manometry .* 2005.

(234) HO YH, TAN M. Ambulatory anorectal manometric findings in patients before and after haemorrhoidectomy. *International journal of colorectal disease.* 1997; 12 (5): 296–297. 10.1007/s003840050109.

(235) Gibbons CP, Read NW. Anal hypertonia in fissures: Cause or effect? *British journal of surgery.* 1986; 73 (6): 443–445. 10.1002/bjs.1800730609.

(236) Reichman EF. Chapter 71. Rigid Rectosigmoidoscopy. In: Reichman EF. (ed.) *Emergency medicine procedures.* McGraw-Hill; 2013.

(237) Pearl RK. *Gastrointestinal Endoscopy for Surgeons.* Boston: Little, Brown & Co; 1984.

(238) MAKOWIEC F, JEHLE EC, BECKER H-, STARLINGER M. Perianal abscess in Crohn's disease. *Diseases of the colon & rectum.* 1997; 40 (4): 443–450. 10.1007/BF02258390.

(239) Stericom. *Proctoscopes.* https://stericom.com/product/proctoscopes/ [Accessed 24 November 2022].

(240) Alimoradi M. *Proctoscopy- Colorectal Medicine.* https://myacare.com/procedure/proctoscopy [Accessed 24 November 2022].

(241) Karunaharamoorthy A. *Anal Canal.* https://www.kenhub.com/en/library/anatomy/the-anal-canal [Accessed 21 October 2022].

(242) Salerno G, Sinnatamby C, Branagan G, Daniels IR, Heald RJ, Moran BJ. Defining the rectum: surgically, radiologically and anatomically. *Colorectal disease.* 2006; 8 (s3): 5–9. 10.1111/j.1463-1318.2006.01062.x.

(243) PILONI V, FIORAVANTI P, SPAZZAFUMO L, ROSSI B. Measurement of the anorectal angle by defecography for the diagnosis of fecal incontinence. *International journal of colorectal disease.* 1999; 14 (2): 131–135. 10.1007/s003840050198.

(244) Bordeianou L, Carmichael J, Paquette I, Wexner S, Hull T, Bernstein M, et al. Consensus Statement of Definitions for Anorectal Physiology Testing and Pelvic Floor Terminology (Revised). *Diseases of the colon & rectum.* 2018; 61 (4): 421–427. 10.1097/DCR.0000000000001070.

(245) Nivatvongs S, Stern HS, Fryd DS. The Length of the Anal Canal. *Diseases of the Colon & Rectum.* 1981; 24 600–601. https://link.springer.com/content/pdf/10.1007/BF02605754.pdf. .

(246) Kuhlmann L, Joensson IM, Froekjaer JB, Krogh K, Farholt S. A descriptive study of colorectal function in adults with Prader-Willi Syndrome: high prevalence of constipation. *BMC gastroenterology.* 2014; 14 (1): 63. 10.1186/1471-230X-14-63.

(247) Kim AY. How to Interpret a Functional or Motility Test - Defecography. *Journal of Neurogastroenterology and Motility.* 2011; 17 (4): 416–420. 10.5056/jnm.2011.17.4.416.

(248) Tirumanisetty P, Prichard D, Fletcher JG, Chakraborty S, Zinsmeister AR, Bharucha AE. Normal values for assessment of anal sphincter morphology, anorectal motion, and pelvic organ prolapse with MRI in healthy women. *Neurogastroenterology and motility.* 2018; 30 (7): e13314–n/a. 10.1111/nmo.13314.

(249) ALTOMARE DF, RINALDI M, VEGLIA A, GUGLIELMI A, SALLUSTIO PL, TRIPOLI G. Contribution of posture to the maintenance of anal continence.

International journal of colorectal disease. 2001; 16 (1): 51–54. 10.1007/s003840000274.

(250) BURNETT SJD, BARTRAM CI. Endosonographic variations in the normal internal anal sphincter. *International journal of colorectal disease.* 1991; 6 (1): 2–4. 10.1007/BF00703951.

(251) Runciman M, Darzi A, Mylonas GP. Soft Robotics in Minimally Invasive Surgery. *Soft Robotics.* 2019; 6 (4): 423–443. 10.1089/soro.2018.0136.

(252) Runciman M, Avery J, Darzi A, Mylonas G. Open Loop Position Control of Soft Hydraulic Actuators for Minimally Invasive Surgery. *Applied sciences.* 2021; 11 (16): 7391. 10.3390/app11167391.

(253) Pelrine R, Kornbluh R, Pei Q, Joseph J. High-Speed Electrically Actuated Elastomers with Strain Greater Than 100. *Science.* 2000; 287 (5454): 836–839. 10.1126/science.287.5454.836.

(254) Blanc L, Delchambre A, Lambert P. Flexible Medical Devices: Review of Controllable Stiffness Solutions. *Actuators.* 2017; 6 (3): 23. 10.3390/act6030023.

(255) Benjamin Gorissen, Wannes Vincentie, Farid Al-Bender, Dominiek Reynaerts, Michaël De Volder. Modeling and bonding-free fabrication of flexible fluidic microactuators with a bending motion. *Journal of Micromechanics and Microengineering.* 2013; 23 (4): 10.1088/0960-1317/23/4/045012.

(256) Karl Friedrich Gauss, James Caddall Morehead, Adam Miller Hiltebeitel. *General Investigations of Curved Surfaces of 1827 and 1825.* ; 2011. .

(257) Runciman M, Avery J, Zhao M, Darzi A, Mylonas GP. Deployable, Variable Stiffness, Cable Driven Robot for Minimally Invasive Surgery. *Frontiers in Robotics and AI.* 2019; 6 141. 10.3389/frobt.2019.00141.

(258) Fitzgerald SG, Delaney GW, Howard D. A Review of Jamming Actuation in Soft Robotics. *Actuators.* 2020; 9 (4): 104. 10.3390/act9040104.

(259) Ching-Ping Chou, Hannaford B. Measurement and modeling of McKibben pneumatic artificial muscles. *IEEE transactions on robotics and automation.* 1996; 12 (1): 90–102. 10.1109/70.481753.

(260) Tondu B, Lopez P. *Modeling and control of McKibben artificial muscle robot actuators.* New York: IEEE; 2000.

(261) Hannaford B, Winters J. Actuator Properties and Movement Control: Biological and Technological Models. *Multiple Muscle Systems.* United States: Springer New York; 1990. pp. 101–120.

(262) Schulte HF, Pearson JR, joint author. *Characteristics of the braided fluid actuator [by] H.F. Schulte, Jr., D.F. Adamski [and] J.R. Pearson.* 1961.

(263) Daerden F, Lefeber D. The Concept and Design of Pleated Pneumatic Artificial Muscles. *International Journal of Fluid Power.* 2001; 2 (3): 41–50. 10.1080/14399776.2001.10781119.

(264) Verrelst Br, Ham RV, Vanderborght B, Daerden F, Lefeber D, Vermeulen J. The Pneumatic Biped "Lucy" Actuated with Pleated Pneumatic Artificial Muscles. *Autonomous robots.* 2005; 18 (2): 201–213. 10.1007/s10514-005-0726-x.

(265) Verrelst B, Van Ham R, Vanderborght B, Lefeber D, Daerden F, Van Damme M. Second generation pleated pneumatic artificial muscle and its robotic applications. *Advanced robotics.* 2006; 20 (7): 783–805. 10.1163/156855306777681357.

(266) Villegas D, Van Damme M, Vanderborght B, Beyl P, Lefeber D. Third-Generation Pleated Pneumatic Artificial Muscles for Robotic Applications: Development and Comparison with McKibben Muscle. *Advanced robotics.* 2012; 26 (11-12): 1205–1227. 10.1080/01691864.2012.689722.

(267) Terryn S, Brancart J, Lefeber D, Van Assche G, Vanderborght B. A Pneumatic Artificial Muscle Manufactured Out of Self-Healing Polymers That Can Repair Macroscopic Damages. *IEEE robotics and automation letters.* 2018; 3 (1): 16–21. 10.1109/LRA.2017.2724140.

(268) Baldwin HA. Realizable Models of Muscle Function. In: Bootzin D, Muffley HC. (eds.) *Biomechanics.* Springer US; 1969. pp. 139–147.

(269) Yong-Lae Park, Wood RJ. Smart pneumatic artificial muscle actuator with embedded microfluidic sensing. *2013 IEEE SENSORS* : IEEE; Nov 2013. pp. 1–4. 10.1109/ICSENS.2013.6688298.

(270) Saga N, Awano K, Nakamura T. Development of Artificial Muscle Actuator Reinforced by Kevlar Fiber. *The Proceedings of JSME annual Conference on Robotics and Mechatronics (Robomec).* 2003; 77. 10.1299/jsmermd.2003.77_1.

(271) Nakamura T, Shinohara H. Position and Force Control Based on Mathematical Models of Pneumatic Artificial Muscles Reinforced by Straight Glass Fibers. *Proceedings 2007 IEEE International Conference on Robotics and Automation* : IEEE; Apr 2007. pp. 4361–4366. 10.1109/ROBOT.2007.364151.

(272) Tomori H, Nakamura T. Theoretical Comparison of McKibben-Type Artificial Muscle and Novel Straight-Fiber-Type Artificial Muscle. *International Journal of Automation Technology.* 2011; 5 (4): 544–550. 10.20965/ijat.2011.p0544.

(273) Wirekoh J, Park Y. Design of flat pneumatic artificial muscles. *Smart materials and structures.* 2017; 26 (3): 35009. 10.1088/1361-665X/aa5496.

(274) Yong-Lae Park, Santos J, Galloway KG, Goldfield EC, Wood RJ. A soft wearable robotic device for active knee motions using flat pneumatic artificial

muscles. *2014 IEEE International Conference on Robotics and Automation (ICRA)* : IEEE; May 2014. pp. 4805–4810. 10.1109/ICRA.2014.6907562.

(275) Niiyama R, Rus D, Sangbae Kim. Pouch Motors: Printable/inflatable soft actuators for robotics. *2014 IEEE International Conference on Robotics and Automation (ICRA)* : IEEE; May 2014. pp. 6332–6337.

(276) Veale AJ, Xie SQ, Anderson IA. Modeling the Peano fluidic muscle and the effects of its material properties on its static and dynamic behavior. *Smart materials and structures.* 2016; 25 (6): 65014–65029. 10.1088/0964-1726/25/6/065014.

(277) Niiyama R, Sun X, Sung C, An B, Rus D, Kim S. Pouch Motors: Printable Soft Actuators Integrated with Computational Design. *Soft robotics.* 2015; 2 (2): 59–70. 10.1089/soro.2014.0023.

(278) Sanan S, Lynn PS, Griffith ST. Pneumatic Torsional Actuators for Inflatable Robots. *Journal of Mechanisms and Robotics.* 2014; 6 (3): 031003:1–np. 10.1115/1.4026629.

(279) Veale AJ, Anderson IA, Xie SQ. The smart Peano fluidic muscle: a low profile flexible orthosis actuator that feels pain. *Proceedings of SPIE, the international society for optical engineering* : SPIE; Mar 27, 2015. pp. 94351V–11. 10.1117/12.2084130.

(280) Kim W, Park H, Kim J. Compact Flat Fabric Pneumatic Artificial Muscle (ffPAM) for Soft Wearable Robotic Devices. *IEEE robotics and automation letters.* 2021; 6 (2): 2603–2610. 10.1109/LRA.2021.3062012.

(281) Niiyama R, Rognon C, Kuniyoshi Y. Printable pneumatic artificial muscles for anatomy-based humanoid robots. *2015 IEEE-RAS 15th International Conference on Humanoid Robots (Humanoids)* : IEEE; Nov 2015. pp. 401–406. 10.1109/HUMANOIDS.2015.7363565.

(282) Li S, Lin J, Kang H, Cheng Y, Chen Y. Bio-inspired origamic pouch motors with a high contraction ratio and enhanced force output. *Robotics and autonomous systems.* 2022; 149 103983. 10.1016/j.robot.2021.103983.

(283) Kellaris N, Gopaluni Venkata V, Smith GM, Mitchell SK, Keplinger C. Peano-HASEL actuators: Muscle-mimetic, electrohydraulic transducers that linearly contract on activation. *Science robotics.* 2018; 3 (14): 10.1126/scirobotics.aar3276.

(284) Park T, Kim K, Oh S, Cha Y. Electrohydraulic Actuator for a Soft Gripper. *Soft robotics.* 2020; 7 (1): 68–75. 10.1089/soro.2019.0009.

(285) Jang JH, Jamil B, Moon Y, Coutinho A, Park G, Rodrigue H. Design of Gusseted Pouch Motors for Improved Soft Pneumatic Actuation. *IEEE/ASME transactions on mechatronics.* 2023; 28 (6): 1–11. 10.1109/TMECH.2023.3244347.

(286) Oh N, Park YJ, Lee S, Lee H, Rodrigue H. Design of Paired Pouch Motors for Robotic Applications. *Advanced materials technologies.* 2019; 4 (1): n/a. 10.1002/admt.201800414.

(287) Chung S, Coutinho A, Rodrigue H. Manufacturing and Design of Inflatable Kirigami Actuators. *IEEE robotics and automation letters.* 2023; 8 (1): 25–32. 10.1109/LRA.2022.3221318.

(288) Shen D, Wu J, Wang X, Tian M. Design and Analysis of a Novel Flat Pneumatic Artificial Muscle. *2021 IEEE 8th International Conference on Industrial Engineering and Applications (ICIEA)* Piscataway: IEEE; Apr 23, 2021. pp. 110–114. 10.1109/ICIEA52957.2021.9436760.

(289) Feng M, Yang D, Ren L, Wei G, Gu G. X-crossing pneumatic artificial muscles. *Science advances.* 2023; 9 (38): eadi7133. 10.1126/sciadv.adi7133.

(290) Kwon J, Yoon SJ, Park Y. Flat Inflatable Artificial Muscles With Large Stroke and Adjustable Force- Length Relations. *IEEE transactions on robotics.* 2020; 36 (3): 743–756. 10.1109/TRO.2019.2961300.

(291) Belforte G, Eula G, Ivanov A, Visan AL. Bellows textile muscle. *Journal of the Textile Institute.* 2014; 105 (3): 356–364. 10.1080/00405000.2013.840414.

(292) Lee J, Rodrigue H. Origami-Based Vacuum Pneumatic Artificial Muscles with Large Contraction Ratios. *Soft robotics.* 2019; 6 (1): 19–117. 10.1089/soro.2018.0063.

(293) Laura Paez, Gunjan Agarwal, Jamie Paik. Design and Analysis of a Soft Pneumatic Actuator with Origami Shell Reinforcement. *Soft Robotics.* 2016; 3 (3): 109–119. 10.1089/soro.2016.0023.

(294) Wu S, Ze Q, Dai J, Udipi N, Paulino GH, Zhao R. Stretchable origami robotic arm with omnidirectional bending and twisting. *Proceedings of the National Academy of Sciences - PNAS.* 2021; 118 (36): 1–9. 10.1073/pnas.2110023118.

(295) Yang M, Grey SW, Scarpa F, Schenk M. Large impact of small vertex cuts on the mechanics of origami bellows. *Extreme Mechanics Letters.* 2023; 60 101950. 10.1016/j.eml.2022.101950.

(296) Han K, Kim N, Shin D. A Novel Soft Pneumatic Artificial Muscle with High-Contraction Ratio. *Soft robotics.* 2018; 5 (5): 554–566. 10.1089/soro.2017.0114.

(297) Yang HD, Greczek BT, Asbeck AT. Modeling and Analysis of a High-Displacement Pneumatic Artificial Muscle With Integrated Sensing. *Frontiers in robotics and AI.* 2019; 5 136. 10.3389/frobt.2018.00136.

(298) Lee J, Rodrigue H. Armor-Based Stable Force Pneumatic Artificial Muscles for Steady Actuation Properties. *Soft robotics.* 2022; 9 (3): 413–424. 10.1089/soro.2020.0117.

(299) Liu S, Lu G, Chen Y, Leong YW. Deformation of the Miura-ori patterned sheet. *International Journal of Mechanical Sciences.* 2015; 99 130–142. 10.1016/j.ijmecsci.2015.05.009.

(300) Sahin I, Ayazi M, Mucchiani C, Dube J, Karydis K, Kokkoni E. A Fabric-based Pneumatic Actuator for the Infant Elbow: Design and Comparative Kinematic Analysis. *2023 IEEE International Conference on Robotics and Biomimetics (ROBIO)* Piscataway: IEEE; Dec 4, 2023. pp. 1–6. 10.1109/ROBIO58561.2023.10354824.

(301) Oguntosin V, Harwin WS, Kawamura S, Nasuto SJ, Hayashi Y. Development of a wearable assistive soft robotic device for elbow rehabilitation. *2015 IEEE International Conference on Rehabilitation Robotics (ICORR)* : IEEE; Aug 1, 2015. pp. 747–752. 10.1109/ICORR.2015.7281291.

(302) Shen Y, Dang Y, Jiang T, Huo W, Yu N, Han J. A Textile-Based Pneumatic Soft Suit for Elbow Joint Rehabilitation. *IEEE ... Annual International Conference on Cyber Technology in Automation, Control, and Intelligent Systems (Online)* : IEEE; Jul 16, 2024. pp. 662–667. 10.1109/CYBER63482.2024.10749338.

(303) Manfredi L, Capoccia E, Ciuti G, Cuschieri A. A Soft Pneumatic Inchworm Double balloon (SPID) for colonoscopy. *Scientific Reports.* 2019; 9 (1): 11109–9. 10.1038/s41598-019-47320-3.

(304) Fathi J, Oude Vrielink TJC, Runciman MS, Mylonas GP. A Deployable Soft Robotic Arm with Stiffness Modulation for Assistive Living Applications. *2019 International Conference on Robotics and Automation (ICRA)* : IEEE; May 2019. pp. 1479–1485.

(305) paolostraffi. *OnScreenProtractor.* https://sourceforge.net/projects/osprotractor/ .

(306) Oblizajek NR, Gandhi S, Sharma M, Chakraborty S, Muthyala A, Prichard D, et al. Anorectal pressures measured with high-resolution manometry in healthy people—Normal values and asymptomatic pelvic floor dysfunction. *Neurogastroenterology and motility.* 2019; 31 (7): e13597–n/a. 10.1111/nmo.13597.

(307) Shafik A. Functional activity of the rectum : A conduit organ or a storage organ or both. *World journal of gastroenterology : WJG.* 2006; 12 (28): 4549–4552. 10.3748/wjg.v12.i28.4549.

(308) Gilbert-Kawai ET, Wittenberg MD. Laplace's law and tension. *Essential Equations for Anaesthesia.* 2014. pp. 24–25.

(309) Niiyama R, Sun X, Sung C, An B, Rus D, Kim S. Pouch Motors: Printable Soft Actuators Integrated with Computational Design. *Soft robotics.* 2015; 2 (2): 59–70. 10.1089/soro.2014.0023.

(310) Lenzi T, Vitiello N, Rossi SMMD, Persichetti A, Giovacchini F, Roccella S, et al. Measuring human–robot interaction on wearable robots: A distributed approach. *Mechatronics.* 2011; 21 (6): 1123–1131. 10.1016/j.mechatronics.2011.04.003.

(311) Nasr A, Inkol K, McPhee J. Safety in Wearable Robotic Exoskeletons: Design, Control, and Testing Guidelines. *Journal of mechanisms and robotics.* 2025; 17 (5): 10.1115/1.4066900.

(312) Niknam Maleki A, Runciman M, Murray J, Mylonas G. Hydraulic endorectal actuator for prostate radiotherapy reduces variations in motion in a silicone rectal phantom. *Frontiers in oncology.* 2026; 16 1686529. 10.3389/fonc.2026.1686529.

(313) Dal Lago A, Minetti AE, Biondetti P, Corsetti M, Basilisco G. Magnetic Resonance Imaging of the Rectum During Distension. *Diseases of the colon & rectum.* 2005; 48 (6): 1220–1227. 10.1007/s10350-004-0933-0.

(314) Castro-Poças F, Dinis-Ribeiro M, Araújo T, Pedroto I. Echoendoscopic characterization of the human colon. *Revista española de enfermedades digestivas.* 2015; 107 (8): 469–475. 10.17235/reed.2015.3721/2015.

(315) Ahmed A, Arbor TC, Qureshi WA. Anatomy, Abdomen and Pelvis: Anal Canal. *StatPearls [Internet].* Treasure Island (FL): StatPearls Publishing; 2023.

(316) Stokes WE, Jayne DG, Alazmani A, Culmer PR. A biomechanical model of the human defecatory system to investigate mechanisms of continence. *Proceedings of the Institution of Mechanical Engineers. Part H, Journal of engineering in medicine.* 2019; 233 (1): 114–126. 10.1177/0954411918756453.

(317) Papaconstantinou HT. Evaluation of Anal Incontinence: Minimal Approach, Maximal Effectiveness. *Clinics in colon and rectal surgery.* 2005; 18 (1): 9–16. 10.1055/s-2005-864076.

(318) Fox M, Thumshirn M, Fried M, Schwizer W. Barostat Measurement of Rectal Compliance and Capacity. *Diseases of the colon & rectum.* 2006; 49 (3): 360–370. 10.1007/s10350-005-0295-2.

(319) Bazira PJ. Anatomy of the rectum and anal canal. *Surgery (Oxford).* 2023; 41 (1): 7–14. 10.1016/j.mpsur.2022.11.002.

(320) Christensen MB, Oberg K, Wolchok JC. Tensile properties of the rectal and sigmoid colon: a comparative analysis of human and porcine tissue. *SpringerPlus.* 2015; 4 (1): 142. 10.1186/s40064-015-0922-x.

(321) *Ecoflex™ Series Product Overview*https://www.smooth-on.com/tb/files/ECOFLEX_SERIES_TB.pdf .

(322) Vaicekauskaite J, Mazurek P, Vudayagiri S, Skov AL. Mapping the mechanical and electrical properties of commercial silicone elastomer

formulations for stretchable transducers. *Journal of Materials Chemistry C.* 2020; 8 (4): 1273–1279. 10.1039/c9tc05072h.

(323) Mui Scientific. *Rapid Barostat Bag Pump User Manual.* 2020. http://www.muiscientific.com/pdf/Rapid%20Barostat%20Bag%20Pump%20Manual%20(July%207,%202020).pdf .

(324) *Tracker video analysis and modelling tool*https://opensourcephysics.github.io/tracker-website/ .

(325) Bohoudi O, Lagerwaard FJ, Bruynzeel AME, Niebuhr NI, Johnen W, Senan S, et al. End-to-end empirical validation of dose accumulation in MRI-guided adaptive radiotherapy for prostate cancer using an anthropomorphic deformable pelvis phantom. *Radiotherapy and Oncology.* 2019; 141 200–207. 10.1016/j.radonc.2019.09.014.

(326) Osgouei RH, Marechal L, Kontovounisios C, Bello F. Soft Pneumatic Actuator for Rendering Anal Sphincter Tone. *IEEE transactions on haptics.* 2020; 13 (1): 183–190. 10.1109/TOH.2020.2968446.

(327) RoyMech Org. *Fluid properties of Water.* https://roymech.org/Related/Fluids/Fluids_Water_Props.html .

(328) Zulina N, Caravaca O, Liao G, Gravelyn S, Schmitt M, Badu K, et al. Colon phantoms with cancer lesions for endoscopic characterization with optical coherence tomography. *Biomedical optics express.* 2021; 12 (2): 955–968. 10.1364/BOE.402081.

(329) Stokes WE. *Development of a physical simulation of the human defecatory system for the investigation of continence mechanisms.* University of Leeds; 2018.

(330) Wang Y, Tai BL, Yu H, Shih AJ. Silicone-Based Tissue-Mimicking Phantom for Needle Insertion Simulation. *Journal of medical devices.* 2014; 8 (2): 10.1115/1.4026508.

(331) Yang J, Runciman M, Avery J, Sun Z, Mylonas G. A Soft Inflatable Robot Driven by Hydraulic Folded Pouch Actuators for Minimally Invasive Surgery. *IEEE robotics and automation letters.* 2024; 9 (5): 4870–4877. 10.1109/LRA.2024.3386022.

(332) Vinod A, Tadmor R, Katoshevski D, Gutmark EJ. Gels That Serve as Mucus Simulants: A Review. *Gels.* 2023; 9 (7): 555. 10.3390/gels9070555.

(333) Thompson AJ, Yang G. Tethered and Implantable Optical Sensors. In: Yang G. (ed.) *Implantable Sensors and Systems.* Cham: Springer International Publishing; 2018. pp. 439–505.

(334) Quan F, Kim KS. Medical applications of the intrinsic mechanical properties of single cells. *Acta biochimica et biophysica Sinica.* 2016; 48 (10): 865–871. 10.1093/abbs/gmw081.

(335) Hammer SJ, Good DW, Scanlan P, Palacio-Torralba J, Phipps S, Stewart GD, et al. Quantitative mechanical assessment of the whole prostate gland ex vivo using dynamic instrumented palpation. *Proceedings of the Institution of Mechanical Engineers. Part H, Journal of engineering in medicine.* 2017; 231 (12): 1081–1100. 10.1177/0954411917734257.

(336) Yang TJ, Phipps S, Leung SK, Reuben RL, Habib FK, McNeill SA. Dynamic instrumented palpation – a new method for soft tissue quality assessment: application to prostate disease diagnosis. *Proceedings of the Institution of Mechanical Engineers. Part H, Journal of engineering in medicine.* 2017; 231 (12): 1101–1115. 10.1177/0954411917734579.

Appendix

A.1 Copyright summary table for third party work

Table A.1 summarises the third-party works used in this thesis and the copyright permissions obtained.

Table A.1: Permissions summary table for third-party copyright works

Page No.	Type of work:	Name of work	Source of work	Copyright holder and contact	permission requested on	I have permission yes /no	Permission note
43	Figure	Figure 2.2 A patient's CT planning scan with annotations analysing the rectum shape and size to assess features between patients who could insert ProSpare™ and those who could not.	Niknam Maleki A, Mylonas G, Murray J. ProSpare tolerability is independent of rectal anatomy. *Proceedings of the 10th World Congress on Electrical Engineering and Computer Systems and Sciences (EECSS'24),* : Avestia; 2024. pp. ICBES 145. 10.11159/icbes24.145.	© 2024 Avestia Publishing copyright@avestia.com		yes	Licensed with a Creative Commons Attribution 3.0 License
43	Table	Table 2.1 Mean (±SD) anorectal angle, anterior-posterior rectal diameter at the anorectal junction, and anal canal lengths in patients	Niknam Maleki A, Mylonas G, Murray J. ProSpare tolerability is independent of rectal anatomy. *Proceedings of the 10th World Congress on Electrical Engineering and Computer Systems and Sciences (EECSS'24),* : Avestia; 2024. pp. ICBES 145. 10.11159/icbes24.145	© 2024 Avestia Publishing copyright@avestia.com		yes	Licensed with a Creative Commons Attribution 3.0 License
44	Figure	Figure 2.3 Distributions of measurements of patients' rectums who could insert ProSpare™ (Green), could not insert ProSpare™ (Red), and had ProSpare™ inside (Blue).	Niknam Maleki A, Mylonas G, Murray J. ProSpare tolerability is independent of rectal anatomy. *Proceedings of the 10th World Congress on Electrical Engineering and Computer Systems and Sciences (EECSS'24),* :	© 2024 Avestia Publishing copyright@avestia.com		yes	Licensed with a Creative Commons Attribution 3.0 License

			Avestia; 2024. pp. ICBES 145. 10.11159/icbes24.145.				
88	Figure	Figure 4.18 Design and fabrication of the soft endorectal actuator	Maleki AN, Thompson A, Runciman MS, Murray J, Mylonas GP. A soft hydraulic endorectal actuator for prostate radiotherapy. *2023 IEEE International Conference on Robotics and Biomimetics (ROBIO)* : IEEE; Dec 4, 2023. pp. 1–6.	© 2023 IEEE	29.06.2025	yes	Permission grant by IEEE attached in A.2.
89	Figure	Figure 4.19 Sagittal view of the device showing the mechanism of action of the internal flexor actuator (in blue).	Maleki AN, Thompson A, Runciman MS, Murray J, Mylonas GP. A soft hydraulic endorectal actuator for prostate radiotherapy. *2023 IEEE International Conference on Robotics and Biomimetics (ROBIO)* : IEEE; Dec 4, 2023. pp. 1–6.	© 2023 IEEE copyrights@ieee.org	29.06.2025	yes	Permission grant by IEEE attached in A.2.
90	Figure	Figure 4.20 Dimensions of the device when (a) deployed and inflated and (b and c) undeployed and folded.	Maleki AN, Thompson A, Runciman MS, Murray J, Mylonas GP. A soft hydraulic endorectal actuator for prostate radiotherapy. *2023 IEEE International Conference on Robotics and Biomimetics (ROBIO)* : IEEE; Dec 4, 2023. pp. 1–6.	© 2023 IEEE copyrights@ieee.org	29.06.2025	yes	Permission grant by IEEE attached in A.2.
91	Figure	Figure 4.21 (a) The maximal angle of flexion with the flexor actuator fully inflated with red-	Maleki AN, Thompson A, Runciman MS, Murray J, Mylonas GP. A soft hydraulic endorectal actuator for	© 2023 IEEE copyrights@ieee.org	29.06.2025	yes	Permission grant by IEEE attached in A.2.

		dyed water, and (b) maximal angle of extension with the extensor actuator filled with black-dyed water.	prostate radiotherapy. *2023 IEEE International Conference on Robotics and Biomimetics (ROBIO)* : IEEE; Dec 4, 2023. pp. 1–6.				
92	Figure	Figure 4.22 Angle changes of the device while the flexor actuator is full and the extensor actuator is inflated from 0 ml to 4 ml	Maleki AN, Thompson A, Runciman MS, Murray J, Mylonas GP. A soft hydraulic endorectal actuator for prostate radiotherapy. *2023 IEEE International Conference on Robotics and Biomimetics (ROBIO)* : IEEE; Dec 4, 2023. pp. 1–6.	© 2023 IEEE copyrights@ieee.org	29.06.2025	yes	Permission grant by IEEE attached in A.2.
93	Figure	Figure 4.23 Measuring force output from the main actuator of the device	Maleki AN, Thompson A, Runciman MS, Murray J, Mylonas GP. A soft hydraulic endorectal actuator for prostate radiotherapy. *2023 IEEE International Conference on Robotics and Biomimetics (ROBIO)* : IEEE; Dec 4, 2023. pp. 1–6.	© 2023 IEEE copyrights@ieee.org	29.06.2025	yes	Permission grant by IEEE attached in A.2.
94	Figure	Figure 4.24 Radial stiffness of the main actuator in relation to the volume it is inflated by	Maleki AN, Thompson A, Runciman MS, Murray J, Mylonas GP. A soft hydraulic endorectal actuator for prostate radiotherapy. *2023 IEEE International Conference on Robotics and Biomimetics (ROBIO)* : IEEE; Dec 4, 2023. pp. 1–6.	© 2023 IEEE copyrights@ieee.org	29.06.2025	yes	Permission grant by IEEE attached in A.2.

94	Figure	Figure 4.25 Force measured vs displacement in compression of the main actuator	Maleki AN, Thompson A, Runciman MS, Murray J, Mylonas GP. A soft hydraulic endorectal actuator for prostate radiotherapy. *2023 IEEE International Conference on Robotics and Biomimetics (ROBIO)* : IEEE; Dec 4, 2023. pp. 1–6.	© 2023 IEEE copyrights@ieee.org	29.06.2025	yes	Permission grant by IEEE attached in A.2.
95	Table	Table 4.1 Force by Newton meter and angle changes. Copyright © 2023 IEEE	Maleki AN, Thompson A, Runciman MS, Murray J, Mylonas GP. A soft hydraulic endorectal actuator for prostate radiotherapy. *2023 IEEE International Conference on Robotics and Biomimetics (ROBIO)* : IEEE; Dec 4, 2023. pp. 1–6.	© 2023 IEEE copyrights@ieee.org	29.06.2025	yes	Permission grant by IEEE attached in A.2.
95	Figure	Figure 4.26 Relationship between the torque acting on the device and the increase in the angle of the device, opposing the bending action by the flexor actuator.	Maleki AN, Thompson A, Runciman MS, Murray J, Mylonas GP. A soft hydraulic endorectal actuator for prostate radiotherapy. *2023 IEEE International Conference on Robotics and Biomimetics (ROBIO)* : IEEE; Dec 4, 2023. pp. 1–6.	© 2023 IEEE copyrights@ieee.org	29.06.2025	yes	Permission grant by IEEE attached in A.2.
96	Figure	Figure 4.27 The absolute pressure over time inside (a) the main body of the device while undergoing anterior-posterior compression.	Maleki AN, Thompson A, Runciman MS, Murray J, Mylonas GP. A soft hydraulic endorectal actuator for prostate radiotherapy. *2023 IEEE International*	© 2023 IEEE copyrights@ieee.org	29.06.2025	yes	Permission grant by IEEE attached in A.2.

			Conference on Robotics and Biomimetics (ROBIO) : IEEE; Dec 4, 2023. pp. 1–6.				
97	Figure	Figure 4.28 Compressive radial stiffness over time	Maleki AN, Thompson A, Runciman MS, Murray J, Mylonas GP. A soft hydraulic endorectal actuator for prostate radiotherapy. *2023 IEEE International Conference on Robotics and Biomimetics (ROBIO)* : IEEE; Dec 4, 2023. pp. 1–6.	© 2023 IEEE copyrights@ieee.org	29.06.2025	yes	Permission grant by IEEE attached in A.2.

A.2 Copyright permission statement from IEEE



CCC RightsLink

Sign in/Register

IEEE Requesting permission to reuse content from an IEEE publication

A soft hydraulic endorectal actuator for prostate radiotherapy

Conference Proceedings:
2023 IEEE International Conference on Robotics and Biomimetics (ROBIO)

Author: Aryan Niknam Maleki

Publisher: IEEE

Date: 04 December 2023

Copyright © 2023, IEEE

Quick Price Estimate

The IEEE does not require individuals working on a thesis to obtain a formal reuse license, however, you may print out this statement to be used as a permission grant:

Requirements to be followed when using any portion (e.g., figure, graph, table, or textual material) of an IEEE copyrighted paper in a thesis:

1) In the case of textual material (e.g., using short quotes or referring to the work within these papers) users must give full credit to the original source (author, paper, publication) followed by the IEEE copyright line © 2011 IEEE.
2) In the case of illustrations or tabular material, we require that the copyright line © [Year of original publication] IEEE appear prominently with each reprinted figure and/or table.
3) If a substantial portion of the original paper is to be used, and if you are not the senior author, also obtain the senior author's approval.

Requirements to be followed when using an entire IEEE copyrighted paper in a thesis:

1) The following IEEE copyright/ credit notice should be placed prominently in the references: © [year of original publication] IEEE. Reprinted, with permission, from [author names, paper title, IEEE publication title, and month/year of publication]
2) Only the accepted version of an IEEE copyrighted paper can be used when posting the paper or your thesis on-line.
3) In placing the thesis on the author's university website, please display the following message in a prominent place on the website: In reference to IEEE copyrighted material which is used with permission in this thesis, the IEEE does not endorse any of [university/educational entity's name goes here]'s products or services. Internal or personal use of this material is permitted. If interested in reprinting/republishing IEEE copyrighted material for advertising or promotional purposes or for creating new collective works for resale or redistribution, please go to http://www.ieee.org/publications_standards/publications/rights/rights_link.html to learn how to obtain a License from RightsLink.

If applicable, University Microfilms and/or ProQuest Library, or the Archives of Canada may supply single copies of the dissertation.

I would like to... reuse in a thesis/dissertation

© 2025 Copyright - All Rights Reserved | Copyright Clearance Center, Inc. | Privacy statement | Data Security and Privacy | For California Residents | Terms and ConditionsComments? We would like to hear from you. E-mail us at customercare@copyright.com